DISS. ETH NO. 21038

On Southern Ocean Eddies and Their Impacts on Biology and the Atmosphere

A dissertation submitted to
ETH ZURICH

for the degree of
Doctor of Sciences

presented by
IVY FRENGER
Dipl. Met., Universität Hamburg
born 21 September 1981
citizen of Germany

accepted on the recommendation of
Prof. Dr. N. Gruber Guyan, examiner
Prof Dr. R. Knutti, co-examiner
Dr. M. Münnich, co-examiner
Prof. Dr. A. Oschlies, co-examiner

2013

Summary

The global ocean's kinetic energy is dominated by mesoscale eddies, with the Southern Ocean (SO, south of 30°S) being a region of particularly high eddy activity. The SO is also dynamically connected to the global deep ocean and is therefore of crucial importance for ocean dynamics and biogeochemistry. This work provides the first study of SO eddies and their impacts based on a Lagrangian approach. More than 1,000,000 snapshots of eddies are identified from satellite observations of sea level anomalies during the time period from 1997 to 2010.

It is shown that eddies cover for more than 30 % of the time the dynamic regions of the SO that include the Antarctic Circumpolar Current (ACC) and the western boundary currents. These regions show both high rates of eddy generation and dissipation, and a seasonal variation of eddy activity of up to 20 %. The dynamic regions also feature the most intense eddies with the largest sea surface temperature anomalies. Regions of very little eddy activity such as shallow topography also exist along the ACC pathway. The local pattern of sea surface temperature anomalies associated with eddies suggest an impact on non-reactive tracers by both eddy *stirring* and *trapping*. The analysis of profiling float data shows that eddies are characterized by deep reaching temperature and salt anomalies and associated large mean trapping depths of more than 1000 m. The float data allow for an estimate of southward heat and salt transports across the ACC caused by eddies due to *trapping*. In agreement with previous in-situ studies this constitutes about 10 % and 1 % of the transports necessary to compensate for the heat loss and freshwater surplus south of the ACC, respectively.

The information on mesoscale ocean eddies is combined with satellite based observations of biology and the atmosphere to examine the local impacts of eddies on their environment. Eddies are collocated with chlorophyll-a (*CHL*), a proxy for phytoplankton biomass. A clear association is found between eddies and *CHL* in the multi-year mean, with *CHL* anomalies larger than 10 % for anticyclonic as well as cyclonic eddies. The spatio-temporal variability of *CHL* anomalies of eddies provides indications for the main causes of the association of eddies with *CHL*. These indications are consistent with a modification of phytoplankton growth by eddies as dominant mechanism in the SO, and *trapping* and *stirring* playing a minor role.

When collocating eddies with winds, cloud properties and rainfall, a distinct relation is detected, with eddies modifying the atmospheric quantities by several percent. The local pattern of the anomalies is consistent with a mechanism where eddies impact the atmosphere by changing its near-surface stability due to their sea surface temperature anomalies, hence modifying atmospheric boundary layer turbulence.

Zusammenfassung

Die kinetische Energie des Ozeans wird von mesoskalischen Wirbeln dominiert. Der südliche Ozean (SO, südlich von 30°S) ist eine Region mit besonders hoher Wirbelaktivität. Gleichzeitig stellt der SO ein Fenster zum Tiefenozean dar und ist daher wesentlich für die globale Ozeandynamik und Biogeochemie. Diese Abhandlung ist die erste Studie zu Wirbeln im Südpolarmeer und ihrer Wirkung, die auf einem Lagrangian Ansatz basiert. Dabei wurden mehr als 1'000'000 einzelne Wirbel aus satellitengestützten Beobachtungen von Meeresoberflächenanomalien zwischen 1997 und 2010 identifiziert.

Es zeigt sich, dass dynamischen Regionen des SO, zu denen der Antarktische Zirkumpolarstrom (ACC) und die westlichen Randströme gehören, mehr als 30 % der Zeit von Wirbeln bedeckt sind. Gleichzeitig sind dies Regionen hoher Raten sowohl von Wirbelerzeugung als auch von -vernichtung, und einer saisonalen Variabilität von bis zu 20 %. Die energetischen Regionen sind auch die Gebiete der stärksten Wirbel mit den grössten Meeresoberflächentemperaturanomalien. Daneben gibt es Regionen mit sehr geringer Wirbelaktivität wie z.B. Untiefen entlang des ACC.

Das lokale Muster der zu den Wirbeln gehörigen Meeresoberflächentemperaturanomalien deutet auf einen Einfluss von Wirbeln auf nicht-reaktive Spurenstoffe (tracer) sowohl durch Vermischung (*stirring*) als auch durch Einschluss (*trapping*) hin. Eine Analyse von Temperatur- und Salzprofilen basierend auf Messungen von *Floats* in Wirbeln zeigen tiefreichende Anomalien und Einschluss (*trapping*)-Tiefen von mehr als 1000 m. Mit diesen Ergebnissen lassen sich südwärtige Wärme- und Salztransporte auf Grund von Wirbeln abschätzen, die den ACC queren. Übereinstimmend mit Abschätzungen von in-situ Studien machen diese nur etwa 10 % bzw. 1 % der Transporte aus, die nötig wären, um den Wärmeverlust und Süsswasserüberschuss südlich des ACC zu kompensieren.

Ich kombiniere die Informationen über die mesoskalischen Wirbel mit satellitengestützten Beobachtungen von Biologie und der Atmosphäre, um den Einfluss von Wirbeln auf ihre Umgebung zu untersuchen. Dabei wird Chlorophyll-a (*CHL*) als Mass für Biomasse von Phytoplankton, also für die Biologie der untersten trophischen Ebene, benutzt. Ein eindeutiger Zusammenhang zwischen *CHL* und Wirbeln wird aufgezeigt, mit langzeitlichen mittleren *CHL* Anomalien von mehr als 10 % für antizyklonische wie zyklonische Wirbel. Dabei variieren Vorzeichen und Stärke dieses Zusammenhangs sowohl räumlich als auch zeitlich.

Mit Hilfe dieser raum-zeitlichen Variabilität werden als Hauptursachen für die *CHL* Anomalien *trapping* und der Einfluss auf das Wachstum von Phytoplankton durch die Wirbel bestimmt. Bezüglich dieser beiden Mechanismen finden sich nur Hinweise auf

den Einfluss des Wachstums von Phytoplankton. Rühren (*stirring*) spielt im SO eine sekundäre Rolle.
Ausserdem kombiniere ich die Wirbel mit atmosphärischen Daten, d.h. Wind, Wolkeneigenschaften und Regenwahrscheinlichkeiten und -raten. Es zeigt sich, dass die Meeresoberflächentemperaturanomalien von Wirbeln in den atmosphärischen Grössen Anomalien von einigen Prozent verursachen. Das lokale Musster des Einflusses von Wirbeln auf die Atmosphäre ist mit einem Mechanismus konsistent, bei dem die Wirbel die Atmosphäre durch oberflächennahe Stabilitätsänderungen beeinflussen und demnach die Turbulenz in der atmosphärischen Grenzschicht ändern.

Contents

1. Introduction

1.1. Ocean Dynamics, Turbulence and the Dominance of Mesoscale Eddies

The dynamics of the ocean and the atmosphere are driven by a spatially inhomogeneous energy supply. At a constant global mean temperature, the Earth system absorbs as much energy from the sun, in the form of shortwave radiation, as it emits back to space in the form of longwave radiation (Figure 1.1a). However, radiative energy is not balanced locally: tropical and subtropical (low) latitudes feature an energy surplus while polar (high) latitudes feature an energy deficit, which is mainly due to the decreasing angle of the sun rays relative to Earth's surface with increasing latitude. The meridional temperature gradient resulting from the spatial energy imbalance triggers air and water to move and transport energy from low to high latitudes, i.e. it triggers winds and currents (Figure 1.1b).

The direct forcings of the ocean motion are momentum input by wind stress and buoyancy changes. Surface currents but also the deep reaching Antarctic Circumpolar Current (ACC) are mainly driven by winds. Winds can cause vertical water motion, too, which is due to Ekman pumping and suction: vertical motion is forced due to mass conservation either where water diverges or converges at the ocean surface due to spatially inhomogeneous wind forcing, or where wind causes water to move perpendicular to the coast. Buoyancy changes arise from the shortwave energy input by the sun, from air-sea fluxes, sea-ice formation and melting, and from riverine input. They cause vertical water motion as water tends to move up or down in the water column until it reaches a level of waters of the same density. For instance deep water is formed this way at the ocean surface in the north Atlantic and in the Southern Ocean (SO). In these regions, water becomes locally very dense at the surface due to atmospheric cooling and brine rejection. This causes it to "plummet" to great depths. The interplay of wind and buoyancy forcing eventually drives the global ocean circulation.

The ocean circulation and its variability span several magnitudes of spatial and temporal scales. The spatial scales reach from less than 1 mm to several 1000 km, which is for instance the scale of immense gyres expanding across the width of ocean basins. The temporal scales reach from seconds to more than 1000 years, where the latter is the time scale since the deep ocean has last been in contact with the atmosphere. Turbulent motions in the ocean cover much of the range of temporal and spatial scales. With the relatively low viscosity of water, small disturbances to the flow are not heavily damped but "free to grow", i.e. turbulence may develop.

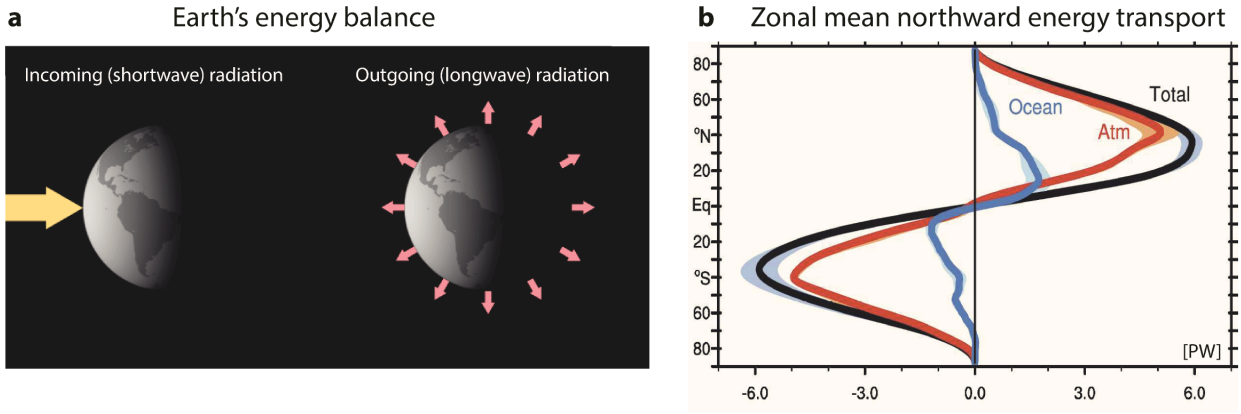

***Figure 1.1.: Earth's heat balance and polar heat transport**; **a** Incoming solar radiation is balanced by outgoing thermal radiation in a steady state, i.e. for a constant global mean temperature; Earth is a sphere and thus the angle of sun rays being perpendicular in (sub)tropics (low latitudes) decrease towards the poles (high latitudes), resulting in high latitudes receiving less energy from the sun per square meter than low latitudes; the outgoing radiation is more homogeneously distributed; thus, high latitudes have a deficit of energy on average and low latitudes a surplus; a poleward energy transport is necessary to prevent low latitudes heating up and high latitudes to cool down (Figure from http://earthobservatory.nasa.gov); **b** The atmosphere and the ocean provide the necessary heat transport; the ocean is crucial for transporting heat out of the tropics whereas the atmosphere is dominant in the heat transport at mid- and high latitudes (Trenberth and Caron, 2001; Wunsch, 2005; Czaja and Marshall, 2006) (Figure from Fasullo and Trenberth, 2008).*

Most of the energy of the turbulent scales is concentrated at the mesoscale, i.e. at features of a few tens to a few hundreds of kilometers. This dominance of the mesoscale was found from observations locally from ship-based measurements and mooring data already in the seventies of the 20^{th} century (Koshlyakov and Monin, 1978). However, the omnipresence of mesoscale features in the ocean became apparent only about two decades ago with the onset of satellite observations resolving features of scales of the order of 100 km (e.g. Stammer, 1997, see Figure 1.2). These data presented an unprecedented observational coverage of the global ocean and triggered extensive research on oceanic mesoscale variability (see reviews by Robinson, 2010; Morrow and Le Traon, 2012).

One of the outcomes of this research has been that the globally ubiquitous non-stationary features already visible in lower resolution satellite data of the seventies and eighties of the 20^{th} century were not linear Rossby waves but mesoscale eddies (Chelton et al., 2007). The latter are coherent circular vortices which populate the worlds oceans at any moment by the thousands (Chelton et al., 2011b) and dominate total ocean kinetic energy (Ferrari and Wunsch, 2009).

To provide background information on this thesis and illustrate where it fits in the current field of research, I will begin with a description of ocean mesoscale eddies, methods of investigating them, and their role in the ocean. Focusing thereafter on the SO, I will highlight its global prominence and the function of eddies for SO dynamics. From this follows the knowledge gap this work will fill and the method applied to achieve this.

1.2. Ocean Mesoscale Eddies

1.2.1. Methods of Examination of Mesoscale Eddies

Eddies are turbulent features and as such are characterized by fluctuations in time and space. Thus, they and their impacts are frequently investigated as deviations from the temporal mean at geographical locations. One measure is the eddy kinetic energy (EKE) which is based on departures of velocities from the mean. Another the heat transport associated with eddies which can be estimated based on velocity fluctuations correlated with associated temperature fluctuations. Similarly, the eddies' diffusivities can be calculated. Further, Fu (2009) derived global propagation characteristics of

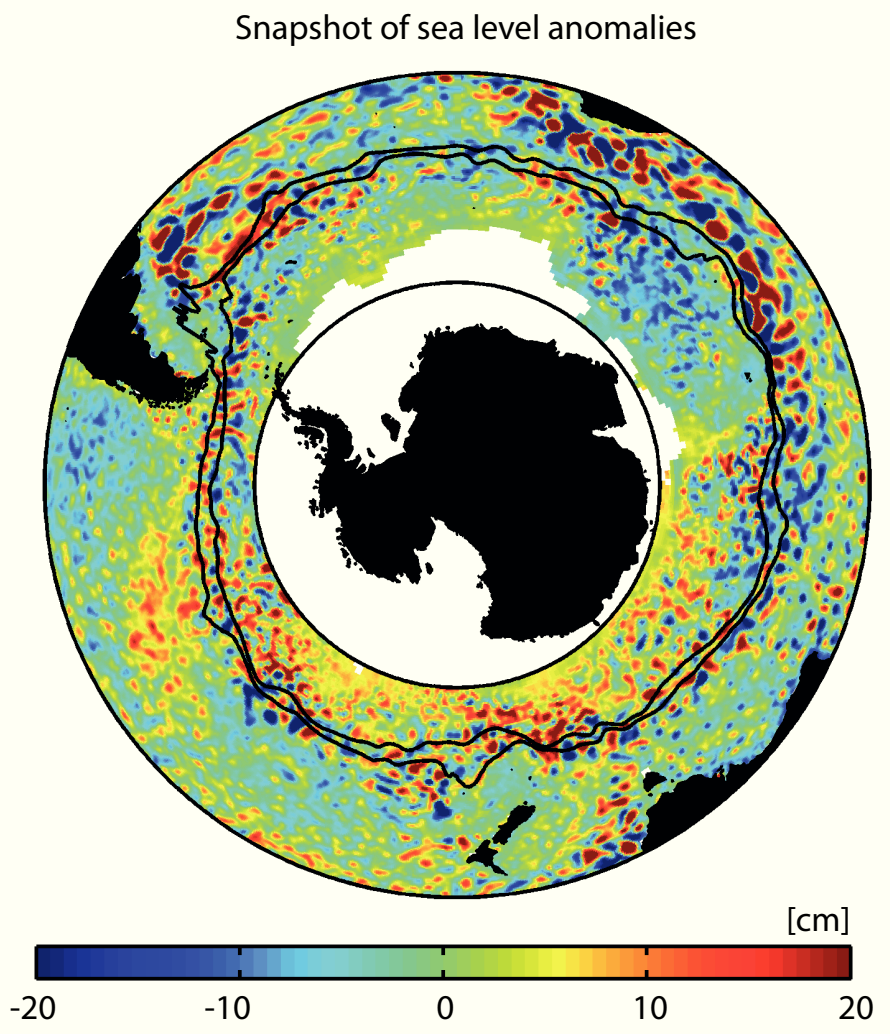

Figure 1.2.: Satellite derived sea level anomalies *for the week centered at 6th November 2002; the imprint in sea level of many of the features of ocean dynamics arises from their density anomalies due to temperature and salt anomalies, which in turn cause a flow; various spatial scales are identifiable in the sea level anomalies, however the mesoscale is clearly dominant; only the domain considered in this study is shown, i.e. 30°S to 65°S; white areas within the domain mark missing values due to sea-ice, and the two black lines denote the major branches of the ACC (see Section 1.3).*

eddies with a maximum cross correlation analysis based on sea level anomalies (*SLA*). All these approaches are Eulerian where the interest is in how eddies and their effects are expressed at certain locations in space, based on fluctuation of flow properties.
Another approach, rather than picking a certain position in space, is to investigate eddies from a position which is fixed relative to the feature itself, i.e. a Lagrangian approach. As eddies are inherently not stationary, the observer migrates with an eddy at a fixed location relative to the center of the respective eddy, over the time the eddy lives. Complementary information can be retrieved with this approach: eddies can be investigated as coherent features and one can examine for instance their shape, evolution over their life time and non-local transport effects.
A substantial spatial and temporal coverage of observational data is necessary to fully characterize eddies and their life cycle. Historically, in-situ observations from research vessels and moorings gave impressions on oceanic eddies. Yet, these data provided snapshots of eddies and barely revelations on their mean characteristics. Besides, it is not trivial to separate turbulent phenomena from characteristics of the mean flow from a mere snapshot. As eddies are typically traceable at the ocean surface, satellite data are well suited for the purpose of an extensive characterization, specifically maps of *SLA*. Covering the globe, they exist in a temporal (weekly) as well as a spatial resolution (considerably higher than one degree of longitude/latitude) which are sufficient to resolve a substantial fraction of mesoscale eddies while they move. In addition, the upper two kilometers of the ocean have been sampled by thousands of coexistent floats since the beginning of the 21^{st} century (*Argo* network). Existing *Argo* floats measure about 100,000 profiles of temperature and salinity per year. These data represent invaluable information on the subsurface ocean and can be combined with the satellite based ocean surface information on eddies.

1.2.2. Features and Dynamics of Mesoscale Eddies

Numerous regional studies have emerged in the last couple of years, taking a Lagrangian approach based on satellite observations and a large number of eddies, e.g for the Mediterranean (Isern-Fontanet et al., 2003, 2006), various areas in the Pacific (Itoh and Yasuda, 2010; Henson, 2008; Chaigneau et al., 2008), the eastern boundary upwelling systems (Chaigneau et al., 2009), Agulhas Rings (e.g. Dencausse et al., 2010) and eddies in the Tasman sea (Everett et al., 2012, based on eddies detected by Chelton et al., 2011b). Chelton et al. (2007, 2011b) are the only global studies applying this method and represent a thorough inventory and a wealth of information on long-lived eddies. Some of the regional studies combined the satellite data with in-situ observations from *Argo* floats.
We have obtained a fairly detailed picture of the main features of ocean eddies from these studies. The temporal and spatial dimensions are the following: ocean eddies have life spans of weeks to months, although, occasionally of more than a year. Their horizontal and their vertical extents are $O(100)$ km and $O(1)$ km, respectively. With the resulting small aspect ratio (ratio of vertical to horizontal length scales), they are basically two dimensional features. The reason being that mesoscale eddies are bound

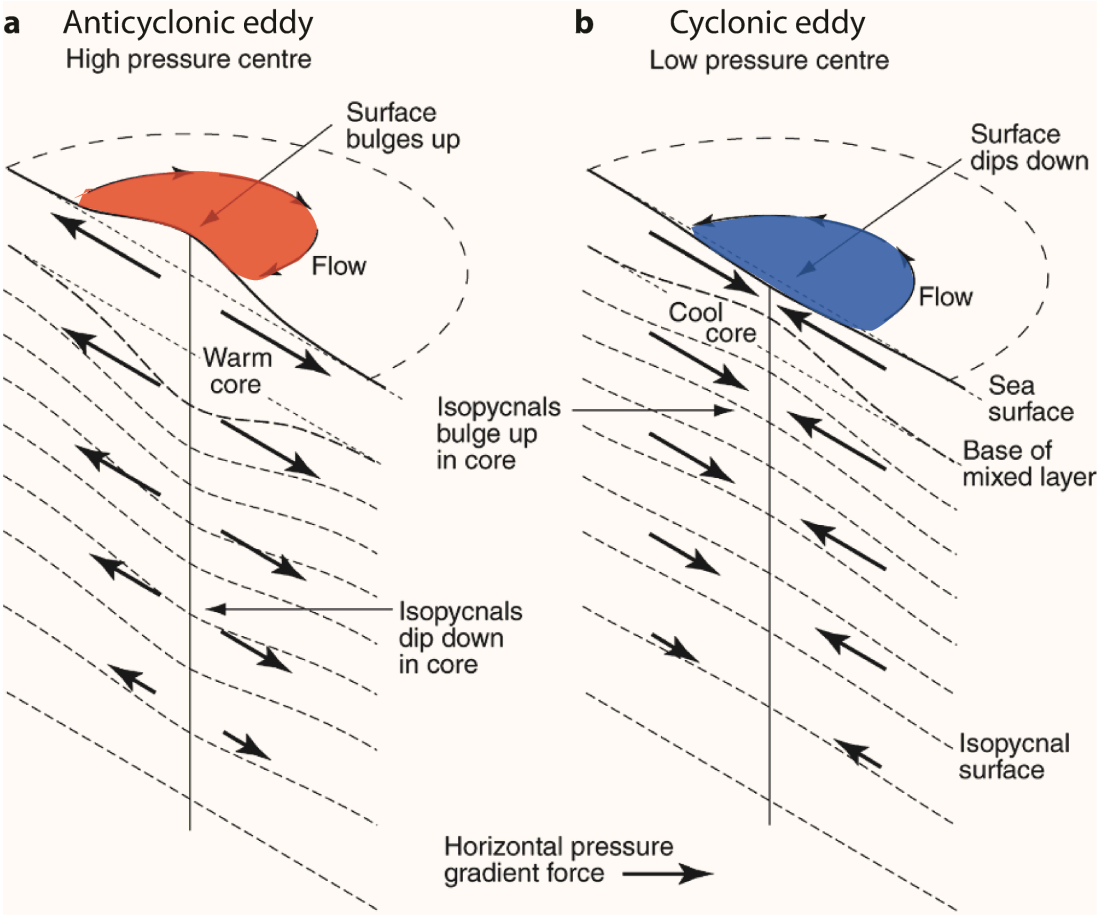

Figure 1.3.: Sketch of three dimensional structure of an anticyclonic (red) and a cyclonic (blue) eddy in the northern hemisphere*, the sense of rotation is opposite in the southern hemisphere, i. e. it is clockwise for cyclones and anticlockwise for anticyclones (Figure from Robinson, 2010).*

by the Earth's rotation as well as ocean stratification.
Eddies are characterized by a density anomaly which is typically surface intensified. The density anomaly results in an anomalous sea level (Figure 1.3, see also Figure 1.2), which can be both, positive or negative. The *SLA* ranges between centimeters and several tenths of centimeters and triggers lateral motion of water. The motion is initiated by the horizontal pressure gradient arising from the *SLA* on the one hand, and constrained by Earth's rotation (Coriolis force) on the other hand, i.e. the motion is geostrophic. The closed *SLA* contours of eddies are closed streamlines for geostrophic flow, likewise. The swirl velocity of eddies is cyclonic for negative *SLA* and anticyclonic for positive ones, and $O(10)$ cm s^{-1}.

The positive density anomaly related to an anticyclonic eddy causes the doming of the *SLA* and a depression of the isopycnals at depths the same time (the opposite for cyclones, see Figure 1.3). This causes a flow counteracting the barotropic geostrophic flow initiated by the *SLA* anomaly. Thus, the geostrophic velocities are not constant with depth, i.e. eddies are baroclinic. However, there may still be substantial velocities even at the ocean bottom related to an eddy detectable at the surface (Adams et al., 2011; Nikurashin et al., 2012). This may lead to energy dissipation when interaction

with small-scale bottom topographical features takes place. Also in-situ studies found vertical extensions of eddies of several thousand meters. Hence, even though most distinct at the surface, eddies may extend well below the thermocline.
The propagation speeds of eddies are similar to the ones of linear baroclinic Rossby waves, even though slightly slower at low latitudes. They are westward and $O(1)$ cm s^{-1} or $O(10)$ km $week^{-1}$ at mid- and high latitudes. Obviously at these speeds, eddies are subject to advection by mean currents, such as boundary current systems and the intense ACC, which exhibit flows of $O(10)$ cm s^{-1} in places on average. In addition to the westward propagation, in both hemispheres cyclonic and anticyclonic eddies tend to propagate inherently pole- and equatorward, respectively.
Even though the characteristics of ocean mesoscale eddies as found from previous studies are in principle also true for SO eddies, no regional study exists with a focus on the characteristics of SO eddies taking a Lagrangian approach.

1.2.3. Effects of Mesoscale Eddies

Ocean mesoscale eddies are crucial not only for ocean dynamics, but also for ocean biogeochemistry and air-sea exchange and subsequently for the Earth system. First of all, they are part of the momentum balance. They transfer momentum from available energy stored in the stratification to dissipative scales, but may also transfer kinetic energy back to larger scales as they interact with the mean flow. (Ferrari and Wunsch, 2009; Thompson and Sallée, 2012)
Further, eddies cause fluxes of active and passive tracers. The former are tracers which have an effect on ocean dynamics, for instance temperature which then imprints on the water density. Eddies can thus impact stratification and water mass formation. The latter, passive tracers, do not feed back directly on ocean dynamics, they are passively advected. Biogeochemical tracers for instance are considered passive, such as carbon.
Eddies redistribute tracers via different ways. On the one hand, they act diffusively on gradients of tracers, referred to as *turbulent diffusion* (e.g. Rhines and Young, 1983): their stirring deforms and hence increases tracer gradients facilitating in turn molecular diffusion. As the term *diffusion* indicates, *turbulent diffusion* acts by definition downgradient. Hence, eddies contribute to the homogenization of tracer fields. On the other hand, eddies act advective as they slantwise exchange water across a front when they form from baroclinic instability (*bolus velocity*, Gent and McWilliams, 1990), as they may trap water of the location of their origin in their core and carry it along while moving around (Flierl, 1981), and as they rotate (Marshall and Shutts, 1981). Advection causes tracer transports which are not necessarily downgradient.
Additional impacts of eddies exist which are related to them interacting with other components of the Earth system: their coupling with biology and with the overlying air. These have received increasing attention in the last couple of years, last but not least due to the increasing availability of observational (satellite) data.
Firstly, eddies may impact ocean biology (Figure 1.4a). By locally changing the physical conditions through their dynamics, eddies may directly and indirectly affect reactive tracers, such as phytoplankton. They may relieve or amplify environmental factors limiting phytoplankton growth (e.g. nutrients and light, Lévy, 2008). Moreover, they can

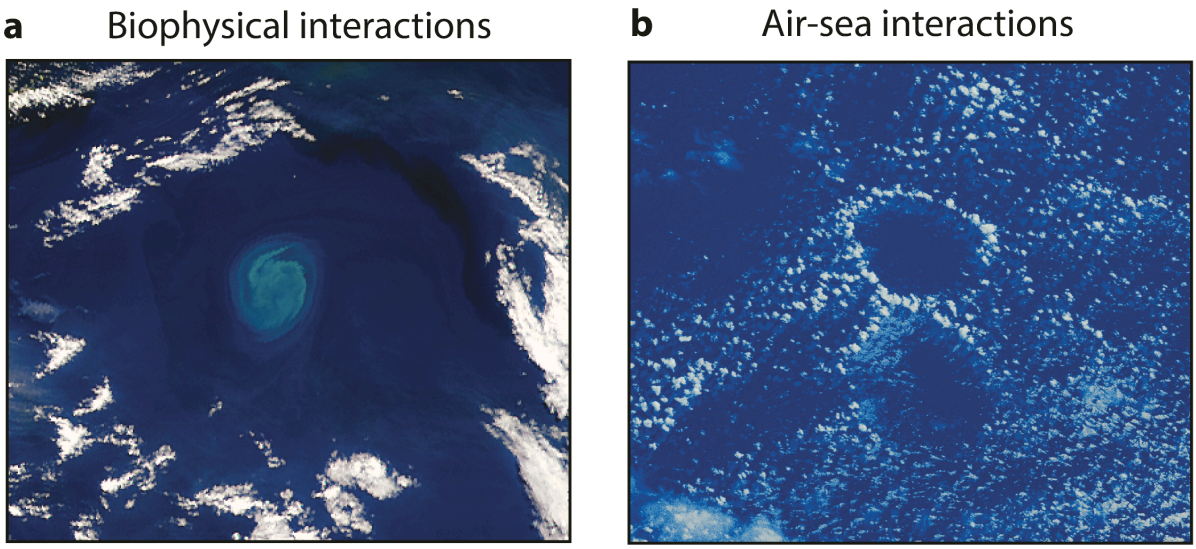

Figure 1.4.: Potential effects of eddies on their environment*; panel* **a** *shows an eddy in the Southern Ocean in the Drake Passage, a bit less than 100 km in size, which is traced by enhanced chlorophyll-a (*CHL*) values; in this situation an individual eddy apparently impacts* CHL*, i.e. biology; however this is a selected situation which may not be representative of how eddies impact* CHL *in the long-term mean; the picture is taken from a satellite (SeaWIFS) on March 4th 1998 (from http://visibleearth.nasa.gov); panel* **b** *is a photograph taken from a space shuttle which shows cloud cover over the ocean: the circular cloud-free areas potentially have arisen from cool sea surface temperatures of (sub)mesoscale eddies with diameters of O(10)km; the image was taken January 15th 1986 at an altitude of approximately 330 km above the South Atlantic (image STS61C-49-31 from http://eol.jsc.nasa.gov, courtesy of the Image Science & Analysis Laboratory, NASA Johnson Space Center).*

impact phytoplankton competition and grazing pressure, as they can provide ecological niches. The latter is the case as high vorticity gradients at the eddy's edge can constitute transport barriers (e.g. Bracco et al., 2000). The eddies' influence may propagate to higher trophic levels in the food web, as for instance grey-headed albatrosses have been detected to forage specific eddies in the SO preferably (Nel et al., 2001). Also this influence of eddies may feed back on biogeochemistry via the effect on nutrient usage, recycling and export. For instance, eddies have been found to impact the carbon pumps (Omta et al., 2007; Moutin et al., 2012), and thus the vertical gradients of biogeochemical tracers.

Secondly, the expression of eddies at the ocean surface e.g. as sea surface temperature (*SST*) anomalies leads to anomalous air-sea fluxes. This way, eddies may impact the overlying atmosphere (Figure 1.4b), and concurrently may themselves be impacted by the changes they triggered in the atmosphere (Small et al., 2008; Chelton and Xie, 2010; Shuckburgh et al., 2011). For instance *SST* fronts affect near-surface winds, and the winds may in turn affect surface ocean mixing and Ekman pumping. Anomalous air-sea fluxes associated with eddies potentially not only include heat and fresh water, but possibly also biogeochemical tracers, such as carbon dioxide.

Despite the increasing interest in these two issues, only a few studies have systemat-

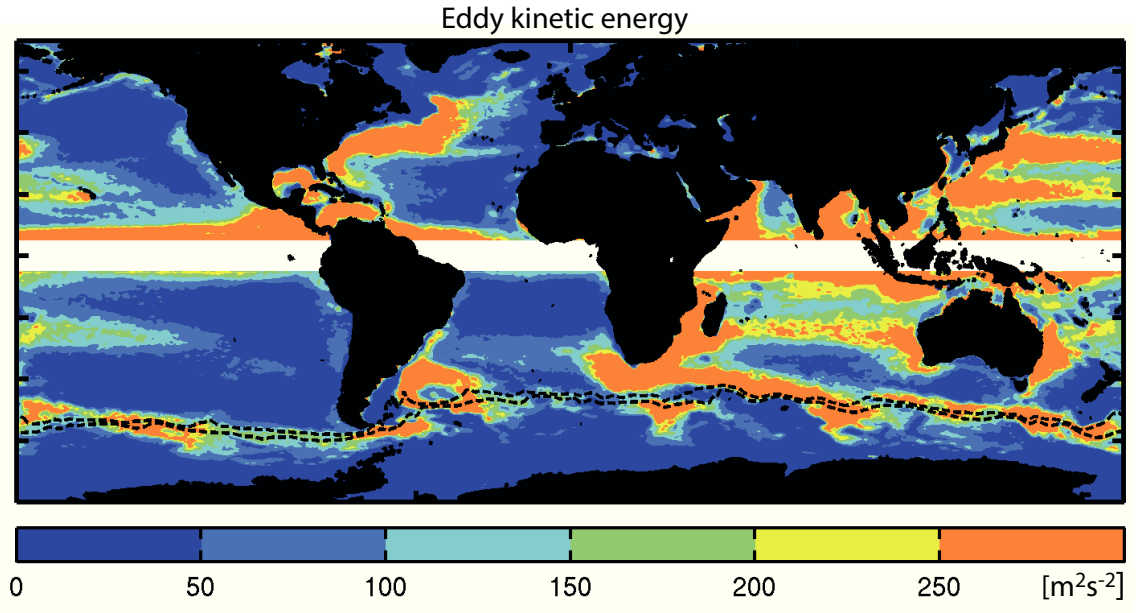

Figure 1.5.: Global mean eddy kinetic energy *based on weekly observations of SLA from satellite altimetry between 1997 and 2010 ; values near the equator are missing due to velocities being derived based on geostrophy, the latter is not valid at very low latitudes where the Coriolis parameter is small; dashed black lines denote the major branches of the ACC. EKE is a measure for mesoscale eddy activity which is frequently used, however it contains other turbulent geostrophic features next to eddies, such as jets.*

ically investigated the eddies' influence on biology and the atmosphere over a larger domain and with sufficient data to conclude on long-term impacts (e.g. Park et al., 2006; Siegel et al., 2011; Chelton et al., 2011a). No previous study has focused on the long-term mean relations of eddies, biology and the atmosphere in the SO.

1.2.4. Occurrence of Mesoscale Eddies

Mesoscale eddies are present throughout the global ocean as mentioned in Section 1.1. However, clear hot spots of frequent and intense eddies exist which are visible in eddy kinetic energy (EKE, Figure 1.5). The uneven distribution of eddies must arise from a combination of an inhomogeneous distribution of generation and dissipation mechanisms of eddies, and the eddies' propagation pattern and evolution while they move.

Clearly a large part of the spatial variability of EKE results from numerous and pronounced eddies developing from ocean currents. Currents become frequently instable and shed eddies, due to baroclinic or barotropic instability. Smith (2007) found the majority of the ocean to be baroclinically unstable. Indeed, the main formation mechanism of ocean eddies is thought to be baroclinic instability (Gill et al., 1974). Baroclinic instability arises from potential energy stored in the ocean stratification being released into kinetic energy, i.e. less dense water (typically warmer and fresher) sliding over denser one (typically colder and more saline). Barotropic instability refers to instabilities of horizontally sheared currents. Atmospheric forcing (stochastic wind or buoyancy forcing) is thought to play less of a role globally but may be important

locally.
The major pathways of the mesoscale energy to dissipation are still not clear (Ferrari and Wunsch, 2009), and thus neither is the contribution of localized dissipation to the spatial pattern of EKE. In principle, to dissipate the energy of geostrophic eddies, it must be transfered to smaller scales where viscous friction can be effective. The mechanism for this to happen is not straightforward as the energy transfer from the first baroclinic and barotropic modes appears to be inverse, i.e. back to larger-scale motions (Charney, 1971; Ferrari and Wunsch, 2009). Possible candidates for the dissipation of the eddy-energy are interactions with the ocean bottom, internal waves and surface ocean submesoscale frontogenesis related to eddies (Ferrari and Wunsch, 2009), with the former mechanism emerging to be the major candidate, at least in the SO (Garabato et al., 2004; Ferrari and Wunsch, 2009; Nikurashin et al., 2012).
The intrinsic propagation of eddies may make a contribution to the spatial pattern of EKE, even though not a tremendous one. For instance the zonal bands of increased EKE in the southern Atlantic and Indian-Ocean as well as in the north Pacific could be caused by very long-lived westward propagating eddies (Chelton et al., 2007, 2011b; Liu et al., 2012).

1.3. Eddies in the Southern Ocean

1.3.1. Southern Ocean Dynamics and its Global Significance

The SO is of global importance for ocean dynamics and biogeochemistry: it is a unique area of water mass modification and formation where on the one hand, water of the different ocean basins is mixed laterally due to the ACC. On the other hand, the SO is only weakly stratified which allows for a vertical exchange between the deep and the surface ocean. Last but not least the global importance of the SO (here south of 30°S) arises due to sheer size: it constitutes about 30% of the area of the global ocean.
A map of the SO with major currents is shown in Figure 1.6. The domain is centered at the southern hemispheric, midlatitude, westerly wind belt where the highest average winds on Earth occur. These winds drive the ACC which is not blocked by latitudinal barriers and thus circles the globe, with a volume transport of about 130 Sverdrup ($\mathrm{Sv} = 10^6\ \mathrm{m}^3\ \mathrm{s}^{-1}$) it is the largest ocean current. The ACC shows strong meridional gradients of temperature and salinity which are concentrated in fronts. The major fronts are the Subantarctic and the Polar Fronts (SAF and PF). Combined, they hold most of the transport of the ACC. As indicated in Figure 1.6 a, the ACC is strongly steered by topography. At topographic obstacles, it is squeezed whereas it broadens in the deep basins downstream of the same obstacles.

The dynamics in the northern part of the domain (north of the ACC and south of 30°S) are determined by the subtropical gyres including the boundary currents. Areas of strong interaction exist between the boundary currents and the ACC, such as the area of the Agulhas Return Current and the Brasil-Malvinas Confluence region, south of Africa and east of South America, respectively. These are areas of intense eddy generation as visible in Figure 1.5.

a Map of Surface currents and topographical features in the Southern Ocean

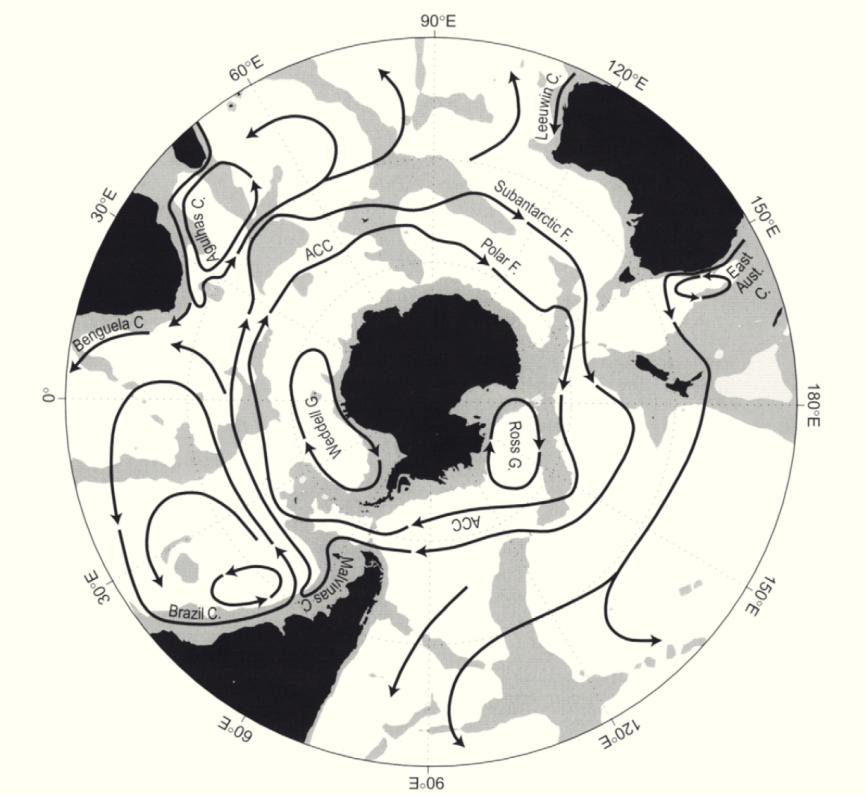

b Transect across the Southern Ocean

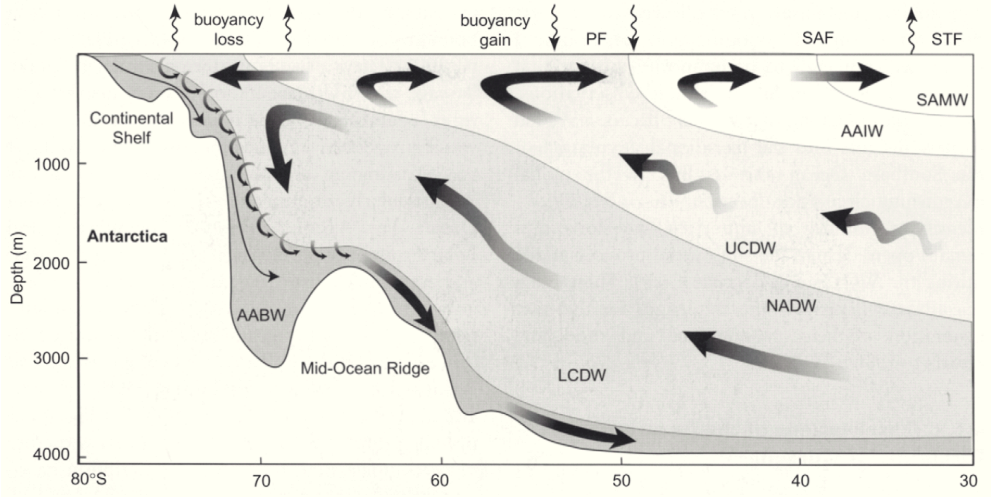

***Figure 1.6.: Sketch of the dynamics of the Soutern Ocean (SO)**; **a** major currents in the southern hemisphere oceans south of 20° S, depths shallower than 3500 m are shaded; the two major cores of the Antarctic Circumpolar Current are the Subantarctic and the Polar Fronts; the ACC frequently interacts with boundary current systems at its northern flank; abbreviations used are F for front, C for Current and G for gyre; **b** meridional overturning circulation in the SO; an upper cell is formed primarily by northward Ekman transport beneath the strong westerly winds and southward eddy transport in the UCDW layer; a lower cell is driven primarily by formation of dense AABW near the Antarctic continent; abbreviations used are PF for Polar Front; SAF for Subantarctic Front; STF for Subtropical Front; AAIW for Antarctic Intermediate Water; UCDW for Upper Circumpolar Deep Water; NADW for North Atlantic Deep Water for , Lower Circumpolar Deep Water; and AABW for Antarctic Bottom Water (from Rintoul et al., 2001).*

A schematic of the cross-section of the SO is depicted in Figure 1.6b. The SO is special in that it is only weakly stratified. Isolines of the same density, referred to as isopycnals, are steeply tilted and outcrop at the ocean surface. This makes a "communication" of deep and surface waters possible.
The westerly winds cause a northward Ekman transport at the ocean surface. The divergent surface transport south of the PF leads to upwelling. The upwelled water origins from great depths due to the weak stratification. A meridional circulation follows which can be separated into two cells. The lower cell is formed by a fraction of the upwelled water moving southward in the Antarctic Zone where Antarctic Bottom Water is formed. The other part of the upwelled water is transported northward where it contributes to the formation of Antarctic Intermediate Water and Subantartic Mode Water. This happens in the Polar Frontal Zone (in between the PF and the SAF) and the Subantartic Zone (north of the SAF and south of the Subtropical Front, not shown here).
Formation of deep water is crucial for the ventilation of the deep ocean, and the intermediate waters transport waters northward into lower latitudes. The Lower and Upper Circumpolar Deep Waters are the main water masses of the ACC which result from the incorporation and mixing of water masses of Pacific, Atlantic and Indian-Ocean waters. As such the SO constitutes a vital part of the global ocean circulation.

1.3.2. The Setting for Biology in the Southern Ocean

Phytoplankton is responsible for about half of the global primary production (Field, 1998). It provides the nourishment for virtually everything existing in the ocean, shapes the biogeochemical composition of the ocean and due to its photosynthesizing, is an essential part of the global carbon cycle (Falkowski, 2012).
The SO forms a special environment with respect to biology as most of this region is a so-called high nutrient low chlorophyll region (HNLC). The upwelled deep waters are rich in nutrients. Biology is not able catch up with this nutrient supply and the leftovers are transported with the Antarctic Intermediate Water and Subantarctic Mode Water to intermediate depths supplying the low latitudes with nutrients (Sarmiento et al., 2004). Phytoplankton is mainly iron and light limited in the Antarctic Zone south of the PF. North of the PF, silicate limitation begins with continuing light limitation as mixed layers depths are with more than 500 m locally very deep, due to strong winds in winter. Nitrate and phosphate limitation starts to occur only north of the SAF.
Biological activity in the HNLC areas occurs mainly as intensive spring blooms in the Subantartic and Polar Frontal Zones, in the Antarctic Zone biological activity starts with the retreat of the sea-ice which covers the area up to about 50-60°S in austral winter. North of the SAF relatively high phytoplankton occurrence in the coastal water contrasts very small occurrence in the open ocean. Phytoplankton is in general heavily nitrate limited within the southern subtropical gyres, as it is typical for the low latitudes.

1.3.3. The Southern Ocean and Climate Change

The SO appears to be sensitive to climate change with major changes related to winds and heat and freshwater fluxes. An increase and poleward shift of the westerlies in the southern hemisphere have been detected (see e.g. Thompson and Solomon 2002; Mayewski 2009). Also, a temperature increase has been observed in the upper ocean layers (penetration until depths of about 1000 m) of the SO and a freshening which is not restricted to the upper ocean layers but extends to Antarctic Bottom Water (e.g. Gille 2008; Böning et al. 2008; Roemmich and Gilson 2009; Turner and Overland 2009). These changes are expected to persist and intensify with climate change progressing (Thompson et al., 2011).
The SO dominates the ocean uptake of excess heat energy due to radiative forcing and is responsible for about half of the the oceanic uptake of anthropogenic carbon. Because of its connection of the surface and the deep ocean, it has the potential to be central with respect to (positive) carbon-climate feedbacks. Indeed, it appears that the SO presently turns from a net sink of the long-lived greenhouse gas CO_2[1] to a net source[2] (Takahashi et al., 2012). It is essential for us to better understand this region and how it might respond to climate change.

1.3.4. Unresolved Issues on Eddies in the Southern Ocean

The SO is characterized by a pronounced zonal band of high EKE (Figure 1.5) and by hot spots of eddy activity where the boundary currents and the ACC interact. Eddies are an integral part of the SO dynamics and as such are of importance for the aforementioned aspects, i.e. SO biology and uncertainties in the context of climate change. Their vital role in the SO has been pointed in many studies based on observations and numerical ocean models (Rintoul et al. 2001; Naveira Garabato et al. 2004; Fyfe and Saenko 2006; Hallberg and Gnanadesikan 2006; Mignone et al. 2006; Hogg and Blundell 2006; Zickfeld et al. 2007; Lachkar et al. 2007; Böning et al. 2008; Hogg et al. 2008; Thompson 2008; Gillett et al. 2008; Morrison and Hogg 2013). The most frequently mentioned effects of eddies in this region are the following:
Firstly, they balance the momentum input provided by the intensive westerly winds by transporting it downwards[3] towards the ocean bottom where it is dissipated. Secondly, they provide the necessary meridional transport of tracers as the zonal flow of the ACC generally acts as a barrier towards meridional transports[4]. Thereby the northward Ekman transport is partly compensated for by southward eddy-fluxes. The extent of this compensation is crucial for instance for the behavior of the SO as CO_2 sink, or source. With regard to climate change, shifts in wind magnitude and pattern are of particular importance for eddies. Winds and subsequent modifications of the ACC in combination with the tilt of the outcropping isopycnals may impact the eddy field. It is still unclear

[1] Due to the uptake of a large fraction of anthropogenic CO_2
[2] Due to the changing winds bringing up deep carbon-rich waters at a higher rate.
[3] Via interfacial form stress, i.e. work done on isopycnal surfaces due to horizontal pressure gradients.
[4] The mean deviations of the ACC from the zonal flow (referred to as standing eddies) are at least as important for meridional heat fluxes as the vortex-like eddies ("transient" eddies) we focus on and refer to as eddies here (e.g. Dufour et al., 2012)

how the latter will respond to these changes resulting from climate change. An *eddy saturation state* may exist, where increased winds do not lead to an increase of the transport of the ACC but to an increase of eddy activity (e.g. Hallberg and Gnanadesikan 2001; Hogg and Blundell 2006). The resulting southward eddy flux would then tend to flatten isopycnals. This again would have an opposing effect to the increased (due to the increased winds) northward Ekman transport, labeled accordingly *eddy compensation*. In this scenario eddies would prevent an increased outgassing of CO_2 due to an intensified upwelling of deep carbon-rich waters. However, Meredith et al. (2012) and Morrison and Hogg (2013) find a decoupling of *eddy saturation* and *eddy compensation* more likely. Indeed, EKE did scale approximately linearly with winds in the high resolution modeling study of an idealized SO by Morrison and Hogg (2013). And so did the northward Ekman transport. In contrast the latter was not compensated for by southward eddy induced transports. The idea put forward by these studies is that the maximum of the Ekman transport and the eddy transport happen at different depths. Thus, the concept of *eddy compensation* might not hold.
Next to these unresolved issues, potential impacts of eddies exist which have not been investigated systematically and which relate to their role in the coupling of components of the Earth system, two of which I mention here.
On the one hand SO eddies have been found to be related to biology, and not only at the lowest trophic level. Perissinotto et al. (2000) for example see a relationship of eddy activity and primary productivity in their in-situ measurements related to the Prince Edward Islands, Kahru et al. (2007) and Gomez-Enri et al. (2007) show the the correlation of eddies with chlorophyll (CHL) and thus biological activity in the SO based on satellite data in and downstream of the Drake Passage. Grey-headed albatross was detected to forage specific eddies in the Southern Ocean preferably (Nel et al., 2001) and Bailleul et al. (2010) found southern elephant seals to forage preferably eddy edges. Thus, an association of eddies and phytoplankton and higher trophic levels is expected, however it is unclear to which extent it exists in the whole of the SO.
On the other hand, with the SO being an area of strong winds and large SST gradients, continuously large air-sea imbalances exist, and hence intense air-sea fluxes which are expected to potentially impact on the atmosphere (as it possibly happens in Figure 1.4b). The "Gulf Stream Rain Band" associated with the narrow sea surface temperature front of the Gulf Stream has been known for a long time Hobbs (1987).The Agulhas Extension has been the focus of some studies investigating this effect (White and Annis, 2003; O'Neill et al., 2005; Liu et al., 2007). It can be anticipated that mesoscale eddies, constituting circular mesoscale SST fronts due to their SST anomalies may have an impact on the overlying air. A modification of winds and cloud fraction by Gulf Stream Rings was indeed found by Park et al. (2006). An investigation of the association of oceanic eddies and atmospheric anomalies is intriguing in an area of highly variable weather such as the SO.
These aspects show that it is vital to increase our knowledge on dynamics and features of SO eddies, and further how they interact with their environment. A better process understanding of SO eddies contributes to a better understanding of the SO as a whole, and hence for instance may serve as basis for an improvement of the skill of climate models which are used for projections of the future of the Earth system.

1.4. Main Objectives

Based on observations I aim to contribute to a better understanding of SO eddies and their impacts with this thesis. SO eddies have not been a focus of a Lagrangian study. Hence first of all, I closely examine SO eddies themselves and retrieve their characteristics. Specifically, I am interested in

- **Where eddies occur, and how frequently.**
- **The eddies' average features, such as their three dimensional structure, where they originate and dissipate, and their variability.**

Secondly, again based on observations, I will investigate the impact of eddies on their environment, an issue which has not been much investigated systematically before. My questions are the following:

- **Is there a relationship between eddies and low trophic levels of biology (phytoplankton)?** I will use *CHL* as a proxy for phytoplankton biomass. Eddies may impact this biomass in several ways: by lateral transport to another environment, vertical transport changing the nutrient content and light exposure as well as trapping, which may lead to spatial segregation and ecological niches. Therefore, I will try to narrow down the causes of the relation I find for instance by analyzing the spatial pattern of the imprint of eddies on *CHL*.
- **Do ocean eddies modify the overlying atmosphere due to their surface properties?** The main reason to anticipate this modification is the *SST* anomaly typically related to ocean eddies, resulting in an air-sea disequilibrium and thus anomalous air-sea fluxes. The latter then may evoke a response in the atmosphere which might become apparent in atmospheric quantities, such as winds, cloud properties and rainfall.

1.5. Approach to Investigate Eddies and Their Impacts

As good data coverage is needed for the above objectives, remote sensing data offering sufficient spatial and temporal coverage form the basis for the majority of this thesis. These data are complemented by in-situ data, specifically *Argo* floats.
I follow a Lagrangian approach where I trace individual eddies during their life cycle. This way, I am able to characterize the mean properties of eddies, and examine how they evolve and where they move to. Simultaneously, I can investigate the state/condition of their nearby environment, thereby estimating the eddies' impacts on the same.
Due to the many (satellite) observations existing by now, it is possible to retrieve statistically significant results even for highly variably data, such as *CHL*.

1.6. Thesis Outline

This thesis is structured as follows: I will present the method to detect and track ocean mesoscale eddies based on *SLA* in Chapter 2, followed by an analysis of the eddies

themselves. I describe my results on the effect of eddies on biology and the lower atmosphere in the Chapter 3 and 4 and conclude with a summary and an outlook in Chapter 5.

2. Southern Ocean Eddy Phenomenology

In preparation for Journal of Geophysical Research – Oceans.

Mesoscale eddies are ubiquitous features in the global ocean, yet their characteristics and mean effects on the ocean circulation as well as tracer distributions are not thoroughly understood. The Southern Ocean (SO) is a vast area of intense eddy activity and crucial for the global ocean circulation at the same time. Here we provide a phenomenology of SO eddies using a Lagrangian approach. We identified and tracked a large number of individual eddies (>1,000,000) with an automated procedure based on satellite observations of sea level anomalies (*SLA*). The eddies' characteristics were deduced from satellite observations in combination with in-situ observations of profiling floats.
We found the Antarctic Circumpolar Current (ACC) and the western boundary currents to be covered by eddy-cores more than 30% of the time. These dynamic areas are also hot spots of variability of eddy occurrence and properties, and they are typical birth places as well as graveyards of long-lived eddies (specifically the ACC). Regions of polarity dominance such as the cyclone-dominated northern flank of the ACC and the anticyclone dominated southern subtropical gyres exist. We also investigated the mean three dimensional structure of SO eddies. By combining the subsurface information with our derived eddy numbers, we calculated an estimate of the heat and salt transports of transient eddies associated with trapped fluid in their cores across the Polar Front (PF), i.e. one of the major branches of the ACC. With O(-10^{-2}) PW/O(-10^{5}) kg s^{-1}, the eddies contribute $O(10^{1})$%/$O(1)$% of the transport necessary to compensate for the heat loss and excess freshwater input south of the PF.

2.1. Introduction

Mesoscale eddies dominate the ocean kinetic energy (Ferrari and Wunsch, 2009). The omnipresence of mesoscale features in the global ocean became apparent only with the onset of satellite observations which resolved scales of O(100)km about two decades

ago. This discovery triggered extensive research on oceanic mesoscale variability such as fronts and eddies (Morrow and Le Traon, 2012). Eddies are coherent vortices of temporal scales of weeks to years and populate the worlds oceans at any moment by thousands (Chelton et al., 2011b). The SO (Figure 2.1) is a vast area of particularly high eddy activity due to the dynamic ACC and its interaction with boundary currents at its northern flank. Until now no study has focused on eddies in the SO with a Lagrangian approach. We fill the gap with this work.

The SO is a unique region of modification and formation of water masses. On one hand water of the different ocean basins in the SO is mixed laterally by the wind-driven ACC encircling the Antarctic continent. On the other hand the SO is only weakly stratified which allows for a vertical exchange between the deep and the surface ocean. Eddies form in the SO due to barotropic and baroclinic instabilities (Treguier et al., 2007) and play a vital role in SO dynamics (e.g. Rintoul et al., 2001; Naveira Garabato et al., 2004; Fyfe and Saenko, 2006; Hallberg and Gnanadesikan, 2006; Mignone et al., 2006; Hogg and Blundell, 2006; Zickfeld et al., 2007; Lachkar et al., 2007; Böning et al., 2008; Hogg et al., 2008; Thompson, 2008; Gillett et al., 2008; Sallée et al., 2010a; Morrison and Hogg, 2013). Two mechanisms are frequently mentioned as causes for their vital role in this region: firstly, they balance the momentum input of the intensive westerly winds by transporting it downwards towards the ocean bottom by interfacial form stress where it is dissipated. Secondly, they provide the necessary meridional transport of tracers as the zonal flow of the ACC generally acts as a barrier against such transports. The northward wind-induced Ekman transport in the ocean surface is partly offset by southward eddy transports. The extent of the compensation of Ekman by eddy transport is essential for instance in the context of the SO currently appearing to change from a net sink to a net source of the long-lived greenhouse gas CO_2 (Takahashi et al., 2012).

A Lagrangian approach is intriguing for the investigation of eddy characteristics as it provides complementary information to the more frequently employed Eulerian framework. We take such an approach by detecting individual SO eddies and tracing them during their life. The SO as a whole has never been considered in a regional study even though a fair amount of regional studies exists by now taking a Lagrangian approach and exploiting satellite data partly in combination with in-situ observations (e.g for the Mediterranean (Isern-Fontanet et al., 2003, 2006), various areas in the Pacific (Henson, 2008; Chaigneau et al., 2008; Itoh and Yasuda, 2010; Kurczyn et al., 2012; Liu et al., 2012), the eastern boundary upwelling systems (Chaigneau et al., 2009), Agulhas Rings (e.g. Dencausse et al., 2010) and eddies in the Tasman sea (Everett et al., 2012, based on eddies detected by Chelton et al., 2011b). Chelton et al. (2007, 2011b) (Chelton et al., 2011b is referred to hereafter as CSS11) are the only global studies applying this method and represent a thorough inventory and rich information on long-lived coherent vortices. Despite having been the focus of many Eulerian as well as Lagrangian studies, many of the eddies' peculiarities and impacts are still not well understood.

We provide a phenomenology of SO eddies by examining their surface as well as subsurface properties including some of their spatio-temporal variability. By using satellite observations as source of information which feature sufficient spatial and temporal coverage, we can make conclusions on the large-scale and climatological distribution and

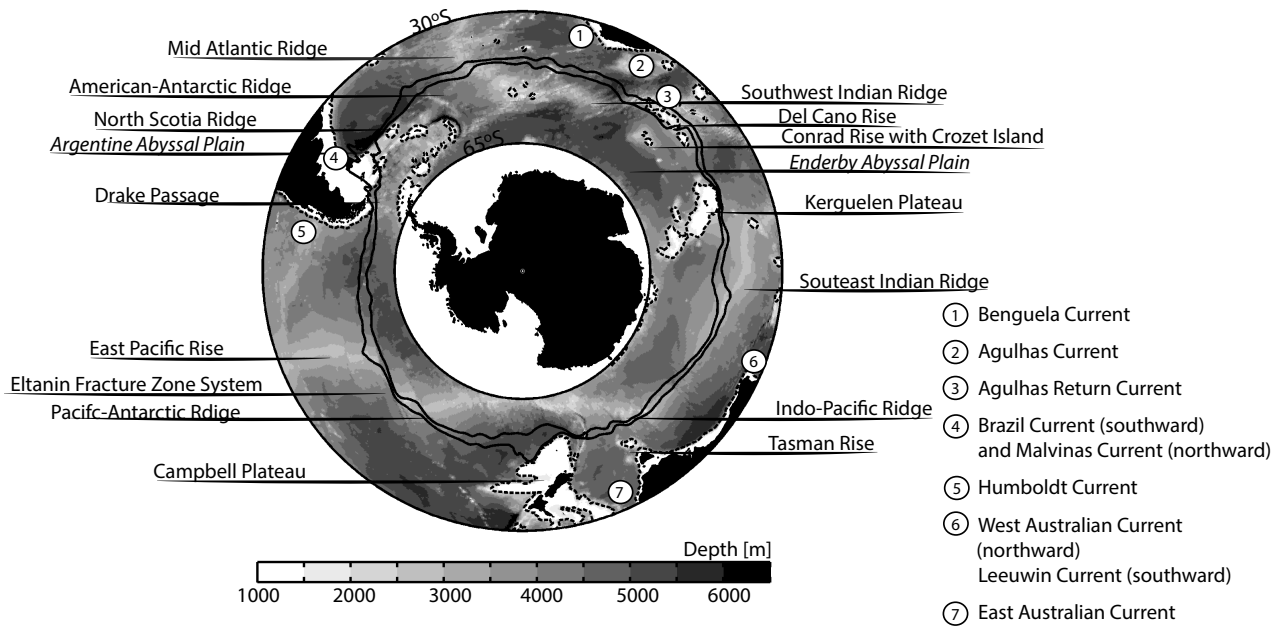

Figure 2.1.: Topography with major topographical rises, abyssal features and boundary currents*; solid black lines show the mean northern (SAF)/southern (PF) boundaries (major fronts) of the ACC; the dashed black lines mark the -2000 m depth contour.*

properties of eddies. We complement the satellite observations by profiles measured by *Argo* floats to obtain subsurface information beyond surface information gained from satellite data.
The paper is structured as follows: we will first describe the data and the methods applied in Section 2.2. We then present results in Section 2.3 and finally give an example of eddy buoyancy transport in Section 2.3.5.

2.2. Method

2.2.1. Data

As the majority of eddies appears to show a signal at the sea surface Peterson et al. (2011) satellite data are suitable for a qualitative study of eddies. Most of our analyses are based on satellite observations. For the eddy identification we made use of the AVISO sea level anomalies (*SLA*, http://www.aviso.oceanobs.com, Delayed-Time v3.0.0, fully reprocessed in March 2010). AVISO is a merged product, it comprises measurements of the altimetry missions Jason-1&2, Envisat, ERS-1&2, Topex/Poseidon and GFO for the chosen time period. The combination of data from different missions significantly improves the estimation of mesoscale features (Pascual et al., 2006). The data have a spatial and temporal resolution of 1/3° and 7 days, respectively. These resolutions are sufficient for the detection of the larger mesoscale features and their tracking over time. We do not correct for steric height effects, as the thermal expansion of water is small at the low temperatures we find in the region we focus on, the high southern latitudes. Additionally, we obtained the AVHRR Pathfinder (version

5) project sea surface temperatures (SST) from `http://www.nodc.noaa.gov` (Casey et al. 2010, 4 km/daily, daytime measurements). We linearly interpolated all data on a common spatial resolution of 0.25° and a temporal one of a week. SST anomalies (ΔSST) are deviations from a monthly climatology which we created from the daily SST fields.
We downloaded profiles of the *Argo* floats (`http://www.Argo.ucsd.edu/Argo_data_and.html`) which sampled the SO to obtain information on the vertical structure of SO eddies. To extract the eddies' anomalies of temperature (T) and salinity (S) we subtracted an *Argo* climatology (`http://apdrc.soest.hawaii.edu/projects/Argo/`, 5°×5°) from the individual profiles before the analysis.
Further, we used the positions of the main ACC fronts (Polar Front, PF, and Sub Antarctic Front, SAF) for geographical analyses by Sallée et al. (2008) (`http://ctoh.legos.obs-mip.fr`). Finally, we needed an ocean current climatology for the tracking of eddies which we derived from the ocean reanalysis SODA (0.5°/monthly, `http://dsrs.atmos.umd.edu`, Carton and Giese (2008), version 2.0.2, 1958 - 2001), and additionally information about the inherent propagation speed of eddies which is similar to the ones of long baroclinic Rossby waves (we used Chelton et al. 1998).
We considered all available data between 30°S and 65°S and in the time period July 1999 to November 2009.

2.2.2. Mesoscale Eddy Detection

2.2.2.1. Eddy Identification

We aim at a comprehensive study of Southern Ocean eddies. As too many eddies exist in the domain at each time step to be identified and tracked manually, we need to apply automated identification and tracking algorithms. We identified eddies applying the Okubo-Weiss parameter (OW, Okubo 1970; Weiss 1991), which has been extensively used for this purpose (e.g. Isern-Fontanet et al. 2003; Chelton et al. 2007; Chaigneau et al. 2008; Henson 2008; Itoh and Yasuda 2010). The OW is a physical criterion whereby the dominance of vorticity over strain in an area (grid box) is determined, $OW = s_n^2 + s_s^2 - \omega^2$ where $s_n = u_x - v_y$ is the normal and $s_s = v_x + u_y$ is the shear component of the strain, and $\omega = v_x - u_y$ the relative vorticity. u and v are the current velocity components in eastward and northward direction respectively, which can be calculated from the SLA under the assumption of geostrophy, and $\partial/\partial x$ and $\partial/\partial y$ denote the partial derivatives in east- and northward direction, respectively. Thus, negative values of OW denote areas where vorticity is dominant and where we thus expect to be eddies. We separated anticyclonic (AE) and cyclonic (CE) eddies by negative and positive vorticity, respectively, and added the constraint of the existence of a local minimum/maximum of the SLA within the eddy area. The former constraint ensured that areas were split into AE and CE which were indicated initially as single large eddies by the OW, but which actually consisted of merged eddies of both polarities.
For the calculation of the OW, we used the AVISO data on the original grid (plus a duplication of ±10° in east and west direction, to not miss eddies crossing the prime

Meridian) and then applied for the identification of eddies $OW < -0.2\sigma_{OW}$ as threshold (as e.g. Pasquero et al. 2001), where σ_{OW} is the spatial standard deviation of the OW. σ_{OW} was calculated for each time step and then averaged over time. The resulting eddy-mask was linearly interpolated to a 0.25° grid as the other data and boxes with values greater 0.5 ascribed to be an eddy-box. We set 4 grid boxes as the minimum of adjacent boxes to form an eddy (thus $2 \times 1/4° \approx 0.5°$) which is at the limit of what is resolvable with the current gridded AVISO data. Thus, we additionally only included eddies which did occur in at least two consecutive maps/time steps as robust features in the analyses unless mentioned otherwise. We also rejected features with a width of only a single grid box to be an eddy. The latter measure was a crude constraint on the shape of an eddy which inhibited elongated features in between eddies to be identified as eddies. The OW has been criticized (e.g. identification of the pure core of the eddy, thus underestimating the total eddy area, overdetection, noise amplification because of the involvement of double derivatives (Chaigneau et al. (2008); D'Ovidio et al. (2009); Chelton et al. (2011b)). However, the OW is well tested and in addition is computationally very efficient. The measures we took as described above counteract the identification of spurious features.

2.2.2.2. Definition of Eddy Characteristics

Our definition of features of eddies are the following: the center of an eddy is the mass center of the same. We defined the diameter L_e and amplitude A_e of eddies similar to previous studies: the former was defined as the diameter of a circle covering the same area A as the respective eddy ($L_e = 2\sqrt{A_{eddy}/\pi}$), and the latter as the absolute difference between the local SLA extremum of the eddy and the mean SLA over the eddy's edge. The eddy intensity ζ is defined as the SLA gradient related to the eddy, i.e. $\zeta = A_e/(L_e/2)$. As it is directly linked to the swirl velocity U (mean of the eddy edge) and the EKE, it is a better proxy for the eddy dynamics than the L_e or A by themselves. An additional advantage is that the latter is not as dependent on the "subjective" choice of the eddy edge. The eddy's age is given in weeks and we start counting with zero when the eddy is detected the first time. As "trapping ability", we chose as applied by CSS11 and already suggested e.g. by Flierl (1981), U/c, with c the propagation speed of the eddy. $U/c > 1$ implies that the eddy is able to trap fluid and carry it along its propagation path.
Concerning the vertical structure of eddies, we used an approach similar to the ones of e.g. Qiu and Chen 2005 and Chaigneau et al. 2011, calculating the mean vertical T/S profiles. With this, we could derive an estimate of the trapped water as well as integrated T/S anomalies applying the thermal wind relation (with the assumption of zero swirl velocities at 2000 m and a cylindrical eddy shape), which gave as the volume of trapped fluid (at $U/c = 1$). We picked from the available *Argo* floats only the ones firstly containing data with quality flag 1 ("best") of the post-processed data (and additionally excluded still existing outliers of $-3\text{C}^\circ > T > 35\text{C}^\circ$ or $30 > S > 35$), secondly spatially surfacing within an eddy core (maximum 0.25° distance from the eddy centre) and thirdly temporally emerging in the same week as the SLA estimate is for. We subtract from these float profiles the *Argo* climatology derived by Von

Schuckmann et al. (2009) at the specific location and month of each float profile and binned the T and S profiles vertically in 5 atm pressure bins. Finally, we sorted the selected floats by polarity of the related eddy.

2.2.2.3. Eddy Tracking

Tracking of mesoscale eddies is more uncertain than the detection (see early online release of Neu et al. 2012, for atmospheric cyclones). We tested various parameters and additions to our algorithm before we found satisfying results based on visual evaluation. To determine matching eddies in consecutive time steps we firstly estimated the location of each individual eddy in the subsequent time step by accounting for advection by mean currents (on the basis of the barotropic current component of the ocean reanalysis SODA) as well as the eddies' intrinsic phase speed (as approximation phase speeds of linear baroclinic Rossby waves, CSS11). For an estimation of the latter, we converted a climatological atlas of the first baroclinic gravity wave phase speed (Chelton et al., 1998) to the theoretical phase speed of nondispersive baroclinic Rossby waves. As this extrapolated eddy propagation is uncertain, we drew a search ellipse around the estimate of the future eddy location on the basis of the zonal and meridional variability of the mean currents (semi-axes of $3\sigma_u$ and $3\sigma_v$). We set one L_e as minimum length for the semi-axes to allow for additional effects as well as uncertainties, such as deviations of the eddies' phase speeds from the ones of baroclinic Rossby waves and the small poleward and equatorward deflection of CE and AE propagation, respectively (Cushman-Roisin Benoit et al., 1989; Morrow, 2004; Van Leeuwen, 2007), as well as for eddy-eddy interactions (Chelton et al., 2011b; Early et al., 2011). When we found more than one potentially matching eddy for e_1 within the search ellipse, for instance e_2 and e_3, we applied a similarity-criteria similar to studies before, i.e. selected the "most similar eddy" as matching eddy (similar to e.g. Penven et al. 2005): $\min(D_{e_1,e_{2,3}})$ with $D^2_{e_1,e_{2,3}} = \frac{1}{4}\left(\left(\frac{\Delta\omega}{\sigma_\omega}\right)^2 + \left(\frac{\Delta A_e}{\sigma_{A_e}}\right)^2 + \left(\frac{\Delta SST}{\sigma_{SST}}\right)^2 + \left(\frac{\Delta d}{d_{min}}\right)^2\right)$, and $\Delta\omega = |\omega_{e_1} - \omega_{e_{2,3}}|$, $\Delta SST = |SST_{e_1} - SST_{e_{2,3}}|$, $\Delta A_e = |A_{e_1} - A_{e_{2,3}}|$ and $\Delta d = |d_{min} - d_{e_{2,3}}|$, where d_{min} is the minimum of the spatial distances of all eddies located within the search ellipse from the projected location of e_1 and σ_ω, σ_{A_e} and σ_{SST}, i.e., the temporal standard deviations of ω, A_e and SST, are taken from maps of temporal standard deviations which we derived based on all identified (not yet tracked) eddies. We applied two final constraints concerning the match-up: firstly, we allowed a match only if $D_{e_1,e_{2,3}} < 1$ to exclude a match which would involve unlikely changes in eddy properties from e_1 to $e_{2,3}$. Secondly, we aimed to filter out "dying eddies" by not allowing an increase (exceeding 5%) of ω if it had decreased the previous three lifetime steps and additionally showed a decrease (>50%) compared to the time of first detection. In the case that either no eddy center was located within the search ellipse or all eddies within the search ellipse were rejected as matching eddies, the eddy was assumed to have died. We did not try to search for a lost eddy in subsequent time steps. Thus, the resulting life times and propagated distances are rather conservative. In comparison to Chelton et al. (2007) and presumably also to Chelton et al. (2011b) (here, the tracking method is not described in great detail), our eddy life times might be shorter,

as CSS11 decided: "If a single eddy was closest to more than one eddy in the earlier map, it was assigned to the eddy with the longest track up to that point", meaning they did not decide based on similarity of the respective eddies but on their age which might result in a bias towards long-lived eddies. Finally, we excluded eddies from our analysis existing in the first or last *SLA* map to consider only eddies with complete life tracks.
The frequently occurring processes of merging and splitting of eddies form a difficulty for the automated tracking algorithm and was not additionally accounted for. A potential future approach would be a "tracking-tree" of eddy trajectories rather than aiming at unique tracks of individual eddies, even though this approach would raise questions on how to interpret the results.

2.3. Results and Discussion

2.3.1. Overview Over the Retrieved Eddy-Dataset

We identified >1,200,000 single eddy events south of 30°S in the analyzed time period 1997 - 2010. More than 90% of these single events belong to tracks of eddies existing at least two consecutive time steps. Expressed in a different way, about 30% of the tracked eddies existed only for one time step, whereas 70% feature life times of more than one week. Thus, the $O(10^6)$ individual eddy events resulted in approximately 260,000 tracked eddies. Of these, slightly more were anticyclonic than cyclonic (140,000 versus 120,000). About 30%, 10% and 5% of tracked eddies existed at least 4, 12 and 16 weeks, respectively. We observed less than 1% to live longer than one year, and a couple of individuals (10 AE and 41 CE) almost exclusively north of the ACC lived longer than 2 years.
The fractionation of polarity is reversed for long-lived eddies relative to the shorter lived ones. Of the very long-lived eddies (more than 1 year old) 30% more eddies were cyclonic than anticyclonic. The maximum life times were 184 weeks for anticyclones and 165 weeks for cyclones, thus more than 3 years for both polarities (see Supplementary Note B.4 for a brief comparison with the global eddy tracking study of CSS11).
We plotted the tracks of all eddies traced at least over 5 time steps (4 complete weeks) in Figure 2.2 to give an illustration of the information contained in the "eddy-data set". It is a qualitative Figure which summarizes many aspects we will get back to in more detail as well as quantify in later paragraphs: it visualizes where eddies occur preferably (in the vicinity of strong currents) and where they propagate to over their life times, how old eddies get (weeks to years) and where we find the long-lived eddies (undisturbed subtropical regions but also the ACC, especially for CE), where eddies are generated (white dots: strong currents, eastern and western boundary currents) and how AE and CE differ in all these aspects (e.g. many more AE than CE populate the south Pacific, and AE and CE propagate in undisturbed waters steadily equatorward and poleward, respectively).

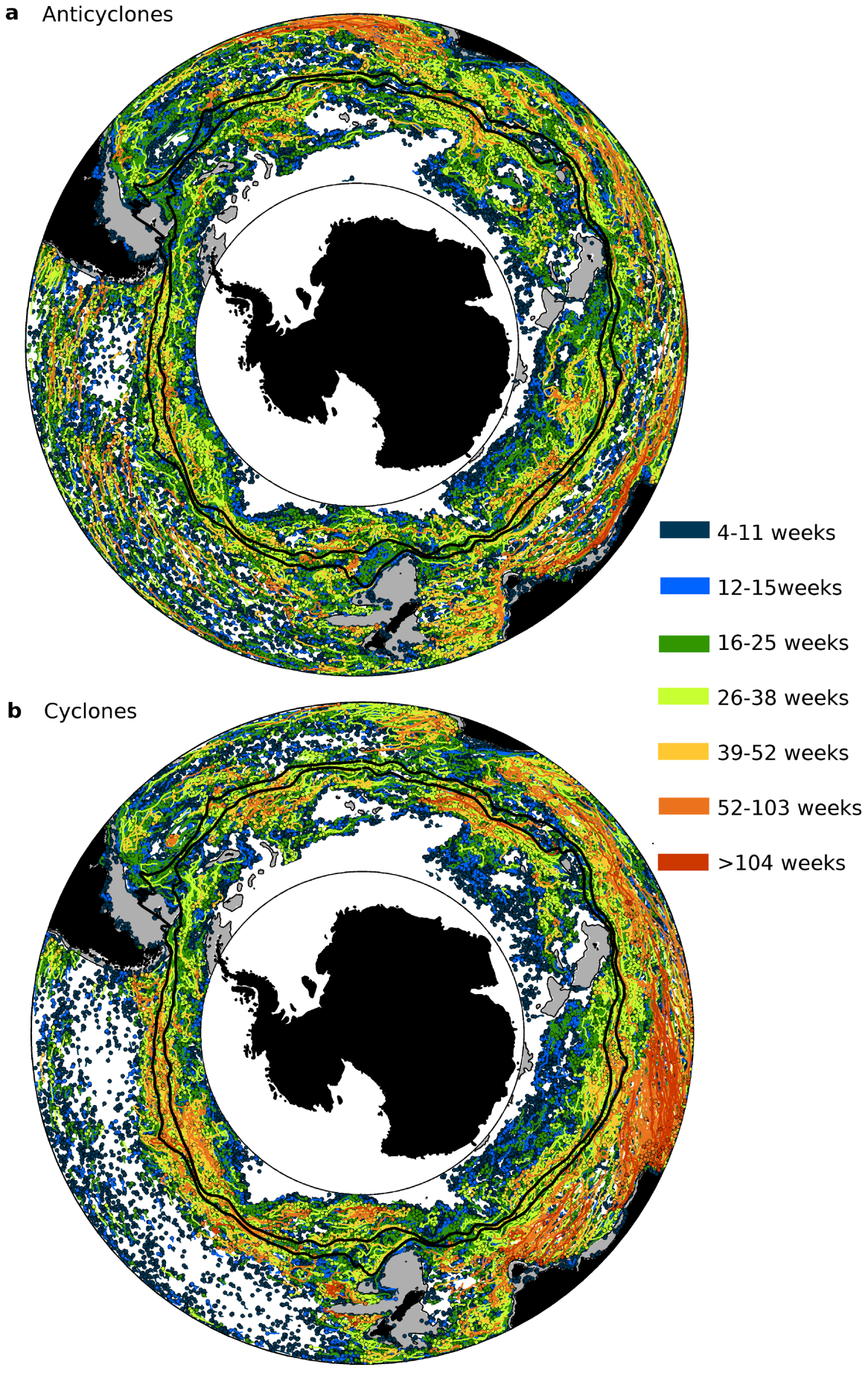

***Figure 2.2**: Caption on next page.*

Figure 2.2.: Tracks of eddies colored by age; a *anticyclonic and* ***b*** *cyclonic eddies detected and tracked over the time period 1997 – 2009; the color code denotes different age groups, eddies with longer lifespans on top of the eddies with shorter ones; note that eddies propagating into or out off the domain are included, thus their lifespans are underestimated; the location of first detection is marked with a circle for each individual eddy; gray shaded areas mark topography shallower 2000 m; black lines show the mean (solid) and maximum (dashed) northern (SAF)/southern (PF) position of the the ACC boundaries in the analyzed time period.*

Examples of average eddy properties as statistically derived from the eddy data-set are for instance the core diameter of 80(61,92) km, the propagation speed of 0.04(0.02,0.05) m s^{-1} (i.e. 22(10,29) km $week^{-1}$), the lifespan (if detected more than once) of 5(1,6) weeks and *SST* anomalies of 0.66(0.25,0.94) °C, with the bracket values denoting the 25^{th} and 75^{th} percentiles, respectively (see also Supplementary Figure B.1). The mean life cycle of eddies shows a spin-up and a spin-down phase 20% of its life time each and a roughly steady phase in between (Supplementary Figure B.4). Further, Figure 2.2 can be translated into maps of long-term mean eddy properties, for instance of mean diameters and amplitudes of eddies (Supplementary Figures B.2 and B.3), or of the dominant propagation direction in a location (not shown): it is largely westward north of the ACC and eastward in the vicinity of the ACC due to advection. In this work, we will focus on the spatial and temporal distribution of eddies and their three dimensional structure.

Before however, we compare the eddy coverage to satellite derived *EKE* as a measure of evaluation of our eddy detection algorithm. CSS11 shows (their Figure 7, lower panel) the contribution of eddies (life times at least 1 month) to the eddy kinetic energy (*EKE*) derived from satellite altimetry which includes for instance also the mesoscale variability caused by e.g. ridges between eddies: they conclude that the larger part (40 - 60%) of mesoscale variability derived from satellite altimetry is indeed caused by eddies.

Overall, the spatial pattern of the area coverage of eddies (Figure Figure 2.3a) is consistent with the natural logarithm of the *EKE* derived from satellite altimetry (Figure 2.3b): strong currents stand out as regions of high *EKE* and at the same time "no-eddy" areas become visible in the same places as in Figure 2.3a.

It is possible that the areas we found to have little *EKE* and detected eddies are actually populated by eddies, but of characteristics beyond the resolution of the *SLA* data, such as less energetic ones and/or of smaller scales (towards the submesoscale). This is anticipated from maps of high resolution infrared *SST* or chlorophyll-a data which show a very rich texture of all kinds of scales. Naturally, *EKE* calculated from satellite altimetry represents only the variability at scales larger than the *SLA* resolution which accordingly underestimates the "true" kinetic energy due to mesoscale variability. If we look at a *EKE* map derived from surface drifters (see e.g. Figure 1d in Thoppil et al., 2011) which we expect to include smaller scales of *SLA* variability than the satellite resolves, the amplitude of the *EKE* is larger (e.g. Kelly et al., 1998 found drifter derived *EKE* to be 13% higher than the one derived from altimetry in the California Current System) but the spatial pattern is still the same. Hence, we conclude that satellite altimetry resolves a substantial fraction of the mesoscale variability.

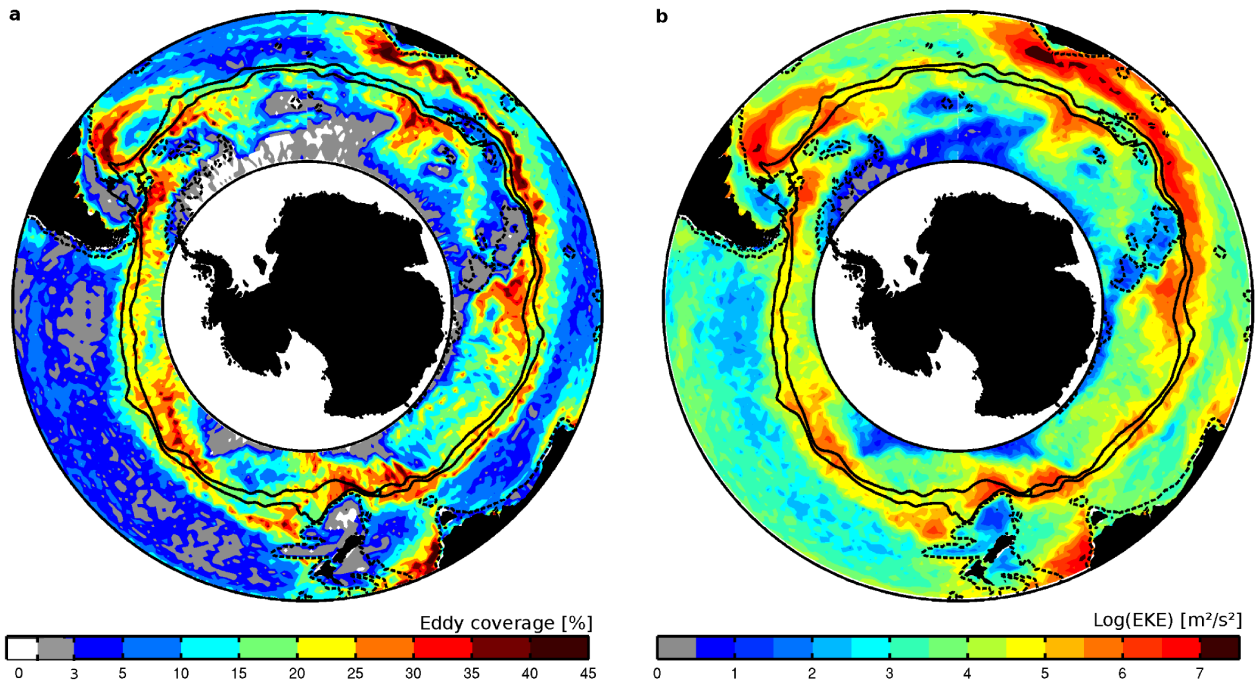

Figure 2.3.: Eddy occurrence; a *eddy coverage over time and* ***b*** *natural logarithm of the mean of the eddy kinetic energy (EKE); aggregated on a 2° grid; as before, solid black lines show the mean northern (SAF)/southern (PF) boundaries (major fronts) of the ACC; dashed black lines mark the -2000 m depth contour; number of eddy occurrences per grid box are converted into area coverages over time on the basis of their mean diameters in the respective area: we bin all occurring eddies into a 1°×1° longitude-latitude grid and calculate the temporal average of the fractional coverage of the grid box area by eddy cores.*

In the following, we turn to the detailed analysis of the pattern as well as to numbers of eddy coverage we found as shown in Figure 2.3a.

2.3.2. Spatio-Temporal Distribution of Eddies and Polarity Dominance

2.3.2.1. Spatial Distribution of Eddies

The cores of mesoscale eddies occupy the dynamic regions of the SO 20 - 40% of the time (Figure 2.3a). Areas of high mean occupation by eddies are contrasted by regions where very little or literally no eddies occur. The former are co-located with strong currents (as found already by an early altimetry study, Chelton et al. 1990), such as the ACC and the western boundary currents and interactions of the same, such as the confluence zone of the Brazil and Malvinas Currents at about 40°S east of South America and the well-studied interaction of the Agulhas Current and the ACC, the Agulhas Retroflection, resulting in the Agulhas Return Current. The latter, the aforementioned "eddy-no-go-areas", include the subtropical waters and specifically the South East Pacific (found also by CSS11). In summary, to first order a largely zonal picture emerges, with weak and strong eddy activity in the north of the domain and along the ACC, respectively. Zonal variability is superimposed on this pattern with

eddy rich coastal waters contrasting relative eddy-poor subtropical gyres in the north of the domain and some variability along the ACC pathway.
The eastern boundary currents (to the extent they are included in our domain) show some but relatively weak eddy activity. One reason for this may be that (as clearly visible from Figure 2.2) eddies originating from the eastern boundary currents typically do not stay there but are free to propagate westward and have long lifespans. The Humboldt Current off the South American coast emerges as the eastern boundary current system with the least eddy activity (in agreement with CSS11, see eddy centroids in their Figure 5). The other two eastern boundary current systems feature next to the cool northward Benguela and West Australian Current warm southward surface currents, the Angola and the Leeuwin Current. Interactions of these opposing cool northward and warm southward currents might well be responsible for increased eddy activity. The Agulhas leakage (forming Agulhas rings) might play an additional role for the high eddy activity associated with the Benguela Current system.
Looking at the ACC eddy band, it appears that eddy coverage drops off quite abruptly at its northern flank but not so much in the south where eddy coverage levels of more gradually. Turning to the zonal pattern one realizes the aforementioned zonal inhomogeneity. Indeed, frequently analyzed using zonal or streamline averages, the zonal asymmetries of the ACC have gotten increased attention relatively recently. Eddy occurrence is especially high in the wake of prominent topographical obstacles (Sokolov and Rintoul, 2009b; Thompson et al., 2010), such as the Drake Passage, the Mid Atlantic Ridge, the Scotia Ridge/American-Antarctic Ridge, the Southwest Indian Ridge, the Kerguelen Plateau, the Indo-Pacific Ridge/Campbell Plateau and the East Pacific Rise/Pacific-Antarctic Ridge (see Figure 2.1). The ACC is strongly steered by topography and the sea surface height (SSH) gradients are steep where the ACC fronts are squeezed together due to obstacles in the bathymetry (Sallée et al., 2008; Sokolov and Rintoul, 2009a). An increased number of eddies spins off in areas of large SSH gradients and downstream where the ACC is more prone to instabilities (e.g. Thompson and Sallée, 2012), and subsequently are advected downstream where the ACC broadens again. This is thought to be of importance for eddy diffusivities and hence meridional eddy transports (Thompson and Sallée, 2012).
One of the prominent areas of almost non-existent eddy activity is located south of the northern-most extent of sea-ice which also surface drifter derived *EKE* maps show. As neither satellite altimetry nor surface drifters sample below sea-ice, this feature must arise from the sea-ice free periods of the year. Hence, even though we cannot draw conclusions about eddy activity under sea-ice coverage it appears that eddy activity is reduced in the sea-ice free ocean in areas of seasonal sea-ice cover. Hypothetically, this is due to a missing generation mechanisms or damping of eddies by sea-ice. Distinct "eddy-no-go-areas" exist also in the ACC influenced region, which are in general areas of "shallow" topography of 2000-3000 m (dashed contours in Figure 2.3, and see Figure 2.1, topography), such as around the Kerguelen Plateau, the Campbell Plateau and the Conrad Rise (as in CSS11, however they did not relate this to topography). We find that the number of eddies occurring over shallow topography increases to a limited extent if short-lived (<1 month) eddies are considered, which are less intense the same time (not shown).

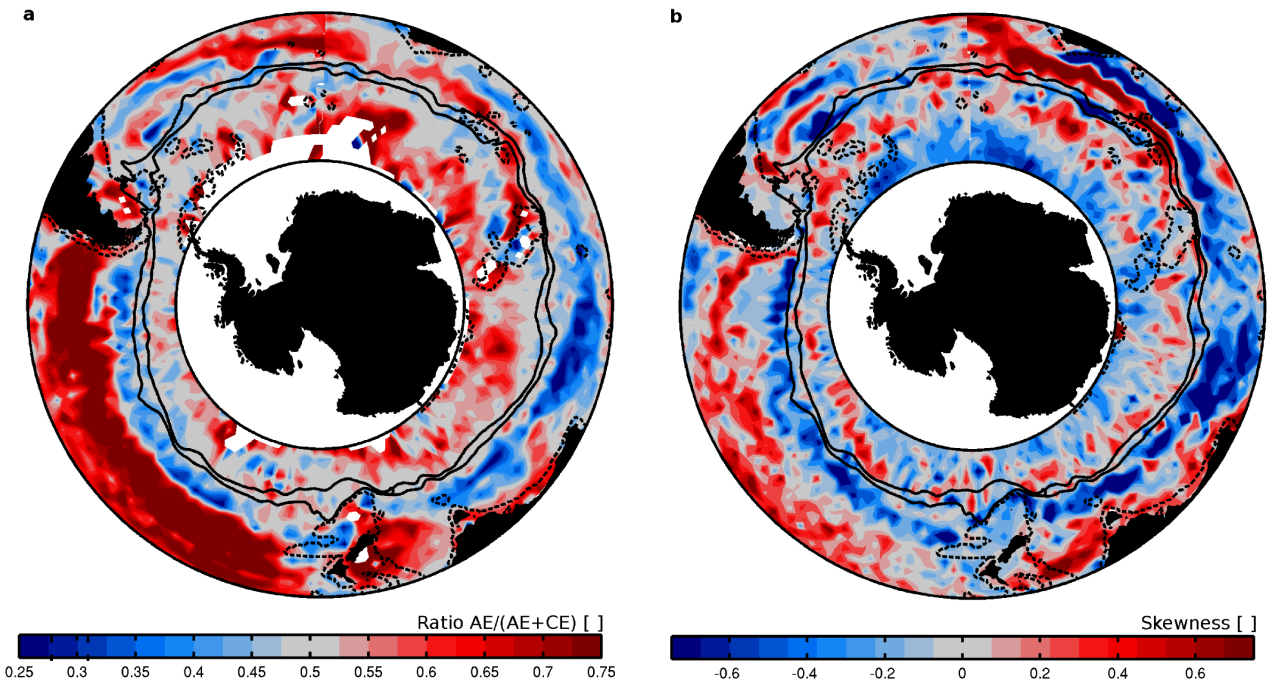

Figure 2.4.: Polarity dominance; a *ratio of area occupied by AE over area covered by all eddies, i.e. a fraction larger (reddish colors) and smaller (bluish) 0.5 marks AE and CE dominance, respectively;* ***b*** *skewness of* SLA*; as before, solid black lines show the mean northern (SAF)/southern (PF) boundaries (major fronts) of the ACC; dashed black lines mark the -2000 m depth contour.*

The area coverage of eddies is dependent on the definition of the eddy-edge. The lateral extent to which eddies influence their surroundings extends beyond the mere eddy core as detected with the OW parameter, and this is not only true for oceanic but also for atmospheric variables: if for instance satellite based observations of sea surface temperatures, chlorophyll-a or wind speeds are collocated with the identified eddies, the "zone of influence" is easily about double the radius of the average eddy (see Section 2.4). If this area is considered as eddy coverage, the numbers in Figure 2.3a become much larger. This is central when investigating the (integrated) impact of mesoscale oceanic eddies on their environment, for instance on biology or their role on water mass formation.
Similarly, it can be of concern in this context how the eddy frequency varies over time, and if the polarity of eddies, i.e. AE versus CE, is variable in space as well as time, as we expect a different impact of AE and CE on their environment due to their opposing dynamics. Hence, we will examine polarity dominance and seasonality of eddies in the following.

2.3.2.2. Dominance of Anticyclones over Cyclones and Vice Versa

A dominance of one polarity of eddies over the other exists which is not evenly distributed in space (Figure 2.4a, e.g. for the ACC also found by Sokolov and Rintoul 2009b, however not specified in detail). We find more AE occurring south of the ACC and in the subtropical regions. In contrast, we find more CE related to the ACC and

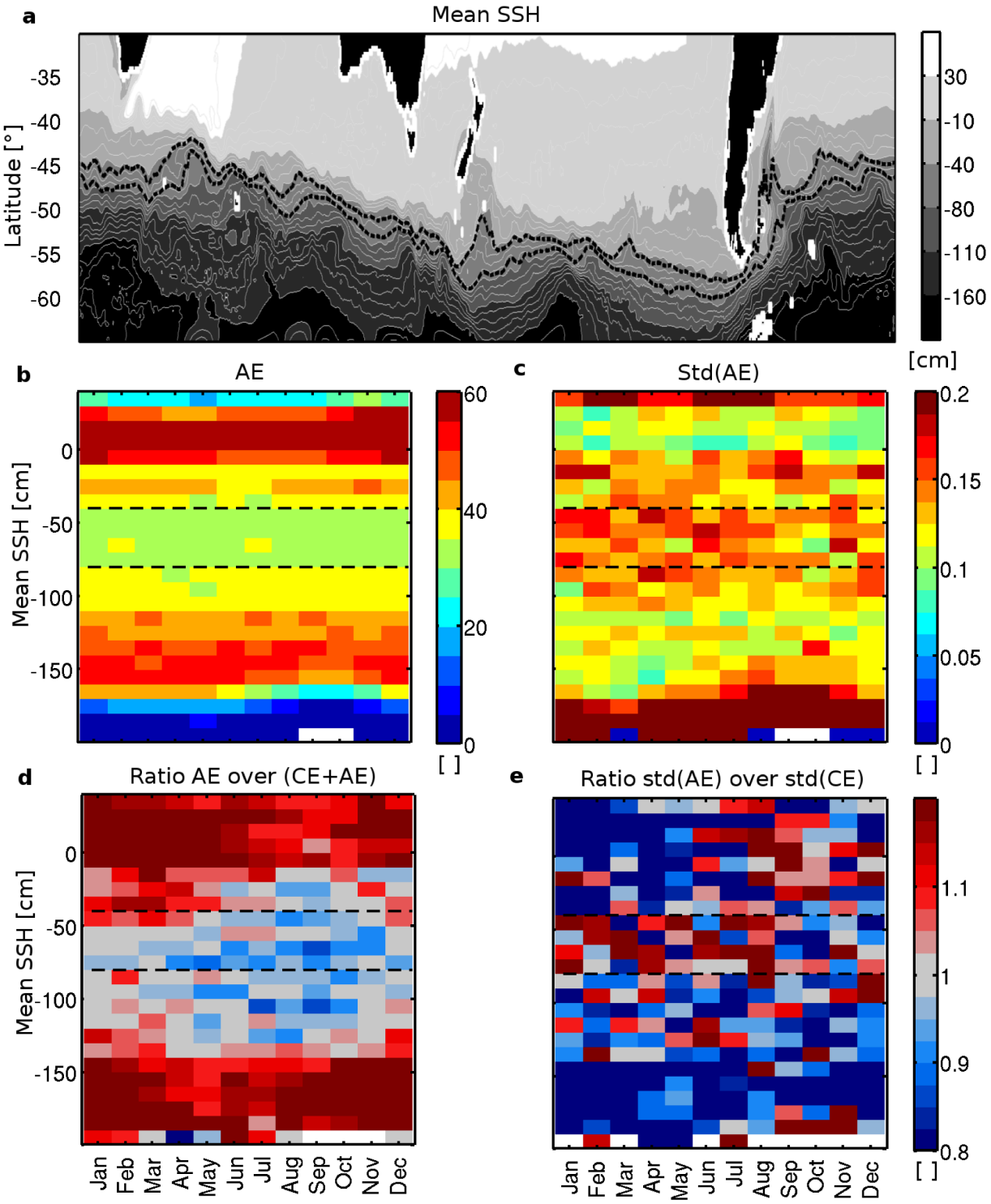

Figure 2.5.: Seasonality and eddy numbers (Hovmoller plot); ***a*** *SSH; as before, solid black lines show the mean northern (SAF)/southern (PF) boundaries;* ***b*** *number of AE and* ***c*** *standard deviation of the number of AE;* ***d*** *and* ***e*** *are* ***a*** *and* ***b*** *divided by the same quantity of CE.*

especially at the northern flank of the current. This large-scale pattern was similarly detected by CSS2011 (see their Figure 8 therein). In addition, we find that other strong currents such as the Agulhas return current and the Malvinas/Brazil currents are related to a dominance of eddies of one polarity on the one side of the front in contrast to the other.
The zonal CE band at the northern flank of the ACC is somewhat extended in the Indian Ocean due to the special area of very long-lived CE originating from the Australian coast and propagating southwestward towards the northern flank of the ACC. These CE emerge potentially due to the special situation of two currents west of Australia, the cool northward West Australian and the warm southward Leeuwin Current. The CE band is interrupted south of Africa, likely due to the extensive and intense Agulhas Retroflection/Return current resulting from the relatively northern position of the ACC in combination with the intense Agulhas current.
The pattern of polarity dominance we find from our Lagrangian approach agrees largely with the skewness of *SLA* variability (Figure 2.4b, Thompson and Demirov 2006). However, the southern part of the SO is an area of prominent disagreement between the former and the latter: we found a dominance of AE where the skewness hints towards a dominance of CE. First of all, we detected only a small number of eddies in this area altogether which makes a ratio, such as we consider here, less trustworthy. Other issues contributing to a mismatch are on the one hand that standing eddies do not show up in the skewness. Eddies do hardly propagate in the south of the domain considered here as no strong currents advect them and also their intrinsic phase speed is small. On the other hand, the skewness includes not only the effects of transient eddies but also for instance the lateral translation of fronts over time. The mentioned factors in common may well result in the partial mismatch between skewness and our CE to AE ratio.
What could be the mechanisms of polarity dominance? It must arise either from a privileging generation mechanism, greater persistence of one of the polarities over the other, or from favored areas eddies of one polarity propagate into.
One of the causes could be symmetric pinching off of eddies from the fronts. One side of the front would then be populated mainly by CE, the other one by AE. This mechanism is likely responsible for the pattern of polarity dominance associated with intense currents, such as the Malvinas-Brazil Confluence or the dominance of CE at the northern flank of the ACC.
Next, high frequency wind forcing is a proposed generation mechanism for mesoscale eddies (see e.g. Tulloch et al., 2011) which hypothetically could favor one of the polarities. Griffa et al. (2008) (their Figure 3a) computed (anti)cyclonic motion in the global ocean from surface drifters and found a dominance of small-scale anticyclonic loopers ($O(100)$km and less, their Figure 4) at the poleward side of the subtropical gyres. These are correlated with (high frequency) wind forcing and hypothetically caused by resulting Ekman transports in the ocean boundary layer (i.e. inertial oscillations). It is unclear if also mesoscale features would be preferably anticyclonic if generated by wind forcing. Looking at the south Pacific in Figure 2.2 it appears to be obvious that more AE than CE are generated in the open ocean (unrelated to boundary currents). In addition, they tend to exist much longer there than CE. We will come back to in-

dications for a potential greater persistence, or in the contrary a quicker dissipation of one of the two polarities in Section 2.3.3.

2.3.2.3. Seasonality of Eddies

The variability in space across SSH contours appears to be much larger than in time (Figure 2.5b). To investigate the former, we use a Hovmöller plot to gain more insight into the spatio-temporal variability of eddy-frequency where we show the occurrence of eddies separated by month and mean SSH bins. Mean SSH contours are very similar to streamlines in the SO (Sallée et al., 2008; Sokolov and Rintoul, 2009a) as can be seen also from Figure 2.5a) where the SAF and PF are added and align nicely with the -40 to -50 cm and -70 to -80 cm SSH contours.
The largest number of AE are found north of the ACC at the -10 to 30 cm contours. A second AE-frequency maximum appears south of the major fronts of the ACC, between the -110 and the -160 cm SSH contours. These two eddy-frequency maxima are presumably due to the western and eastern boundary current systems and due to the high SSH gradients related to topographic obstacles along the pathway of the ACC (whose impacts extend quite far south) as elucidated before. Near the southern edge of our domain, we find only a very small number of AE. Again, besides an actual occurring lack of eddies this can be also due to finite data coverage and too small eddies to be resolved by the satellite observations. The vicinity of the major fronts of the ACC is an area of still large eddy numbers, however less so than the regions both, north and south of the ACC. A reason for this could be shear destruction of eddies by jets. In a snapshot, the ACC is composed of a large number of filaments and jets instead of two major fronts. A suppression of eddy mixing related to jets was found e.g. by Naveira Garabato et al. (2011) and Thompson and Sallée (2012) and we will briefly get back to it in Section 2.3.3 on eddy dissipation.
Examining the standard deviation of the occurrence of AE (Figure 2.5c), we find the seasonality of eddy frequency with 10 - 20% (relative to local absolute numbers) not to be as large as the spatial one (agreeing with Chaigneau et al., 2009 who found a seasonal and interannual variability of about 20%). Here, the standard deviation in the vicinity of the ACC fronts is actually larger than in the very eddy-rich regions demonstrating a larger interannual variability of eddies in the ACC, which possibly could be due to winds or a variability of the interaction of eddies with ACC jets. The latter are in constant interaction with the eddies which may result in up- and downscale energy transfers as proposed by Thompson and Sallée (2012), which potentially contributes to the eddy-frequency variability in this area. The standard deviation contains all lower-than-monthly frequency variability, thus interannual and decadal variability, and trends. The seasonal variability is about as large as this longer-term variability (not shown). Still, the spatial variability of eddies is clearly of larger magnitude than the temporal one.
The general pattern of the eddy number variability looks similar for CE as for AE as visible from the ratio of the two (Figure 2.5d). In terms of absolute numbers, more (10%) AE exist north as well as south in the domain, which is approximately where we have the SSH-bands of high eddy numbers (as already apparent from Figure

2.4). In the vicinity of the SAF and PF, we find slightly (up to 10%) more CE. This band of CE dominance expands somewhat north- and southward in late austral winter. Additionally, it shifts somewhat south in austral autumn and north in austral spring so that the AE dominance is weakened to some extent in the SSH-bands south and north of the ACC. The seasonality of the Westerlies may possibly play a role in this, as SO stratification and the ACC and thus eddy activity may respond to a change in winds.
The ratio of the standard deviations of the eddy numbers (Figure 2.5d) is noisy within the ACC. There is a tendency for a greater variability of CE north of the ACC in austral summer, and south of the ACC all year round. The causes of the seasonality of the dominance of the variability of CE over the variability of AE is unclear. Potentially, the boundary currents feature a seasonality which results in a meridional shifting of polarity dominance.
We have not considered the zonal variability here as it is in general smaller than the meridional one. However, as discussed in the context of Figure 2.3, zonal variability of eddy activity exists north of the ACC and along the ACC which has received increased attention recently (Sallée et al., 2010b, 2011; Thompson and Sallée, 2012; Sallée et al., 2012).

2.3.3. Spatial Distribution of Eddy Genesis and Dissipation

The eddy coverage as examined in Section 2.3.2.1 at any location depends obviously on whether eddies are formed in the very place or if they propagate to the location from somewhere else. Here, we turn to the question of where they form and where they die, i.e. if we can determine the eddy "nurseries" and "graveyards".
The pattern of eddy generation regions resemble to some extent the one of *EKE* or the eddy coverage (Figure 2.3). This is expected as instabilities of ocean currents are the main eddy generation mechanism. The ACC downstream of topography, slightly south of the PF, stands out as eddy nursery, i.e. a large number of eddies is detected there the first time (not shown). In contrast to *EKE*, these topographically stimulated regions clearly outrival the (western) boundary currents as eddy nurseries. The areas in between the eddy-generation-hot spots strung along the ACC show an eddy formation rate at least as large as in the boundary current systems. The subtropical gyres are barren with respect to eddies as strong currents are absent.
We are more interested in generation sites of long-lived eddies, i.e. robust features. The general picture of the distribution of eddy nurseries changes somewhat if we weight individual eddies at the location of first detection with their maximum age (Figure 2.6a, only for AE). With this measure, we get an impression of nurseries of persistent eddies: besides the ACC the boundary currents emerge as important eddy production regions. As mentioned before, eddies born in the eastern boundary current systems can propagate relatively undisturbed westward across the subtropical gyres once they escape the current systems allowing for long lifetimes. The longevity of eddies generated in the western boundary currents is possibly related to their large intensity (alike the ACC eddies, see section B.2) which allows for a stable coherence and thus persistence. Also within the ACC, the nurseries of long-lived eddies are zonally expanded relative to the

"normal ones", thus the ACC is important as nursery for durable eddies as a whole. Finally, also the subtropical gyres loom as places where (although not as many) long-lived AE are born. They are potentially generated due to wind forcing, as mentioned before (also the wavenumber spectrum analysis by Xu and Fu (2011) supports air-sea interactions and short-term atmospheric variability as eddy generation mechanism in quiescent ocean regions). Once these eddies are generated, again, they are relatively undisturbed in the subtropical gyres.

The relative zonal homogeneity of the ACC with respect to nurseries of long-lived eddies makes apparent that in the dynamic regions downstream of shallow topography a bulk of eddies is formed which right away dissipate again. This is also visible from the map of "graveyards" of AE which indeed looks similar to the one of formation regions. The ratio of the two does not highlight prominent areas where nurseries and graveyards differ (Figure 2.6b). One reason for the ephemerality of many of the eddies in the eddy-generation-hot spot locations hypothetically is that newly generated eddies are subject to instantaneous distortion by interactions with jets (Thompson and Sallée, 2012). Speculating further, eddies may be especially vulnerable to distortion in their early life stage as they develop their maximum intensity only about after the first $^1/_5$ of their life time (see Supplementary Figure B.4). The combination of these two mechanisms would result in a preferential dissipation of young eddies in dynamic regions of the SO.

An indication for shear suppression to be possible to happen is if the eddies' swirl velocity is small compared to the shear of the ambient flow, i.e. if the ratio of the lateral shear rate $\gamma = |\Delta u/\Delta y| + |\Delta v/\Delta x|$ over the eddy turnover time τ is smaller than one (Terry, 2000; Shats et al., 2007). In fact, this is the case in the ACC for the most part for all eddies (not shown).

In addition, also vortices themselves incessantly interact, merge and split which may result in "young weak" eddies being absorbed by more "mature intense" ones. Obviously though, the increased difficulty of eddy tracking in the dynamic areas of the ACC has to be kept in mind. Also CSS11 note "we do not feel that this is a major problem, but we are not able to quantify how frequently this occurs". Likewise we can not exclude a bias with respect to generation and dissipation sites of eddies and their life spans. However, the frequent formation and concurrent dissipation of eddies in dynamic regions is supported by Xu et al. (2011a) and D'Asaro et al. (2011).

It is noteworthy, that even though eddies may live long, propagate and get advected, they are restricted to propagation distances of $O(100)$ km over their lifetime. This is as their intrinsic phase speed is relatively slow especially at high latitudes, and also, the eddy propagation direction and the zonal advection by ACC work in opposing directions. Thus, eddies do not get very far away from where they form. Even if they propagate $O(1000)$ km which the long-lived ones in the subtropics do, it still implies that the majority of eddies stays in the same ocean basin. The fact that eddies do generally not cover vast distances over their life time indicates an overlapping of eddy generation and dissipation areas as well. Here, partial exceptions are the western boundaries of the ocean basins which are anticipated to be typical dissipation regions of very long-lived eddies propagating westwards across the subtropical gyres towards the continents. CSS11 found this to be the case and this is supported also by Zhai

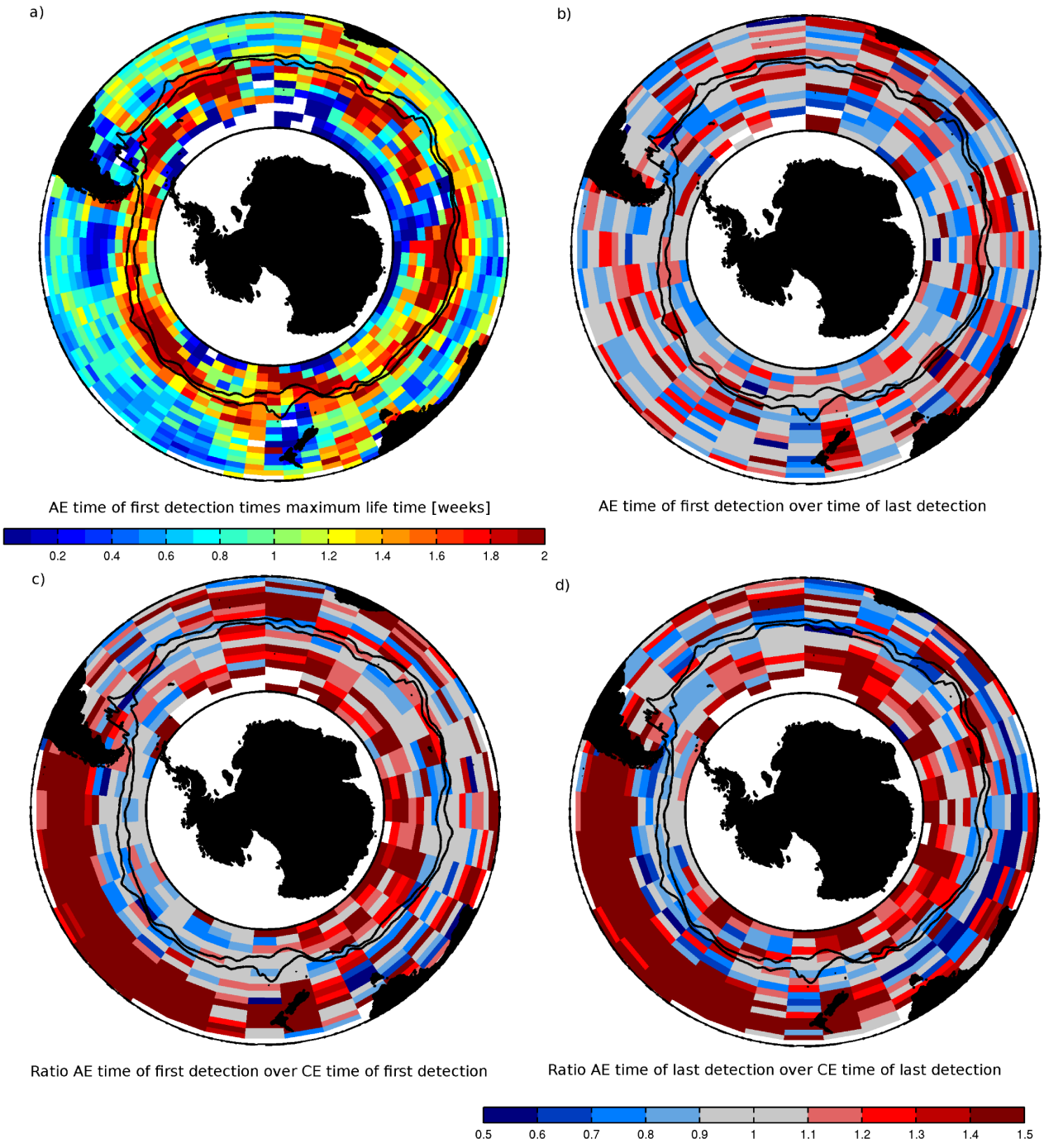

Figure 2.6.: Eddy generation and dissipation; *binned in $2° \times 1°/5° \times 2°$ grids* ***a*** *number of AE detected the first time times their maximum life time,* ***b*** *ratio of* ***a*** *over number of AE detected the last time times their maximum life time,* ***c*** *ratio of* ***a*** *over the same for CE and* ***d*** *ratio of* ***b*** *over the same for CE; main fronts are shown again as black contours.*

et al. (2010). We can give no evidence for this here, mainly because we miss a large fraction of the long-lived gyre AE (they are north of our domain or "leave" it while they are migrating westward).
We now focus on the formation and dissipation regions of CE. As they to first order are similar as the ones of AE, we only touch on the discrepancies (Figure 2.6c, d). The latter must be present as the existing dominance of absolute numbers of one polarity over the other (section 2.4) arises (as noted before) either from a larger formation of one polarity and/or from a quicker dissipation of the opposite polarity.
The pattern of polarity dominance in formation and dissipation areas actually looks similar as the one of polarity dominance of the total number of eddy events (Figure 2.4): the subtropical regions, but specifically the South Pacific stand out as areas of dominance of AE formation and dissipation. And so does the region south of the ACC, however this is less robust due to the small number of detected eddy events. The ACC is an area of a slightly larger number of CE generation and dissipation (if weighted by lifespan). The dominant areas of AE are already visible in the maps not weighted by lifespan (not shown) but intensify when weighted by the maximum age. This means that more AE form in general, but they are also more long-lived than the CE, thus they dissolve not as fast. In contrast (as mentioned) the dominance of the CE emerges in the vicinity of the ACC only when the formation and dissipation numbers are weighted with the lifespan. Thus, the total number of CE generated is not necessarily larger, however the CE dissipate not as quickly.
Why would one polarity be "preferred" with respect to dissipative processes? Regarding to CE, this could be related a larger total energy which makes them live longer if a uniform/steady dissipation is assumed. Additionally, the greater intensity of CE makes them also less vulnerable to the aforementioned shear suppression as path of energy loss. If only the eddy intensity, i.e. EKE mattered, one would expect a generally longer lifetime for CE. Surprisingly though, AE tend to live longer in the quiescent subtropical areas. Thus, it appears an eddy "energy drainage" other than linked to their kinetic energy must be at work, for instance air-sea interactions damping the eddy. Indeed, SST anomalies of CE are somewhat larger than of AE north of the ACC. This could hint towards surface intensified CE as found by Chaigneau et al. (2011) for the Humboldt upwelling system which are more susceptible to damping by the atmosphere. This contrasts the eddy T/S profiles (see section 2.3.4.2) which does not indicate a surface-intensification of CE. To clear up the picture, it could help to separate the long-lived CE forming next to Australia as they show for CE untypical *positive* SST anomalies as they propagate southward.
Closing, we can not draw conclusions about the pathways of the mesoscale energy to dissipation. The major pathways of dissipation of mesoscale energy in the ocean are still unclear (Ferrari and Wunsch, 2009). Dissipation at the ocean bottom, internal waves and surface ocean submesoscale frontogenesis related to the eddies are possible candidates. Eddies rubbing at the bottom (bottom friction) is a major candidate (Ferrari, 2011; Whalen et al., 2012; Nikurashin et al., 2012) as surface dissipation at fronts appear to contribute only $O(10)\%$ (Ferrari, 2011) and eddies may cause significant velocities at the ocean bottom (Adams et al., 2011; Liang and Thurnherr, 2012; Nikurashin et al., 2012). This could especially be the case in the deep reaching ACC

where eddies are thought to close the momentum budget by vertical momentum transfer in the fist place and eddies were found to be particularly deep reaching (Petersen et al., 2013).
A last issue we like to discuss in this context is the eddy-lacking areas. To some extent, these areas are lacking also intense currents able to shed eddies and advect them along their way into these areas, thus they are areas missing the major eddy generation process. The question is more why these areas are no eddy graveyards either. One would expect that a fraction of the eddies would leak from the influence area of strong currents, "wander about" with their intrinsic propagation speed and direction (see Chelton et al., 1998), and subsequently migrate also into eddy-lacking areas. The latter are indeed in reachable distance of areas featuring eddy populations (for instance eddies forming next to the South American coast). As the ACC is strongly topographically steered and eddies are in turn advected by the current (Fu, 2009), it is not trivial to separate between eddy advection and direct topographical steering. Yet, it seems that some eddies are steered by topographic contours directly (see again Figure 2.2, e.g. the CE in the Argentine Abyssal Plain or Chatham Island). This would necessitate them extending below the thermocline and them being rigid (alike a Taylor column, Hogg, 1973; Johnson, 1977; Velasco Fuentes, 2009); also, solid-body rotation is suggested by CSS11 due to homogeneous vorticity in the eddy core). In-situ measurements have frequently found deep reaching eddies (for instance Agulhas rings reaching as deep as 4000 m, Van Aken et al., 2003, or ACC eddies, Swart et al., 2008) and also semi-stationary eddies related to topography, "eddy-Taylor-columns" (Boehlert, 1988; Meredith, 2003; Bigorre, 2005). And again, this would fit the idea of eddies "rubbing off" at the sea floor (De Steur and Van Leeuwen, 2009; Ferrari, 2011).

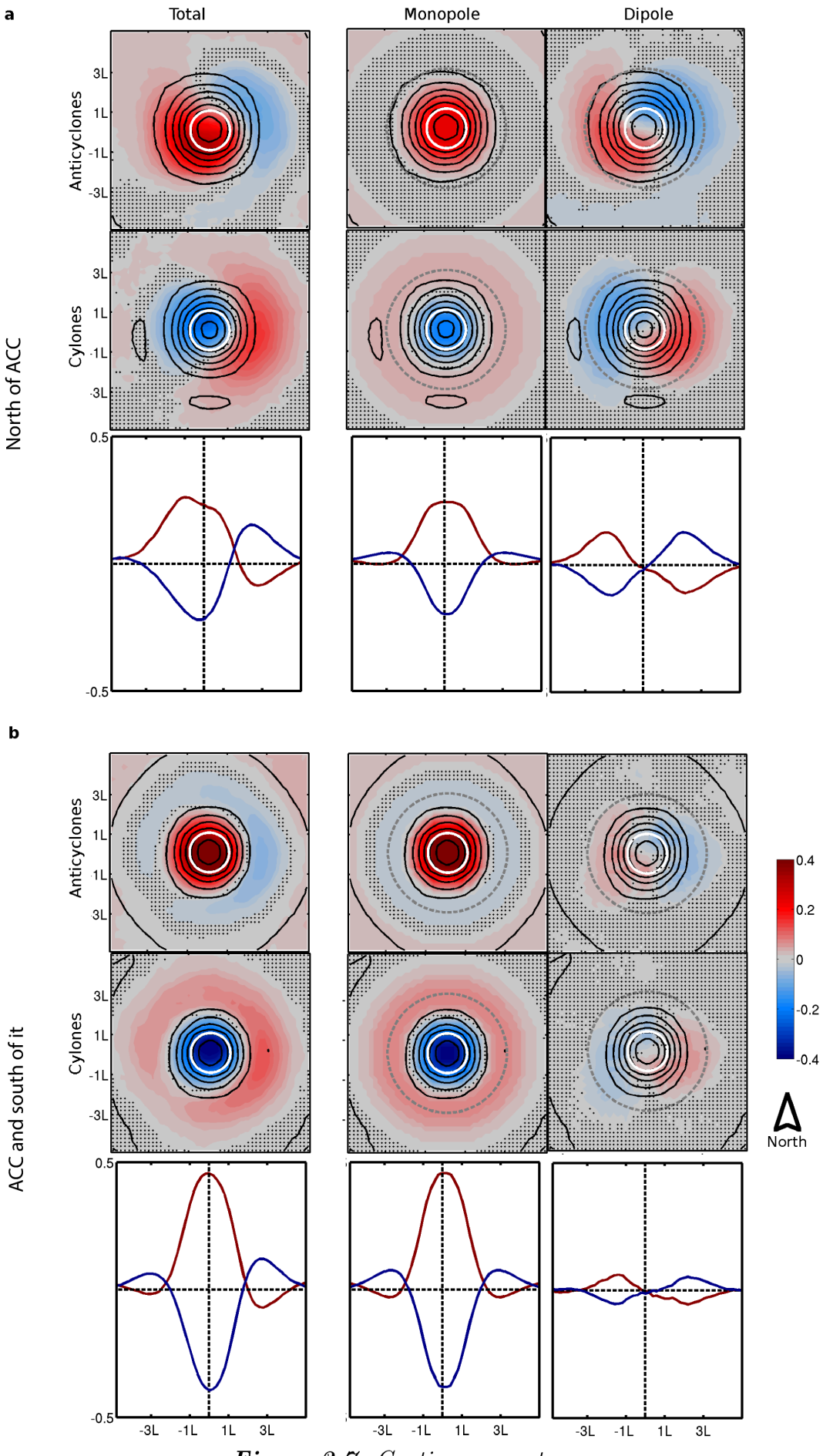

***Figure 2.7**: Caption on next page.*

Figure 2.7.: Average two dimensional structure of eddies at the surface; a *north and* ***b*** *south of the -10 cm SSH contour; colors denote the* SST *anomalies, black contours the* SLA *contours (before averaging they were normalized with the maximum* SLA *anomaly for each eddy, contours in 0.05 levels), white circle marks the eddy's center as detected with the* OW*, gray dashed line three eddy radii; stipplings are areas outside the x confidence level; the monopole was calculated by radial averages around the eddy center, the "dipole" is the remainder if the monopole is subtracted from the total (total=monopole+dipole); the third panel in a) and b) are east-west cross sections through the eddy's core.*

2.3.4. Three-Dimensional Structure of the Average Eddy

2.3.4.1. Appearance at the Sea Surface

We change in this paragraph from treating eddies as point features to an examination of the three dimensional structure of the average eddy. Again, we distinguished by polarity and eddies occurring north versus south of the -10 cm SSH contour. First, we resolved the horizontal structure of the mean eddy as detected at the surface. To this end, we cut out all identified eddies from weekly maps of *SLA* as well as *SST*. The size of the extracted rectangle is five mean diameters (10 radii) containing the core of the eddy at the center. This is certainly a large enough area to include the eddy's impact on its surroundings. The choice of the extracted area around the eddy measured by eddy radii implies an implicit standardization according to the length scale of the individual eddy. For the *SLA*, we standardized additionally with the maximum anomaly of the individual eddy as we are here interested in the typical eddy-shape instead of quantifying the eddy's amplitude as done in Section B.2. Finally, we averaged over all eddies.

The resulting Figure (Figure 2.7, black contours) shows a basically axisymmetric eddy (as found by CSS11). Vortices tend to relax back to an isotropic shape after incidents of deformation for instance caused by shear flow (Melander et al., 1987). Again as CSS11, we find an approximately Gaussian shape. An alternative fit by CSS11 is a quadratic which would imply a more homogeneous core with respect to vorticity resulting in solid-body rotation. Also Oh and Zhurbas (2000) argue for the eddy consisting of a core of solid-body rotation and a larger peripheral ring with velocities leveling of in a relatively long tail. It becomes obvious from Figure 2.7 that the eddy edge as detected with the *OW* parameter clearly marks purely the eddy core. The eddy and its influence on the surrounding extents from the center at least double the radius of the eddy core. It appears that eddies north of the ACC feature closed contours of *SLA* beyond two of the core-radii whereas eddies related to the ACC impact their surroundings up to two radii "only". Thus, eddies in the southern subtropical gyres feature not only larger cores (as shown in section B.2) but a greater "length scale of impact" relative to their core-size the same time. Likely, this is due to them propagating through a more quiescent SSH environment.

The extension of the eddies' impact beyond the *OW*-core becomes clear also when examining the *SST* anomaly related to the eddy (Figure 2.7, colors). AE (CE) feature

positive (negative) *SST* anomalies of several $^1/_{10}$ °C (Figure 2.7, left column) where the *SST* anomalies are generally more pronounced in the ACC area relative to the north of the ACC. A systematic lag between the eddy and the *SST* anomaly exists (east-west section shown in Figure 2.7, lower panel in a and b), which is smaller in the ACC compared to north of it. Hausmann and Czaja (2012) found the same and explained the feature with the nearly pure westward propagation of eddies in low-energetic areas in contrast to the much more complex propagation pattern in areas of intense mean currents such as the ACC. We add here an additional possible explanation for the lag. To this end, we separate the *SST* anomaly associated with the center of the eddies from the remainder. We do this by taking the radial average relative to the eddy's center. This returns a monopole (Figure 2.7 middle column). The residual (Figure 2.7 right column) shows a surprisingly symmetric dipole. This dipole reflects the sense of rotation of AE (CE) which is anticlockwise (clockwise) in the southern hemisphere. One can hypothesize now that the monopole anomaly is due to the trapped fluid in the core of the eddy. It is larger in the ACC than north of it which is consistent with eddies exhibiting higher swirl velocities and accordingly are more likely able to trap fluid. The dipole is more prominent north of the ACC which results in the apparent larger phase shift of *SLA* and *SST* there (Hausmann and Czaja, 2012). A larger and smaller large-scale *SST* gradient eddies are embedded in could explain the larger and smaller dipole of eddies north and in the ACC, respectively. As noted before, north of the ACC eddies exhibit a larger periphery around the inner core where they impact the adjacent waters with their rotation. Additionally, their surrounding waters are less disturbed by neighboring eddies/mesoscale features (as these regions are more quiescent). Thus, the "environmental conditions" in combination with the eddies' "rotational length scales" could result in the larger dipole signal.
An additional complicating aspect noted by Chelton et al. (2011b) is that eddies perturb the temperature field as they propagate through it. Thus, the trailing side (here right side) of the eddy may feature a smaller tracer anomaly as it distorts an already perturbed tracer field. Whereas the leading side of the eddy impacts an assumed unperturbed one. As the eddy is propagating this leading side anomaly might be entrained into the eddy-core. The contribution of this effect to the *SST* pattern related to eddies is difficult to quantify based on the satellite data. However, the fact that the average absolute value of the *SST* signal related to the eddy-core is larger than the *SST* in the eddy-periphery impacted by the eddies' rotation (not shown) supports the hypothesis that the origin of the *SST* anomaly related to the eddy-core is the trapping effect. This is supported by Early et al. (2011) whose results based on idealized model simulations show a strong trapping of an eddy in addition to a continuous exchange of fluid with the surrounding at the eddy's periphery.
A side note here: if the *SST* anomalies related to eddies are examined on a map (not shown), there are exceptions to CE featuring negative *SST* anomalies: the prominent CE southwest of Australia exhibit a positive temperature anomaly at the surface as they are migrating southward. This is potentially due to a "warm cap" induced by additional solar energy input not uncommon for CE (in contrast, it takes longer for AE to loose energy by longwave radiation). Even though this is not essential for the southward oceanic heat transport caused by the eddies, it is determining for the ex-

change with the atmosphere. Hence, with regard to eddy identification on the basis of *SST* (Fernandes et al., 2011; Dong et al., 2011) and concerning impacts of eddies, one can not by default relate anticyclonic and cyclonic eddies with a positive and negative temperature anomaly at the surface, respectively.

2.3.4.2. Subsurface Structure

If one is interested for instance in transport caused by eddies one may want to know if the *SST* signature is representative for the general anomaly/vertical structure of the eddy and about the vertical extent of eddies. Hence, we investigate some of the vertical structure of SO eddies. For the objective of retrieving information on the vertical structure of eddies, we obviously cannot rely on the ocean surface information obtainable from satellite but need to use in-situ observations. We used data from *Argo* floats which collect temperature and salinity data down to approximately 2000 m depth (see Section 2.2.1).
The anomaly profiles, again separated by polarity and position relative to the ACC reveal that eddies extend down to as deep as 2000 m. The major anomaly persists down to 500 m (ACC) or 1000 m (north of the ACC) (Figure 2.8a, upper panel). An extent of eddies much deeper than the thermocline has been found in various in-situ studies based on floats or on data collected with research vessels (Keffer and Holloway, 1988; Ansorge et al., 2009; Morrow, 2004; Chaigneau et al., 2011). Secondly, the maximum anomaly for eddies north of the ACC is on average not located at the surface but at depth (Chaigneau et al., 2011). Thereby, the maximum of CE is located lower in the water column than for AE (in contrast to the findings of Chaigneau et al., 2011, for southeast Pacific eddies) (300 - 500 m versus 100 - 300 m).
Contrarily, eddies of both polarities in the ACC are surface intensified (Figure 2.8a, lower panel). Thus, the larger temperature anomaly of ACC eddies at the surface in contrast to eddies north of the ACC does not hold at depth, i.e. *SST* can be a misleading proxy for the integrated temperature anomaly for subtropical eddies. It is somewhat anticipated that this is the case in the stratified subtropical gyres, whereas the ACC area is weakly stratified and also intensely mixed by strong winds. A factor determining the vertical structure of eddies is their generation mechanism. Chaigneau et al. (2011) hypothesize the interaction of overlying vertically sheared boundary currents as the origin for the southeast Pacific eddies.
The salinity profiles reveal a major salty and fresh anomaly for AE and CE, respectively. The maximum salt anomalies are located at similar depths as the temperature anomalies. However, the general shape of the temperature and salt profiles differ slightly with the salinity anomaly extending not as deep as temperature anomaly. This may be due to systematically different climatological hydrographic conditions at the eddy's origin compared to the location where the profile was measured, as local climatological conditions were used to calculate the anomaly profiles of an eddy.
To calculate the volume of trapped water, we compute the depth to which the eddy is nonlinear (Flierl, 1981). As *Argo* floats do not provide current velocities, we assume geostrophy and calculate the geostrophic velocities based on the T and S anomalies.

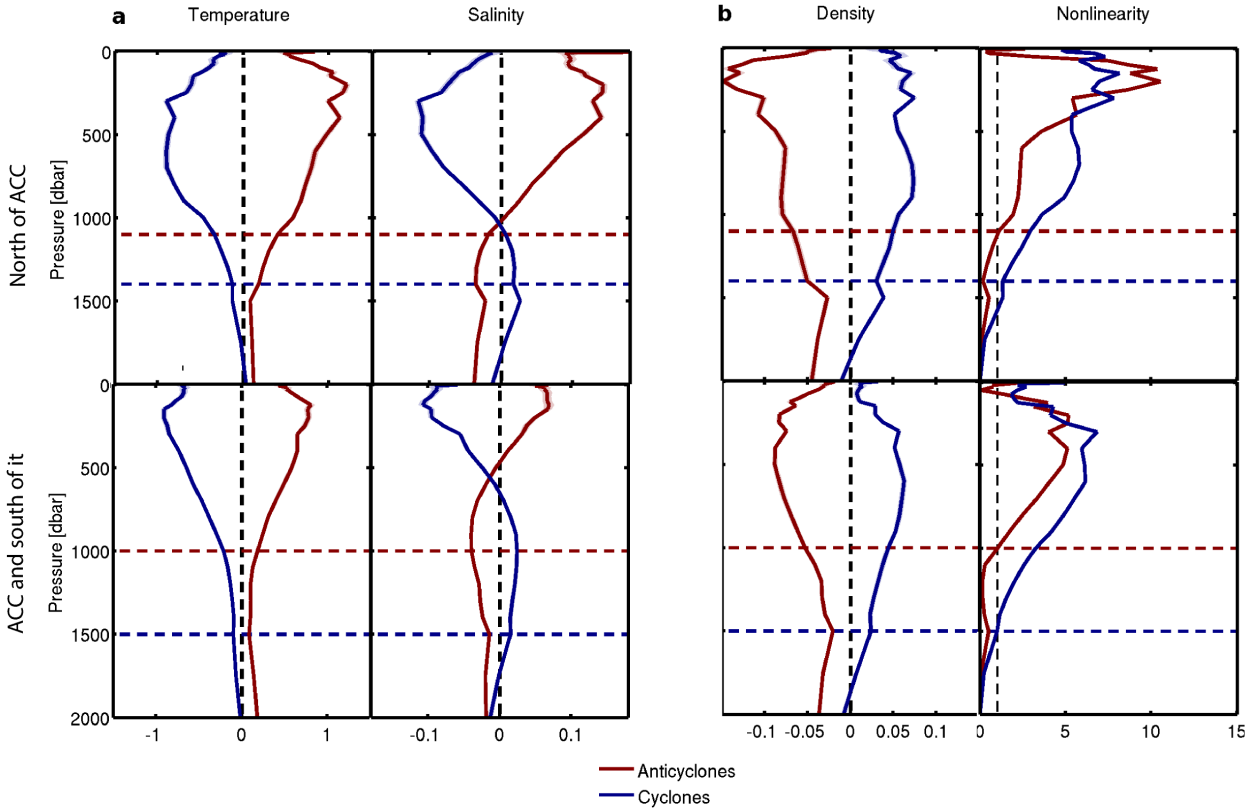

Figure 2.8.: Mean anomaly-profiles from* Argo *floats; a *temperature and salinity and* ***b*** *density and nonlinearity derived from* ***a****; upper row north of the -10 cm SSH contour and lower one south of it; dashed lines mark the level down to which fluid is trapped.*

We chose 2000 m as the level of no motion, thus assuming the eddies' velocities approach zero at this level. Then, we calculate the vertical change of the density anomaly related to the eddies (see Figure 2.8b derived from T and S and EOS-80) which further relates to the baroclinic velocity. Assuming a mean propagation speed of 0.4 m/s of eddies (as Chaigneau et al., 2011, which is very similar to our estimate), we can derive the vertical profile of nonlinearity. We arrive at 1100 and 1500 m as the trapping depths for AE and CE, respectively.

2.3.5. Integrated Meridional Heat and Salt Transports

The southern part of the SO experiences a net heat loss and fresh water surplus. Next to northward Ekman transport eddies are thought to be important for the meridional transports of buoyancy. With the information on numbers of eddies, their associated heat and salt anomalies and trapping depths, we can derive an estimate of the yearly meridional heat and salt transports across the PF.
To this end, we calculate heat and salt anomalies of the average AE and CE along the PF (profiles up to 1° distant from the front), and multiply with the average number of eddies crossing the front. The available heat anomaly of the mean eddy is calculated as AHA$= \rho c_p V \Delta T$, with V the eddy's volume calculated with the mean diameter and the trapping depth, ΔT the heat anomaly associated with the mean eddy, a density of

$\rho = 1000$ kg m^{-3} and a heat capacity of $c_p = 4000$ J kg^{-1} K^{-1}. Similarly, the available salt anomaly is computed as ASA$= \rho \Delta S \times 0.001$, with ΔS the salt anomaly associated with the mean eddy.
The resulting transports due to *trapping* are $O(10^{-2})$ PW and $O(10^5)$ kg s^{-1} and relatively small. They constitute about $^1/_{10}$ and $^1/_{100}$ of the heat and salt transport necessary to compensate for the heat loss and fresh water surplus south of the PF.
Our numbers of heat and salt anomalies of an individual eddy are somewhat large compared with in-situ studies (see Table 2.1), but for AE around the PF where we find a net negative ASA. The resulting meridional transport (southward heat and salt transport) roughly agrees with previous in-situ estimates (if approach a is chosen for the number of eddies crossing the front, see Table 2.1). Also, we agree with Hausmann and Czaja (2012) who calculated eddy heat transport due to *trapping* at the latitudes of the ACC. They found in the same study that the advective transport due to *stirring* is an order of magnitude larger then the one due to *trapping*. Thus, *stirring* appears to be the dominant transport mechanism of eddies and appears to be of the magnitude (for heat) which compensates for the heat loss in the southern SO Hausmann and Czaja (2012). However, it has been pointed out recently that "standing eddies", i.e. the time mean meridional geostrophic flow may compensate for a large fraction of the heat loss in the southern SO Olbers et al. (2004); Dufour et al. (2012).

Study/location	Single eddy anomaly				Upscaled/integrated transport estimate
	Anticyclones		Cyclones		
	AHA [10^{19} J]	ASA [10^{11} kg]	AHA [10^{19} J]	ASA [10^{11} kg]	
Joyce et al. (1981)/Drake Passage, from PF			−1.2	−2.5	
Rae et al. (1996)/Agulhas Rings	+5.5	+35			-0.007 PW, -14-21×10^{12} kg yr^{-1} (=444-466×10^3 kg s^{-1})
Morrow (2004)/South of Australia, PFZ (from PF)			−5.6±1.5	−8.1±1.5	−16.8×10^{19} J and −24.3×10^{11} kg, annual, local (=0.0053 PW and 77.1×10^3 kg s^{-1})
Morrow (2004)/South of Australia, SAF (north of it)			−1.9	−8.2	-0.04 PW
Swart et al. (2008)/South of Africa	+5.4				
This study/SAF	+20.0	+4.9	−21.2	−36.5	−0.01 PW/−209.1×10^3 kg s^{-1a}, -0.01 PW/−79.0×10^3 kg s^{-1b}
This study/PF	+5.3	−30.9	−24.3	−25.9	−0.03 PW/−229.2×10^3 kg s^{-1a}, -0.01 PW/−45.1×10^3 kg s^{-1b}

Table 2.1.: Mean eddy heat (AHA) and salt (ASA) anomalies from in-situ studies and integrated numbers of T ***and*** S ***transports northward across the PF by eddies****; according to (De Szoeke and Levine, 1981; Walkden et al., 2008) 0.45 PW heat are lost to the atmosphere south of PF; Joyce et al. (1981) (from Gordon and Taylor, 1975) have an estimate of 0.4 PW and* 10^7 *kg* s^{-1}*; superscript a denotes the northward transport across the PF if one considers eddies originating at one and dissipating at the other side of the front, and superscript b denotes the transport considering each single crossings of eddies across the front.*

2.4. Summary and Conclusions

We provide the first regional study of mesoscale eddies in all of the SO based on a Lagrangian approach. We did this based on *SLA* data of multiple simultaneous altimeter missions resolving scales of $O(100)$km and covering more than a decade. By tracking eddies over their life time we assembled an eddy dataset for the area south of 30°S. Next to eddy characteristics such as diameters, amplitudes, propagation velocities as presented by the global study of CSS11, we did further analyses on eddies, for instance on their seasonality and subsurface structure. Our major findings are the following (partly summarized in Figure 3.1):

- The dynamic areas of high SSH gradients in the SO are covered by eddy-cores more than 30% of the time; if one includes the influence area of eddies ("peripheral area"), the coverage easily doubles.

- The dynamic areas are also regions of both, high rates of eddy generation and eddy dissipation.

- *Eddy deserts* are the southeast Pacific and waters over topographical plateaus along the ACC pathway. The area in between the major fronts of the ACC shows a noteworthy reduction of eddy occurrences, relative to the northern and southern flank of the ACC.

- The temporal variability of eddy occurrence in general is much smaller than the spatial one; the temporal variability is larger in the ACC than in the boundary currents north of the ACC, with local temporal standard deviations of eddy-incidences between 10% and 20%.

- Regions of polarity dominance exist: the southern subtropical gyres are generally dominated by AE, whereas the northern flank of the ACC is dominated by CE.

- Based on the analysis of the surface imprint of eddies on temperature, we found a combination of the *trapping* and *stirring* effect of eddies to act on tracers. The former is associated with the eddy's core, the latter with the eddies periphery which is in continuous exchange with ambient waters (see also modeling study by Early et al., 2011).

- Subsurface information on eddies based on *Argo* floats shows major temperature and salt anomalies down to 500 to 1000 m depth and trapping depths of more than 1000 m; eddies in the vicinity of the ACC appear to be slightly shallower than eddies north of the ACC.

- With this data we could provide an estimate of heat and salt transports across the ACC due to the eddies' *trapping* effect. Our result shows southward heat and salt transports which are about $^1/_{10}$ and $^1/_{100}$, respectively, of what is necessary to compensate for the surplus of freshwater and heat loss south of the PF.

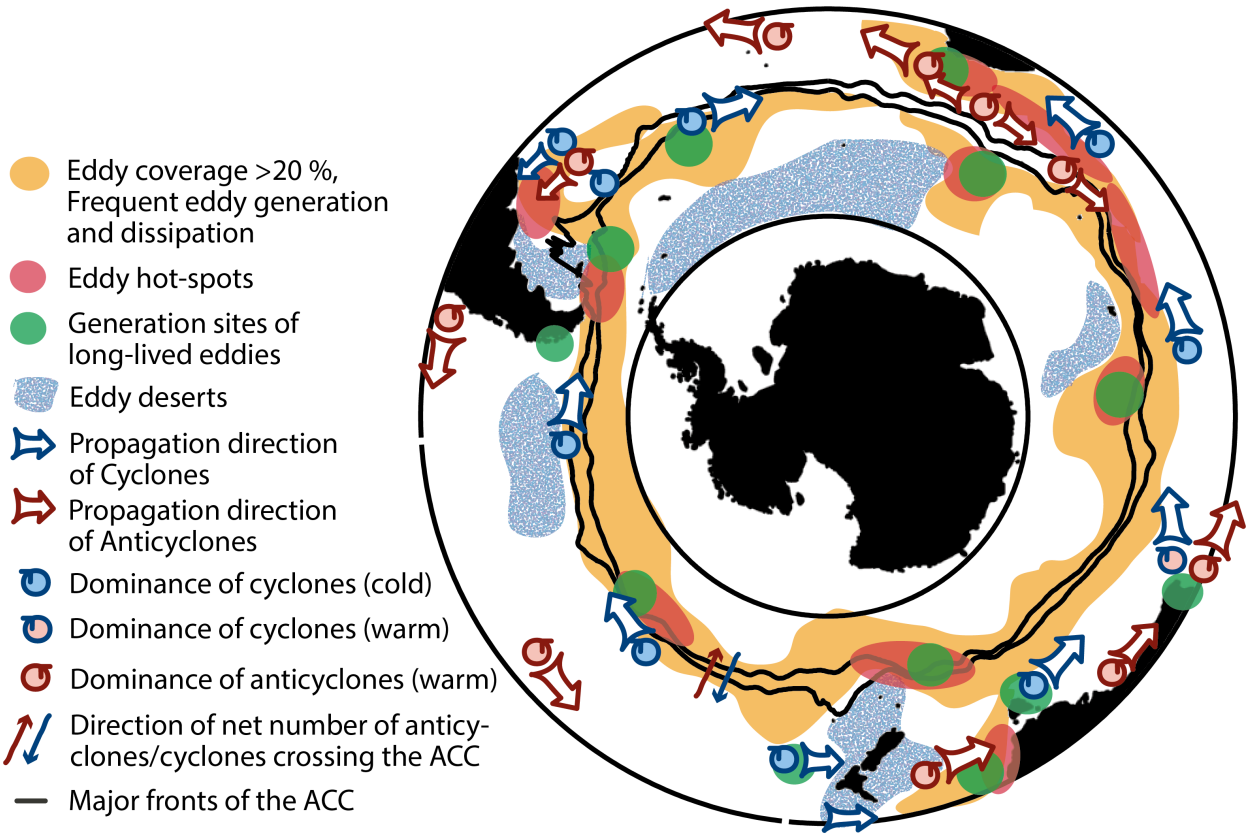

Figure 2.9.: Summary of major findings with respect to SO eddies.

The major drawback of this work are results which are dependent on the tracking algorithm, as these are less robust than the ones based only on eddy detection; this concerns for instance generation/dissipation locations as well as lifespans and propagation directions. Having said that, we believe the tendencies of our results to be robust. There are several implications of our findings. Eddies are frequently investigated in terms of EKE but it is not differentiated by polarity. Dependent on the context and the question asked we believe it may be of importance to consider the inhomogeneous distribution of AE and CE. We note that one may not be able to determine an eddy's polarity by solely relying on *SST* information, which is of importance for *SST* based eddy detection. Further, the extent eddies are able to trap fluid is vital for non-local effects of eddies. *Trapping* is not accounted for in parametrizations of eddies in coarse resolution numerical models.

The Lagrangian approach to examine eddies has become more widely used in the last decade. It provides plenty of possibilities for further research on ocean eddies. One interesting aspect would be to closely examine eddy "graveyards" to get more information on dissipation mechanisms. Also, one may examine vortex interaction, such as merging and splitting which frequently happens especially in the highly dynamic regions. Further, one could investigate the temporal variability and trends of eddies on longer time scales, i.e. years to decades. In combination with the impacts of eddies, such as their transports, this could be of importance with respect to impacts of climate change. The last issue to be mentioned here is that one could investigate the eddies'

impacts on their environment. Examples of these are given in Chapter 3 and 4.

Acknowledgments

The altimeter products used for this study were produced by Ssalto/Duacs and distributed by Aviso, with support from Cnes (`http://www.aviso.oceanobs.com/duacs/`). The *chl* and *cf* used were processed and distributed by ACRI-ST GlobColour service, supported by EU FP7 MyOcean & ESA GlobColour Projects, using ESA ENVISAT MERIS data, NASA MODIS and SeaWiFS data. QuikScat data are produced by Remote Sensing Systems and sponsored by the NASA Ocean Vector Winds Science Team. Data are available at `http://www.remss.com`. These data were collected and made freely available by the International *Argo* Program and the national programs that contribute to it. (`http://www.Argo.ucsd.edu`, `http://Argo.jcommops.org`). The *Argo* Program is part of the Global Ocean Observing System.

3. On the Impact of Southern Ocean Eddies on Biology

In preparation for Journal of Geophysical Research – Oceans.

The Southern Ocean (SO) is a region of intense eddy activity and high spatio-temporal variability of phytoplankton biomass, yet the long-term mean influence of eddies on phytoplankton is essentially unknown. Eddies are expected to impact the distribution of phytoplankton by modifying lateral transport (eddy stirring and advection) as well as by changing the environmental conditions that are vital for phytoplankton growth (vertical mixing, up- and downwelling). We investigated the long-term mean association of SO eddies and variations in phytoplankton biomass by tracking more than 100,000 eddies in the SO over 14 years, and determining the changes in phytoplankton biomass using satellite based chlorophyll-a (*CHL*) measurements as a proxy. Our findings reveal significant eddy-related *CHL* anomalies in the long-term mean with magnitudes of more than ±10% over large areas of the SO. The anomalies have a zonal structure with positive anomalies north of the Antarctic Circumpolar Current (ACC) and negative anomalies within the circumpolar belt of the ACC and south of the ACC for cyclonic eddies. The pattern is similar but of opposite sign for anticyclonic eddies. The seasonality of the eddy-related *CHL* anomalies is weak north of the ACC whereas it is pronounced in the vicinity of the ACC. The distinct spatial structure and seasonality of the long-term mean *CHL* anomalies associated with SO eddies is consistent with the dominant mechanisms being advection of trapped properties within each eddy as well as local stimulation of phytoplankton growth, with stirring due to rotation of eddies being of secondary importance.

3.1. Introduction

Mesoscale ocean eddies have been shown to impact biology, especially phytoplankton. The SO is an area of high eddy activity. With this study we examine the large-scale long-term impact of SO eddies on phytoplankton biomass taking chlorophyll-a (*CHL*) as a proxy.

The SO is a special area with respect to biology: light and micro-nutrient (iron) limitation of phytoplankton south of approximately 40°S contrast nitrate limitation at lower

latitudes further north, i.e. the SO is largely a high-nutrient-low-chlorophyll (HNLC) area. It shows a strong seasonality of *CHL* depending on the availability of light and iron. The latter is assumed to be provided largely by atmospheric dust as well as sediment input. In addition, the SO is also an area of large spatial gradients of *CHL*. These gradients provide the potential for an efficient stirring and transport effect by eddies.

The association of eddies and ocean biology (and not only for the lowest trophic levels) has been found frequently from in-situ studies, with only a few studies mentioned here: grey-headed albatross and fish was detected to forage in eddies (Nel et al., 2001; Godøet al., 2012); McGillicuddy et al. (1998) found eddies in combination with winds to stimulate phytoplankton blooms in the Sargossa Sea; Xiu et al. (2011) and Peterson et al. (2011) investigated *Haida* eddies in the northern Pacific and concluded that they might be important for iron supply in the ocean beyond the shelf area, and in addition exhibited enhanced production at their edge. Bernard et al. (2007) and Ansorge et al. (2009) found eddies in in the SO whose biographical provenance was clearly from a different SO zone, demonstrating the advective effect of eddies. Lehahn et al. (2011) followed an Agulhas ring and its *CHL* for several months based on satellite observations, pointing out that it carried along a *CHL* anomaly originating from the time of its formation. There exist also studies based on remote sensing and modeling results which point out the advective effect of eddies (e.g. Oschlies, 2002; Dandonneau et al., 2003; Siegel et al., 2011; Chelton et al., 2011a).

As phytoplankton forms the base of the food web, it is of general interest to investigate the factors impacting it. It contributes about half to global primary productivity even though it comprises only about one percent of the global photosynthetic biomass (Field, 1998; Falkowski, 2012). The latter is due to its quick turnover time. Phytoplankton only lives a couple of days, then it dies or is being grazed. With a fraction of its biomass accumulating in higher trophic levels it is critical eventually also for fisheries. With another (the larger) fraction of its left overs being quickly recycled in the (surface) ocean, phytoplankton forms an integral part of global biogeochemical cycles and even determines the biogeochemical composition of the ocean (Redfield, 1958). This is of special interest in the SO with its importance for global biogeochemistry.

Indications based on satellite observations that mesoscale structure in the ocean affect phytoplankton were already found by Gower et al. (1980). They found patterns of a north Atlantic phytoplankton bloom to trace mesoscale features from a LANDSAT multispectral scanner images of 1976. Later, satellite derived maps of *CHL* in the oceans were combined with physical properties, with the objective to explain the spatial and temporal variability of *CHL* with physical variables (Comiso et al., 1993; Kahru et al., 2010), one of these variables being sea level anomalies (*SLA*). The relation of *CHL* and *SLA* has been noticed more than a decade ago (Cipollini et al., 2001; Dandonneau et al., 2003; Doney, 2003), however this was initially attributed to planetary waves similarly propagating westward in the ocean gyres as mesoscale eddies. A major reason for this being that the satellite based *SLA* where not yet resolving the mesoscale sufficiently. With the propagating features defined as eddies, the link to the concurrently westward propagating *CHL* pattern could be made: it was suggested that the covariability of westward propagating *SLA* and *CHL* in the low and mid latitudes

was mainly due to mesoscale eddies (Chelton et al., 2011a).
More than one mechanism exists how eddies may affect phytoplankton. Phytoplankton is barely able to actively move. Thus, it cannot choose where it lives but is passively advected by the motions in the ocean inevitably subject to the environmental conditions provided in its surroundings. Phytoplankton thrives where these conditions are favorable and perishes where they are not. The factors determining the well-being of phytoplankton are nutrient and light conditions, competition with other species and grazing pressure. Furthermore, phytoplankton is affected by being advected, dispersed and accumulated by the ambient flow. Indeed, ocean mesoscale eddies can impact phytoplankton by all of these mechanisms: they advect due to their rotation and propagation, they disperse, and they may modify phytoplankton growth as they may change the supply of nutrients either by lateral advection or from deeper ocean layers by lifting the nutricline. Furthermore, they may provide ecological niches in their core where phytoplankton may escape competition or foraging by zooplankton.
Here we quantify the imprint of mesoscale SO eddies on *CHL* based on satellite observations, and discuss potential mechanisms for this imprint. The paper is organized as follows: in Section 3.2 we provide information on the data and methods used, show our results in Section 3.4 where we first examine the relations of eddies with *CHL* (Section 3.4.1) and thereafter examine the potential mechanisms (Section 3.4.3) playing a role thereby.

3.2. Methods

3.2.1. Data

We use the same data set of Southern Ocean eddies and their characteristics as in Chapter 2 (Section 2.2), whose retrieval we describe in detail therein. The data set contains about 1,000,000 snapshots of eddies. We consider all data between the 30°S to 65°S latitude band, and from September 1997 to March 2010. This is the overlapping time period for sea level anomalies *SLA* and *CHL*.
For *CHL* we used the merged ESA GlobColour Project product (`http://www.globcolour.info`, case-1 waters and merged according to Maritorena and Siegel, 2005) with a spatial and temporal resolution of 0.25° and one day, respectively. We chose a merged product for *CHL* as the merging on average doubles the spatial coverage of the daily data (Maritorena et al., 2010). Of the data of up to three available sensors, SeaWIFS (SeaStar), MODIS (Aqua) and MERIS (Envisat), SeaWIFS data generally features the best spatial coverage but its contribution drops below 40% in high latitudes and partly in the western ocean basins of the Southern hemisphere. For these areas, SeaWIFS data is complemented with MODIS as well as MERIS data. Due to *CHL* being lognormally distributed (Campbell, 1995), we log-transformed *CHL* for all analyses. We averaged the daily CHL data to weekly fields to match the temporal resolution of the eddy dataset.
To examine the *CHL* anomalies of eddies (ΔCHL), we compared their related *CHL* data to background fields of *CHL*. *CHL* is temporally and spatially very variable, a

monthly climatology of *CHL* proved not to be appropriate as a background field. We obtained the latter the following way: we applied a moving spatio-temporal Gaussian filter (Weierstrass transform, spatial filter similar to e.g. Siegel et al., 2008, with 2σ of 10 boxes/∼200 km at 45°S, 8 boxes/∼200 km and 1 week in longitudinal, latitudinal and temporal dimensions, respectively) to each of the weekly *CHL* fields. We then subtracted the resulting from the original fields to produce ΔCHL fields. The resulting ΔCHL fields were found to be not sensitive to the selected σ. Due to our choice of a rather small filter, our estimate of ΔCHL related to eddies is a conservative one.
As AE and CE frequently show a *CHL* signal of opposite sign. For reasons of clarity, we only describe the signals related to the one polarity in these situations. As mentioned before, all analyses were done using log-transformed *CHL*, however eddy anomalies in the figures are frequently given in percentage change with *e* and *bg* denoting *eddy* and *background*, respectively. I.e. ΔCHL represents the *CHL* anomaly in percent relative to the local background *CHL*. When we show absolute *CHL* in a logarithmic scale, it is the common (base 10) logarithm. Regarding the spatial, i.e. geographical analysis, we used on the one hand the positions of the main ACC fronts (Polar Front, PF, and Sub Antarctic Front, SAF) for geographical analyses as determined by Sallée et al. (2008). On the other hand, we made use of a climatology of sea surface height contours (Maximenko et al., 2009) which are representative for the long-term geostrophic flow in the area. The mean positions of the PF and SAF align approximately with the mean SSH contours of about -40 cm and -80 cm, respectively.
We investigated the impact of eddies on biology in various "environmental conditions", As there is no temporally adequately resolved data available, we in addition used fields of monthly climatologies of nitrate (World Ocean Atlas 2009, available at http://www.nodc.noaa.gov) and mixed layer (based on Argo floats, available at http://www.locean-ipsl.upmc.fr). We collocated weekly QuikSCAT wind speeds with eddies (available at http://www.remss.com), and considered if the effect of eddies on *CHL* was related to the local water depth (ETOPO2v2 from NGDC, 2006).

3.2.2. Handling of Measurement Error and Data Gaps in Chlorophyll

As the error of the satellite retrieved *CHL* for each individual eddy can easily be as large as the anomaly related to the individual eddy, the significance of our results arises from the large number of analyzed eddies. Thereby the frequent cloud cover in the SO is an issue. The resulting missing values in the *CHL* data pose a challenge to the objective to extract the *CHL* signal related to eddies, especially since the latter is anticipated to be small (Siegel et al., 2011).
On average 45% of *CHL* values associated with eddies were missing. Missing values due to cloud cover-only (leaving aside irradiation changes) increase from 20% at 30°S to 60% at 65°S. Of all detected eddy events >30% and >20% feature none and 100% missing values, respectively. CE thereby show less events with missing values 100% as well as more events with 0% missing values. Thus, AE exhibit a higher percentage of data gaps than CE (47% versus 42%), which can be explained by the impact of ΔSST on cloud cover (see Small et al., 2008, and Chapter 4).

However, due to the large number of eddies we were able to track, the majority of our results are statistically significant at the 95% level. As the data is about normally distributed in the log-space, all significance estimates were based on simple t-tests.

3.3. Proposed Mechanisms of Eddies Impacting Chlorophyll and The Local Pattern of Their Chlorophyll Imprint

We distinguish four potential mechanisms of eddies impacting the CHL distribution, where two are due to lateral displacements of *CHL* by eddies and two are due to eddies modifying *CHL* by actually modifying phytoplankton growth (Figure 3.1). *Stirring* and *trapping* relate to the pure lateral redistribution of CHL by eddies. *Stirring* leads to a distortion of the large-scale CHL gradient caused by the rotation or swirl velocity of the eddy. *Trapping* describes the ability of eddies to transport along fluid in the core while they move. That eddies are able to trap fluid in their core can be seen from observations where eddies carry the signature of their origin in their core (e.g. Bernard et al., 2007; Ansorge et al., 2009; Lehahn et al., 2011) and is supported by the modeling study of Early et al. (2011). *Trapping* can occur if the eddies' swirl velocity is larger than their propagation speed relative to ambient water (Flierl, 1981). This is the case for eddies in the SO (Chelton et al., 2011b, see also Chapter 2).

The other two mechanisms of eddies affecting *CHL* by a modification of phytoplankton growth are associated with vertical displacements of isopycnals due to the eddy dynamics, i.e. geostrophic balance. Nutrients from deeper (nutrient-rich) unlit waters are brought up to the euphotic zone and used by phytoplankton or pushed down into unlit waters where phytoplankton can not thrive. Also, the exposure of phytoplankton to light may change due to vertical displacements of isopycnals.

AE lower, while CE lift isopycnals. If wind comes into play which interacts with surface currents of an eddy a convergence or divergence of Ekman transport occurs over the center of the eddy which results in Ekman pumping or suction. This mechanism has the opposite effect on isopycnals than the eddy has by itself, may potentially overcompensate it and result in lifted isopycnals for AE and suppressed isopycnals for CE (see also Chapter 1, Figure 1.3). There is an additional complicating factor concerning the "vertical" effect of eddies: it might depend on the life stage of an eddy. The process as illustrated is expected for a young eddy in the spin-up phase. However, effects may be opposite if an eddy is close to dissipating, i.e. if it is dying. In this case, isopycnals would relax, i.e. deepen for CE and lift for AE (leaving aside the interference of wind). An influence of eddies we do not consider here are submesoscale effects occurring at eddies' edges.

The effectiveness of *advection* by eddies of *CHL* on the one hand depends on the spatial scales of the horizontal *CHL* distribution, on the other hand on the time scale of *CHL* as a reactive tracer. The steeper the large-scale *CHL* gradient, the more effective is the eddy expected to be in advecting *CHL* into areas with ambient *CHL* of different magnitude. For *stirring* to operate the large-scale gradient must be noticeable at length

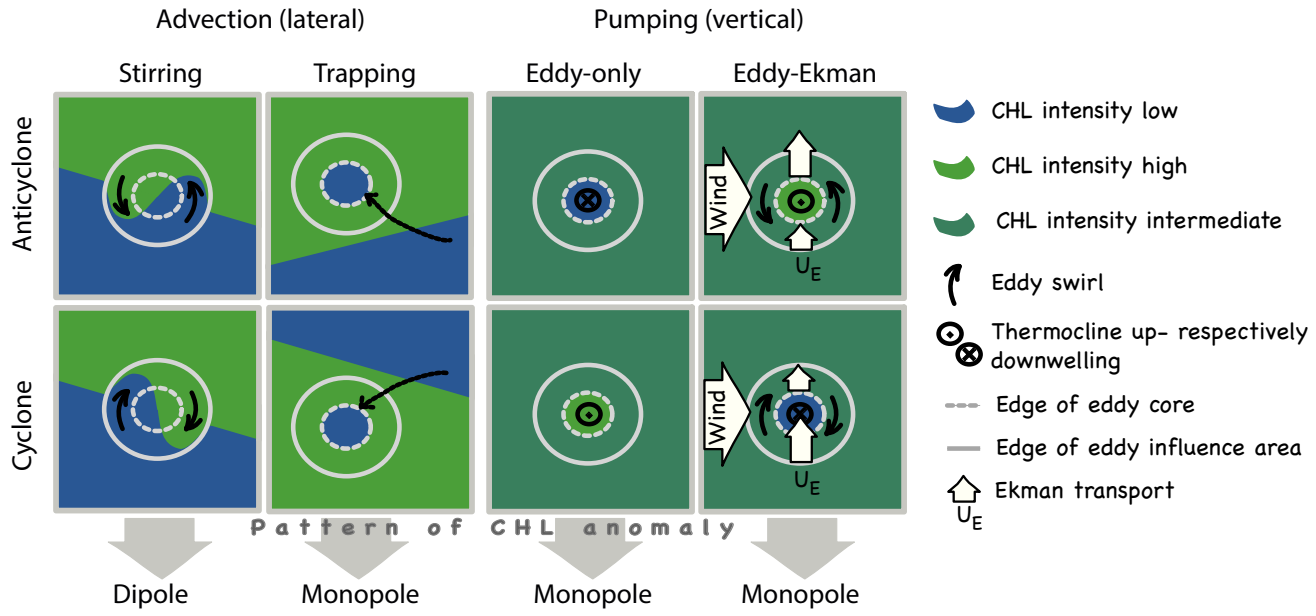

Figure 3.1.: Schematic illustrating the mechanisms of how eddies may impact the chlorophyll (CHL) distribution*, separated by anticyclones (top row) and cyclones (bottom row); the left two columns show the effects of advection (lateral displacements) due to the eddies' rotational speed (stirring) and lateral propagation (trapping); trapping can cause CHL anomalies of either sign (here a negative anomaly is depicted); the right two columns show the potential effect of eddies on CHL by modifying phytoplankton growth due to vertical displacements of isopycnals by eddies; this may change the nutrient availability for and/or light exposure of phytoplankton; the third column shows the effect of eddies-only and the forth column the possible effect of Ekman pumping if surface currents of an eddy and winds act together; the spatial pattern of the CHL anomaly is anticipated to look different depending on the mechanism active, i.e. a monopole ΔCHL imprint is expected for all eddy-effects except for Stirring where a dipole imprint is anticipated (Figure expanded from Siegel et al., 2011).*

scales of the eddy's diameter, whereas for *trapping* it can have larger length scales. The time scales of the reactive tracer, i.e. *CHL* need to match the time scales of the rotation and the propagation of eddies for eddies to have an effect. If the time scale of a reactive tracer is very short compared to the ones of an eddy, it is degraded before the eddy can affect it.

The spatial and temporal scales of eddies and phytoplankton overlap: *CHL* gradients in the SO can easily occur on spatial scales of 100 km, the typical scale of eddies. The turnover time of phytoplankton is on the order of days to one week. A phytoplankton population can be sustained by recycling of nutrients within the euphotic zone for weeks to months. The lateral turnover time of an eddy is about one week or a bit longer with which it can affect already the same plankton generation. Propagation of eddies happens on time scales of weeks to months. Thus eddies can impact the pattern of phytoplankton blooms by *stirring* as well as *trapping*.

Even though the relation of eddies and biology has been found frequently in in-situ studies, the overall effectiveness of eddies impacting phytoplankton growth is an issue of debate. The pumping of nutrients by CE had been hypothesized to be crucial in

the nutrient-wise desert-like subtropical gyres (Falkowski et al., 1991). However, this idea has been challenged with the argument of a missing mechanism of resupplying the thermocline with nutrients (Oschlies, 2002). Then, eddies were found to be able to pull up iron-rich sediments from the coastal shelf in the north Pacific, which is crucial in this HNLC region (Xiu et al., 2011). Also in the SO this could play a role downstream of shallow topography in the ACC (Boyd et al., 2012). Further Mahadevan et al. (2012) argue that CE help initiating the Atlantic spring bloom as they increase stratification and thus light exposure. Again an effect of potential importance in the SO with its deep mixed layers which has been shown to be locally vital south of Africa (Llido, 2005). Obviously, the effect of eddies needs to meet the "phytoplankton's needs" to actually make an impact on phytoplankton growth. Hence, the extent of the effect of eddies on phytoplankton growth is dependent on the concurrent limitation of phytoplankton growth in combination of the coincidental state of the eddy's properties.
The local pattern of the *CHL* imprint of eddies can be used to differentiate between stirring and the other mechanism. Further, the *CHL* anomaly associated with eddies can be related to various quantities which may play a role, such as factors limiting phytoplankton growth or the large-scale *CHL* gradient. We will make use of these approaches in Section 3.4.3.

3.4. Results and Discussion

3.4.1. Chlorophyll Anomalies of Anticyclonic and Cyclonic Eddies

3.4.1.1. The Mean Imprint of Eddies on Chlorophyll

Overall, we detect a mean imprint of eddies on CHL (Figure 3.2a). Both AE and CE in certain regions feature positive and negative CHL anomalies. The distribution of the anomalies is overall shifted towards negative values for AE and towards positive values for CE (Figure 3.2a, b), which causes the mean negative anomaly for AE, and likewise the mean positive anomaly for CE. Thereby a small asymmetry exists in these distributions with a greater excess of negative anomalies for AE versus a smaller excess of positive anomalies for CE. This again results in the in absolute terms larger mean anomaly of AE.
Even though the mean anomalies are relatively small averaged over positive and negative anomalies, i.e. -4% and 1% averaged over AE and CE, respectively, they are statistically different from zero. In the following, we further examine the variation of *CHL* anomalies in space and time.

3.4.1.2. The Spatio-Temporal Variability of the Imprint

The geographical areas of prominent positive and negative ΔCHL of eddies emerge if we bin the ΔCHL associated with each eddy into $2^\circ \times 2^\circ$ longitude-latitude boxes (Figure 3.3). We find a distinct spatial variability of the long-term mean imprint of eddies on *CHL*. The mean local anomalies are larger 10%. Thus, even though the aforementioned overall mean imprint of eddies on *CHL* is small, the local mean imprint is substantial.

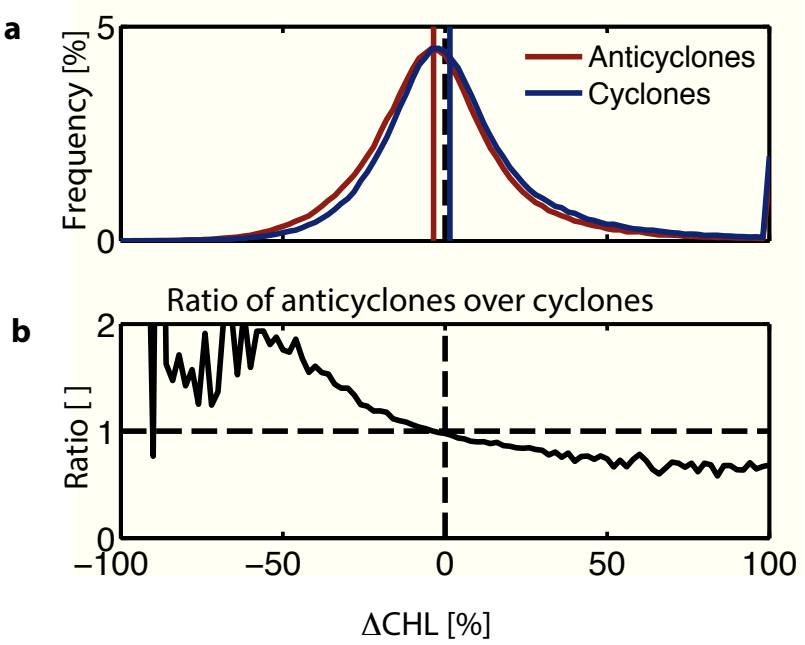

Figure 3.2.: Chlorophyll (CHL) anomaly distribution associated with eddies; a *distribution of CHL anomalies (based on 2% bins) of eddies existing at least 3 weeks; vertical colored lines mark the mean;* ***b*** *is the ratio of the two distributions as shown in* ***a*** *with anticyclones over cyclones.*

Similar to the large-scale climatological *CHL* distribution, the large-scale geographical pattern of the mapped ΔCHL is mostly zonal. The negative imprint of AE is most clearly expressed north of the ACC in the southern subtropical gyres (north of the -20 cm SSH contour). The prevailing negative imprint is contrasted by positive anomalies related to the ACC (south of the -20 cm SSH contour). In addition AE show positive *CHL* anomalies in some of the shelf areas, especially south southwest off the Australian and South-American coasts, and west of New Zealand. CE show a largely similar spatial pattern but of opposite sign compared to the AE: the prevailing positive CHL anomalies north of the -20 cm SSH contour are opposed by a band of negative anomalies along the ACC. Southwest of Australia forms an exceptional region of pronounced negative anomalies for CE. Also the western subtropical ocean basins feature negative anomalies for CE, even though of weaker magnitude. The ΔCHL pattern is spotty for AE as well as CE south of the PF, with AE and CE featuring average positive and negative anomalies, respectively. We will next examine the seasonality of the *CHL* imprint of eddies.

The seasonality of ΔCHL associated with eddies is large in the ACC influence area and south of it, but small in the southern subtropical gyres (Figure 3.4). The *CHL* anomalies in the southern subtropical gyres of AE and CE are positive and negative, respectively, all year round. In winter (austral, i.e. June/July/August), they tend to expand from the -20 cm SSH contour further southward. In the vicinity of the ACC and south of it, the ΔCHL changes sign over the course of the year: around the SAF, AE exhibit negative anomalies in winter and spring, followed by positive anomalies in summer and autumn. CE feature negative anomalies in spring to autumn, with almost

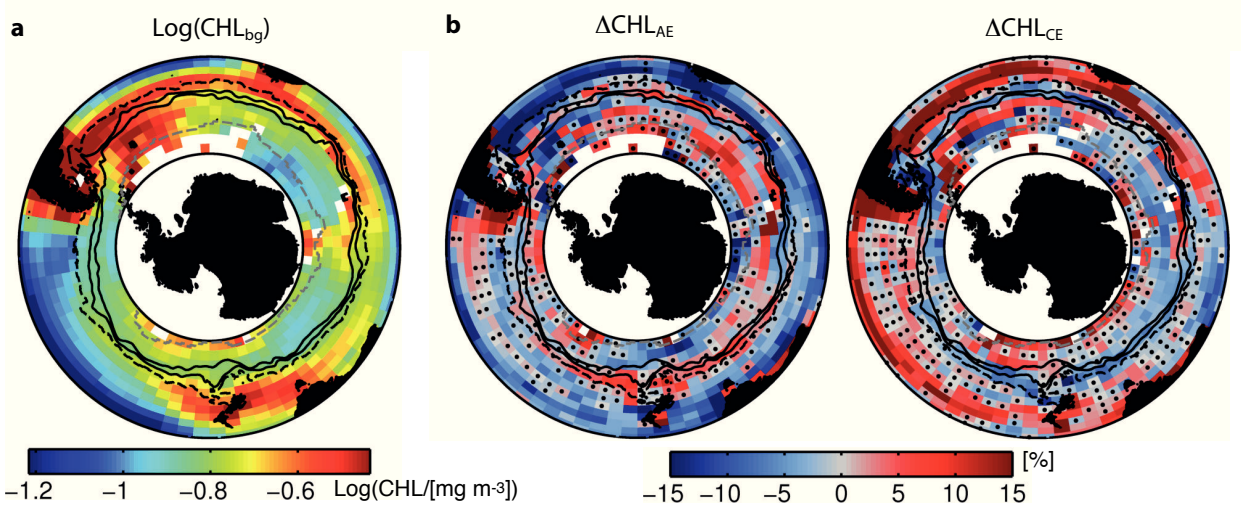

Figure 3.3.: Maps of chlorophyll (CHL) anomalies associated with eddies; a *Common logarithm of the climatological CHL for reference, and* ***b*** *anomaly ($CHL_{eddy}/CHL_{bg} - 1$, see Methods Section for details) related to anticyclones and cyclones; the anomalies are the mean of all eddies existing at least 3 weeks binned in $5° \times 3°$ lon-lat-grid boxes; dots mark boxes where the mean anomaly is not significantly different from zero (t-test, p=0.05); solid black lines show the mean northern (SAF) and southern (PF) boundaries (major fronts) of the ACC, respectively; the dashed black line denotes -20 cm SSH contour and the dashed gray line the northernmost extension of the sea-ice cover.*

none to slightly positive anomalies in winter. The anomalies around the PF feature basically a bipolar signal with negative and positive anomalies for AE in spring and autumn, respectively[1].
The seasonal variability of ΔCHL is as large as the meridional variability. In contrast, the magnitude of the zonal variability and its seasonality is smaller (Supplementary Figure C.1). Here, locations of prominent *CHL* anomalies coincide with areas downstream of topographical obstacles, such as the Kerguelen Plateau. Once more, these are areas where the absolute *CHL* values are high, too[2]. With respect to ocean basins the anomalies related to eddies are largest in the Atlantic sector, especially north of the -20 cm SSH contour, i.e. the area of the Brazil-Malvinas Confluence.

3.4.2. Integrated Impact of Eddies on Chlorophyll

3.4.2.1. Contribution to the Climatological Chlorophyll Distribution

We now address the overall impact of AE and CE independent of polarity (Figure 3.5). We have seen in Chapter 3.4.1 that the imprint on *CHL* is generally opposite for anticyclones and cyclones thus we expect a large cancellation of the effect of AE and CE. Indeed, the anomalies averaged over AE and CE are much smaller than if we consider eddies separated by polarity (Figure 3.5a). Nevertheless, we find significant

[1] Vice versa for CE.
[2] Sokolov and Rintoul (2007) argue that these elevated *CHL* values are due to large-scale upwelling of deep iron-rich waters resulting induced by bottom torque.

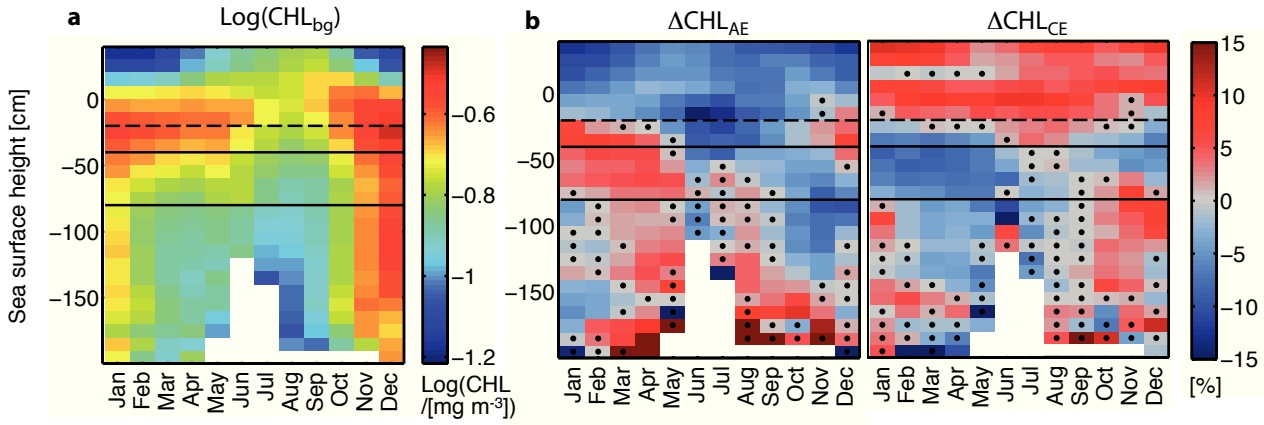

Figure 3.4.: Seasonality of chlorophyll (CHL) associated with eddies; a *Common logarithm of the climatological chlorophyll (CHL) for reference, and* ***b*** *anomaly of CHL associated with eddies (ΔCHL) related to anticyclones (AE, left) and cyclones (CE, right); the anomalies are the mean of all eddies existing at least 3 weeks binned in monthly -10 cm sea surface height (SSH) bins; black dots mark bins where ΔCHL is not significant (t-test, p=0.05); solid black lines show the mean northern (SAF) and southern (PF) boundaries (major fronts) of the ACC, respectively; the dashed black line denotes the -20 cm SSH contour.*

CHL anomalies of 5-10%. Areas of persisting positive *CHL* anomalies include the coastal areas west of South-America, New Zealand and south of Australia. Areas of persistent negative anomalies cover the larger fraction of the SO, specifically the southern subtropical gyres and the vicinity of the ACC. Thus, the effect of anticyclones and cyclones does not completely cancel.
In addition, we can derive the net impact of eddies on the mean by taking into account the spatial varying occurrence of eddies (Figure 3.5b, see also Chapter 2). This impact is small, with eddies causing a net decrease of *CHL* by 1-2% around Australia, east of South-America and west of South Africa. A localized increase is visible in some coastal areas and the vicinity of the ACC. It should be kept in mind however, that we consider here the contribution only of the core of the eddies, the contribution increases if the influence area of the eddy around its core is considered as well.

3.4.2.2. Chlorophyll Transport Across the Antarctic Circumpolar Current

The SO is of major importance for the global carbon cycle. It has acted as a net sink with respect to carbon in the past, however its behavior in the future is uncertain (Gruber et al., 2009). The contribution of mesoscale eddies to lateral and vertical carbon fluxes in the SO is unclear (e.g. Ito et al., 2010; Sallée and Rintoul, 2011). Here, we provide a back on the envelope calculation of meridional carbon fluxes associated with eddies. This estimate has to be taken with care as it includes several strong assumptions[3].
With our study, we have information on the *CHL* anomalies related to eddies ($\Delta CHL \approx$

[3]The estimate of meridional heat transport associated with eddies which is based on similarly crude assumptions agrees rather well with previous studies (see Chapter 2); this provides some confidence for the carbon estimate, even though the latter includes additional strong assumptions.

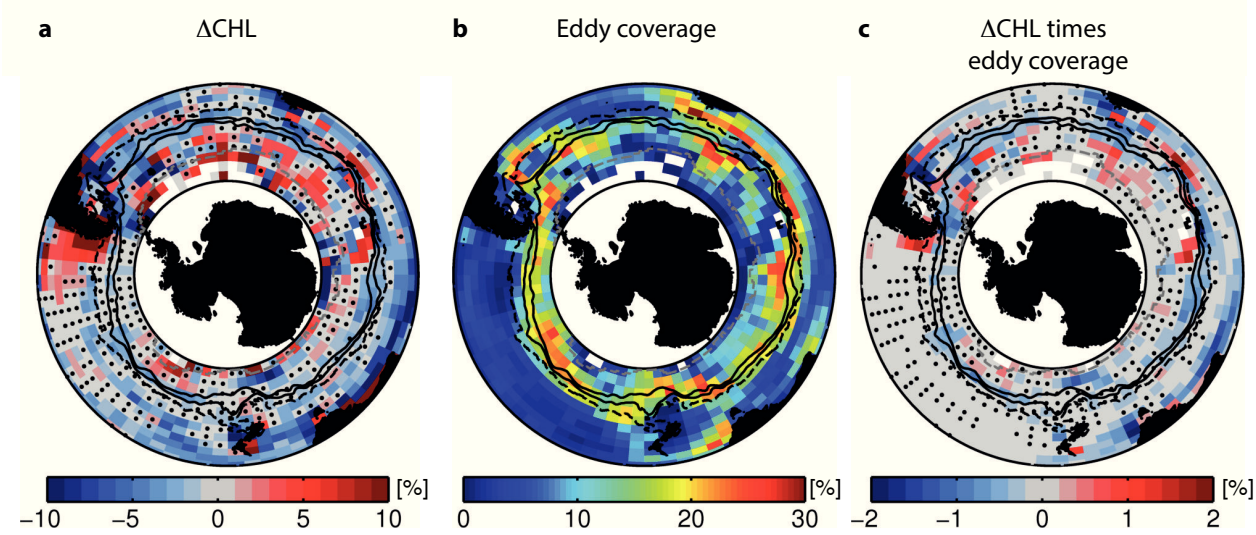

Figure 3.5.: Average chlorophyll (CHL) anomalies related to eddies independent of polarity. ***a*** *Mean* ΔCHL *of eddies independent of polarity;* ***b*** *eddy coverage and* ***c*** *modification of the total CHL due to eddies (****a*** *weighted with* ***b****); solid black lines show the mean northern (SAF) and southern (PF) boundaries (major fronts) of the ACC, respectively; the dashed black line denotes -20 cm SSH contour and the dashed gray line the northernmost extension of the sea-ice cover.*

10^{-3} mg m^{-3}), on the eddies' sizes (radius R≈40 km) and their meridional displacements. We assume a constant carbon to chlorophyll ratio (exemplary $r_{c:chl}$=10 and $r_{c:chl}$=100, the first being rather small, the second a rather large number, see e.g. Dehairs et al., 1997; Calbet et al., 2011; Behrenfeld et al., 2005), and further that the surface *CHL* as detected by the satellite is representative for a (well-mixed) mixed layer which is a reasonable assumption in the SO due to high wind speeds. We use an Argo float derived monthly climatology for information about the mixed layer depth at the location of each eddy (MLD_e ≈100 m). Assuming a cylindrical shape of the eddy and a perfect trapping by the eddy of the fluid in its core, the trapped volume is calculated as $V = \pi R^2 MLD_e \approx 500 \times 10^3$ m^3. The mean carbon anomaly of AE and CE is then computed as

$$\Delta C_e = V \Delta CHL r_{c:chl} \times 10^{-15} \approx -10 \times 10^3 \text{kg}$$

of carbon for $r_{c:chl} = 10$, and -100×10^3 kg for $r_{c:chl} = 100$. The transport across the major ACC fronts (PF and SAF) is obtained by multiplying this average anomaly with the average number of eddies per year being formed at the one side of a front and dissipated on the other side. Both AE and CE form and dissipate on either side of the fronts. Only in the net do a small number of AE cross from north to south and CE south to north. AE and CE both carry negative carbon anomalies, however, AE are more efficient with a southward transport and thus end up with a positive northward transport. Whereas CE cause a negative northward carbon flux.
The resulting transport is a negative northward flux of $O(10^{-5})$ Pg C yr^{-1} and $O(10^{-6})$ Pg C yr^{-1} for $r_{c:chl} = 10$ and $r_{c:chl} = 100$, respectively[4]. The impact of eddies on carbon

[4]The sensitivity of this number to the major uncertainties of some of the input numbers into the equation remains to be tested

fluxes due to carrying along of phytoplankton appears to be small compared to the total meridional carbon fluxes, where only the anthropogenic fraction amounts to about $O(10^{-1})$ Pg C yr^{-1} at these latitudes (Ito et al., 2010). However, two issues need to be considered in this context: Hausmann and Czaja (2012) found the transport of eddies caused by their rotation to be about one order of magnitude larger than the transport related to eddies trapping water in their core. It remains to be checked if this is also true for *CHL*, respectively carbon. Then, this is solely a carbon transport estimate associated with eddies based on "alive"[5] organic matter. There may be additional components, such as transport of inorganic carbon or even indirect effects, such as eddies laterally transporting nutrients which lead to increased productivity in remote areas.

3.4.3. Causes of the Imprint on Chlorophyll by Eddies

3.4.3.1. Advective Effect of Eddies Part I: *Stirring*

As seen from section 3.4.1 we detected a distinct *CHL* anomaly associated with eddies. Further, there are possibly several mechanisms simultaneously involved which result in the detected imprint (Siegel et al., 2011). It is not straightforward to separate these mechanisms. The idea is to make use of the spatio-temporal pattern of the imprint as illustrated in Section 3.4.1 to find the dominant mechanisms. We will try this in the following with several approaches. A first approach is to make use of the different spatial structure of the *CHL* imprint which is expected from different mechanisms, as suggested by Siegel et al. (2011) and depicted in Figure 3.1. For this purpose we isolate *stirring* from the other effects (as in Section 2.3.4.1 for temperature).
The mean local imprint of eddies on *CHL* is shown in Figure 3.6. The ambient *CHL* gradient and the distinct imprint on *CHL* associated with the mean eddy is clearly visible in Figure 3.6a. The *CHL* anomaly of the mean eddy (Figure 3.6b) features a monopole shape. We separate the monopole from this imprint by taking radial averages of the total imprint relative to the center of the eddy. The monopole is of much larger magnitude than the residual (Figure 3.6c-d). The contribution of the monopole to the spatial variance of the pattern of the *CHL* anomaly associated with the eddy is >95%, with the residual, i.e. dipole, contributing the remaining several percent. Thus, mechanisms causing a monopole of the pattern, i.e. *trapping*, *eddy pumping* and *eddy-Ekman pumping* appear to be clearly dominant. The residual is a surprisingly symmetric dipole which we attribute to *stirring*.
The importance of *stirring* varies regionally, it contributes several 10% to the *CHL* imprint north of the ACC (see Section 2.3.4.1). This agrees with the finding of Hausmann and Czaja (2012) that the lag of an eddy and its temperature anomaly is larger in the more quiescent compared to dynamic areas, which results in a more distinct dipole pattern in the former compared to the latter. Also Chelton et al. (2011a) explained the *CHL* imprint they detect mainly with *stirring*[6]. Besides, they detect a contribution

[5] Or only recently died.

[6] They consider only *CHL* on time scales of more than 2 to 3 weeks (and seasonality removed) aiming to exclude the pumping mechanisms.

of a monopole, too, but attribute it to yet another process: as eddies propagate their leading side stirs an undisturbed *CHL* field whereas their trailing side stirs an already perturbed *CHL* field. Thus, firstly, the tail anomaly would be less distinct (asymmetric dipole) and secondly, ambient *CHL* of the leading side would entrain into the eddy's interior causing the monopole contribution. We do not believe this effect to be dominant. Firstly, the maximum anomaly of the monopole is larger in magnitude than the *CHL* in the direct influence area of the eddy. Secondly the sign of the monopole one would expect from this effect does not agree in 1/3 to 1/2 of the situations (see Supplementary Figure C.2). Possibly, the explanation for the monopole imprint found by Chelton et al. (2011a) is *trapping*. Chelton et al. (2011b) themselves pointed out the high trapping ability ("nonlinearity") of eddies in their paper on physical characteristics of eddies and Early et al. (2011) found an almost complete *trapping* by eddies within the zero vorticity contour of eddies from an idealized modeling study. Siegel et al. (2011) conclude the advection effect of eddies to be important (in the Sargossa Sea), with other effects, specifically wind, playing a role as well.
We conclude from Figure 3.6 that the effect of *stirring* it is overall small in the domain considered here (especially in the ACC area) which partly contrasts conclusions of the aforementioned studies for lower latitudes and more quiescent areas. One reason for this may be the steady year-round north-south gradients of *CHL* facilitating *stirring* in the lower latitudes (subtropical waters), whereas in high latitudes phytoplankton occurs primarily in prominent blooms. Another reason may be that *stirring* happens mainly at the periphery of eddies (supported by the modeling study of Early et al., 2011) which is nicely visible relative to the background in the quiescent subtropical gyres, whereas the eddies periphery is subject to frequent interactions with other eddies and jets in dynamic areas such as the ACC.
In the following two paragraphs we try to tease out indications on the importance of the other mechanisms we introduced in Figure 3.1, i.e. *trapping* versus *eddy-pumping* and *eddy-Ekman-pumping*. As we find the *CHL* imprint of eddies to be mainly a monopole, we do not separate the dipole from the total imprint in the following.

3.4.3.2. The Advective Effect of Eddies Part II: *Trapping*

The swirl velocity is larger than the propagation speed for SO eddies (see Chapter 2 and Chelton et al., 2011b), i.e. they are predisposed to trap fluid. Based on an idealized model Early et al. (2011) found effective trapping in the eddy's core. *Trapping* has also been observed by e.g. Lehahn et al. (2011) who were able to follow an Agulhas ring trapping a *CHL* patch for almost a year. Further, trapping is happening also for the non-reactive tracer temperature (see Section 2.3.4.1). Thus, we anticipate a significant contribution of *trapping*.
In a case of perfect trapping the magnitude of *CHL* within the eddy does not change while it propagates away into a different *CHL* surrounding. The assumption hereby is that the temporal change of *CHL* is small compared to the spatial variation, which may be the case if we focus on a "short enough" time period of weeks. In this case, one expects no difference between the current *CHL* of the eddy and the one at the time t_o of the eddy's formation ($\Delta\mathrm{CHL}_{to} = 0$), and the absolute *CHL* anomaly ($|\Delta CHL|$) of

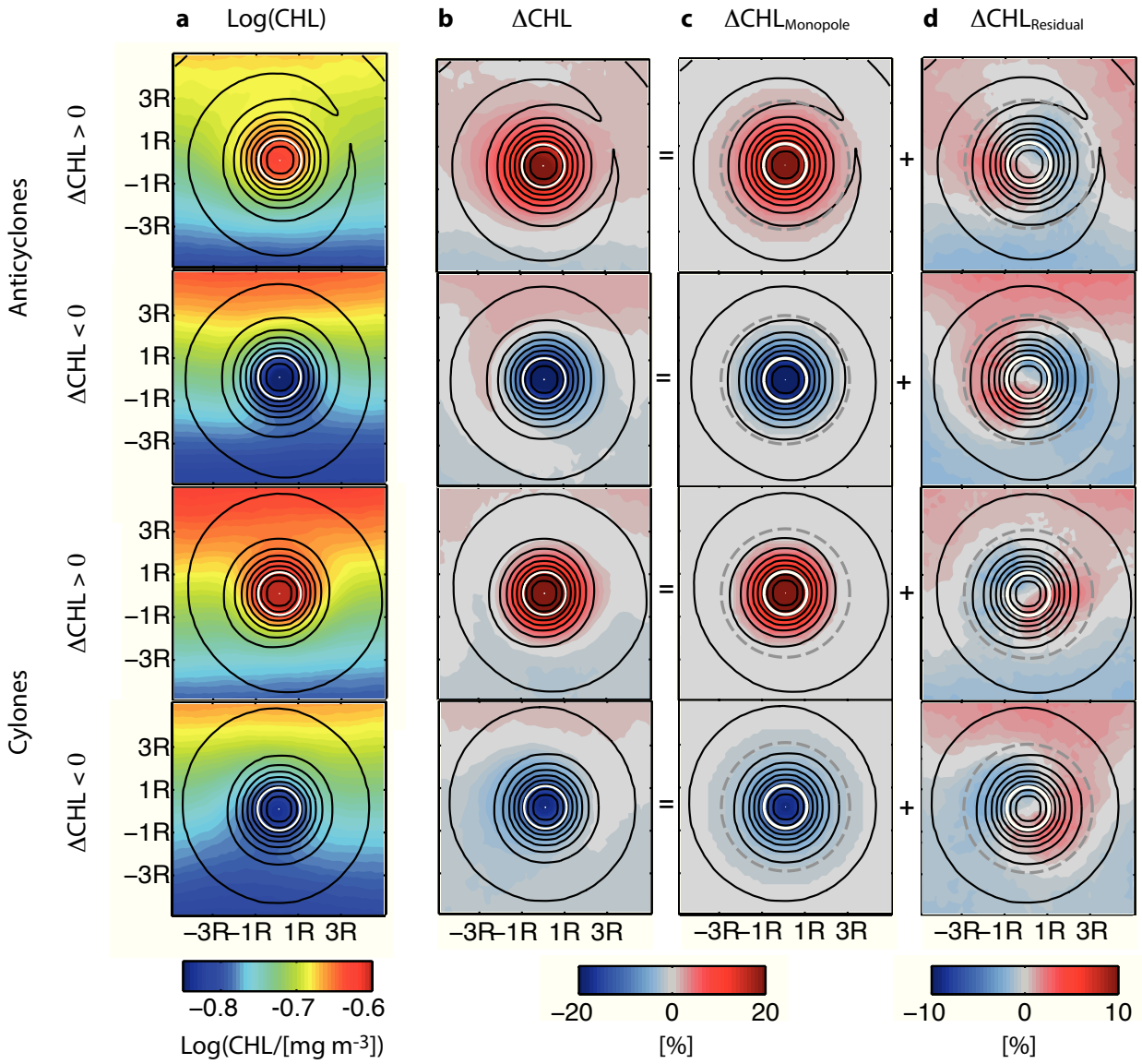

Figure 3.6.: Eddy composite of chlorophyll (CHL)*; separated by anticyclones (top two rows) and cyclones (bottom two rows), and by positive and negative CHL imprint, respectively;* ***a*** *shows the absolute log(CHL) and* ***b*** *the CHL anomaly (ΔCHL);* ***b*** *is decomposed into a monopole pattern as depicted in* ***c*** *and a residual as shown in* ***d****;* ***d****, the residual, shows in fact a dipole pattern; sea level anomaly contours are shown in black (0.05 spacing, normalized before averaging); eddy core and eddy center are shown as white circle and dot, respectively; the individual eddies are rotated according to the large-scale CHL gradient (top high to bottom low CHL) and scaled according to the eddy's radius (R); the dashed gray circle as marked in* ***c*** *and* ***d*** *is used for the computation of the contribution of the monopole and the residual (dipole) to the pattern as seen in* ***b****; several 10,000 eddies go into each of the four composites.*

the eddy relative to its immediate surrounding increases the further the eddy propagated into waters featuring different *CHL*, i.e. it would scale with the difference of the surrounding *CHL* of the eddy's origin and current position ($\Delta CHL = a\Delta CHL_{bg}$, with $a = 1$)[7]. If *trapping* is not perfect, i.e. entrainment of surrounding *CHL* into the eddy's core occurred, then the eddy's *CHL* accordingly ranges between the background *CHL* of its origin and current position ($\Delta CHL = a\Delta CHL_{bg}$, with $0 < a < 1$). The eddy's anomaly were zero if it did not trap at all, i.e. a continuous complete exchange with its surrounding happened ($\Delta CHL = a\Delta CHL_{bg}$, with $a = 0$).
Contrary to our expectation, we do not find any indication for *trapping* (Figure 3.7): ΔCHL tends to be very small to zero if examined with respect to the gradient of the background *CHL* (ΔCHL_{bg}). The difference of the eddy's *CHL* relative to the time of its origin scales with the background *CHL* gradient ($\Delta \mathrm{CHL}_{to} = a\Delta CHL_{bg}$, with $a > 1$ actually) indicating that the entrainment of *CHL* into the eddy's core is much stronger than *trapping*.
Possibly, we do not detect *trapping* as the effect is not as trivial to detect as we pretended it to be with the above analysis. Another approach could be to track individual eddies and investigate the associated *CHL* in detail as Lehahn et al. (2011) did. Indeed, the latter found the *CHL* patch related to an Agulhas ring to exhibit a distinct variability over time, which was triggered for instance by mixing events caused by winds. Hence, the temporal variability and patchiness of *CHL* (seasonality, "bloom behavior") could hamper the identification of trapping.
If we believe the above trapping-analysis, we can conclude that the largest part of the imprint of eddies on *CHL* is due to a modification of phytoplankton growth by eddies. We will illustrate evidence for this mechanism in the following paragraph.

[7]With the assumption of a monotonic background change of *CHL*

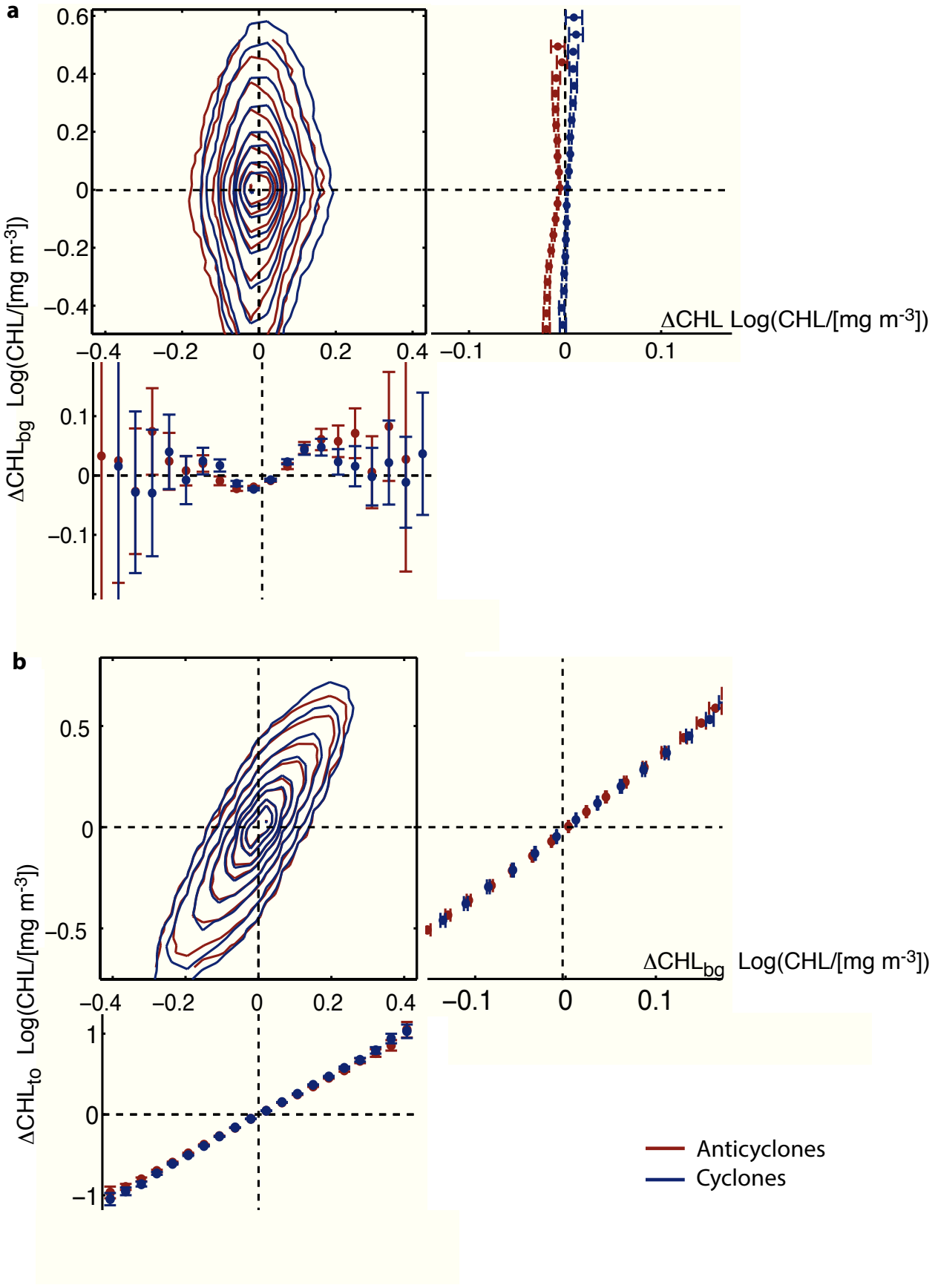

***Figure 3.7**: Caption on next page.*

***Figure 3.7.: "Chlorophyll (CHL)−chlorophyll relations"**; **a** two-dimensional histogram of CHL anomalies associated with eddies (relative to surrounding, ΔCHL) and difference of background CHL at the eddies current location relative to the location (and time) at its origin (ΔCHL_{bg}), and **b** ΔCHL_{bg} and the difference of the current CHL of an eddy relative to its CHL when it originated (ΔCHL_{to}); 2-dimensional histogram (in **a** and **b**): binning according to the quantity of the x-axis and concurrently according to the quantity of the y-axis (about 40 bins for both); the normalized occurrences ranging from 0 to 1 are depicted with only selected (unevenly spaced) contours shown for reasons of clarity (contour 0.01, 0.02, 0.05, 0.1, 0.2, 0.3, 0.5, 0.7 and 0.99); the panels on the right and bottom of **a** and **b** show the projection onto the x- (19 bins) and y-axis (20 bins), respectively; 3 errors of the mean are marked with error bars; note the different scales; not the different scales for the projections (zoom-in); only eddies with an age of 3 to 12 weeks are considered.*

3.4.3.3. Are there Indications for Eddies Stimulating Phytoplankton Growth?

As elucidated in Section 3.3 various ways exist how eddies may impact the phytoplankton's well-being. An indication for the latter to happen is visible from the slope of Figure 3.7, which is larger than one (see also Supplementary Figures C.4 and C.5 for a modified version of the Figure and a detailed interpretation). As to the environmental conditions, we consider here the macro-nutrient nitrate (monthly climatology), the mixed layer depth as indication for light limitation (monthly climatology) and wind speeds (weekly data). The latter provides an indication for eddy-Ekman interactions, i.e. a reversing of the original pumping effect. We find similar results for silicate as for nitrate, even though for silicate less distinct (not shown). Information on the iron distribution would be of great interest for the HNLC region. Unfortunately, iron observations are very sparse. We tested the topography as indicator for iron (not shown), as for instance over shallower topography iron may potentially be brought up from sediments. However, we could not find a clear relation besides very shallow topography, i.e. shelf areas featuring increased *CHL*.
We detected indications for eddies having an impact on phytoplankton if we bin environmental variables according to certain *CHL* levels and vice versa:

- CE *CHL* anomalies tend to be elevated in areas of low nitrate levels, and nitrate levels tend to be lowest for positive *CHL* anomalies, indicating nutrient supply (Figure 3.8 a); the opposite is the case for AE.

- Positive *CHL* anomalies decrease with increasing wind speeds for CE indicating an eddy-Ekman effect (Figure 3.8 b), and vise versa for AE;
  this effect occurs mostly north of the ACC (not shown).

- CE show positive *CHL* anomalies in both shallow (supporting nutrient supply) and deep mixed layers (supporting revelation of light limitation); *CHL* anomalies in the vicinity of the ACC are positive in spring supporting the proposed mechanism that CE alleviate light limitation; hence, eddies may contribute to initiate spring blooms.

In addition, one would expect a larger impact of eddies if they are "more powerful", i.e. of larger size and/or amplitude. As a matter of fact, we find indications for this (Figure 3.9):

- For CE, *CHL* anomalies show a positive correlation with size, for AE the correlation is negative (similarly for other eddy characteristics such amplitude, not shown).
- The *CHL* anomaly associated with eddies tends to increase if the eddy evolved between the previous and the current time step (week), this is true with respect to amplitude, diameter and kinetic energy; hence, it appears, eddies have an effect if they dynamically evolve (not shown).

Likewise however, we detect relations which are not completely consistent with eddies modifying phytoplankton growth or else question its importance:

- The above mentioned effects become visible only after projecting the two-dimensionally binned Figure onto the x- and y-axes and after one zooms in, i.e. the effects are small.
- The clearest effect the Figure shows is the before analyzed general positive ΔCHL of CE versus general negative ΔCHL for AE.
- *CHL* anomalies of eddies tend to level off during the eddies life time (Supplementary Figure C.3); this supports less an impact on phytoplankton growth but rather the trapping of a *CHL* patch.

We here presented some of the possibilities of interpretations of the figures shown. Altogether the interpretation of these figures are not completely consistent with an impact of eddies on phytoplankton growth. Besides, a few of the features of the figures are not unequivocally explainable, and further the spatial separation of environmental regimes based on nitrate, MLD and winds is not independent. For instance the MLD tend to be shallow in areas of nitrate limitation. Further, cross-dependencies may occur, such as CE only providing nitrate in shallow mixed layers. And finally the *CHL* anomalies of eddies exhibit a clearly more pronounced seasonality than the limitation of phytoplankton.
In the end the mechanism of eddies impacting phytoplankton growth is more complex than pictured in section 3.3. We point out only some aspects here: for vertical nutrient supply to be feasible a steep enough vertical gradient of the respective nutrient must exist for the "eddy-lifting" to be effective. This is not necessarily the case for iron in the SO for instance. Secondly, a mechanism of (diapycnal) recharging the upper thermocline with nutrients must exist once they have been depleted (Oschlies, 2002). Another issue is that the impact of eddies depends on their life stage, i.e. they might show an opposing signal in the first versus the last life stage: the thermocline relaxes back down to its original level as CE mature and "die". In this situation they actually may have a similar impact as AE in the beginning of their life time as they "spin up". However, we do not find a significantly different imprint of eddies if we compare

the first versus the last few weeks of their life cycle (not shown). Then, there is the yet more difficult detectable effect of eddies spatially isolating plankton groups due to their trapping ability. This may impact plankton competition for resources as well as exposure to grazing. A top-down control we neglect altogether. Finally, it may be possible that eddies have a remote impact in contrast to a local one by transporting nutrients in their core and releasing them where they dissolve.
The key drawback is that solely surface information is provided by satellite observation. It is questionable to which extent a stimulation/damping of phytoplankton growth happening at the lower euphotic zone propagates to the ocean surface where it is detected by satellite sensors.
Nevertheless, these are the only hints we find for explaining the relation of eddies and ΔCHL. One could argue that eddies stimulate phytoplankton growth in the nutrient depleted areas north of the ACC. Thereby can CE pump up nutrients, whereas AE might decrease the availability of nutrients by pushing even further down the nutricline (out of the euphotic zone) where some diapycnal small-scale mixing may transfer nutrients up. In the ACC area CE would alleviate light limitation (AE reinforce it). High winds in the ACC area would partially reverse the stimulating effect of CE by eddy-Ekman interplay, and so the suppressing effect by AE. The interplay of the two may explain the "spotty nature" of the CHL imprint of eddies in this area.

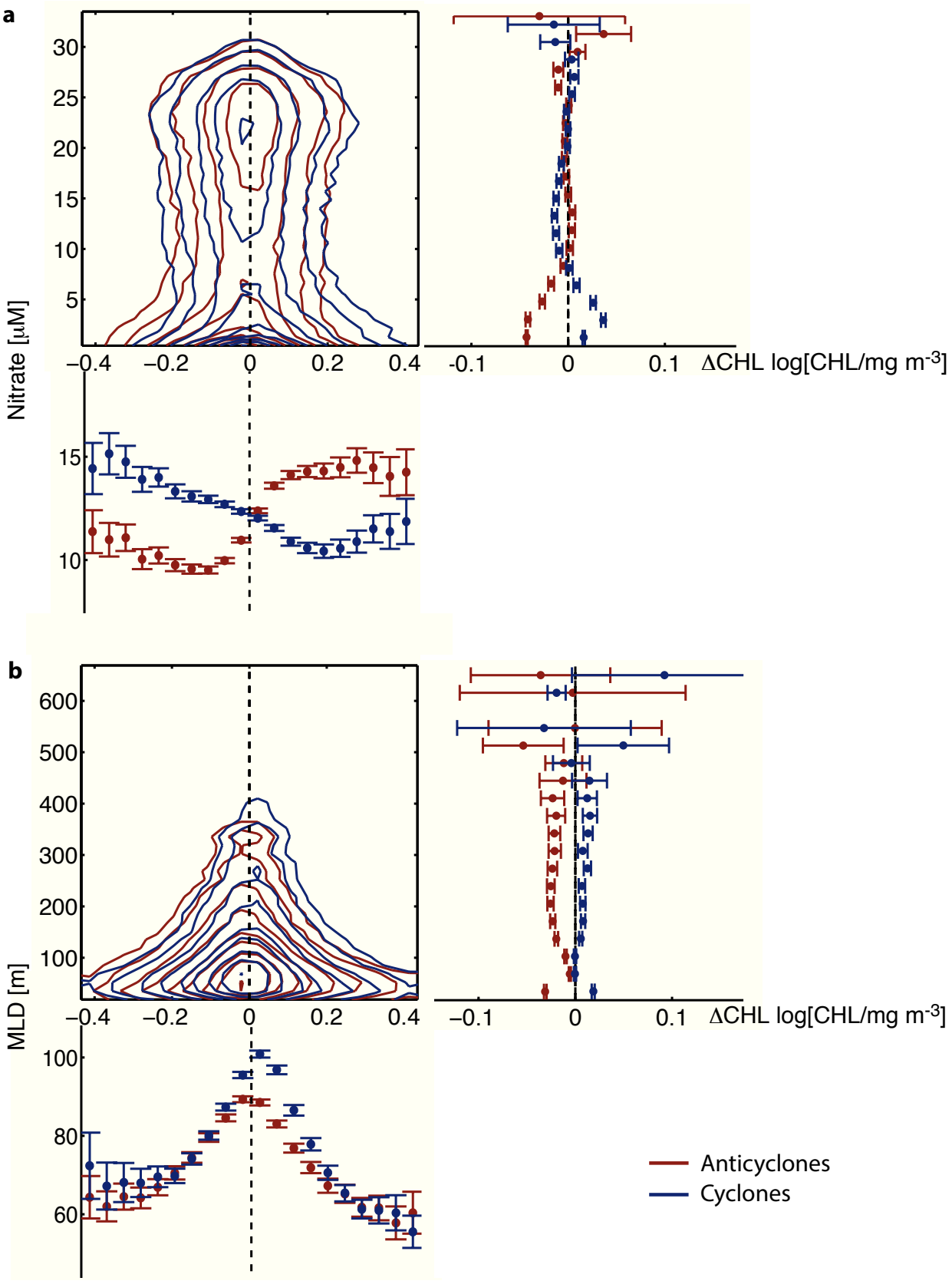

Figure 3.8.: Relations of chlorophyll anomalies (ΔCHL) of eddies with environmental conditions and eddy properties. *As Figure 3.7 but with* **a** *nitrate and* **b** *mixed layer depth (MLD).*

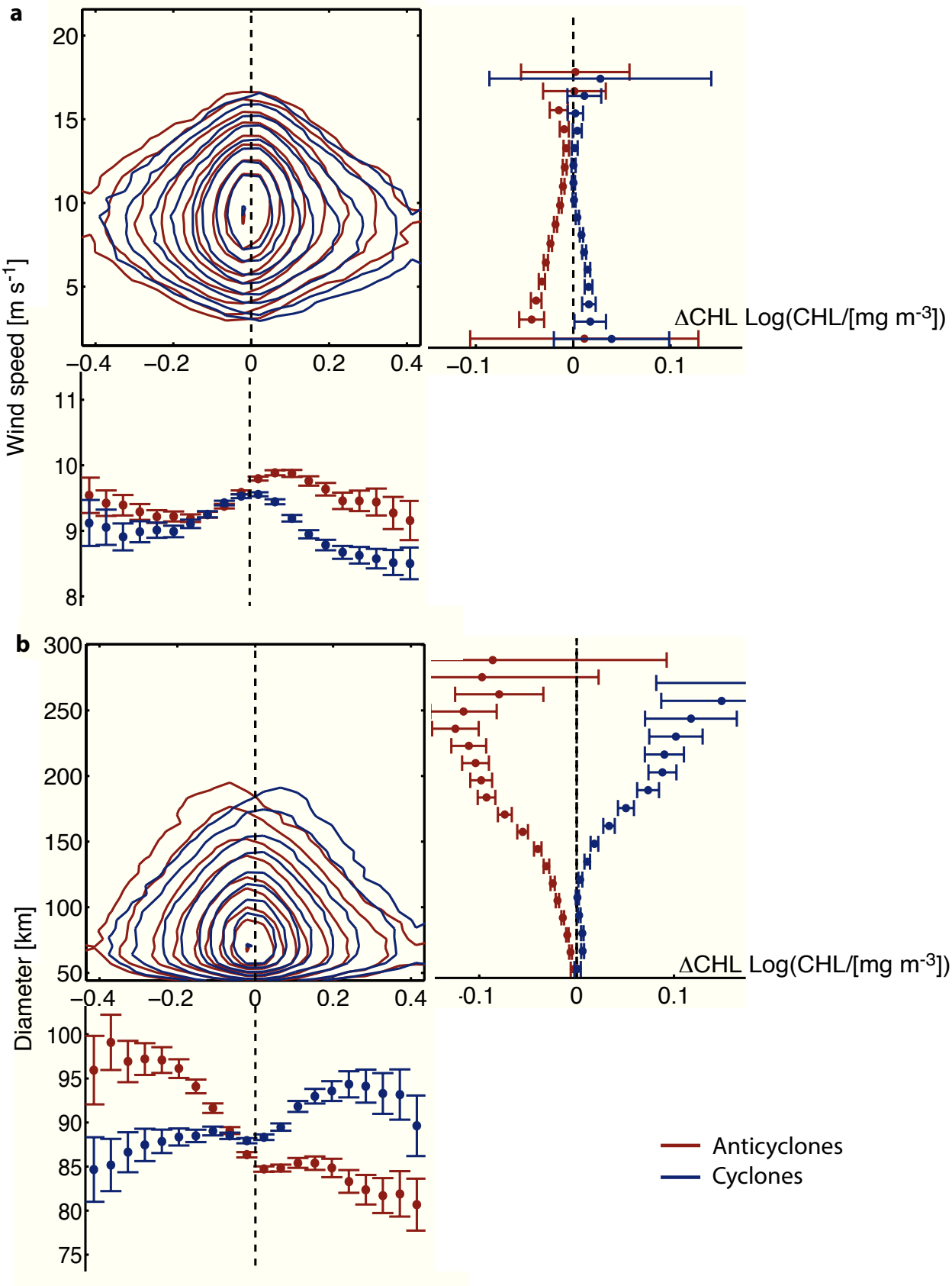

Figure 3.9.: Continued from Figure 3.8. *As Figure 3.7 but with* ***a*** *wind speed* ***b*** *eddy diameters; the former is thought to have an impact on the eddy dynamics.*

3.5. Summary and Conclusions

Spatial scales of *CHL* patchiness and (sub)mesoscale variability have intrigued substantial research but many unresolved issues remain (e.g. Lévy, 2008). With this study, we provided the first estimate of the long-term mean association of eddies and *CHL* in the SO. We obtained this by combining ocean eddies detected and tracked based on satellite observations of *SLA* with *CHL*. Statistically robust results could be retrieved due to the large number of collocations of eddies and *CHL*. This is not self-evident as *CHL* is a variable with large spatial and temporal variability, and additionally frequent data gaps due to cloud cover, especially in the SO. Our major findings are summarized in the following:

- Distinct *CHL* anomalies associated with eddies of >10% are found in large areas in the SO.
- *CHL* anomalies are different for AE and CE, and a large spatio-temporal variability comes on top of that: the large-scale pattern is that CE exhibit positive and negative anomalies north and in the vicinity of the ACC, respectively; AE show a similar pattern, however of opposite sign; in addition, a strong seasonality is superimposed on the mean *CHL* imprint of eddies in the vicinity of the ACC.
- We sought to unravel the causes of the association of eddies and *CHL* making use of the local spatial pattern of the *CHL* imprint and its large-scale spatio-temporal variability; from the mechanisms as proposed in the literature, we find indications for eddies influencing phytoplankton growth based on climatological bottom-up limitations (macro-nutrients and light); it appears that *stirring* plays a secondary role in the SO; further, we can not verify relations of eddies and *CHL* due to *trapping*.

Our findings on the importance of the various mechanisms of the relation of eddies and *CHL* are first steps and should be tested further. This is independent of the actual existence of the relation of eddies and *CHL*. From the latter, the main questions which arise are what the implications for biogeochemistry are, and for higher trophic levels. We suggest directions for future research with respect to both, mechanisms of the eddy-*CHL* association as well as their implications:

- Refine the examination of the mechanisms based on the same observational data used already in this work; as SO eddies are clearly capable of *trapping*, it is surprising that we do not find indications for it to happen; in the future we seek to make use of temperature as a non-reactive tracer (see also Chapter 2) to be able to better quantify the contribution of the trapping effect versus the effect of eddies on *CHL* as a reactive tracer.
- In-situ observations are still sparse in the ocean, especially with respect to biogeochemistry; targeted observations could be of great use to learn more about the relations of eddies and biology, especially and crucially their about subsurface structure: for instance, autonomous gliders have become available recently and

are more and more frequently used to carry out directed measurement efforts on special structures in the ocean, such as eddies.

- Refine the examination of the mechanisms based on a numerical model: the extent of trapping to happen can be investigated with a model for instance with dye or particle experiments similar to Early et al. (2011); furthermore; in these studies limitations of phytoplankton may selectively be switched on and off and hence the importance of specific limitations tested.

- A numerical model may be also applied to examine the impact of eddies not only on *CHL* but also on biogeochemistry; for instance, associated carbon fluxes are of especial interest in this field with the SO being a major CO_2 sink and source the same time.

- Finally, the severity of the key drawback of our study should be investigated which is the reliance on surface information on *CHL*: here, the main questions are if the magnitude of surface *CHL* is representative for *CHL* in the euphotic zone/mixed layer (for temperature it appears to be mostly, see Chapter 2), and also, to which degree phytoplankton growth modifications at the bottom of the euphotic zone (due to *eddy-pumping*) are reflected in *CHL* as measured at the ocean surface.

Acknowledgments

The altimeter products used for this study were produced by Ssalto/Duacs and distributed by Aviso, with support from Cnes (http://www.aviso.oceanobs.com/duacs/). The *CHL* used were processed and distributed by ACRI-ST GlobColour service, supported by EU FP7 MyOcean & ESA GlobColour Projects, using ESA ENVISAT MERIS data, NASA MODIS and SeaWiFS data. QuikScat data are produced by Remote Sensing Systems and sponsored by the NASA Ocean Vector Winds Science Team. Data are available at http://www.remss.com.

4. Imprint of Southern Ocean Eddies on Winds, Clouds and Rainfall

Published as:
Frenger, I., Gruber, N., Knutti, R., and Münnich, M. (2013). Imprint of Southern Ocean eddies on winds clouds and rainfall. *Nature Geoscience*, 6:608-612, doi:10.1038/ngeo1863.

Owing to the turbulent nature of the ocean, mesoscale eddies are omnipresent. The impact of these transitory and approximately circular sea surface temperature fronts on the overlying atmosphere is not well known. Stationary fronts such as the Gulf Stream have been reported to lead to pronounced atmospheric changes (Hobbs, 1987; Minobe et al., 2008). However, the impact of transient ocean eddies on the atmosphere has not been determined systematically, except on winds and to some extent clouds (White and Annis, 2003; Chelton et al., 2004; Park et al., 2006; Bryan et al., 2010). Here, we examine the atmospheric conditions associated with over 600,000 individual eddies in the Southern Ocean, using satellite data. We show that ocean eddies locally affect near-surface wind, cloud properties and rainfall. The observed pattern of atmospheric change is consistent with a mechanism in which sea surface temperature anomalies associated with the oceanic eddies modify turbulence in the atmospheric boundary layer. In the case of cyclonic eddies, this modification triggers a slackening of near-surface winds, a decline in cloud fraction and water content, and a reduction in rainfall.We conclude that transient mesoscale ocean structures can significantly affect much larger atmospheric low-pressure systems that swiftly pass by at the latitudes investigated.

Although the ocean and atmosphere form a closely interacting system, it has generally been assumed that these interactions occur primarily at the synoptic and global scale. At these scales the atmosphere drives the ocean via buoyancy changes and momentum input through winds, while the ocean affects the atmosphere through heat and moisture fluxes (Xie, 2004).
It has been less clear, however, how strongly the ocean and atmosphere interact on the mesoscale, especially in the extra-tropics. What is known is that mesoscale sea surface temperature (SST) anomalies are globally correlated with near-surface winds and albedo (Chelton et al., 2004; Bryan et al., 2010). Concurrent modifications of winds

and clouds were detected for the distinct Gulf Stream rings (Park et al., 2006) and for large-scale fronts such as the semi-permanent Agulhas Return Current (O'Neill et al., 2005; Liu et al., 2007). In addition, an *SST* related change of rain rate was observed for the Gulf Stream and the Kuroshio (e.g. Hobbs 1987; Xu et al. 2011b).
But large-scale fronts are outnumbered by mesoscale eddies, which dominate the ocean's kinetic energy (Ferrari and Wunsch, 2009) and typically feature an *SST* anomaly (Hausmann and Czaja, 2012). Despite their prevalence, little is known about systematic atmospheric perturbations related to these non-stationary mesoscale *SST* anomalies. Here we close this gap, and show based on observations how oceanic mesoscale eddies impact the atmosphere by changing not only wind, but also clouds and rainfall.
Our analysis is based on the identification of more than 600,000 oceanic eddies south of 30°S over a period of more than seven years (06/2002 through 11/2009). To identify the oceanic eddies, we applied a standard detection method based on the Okubo-Weiss parameter (Okubo, 1970; Weiss, 1991) to weekly maps of satellite derived sea level anomalies (see Method Section for details). For each eddy that was detected at least twice, we collocated satellite derived *SST* and atmospheric data (wind speed and direction, cloud fraction, liquid cloud water content, rain rate and rain probability).
The vast majority of the identified eddies is located in the frontal region of the intense Antarctic Circumpolar Current especially in the Indian and Pacific sectors (Figure 4.1a) with both cyclonic and anticyclonic eddies occurring in the same regions. We found relatively little seasonality in the number of detected eddies as well as their atmospheric impact (Supplementary Figure D.1). Therefore, we only analyse and present the long-term mean results. The average detected eddy-core has a radius of about 40 km, propagates by more than 20 km a week and is characterized by an *SST* anomaly of about -0.5 °C in the case of a cyclonic (cold-core) eddy, and +0.5 °C in the case of an anticyclonic (warm-core) eddy. These SST anomalies induce a sufficiently large anomalous air-sea heat flux to cause measurable changes in the marine atmospheric boundary layer (Supplementary Note D.2).
Indeed, *SST* anomalies associated with the cyclonic and anticyclonic eddies are positively correlated with anomalies in near-surface wind speed, cloud fraction, cloud water content, rain rate and rain probability throughout the Southern Ocean (Figure 4.1b-d and Supplementary Figure D.2). The correlations are highly significant almost everywhere. When computing the significance, we assumed that the weekly composites of the atmospheric quantities were independent - an assumption supported by the short decorrelation time scale of atmospheric quantities over the Southern Ocean (Supplementary Figure D.3).
The positive correlation indicates that the oceanic *SST* anomalies associated with eddies are responsible for the atmospheric anomalies, and not vice-versa, as the latter would tend to lead to negative correlations (Xie, 2004). The correlation is highest for wind speed and cloud fraction, smaller for cloud water content and the lowest for rain. Further, it is strongest in regions of large *SST* anomalies, high eddy activity and for high wind speeds (in agreement with ref. Spall 2007), and similar for both cyclonic and anticyclonic eddies, indicating a linear effect of the oceanic forcing on the atmosphere (Supplementary Figure D.4).

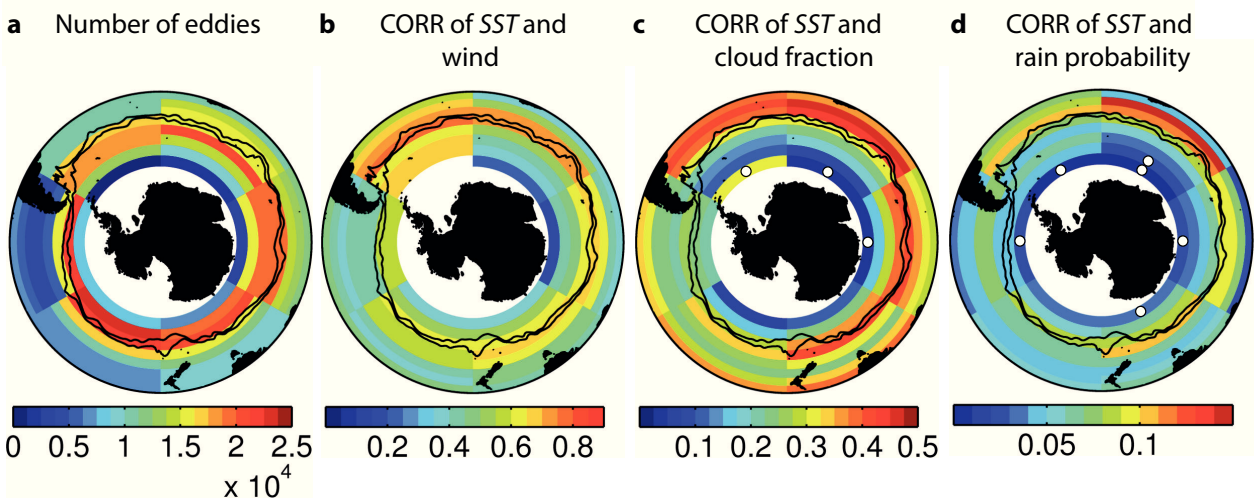

Figure 4.1.: Polar orthographic maps of the eddy statistics. ***a*** *Number of detected eddies in each 60°×4° bin and correlations (CORR) of anomalies of sea surface temperature (*SST*) with anomalies of* ***b*** *wind,* ***c*** *cloud fraction and* ***d*** *rain rate. White dots mark bins where correlations are not significant (p>0.01) and white areas feature insufficient data; black contours denote the two major fronts of the Antarctic Circumpolar Current (the Subantarctic and the Polar Fronts Sallée et al. 2008).*

To investigate the mechanisms underlying this mesoscale oceanic forcing of the atmosphere, we computed mean composites of the spatial pattern of the imprint on the *SST* and the atmosphere for all identified eddies. To this end, we centred the *SST* and atmospheric quantities relative to the eddy-core, scaled them relative to the individual eddy radius, and rotated them according to the current large-scale wind direction.
A smooth picture of the mean impact of oceanic eddies on the atmosphere emerges, with the anomalies related to the eddy-cores distinctly standing out from the background (Figure 4.2 and Supplementary Figure D.5). This background largely reflects the large-scale north-south gradients, as the winds are predominantly westerly at these latitudes. In view of the tight spatial coupling and the similar circular shape of the atmospheric response and the *SST* anomalies associated with the eddies, we conclude that we detected a direct response of the atmosphere to *SST* anomalies of ocean eddies and not to the large-scale *SST* fronts these eddies are frequently embedded in. The pattern of the atmospheric imprint by the oceanic eddies is nearly symmetric between the cyclonic and anticyclonic eddies but of opposite sign, and the maximum radial extent of the imprint corresponds roughly to 2-3 eddy-core radii (80-120 km).

The atmospheric imprints are well quantifiable, and although of moderate magnitude relative to the mean state (2-5%), they are statistically significant (K-S test, p=0.01). Anticyclonic and cyclonic eddies cause maximum positive and negative anomalies (see Methods Section), respectively, with maximum mean anomalies of wind of 0.31±0.01 m s^{-1}, of cloud fraction of 1.7±0.1%, of cloud water content of 2.9±0.3×10^{-3} mm, of rain rate of 4±1×10^{-3} mm h^{-1} and of rain probabilities of 1.7±0.3%. Relative to the atmospheric variability, the magnitude of these anomalies represents 13-15% (wind, cloud fraction), 6-10% (cloud water content) and 2-6% (rain).
Two main mechanisms, downward momentum transport and pressure adjustment, have

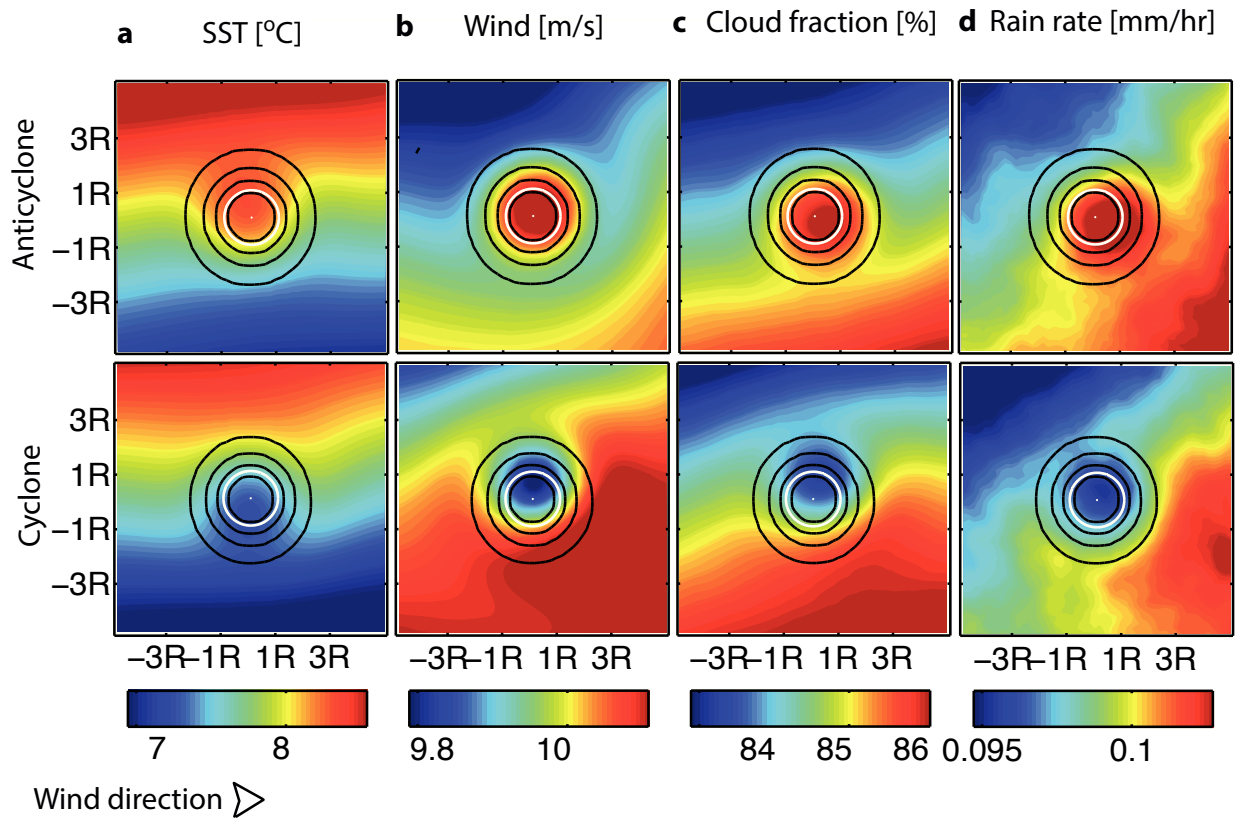

Figure 4.2.: Mean eddy and pattern of its atmospheric imprint. ***a*** SST *(±0.04 °C),* ***b*** *wind speed (±0.01 m* s^{-1}*),* ***c*** *cloud fraction (±0.1%) and* ***d*** *rain rate (±*10^{-3} *mm* h^{-1}*); mean composite maps of the >600,000 individual eddy realizations south of 30° S, divided into anticyclones and cyclones; white circles mark the eddy-core as detected with the Okubo-Weiss parameter; black lines denote sea level anomaly contours associated with the eddy; before averaging, the eddies were scaled according to their individual eddy amplitude and radius (R), interpolated and rotated so that the large-scale wind is from left to right.*

been proposed to explain the adjustments in the atmosphere resulting from *SST* gradients (Small et al., 2008; Chelton and Xie, 2010). The former relates to a decrease of the vertical stability of the atmosphere as air moves from cold to warm water. This leads to an intensification of the turbulence within the atmospheric boundary layer and thus an increased downward momentum transport. Subsequently, the near-surface vertical wind shear is increased and the near-surface wind intensifies centred over the *SST* anomaly. The pressure adjustment mechanism relates to changes of the near-surface air density and thus of the sea level pressure. Here, negative sea level pressure anomalies arise over a warm *SST* anomaly from modified air-sea fluxes, yielding an acceleration of wind upstream of the warm *SST* anomaly and a deceleration downstream of it. Which mechanism is dominant can be estimated from the spatial pattern of the *SST* in combination with the wind divergence (Figure 4.3a). In the case of the pressure adjustment mechanism, one expects a monopole pattern corresponding to the divergence of the SST gradient (Minobe et al., 2008), as the surface wind converges over a positive *SST* anomaly. In contrast one expects a dipole pattern for the downwind momentum transport mechanism (Chelton et al., 2004). This is because the wind speed

increase over the *SST* anomaly is accompanied by a wind divergence upstream and a convergence downstream of the *SST* anomaly, and hence it has the same structure as the dipole-shaped downwind gradient of *SST*

The resemblance of the wind divergence and the downwind *SST* gradient in Figure 4.3a favours the downwind momentum mixing mechanism as an explanation. This implies that the perturbed air-sea fluxes associated with the steep gradients of the *SST* upstream and downstream of the eddy-core lead to the changes in the near-surface wind by changing the turbulent mixing in the atmospheric boundary layer, as anticipated under conditions of strong cross-frontal winds (Spall, 2007) (Figure 4.3b). Similarly, the nearly in-phase relationship of cloud and rain anomalies with those of *SST* and wind speed points to a modification of the atmospheric boundary layer stability and hence convection (enhancement/suppression) in combination with changes in the moisture supply as the likely cause, in contrast to vertical air motion triggered by the wind divergence/convergence. Thus, the thermodynamical and dynamical adjustments in the marine atmospheric boundary layer due to the eddies' *SST* anomalies become apparent in a modification of local weather. These modifications are presumably accompanied by a change of the atmospheric boundary layer height (Small et al., 2008) but likely remain restricted to the atmospheric boundary layer.

The mesoscale modifications of the atmosphere related to oceanic eddies represent yet another piece of the puzzle of the energy and hydrological cycle of the Earth system. Southern Ocean eddies provide a source of atmospheric variability in the latitudes of the prevailing westerlies in the southern hemisphere at spatial scales of $O(100)$ km. We thus suggest to incorporate this additional *SST* variability in numerical weather prediction models to improve their skill (Iizuka, 2010). The subsequent feedbacks of the atmosphere on the ocean may be of significance for ocean dynamics including the mesoscale eddy field (Jin et al., 2009). Firstly, changes of the wind stress curl due to *SST* anomalies are directly related to upwelling and suction in the surface ocean. Secondly, changes in wind speed as well as cloud fraction constitute negative feedbacks by damping the *SST* anomalies and potentially leading to an acceleration of eddy dissipation (Shuckburgh et al., 2011). Thirdly, and in contrast to the above, the eddy-induced changes of rainfall could constitute a positive feedback: in the case of anticyclonic eddies, the increased fresh water input decreases further the low density anomaly, and vice-versa for cyclonic eddies.

Mesoscale eddy induced atmospheric responses might also be relevant for ocean biogeochemistry, especially for the oceanic uptake of carbon dioxide (CO_2). For cold-core cyclonic eddies, for which the partial pressure of CO_2 (pCO_2) is $\sim$2% lower than that of the surrounding waters, a $\sim$4% lower gas transfer rate due to the concurrent attenuated winds leads to a reduction of the anomalous sink associated with these eddies. In contrast, in the case of the warm-core anticyclonic eddies, whose pCO_2 tends to be higher than that of the surrounding waters, the accelerated gas transfer due to the stronger winds causes this anomalous source to be more strongly expressed. The net effect of this mesoscale correlation between wind speed and pCO_2 makes the ocean locally take up about 5-10% less CO_2 from the atmosphere. While this is a small effect (see also (Wanninkhof et al., 2011), based on monthly data), it may be of significance when considering that the Southern Ocean is globally the most important sink for an-

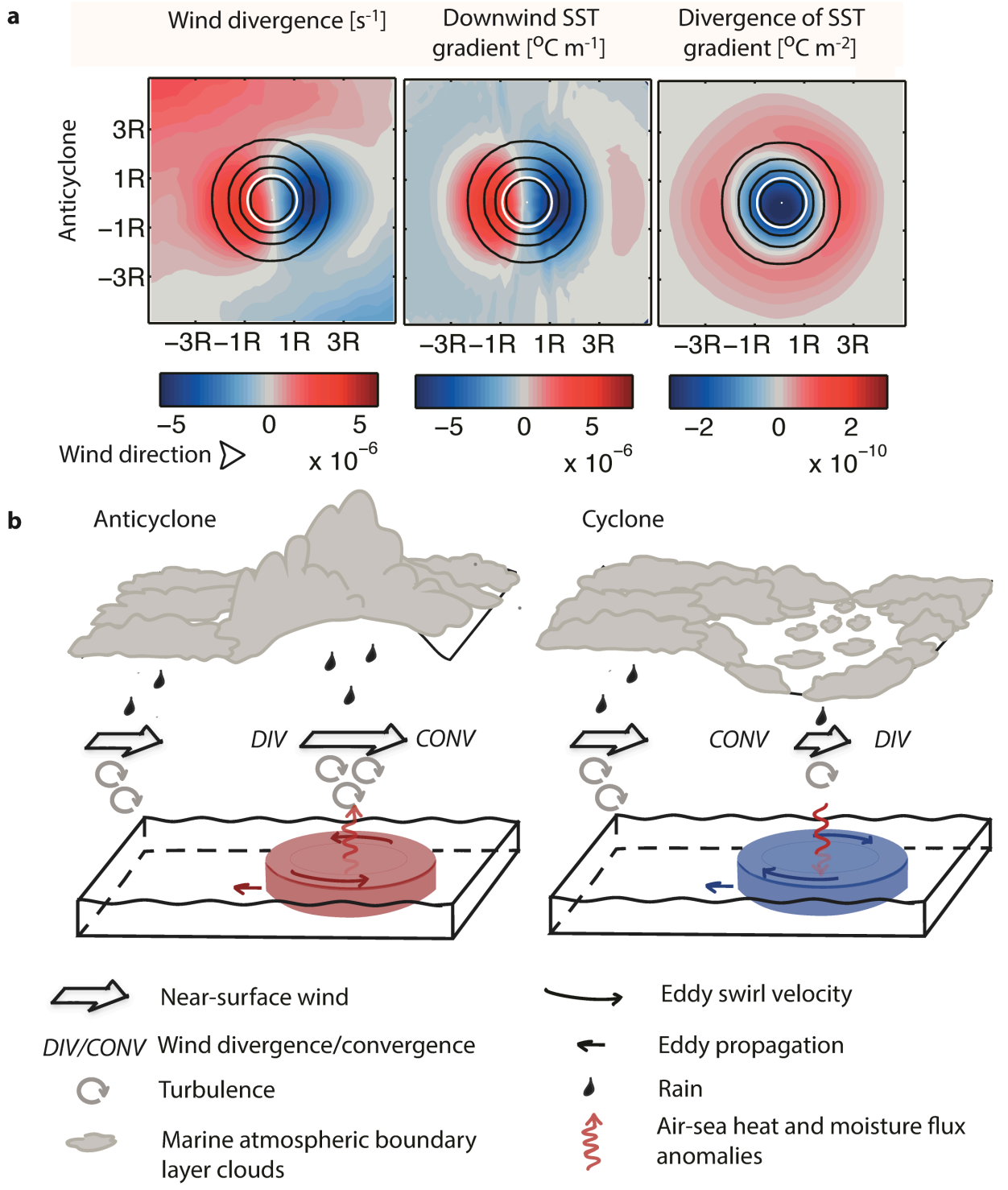

Figure 4.3.: Impact of mesoscale oceanic eddies on the atmosphere. ***a*** *Mean composite of the wind divergence (left), downwind* SST *gradient (middle) and divergence of the* SST *gradient, i.e. the Laplacian of the* SST *(right); the graph is very similar but of opposite sign for cyclonic eddies (not shown); otherwise as Figure 4.2.* ***b*** *Schematic summarizing the impact of oceanic eddies on the lower atmosphere for a southern hemispheric warm-core anticyclone (red, left) and a cold-core cyclone (blue, right).*

thropogenic CO_2 (Mikaloff Fletcher et al., 2006). In addition, with the eddies likely causing an anomaly of the air-sea CO_2 partial pressure difference of the order of 100%, eddies are a substantial source of variance for the Southern Ocean carbon sink. Finally, modification of mixing and Ekman pumping due to the coupling of winds and eddy currents could result in a modulation of biological productivity (McGillicuddy et al., 2007).

We have shown that transient mesoscale structures in the ocean can significantly alter atmospheric patterns introducing an "oceanic mesoscale imprint" in the atmosphere, disproving the common assumption of the atmosphere being independent of smaller-scale variability in the ocean. We suggest that air-sea interactions at the mesoscale may need to be considered in observational data analyses and numerical model simulations.

Methods

Data

Our analysis is based on satellite observations of oceanic and atmospheric properties: we analyzed sea level anomalies from Aviso, *SST*, liquid cloud water and rain rates from AMSR-E (microwave radiometer), wind speeds from SeaWinds/QuikSCAT (microwave radar) and cloud fraction from GlobColour (see Supplementary Methods). Besides the rain rate we also looked at "rain probability" by assigning 0 to "no rain" conditions and 1 to conditions of âĂIJrain of any intensityâĂİ.
The data were analyzed at weekly resolution which is long enough to largely filter out synoptic perturbations in the atmospheric data and are hence assumed to represent independent data points (Figure 5 in (O'Neill, 2012) and Supplementary Figure D.3). At the same time, this is sufficient to resolve the migration of eddies which is of the order of 10 km per week on average. The data are provided at a spatial resolution of 0.25° except for the sea level anomalies ($^1/_3$°, however the feature resolution is coarser, due to the processing of the observational data by the providers).

Eddy Identification

We identified oceanic mesoscale eddies on the basis of sea level anomalies and the Okubo-Weiss parameter (OW) (Okubo, 1970; Weiss, 1991), which has been widely used for this purpose (e.g. Isern-Fontanet et al. 2003). The OW separates areas of dominance of vorticity from areas of dominance of strain: $OW = s_n^2 + s_s^2 - \omega^2$, where $s_n = u_x - v_y$ is the normal, $s_s = v_x + u_y$ is the shear component of the strain, $\omega = v_x - u_y$ the relative vorticity. u and v are the current velocity components in eastward and northward direction calculated from sea level anomalies under the assumption of geostrophy, and the subscripts x and y denote the partial derivatives in east- and northward direction, respectively. Vorticity dominates for $OW < 0$. We used $OW < -0.2\sigma_{OW}$ as threshold to determine the edge of the eddy-core (as e.g. (Isern-Fontanet et al., 2003)), where σ_{OW} is the temporal mean of the spatial standard deviation of OW. The eddy radius is defined as the radius of the core. The resulting eddy-masks (with 1 for âĂIJeddyâĂİ and 0 for âĂİnon-eddyâĂİ) for each week were then linearly interpolated onto a 0.25° grid matching the atmospheric and *SST* data. We assigned all grid boxes containing a value greater than 0.5 to 1 (âĂİeddyâĂİ) and below 0.5 to 0 (âĂİnon-eddyâĂİ). Cyclonic and anticyclonic eddies were separated depending on vorticity. We require an eddy to cover at least 4 adjacent grid boxes, reject shapes with a width of only a single grid box to avoid elongated features to be detected as eddies, and only eddies detected in at least two consecutive time steps (see Supplementary Methods) are included in our analysis as robust features.

Definition of Anomalies Related to Eddies

Anomalies of all quantities related to the oceanic eddies are calculated as differences of the respective quantity between the "eddy-impact-area" and the "background". The former is defined as a circle of two radii around the centre of the eddy and the latter as a ring of three radii around this circle. The anomaly is defined as the difference of the mean of the two (used in Figure 4.1 and Supplementary Figures D.1, D.2, D.4, D.6, D.7), except when interpreting the mean composite eddy (Figure 4.2, Supplementary Figure D.5) where we examine the maximum of the anomaly relative to the background.

Error and Uncertainties

The error of the atmospheric quantities and *SST* for each individual eddy can easily be as large as the anomaly related to the individual eddy. The significance of our results arises from the large number of analyzed eddies. A number of potential biases and errors need to be considered in more detail, though.
Our consideration of all eddies existing at least two weeks may cause a skewed result: the Aviso sea level anomalies were time filtered which could lead to some frontal systems erroneously being classified as eddies. An additional potential bias may stem from the assumption that the atmospheric data are decorrelated after one week. In order to test for the influence of these two effects, we analyzed a case where we required all eddies to be at least 1 month old, and where we used the atmospheric data only from every other week. This entailed a reduction of the sample size by more than half but caused minor changes in the results and did not affect our conclusions: the patterns in the Figures remained nearly the same (see Supplementary Figs. D.6-D.9 in comparison to Figs. 4.1, 4.2, D.2, D.5). The error of the anomalies associated with eddies increased slightly (doubling at most) and a few more of the bins in Figure 4.1 became insignificant (at p=0.01) at the southern boundary and in the southern subtropical gyre in the Pacific where the least data is available (see Figure 4.1a and Supplementary Figures D.6-D.9). *SST* is not available under rainy conditions and wind speed is subject to contamination by rain. The former is inconsequential as the decorrelation time scale of *SST* is typically longer than a week and therefore *SST* values a week before/after a rainy event are considered representative for the rain event also. Wind speed shows a positive bias with increasing rain rates at the wind and rain conditions of the *SO* (Hilburn et al., 2006) which may inflate the signal we find in wind speeds related to eddies due to their modification of rain. Because of that, we only use wind data without rain events for the calculation of correlations (Figure 4.1, Supplementary Figures D.1, D.4, D.6). Rain-free data are regarded as independent: these are derived making use of distinct spectral and polarization signatures in the microwave brightness temperatures (Wentz, 1997). The bias of wind speed due to the change of water viscosity related to *SST* as well as the deviation of actual winds from the equivalent neutral satellite winds have been found to be small relative to the changes of winds due to atmospheric boundary layer adjustments in the course of *SST* anomalies (Park et al., 2006; Liu et al., 2010).

5. Synthesis

5.1. Summary

In this work I examined on ocean eddies constituting a vital part of ocean dynamics and I highlighted two more aspects of the close interaction of components of the Earth system, i.e. aspects of biophysical and ocean-atmosphere coupling at the mesoscale. The regional focus of the study was the Southern Ocean, a crucial area for the climate system. The results are based on observations. The major findings were

- **The coverage of eddies in the Southern Ocean (SO) is larger than 30% in "hot spots",** i.e. downstream of topographical obstacles in the Antarctic Circumpolar Current (ACC) and in regions of interaction of the ACC and boundary currents. If one considers not only the core but the entire impact area of eddies, this number easily doubles. A large spatial variability of eddy coverage exists (as visible also from eddy kinetic energy) with the regions of very high coverage being contrasted by regions of very low coverage. The latter include areas over "shallow" topography. We confirmed with a different method the finding by Thompson and Demirov (2006) that the occurrence of anticyclones and cyclones is not distributed completely uniformly in space. Areas exist with a dominance of one polarity, e.g. anticyclones dominate the southern subtropical gyres whereas cyclones dominate the northern flank of the ACC. This may play a role for the integrated impact of eddies.

- **A general agreement of eddy characteristics compared to previous studies**, e.g. the eddies' mean properties (e.g. amplitudes, diameters), their origin and dissipation locations (overall in the same locations) are similar as e.g. found by Chelton et al. (2011b), and their evolution over time similar as found by Liu et al. (2012). An analysis of the three dimensional structure of eddies based on *Argo* floats shows a large vertical extent of these mesoscale features of more than 1000 m on average (e.g. Arhan et al. 2011, somewhat deeper than Chaigneau et al. 2011); the eddies appear to be more surface intensified in the ACC vicinity whereas they show a subsurface maximum anomaly north of the ACC.

- **An estimate of the non-local (due to *trapping*) heat and salt transports across the ACC associated with eddies turned out to be small** relative to the transport necessary to compensate for the heat loss and freshwater surplus south of the ACC (i.e. compared to the difference of evaporation minus precipi-

tation). It ranges amongst other observational estimates which vary substantially (e.g. Morrow 2004; Hausmann and Czaja 2012).

- **A relation of eddies with *CHL* is clearly detectable.** Here, we followed the analyses of Siegel et al. (2011) for Gulf Stream rings or Chelton et al. (2011a) for the southeast Pacific (and some global analysis between 15°S and 45°S). The imprint of eddies on *CHL* is distinct in the long-term mean but varies in space and time and depending on polarity (frequently being >10%). The anomalies have a zonal structure with positive anomalies north of the ACC and negative anomalies within the circumpolar belt of the ACC and south of the ACC for cyclonic eddies. The pattern is similar but of opposite sign for anticyclonic eddies. The seasonality of the eddy-related *CHL* anomalies is weak north of the ACC whereas it is pronounced in the vicinity of the ACC. The spatio-temporal pattern of the anomalies indicates that they are largely due to *trapping* and stimulation/damping of phytoplankton growth, with pure *stirring* being of secondary importance; the latter is in partial disagreement with Chelton et al. (2011a).

- **A systematic impact of eddies on the atmosphere.** Winds, cloud fraction and liquid cloud water, rainfall rates and probabilities are modified by several percent associated with ocean eddies. Eddies cause these modifications due to their *SST* anomalies, similarly as large-scale *SST* fronts (e.g. the *Gulf Stream rainband*, Hobbs, 1987). We expanded thereby work done e.g. by Park et al. (2006) systematically looking at the "weather impact" of ocean eddies over an immense domain, the SO. We suggest as mechanism for the "weather impact" the *downward momentum mixing* mechanism where eddies affect the atmosphere via stability changes.

5.2. Implications and Suggestions for Further Research

We could show in this work that a relation of eddies with biology as well as eddies with the atmosphere indeed exists. This raises two main questions immediately:

- **What are the mechanisms for the biophysical interactions we found? Does the proposed mechanism for the air-sea interactions hold?**

- **What are the integrated impacts resulting from these interactions?** For instance what is the role of eddies in carbon export to the deep ocean? Do the biophysical interactions at the phytoplankton level propagate to higher trophic levels in the food web (e.g. Nel et al. 2001)? How do eddies impact ocean stratification and water mass formation due to their density anomalies and transports? Does an effect of eddies exist beyond the atmospheric boundary layer? Do the net air-sea heat, freshwater, momentum and gas (such as CO_2) fluxes change due to eddies?
  Even though the net effect of eddies on the mean appears to be rather small, it can be high in certain regions. In addition, eddies may have an effect not only on

the mean but also on the variability of properties. Furthermore, being transient, eddies may have non-local impacts.

Further subsequent issues of interest would be

- **To explore the coupling:** We interpret our findings as impact of eddies on their environment. However, the system is coupled. For instance, modified winds feed back on the ocean by modifying ocean surface mixing and Ekman pumping. Similarly, biology can feed back on the surface ocean by changing the depth of light penetration, or on the atmosphere by providing additional cloud condensation nuclei (*CLAW* hypothesis, Charlson et al., 1987). In turn, the change in cloud properties changes irradiation and hence the depth of the euphotic zone, impacting phytoplankton growth. The latter two effects would represent a coupling of the eddy-modified atmosphere and the eddy-modified biology (Figure 5.1).
- **How is the role of the mesoscale relative to other scales concerning coupling?** For instance submesoscale motions are triggered at the eddies edges which are thought to be crucial for biology due to their large vertical velocities (Figure 5.2). Another question would be how the impact of eddies embedded in large-scale *SST* fronts (as eddies frequently are) such as the ACC fronts is on the atmosphere, compared to the larger-scale front.

The above points are not only important to investigate due to pure scientific curiosity that results in the aspiration to better understand the Earth system. In the context of weather prediction and climate projections they relate to our continuous quest for increasing the skill of numerical models of the Earth system, or components of it. If we find processes in observational data which have significant impacts, we need to include those in models which we use for weather and climate simulations.
In the following we point out some specific suggestions for directions of further research. One approach is to apply a regional coupled ocean-atmosphere-biogeochemistry model to investigate some of the above matters. The tremendous advantage of models compared to observations are firstly the possibility of repetition of an experiment with the option to vary conditions according to the investigators wishes. Secondly, one has access to an unmatchable data coverage in space and time. Simulations and/or analyses one could carry out are:

- **For the purpose of investigating the integrated impact of eddies on their environment**: run "eddying" and "non-eddying" simulations (e.g. by running the model in various resolutions, from non-eddying to eddy-resolving), carry out a Reynolds decomposition or by doing a budget analysis, for instance for carbon. The differences between the runs then provide indications on the integrated contribution of eddies, for instance to carbon export or cloud fraction.
- **For the purpose of investigating the extent of the coupling**: one-way and truly coupled simulations can be run and compared. The ocean model may be run once with a passive atmosphere and once with an atmosphere which responds to the ocean, for instance to *SST* anomalies. From the difference of the runs on obtains the effect of the coupling on the ocean where one could focus on eddies.

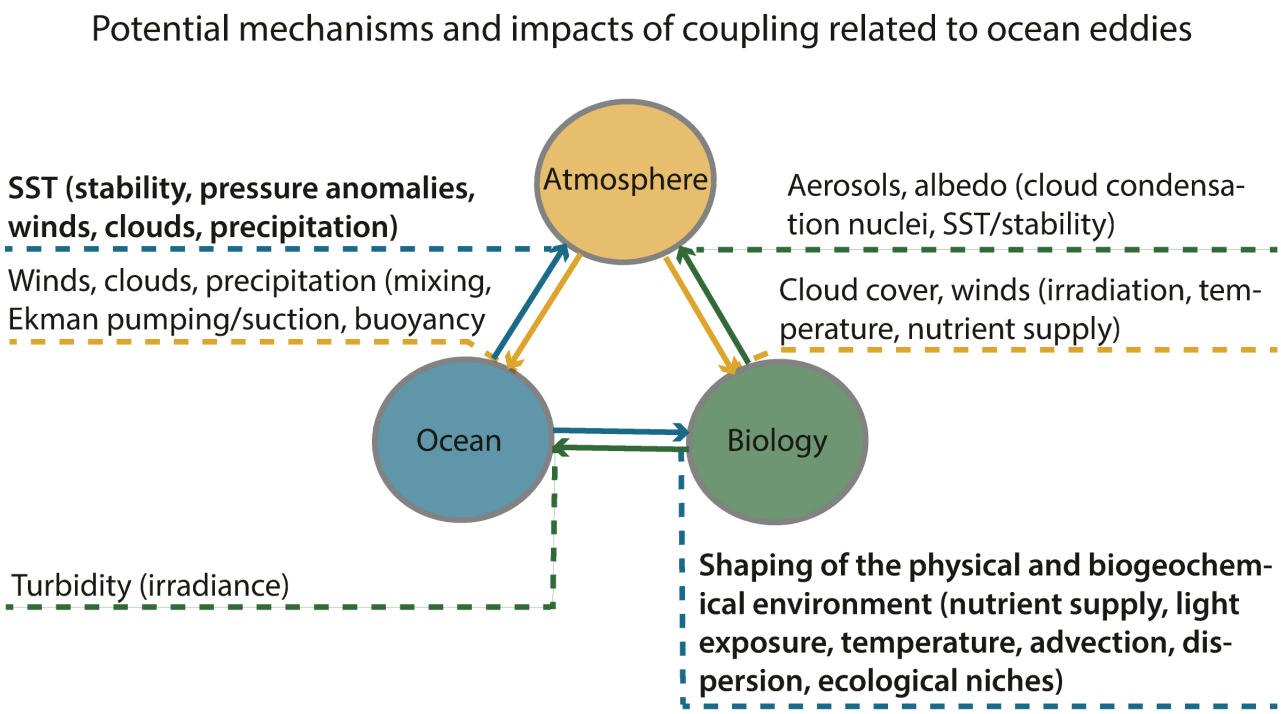

Figure 5.1.: Examples of Potential mechanisms and impacts of coupling of eddies and their environment*; we looked in this work into the issues in bold writing, the other depicted interactions and impacts could be topics of further research.*

- **For the purpose of investigating the mechanisms of the coupling**: the various mechanisms of the relation of eddies with *CHL* could be disentangled and the magnitude of their contributions separately quantified. To this end, one could switch off/on the various limitations of phytoplankton growth and check if the relation of eddies and *CHL* changes, or compare the behavior of *CHL* with a passive tracer released in the model.
- **Sensitivity of eddies and their impacts to climate change:** for this purpose, one could run simulations of the SO with different "climatic conditions", for instance strengthened and shifted westerly winds or changes in stratification. From this, one could obtain indications on the changes of the eddy field and eddy fluxes in a changing climate. These tests would fit in nicely in the current debate on *eddy saturation* and *eddy compensation* (Morrison and Hogg, 2013).

The drawbacks of working with models are their inherent imperfection which needs to be kept in mind for any analysis, and the constraint of computer power, because coupled as well as highly-resolved simulations are expensive to run. Therefore, model work inevitably needs to be combined with observational and experimental work. An other approach is an assemblage of various observations of eddies themselves in combination with their surroundings, with a focus on in-situ data. I imagine something like the combination of satellite observations with Argo floats and autonomous gliders measuring the ocean and concurrent radiosondes measuring the atmosphere. We suggest to focus on:

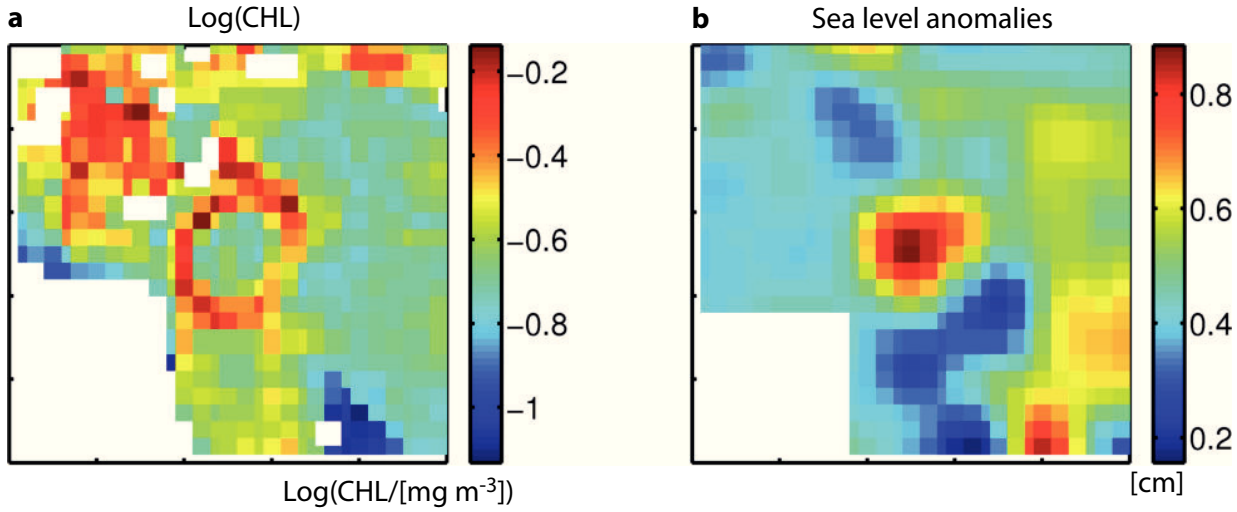

***Figure 5.2.: Anticyclonic eddy east of Australia**; **a** composite of chlorophyll (*CHL*) and **b** sea level anomalies; enhanced* CHL *is clearly visible associated with the edge of the eddy where mesoscale motion is triggered.*

- **"Three dimensional" measuring, i.e. vertical spatial resolution**: with satellite data we obtain observations with good spatial and temporal coverage on the interface between the ocean and the atmosphere for the purpose of investigating mesoscale eddies. We would like to obtain subsurface ocean information, as well as atmospheric observations which are not column-integrated (such as liquid cloud water content) but vertically resolved (some approaches with satellite based measurements exist already, however they are of limited resolution, specifically in the atmospheric boundary layer).

- **Simultaneous measurments of the ocean, the atmosphere and biogeochemistry**: "physical" measurements have the longest history and measurement sensors and devices are best developed. However, for studies such as this thesis, it is vital to not only have information available on the physical but also on the biogeochemical state. Increasing efforts are made to realize this, for instance some *Argo* floats have been equipped with oxygen sensors.

Even though observations in the ocean are sparse, there is plenty of data which has not been analyzed. In addition, great potential exists in combining different kinds of observational data which is already available, such as remote sensing data and measurements collected with research vessels or drifters. Beyond an effort concerning a collection of already existing data related to eddies, targeted measuring of eddies and their environment is vital. The latter has been done for instance by Messager et al. (2012) who measured the atmospheric boundary layer south of Africa over ACC fronts and warm-core eddies, or was tried with the Polarstern cruise carrying out the *Eddy Pump* project (see e.g. http://www.awi.de) where the goal was to measure the physics, chemistry and biology of ocean eddies for the examination of the carbon pumps.
The last point we note here with respect to our work is that -as indicated before- our

results can be used to improve numerical models:

- **Model evaluation**: the "eddy-data set" assembled in the framework of this thesis can be applied for the purpose of evaluation, i.e. to test the skill of a numerical model (ocean/atmosphere/biogeochemistry) with respect to the characteristics of eddies and their impacts found in this work. For instance, one may compare the temperature and salt anomalies and the vertical structure of eddies as found in satellite observations and *Argo* floats with eddies from model simulations.

- **Improvement or development of parameterizations:** if one finds processes with significant impacts from observations which are not resolved in typical numerical models, one needs to represent their impacts based on quantities which are resolved by the model; the eddy impacts we found are partly not included in global general circulation models and depending on the questions one is interested in might be needed to be incorporated. For instance a potential net effect on clouds due to eddies may play a role in the local radiation budget or for biological production.

Obviously the above suggestions require quite different investments of time and cost (for instance computer power for expensive model simulations, or for elaborate in-situ observations or laboratory work). My specific next research steps following up on this work will be to

- expand the preliminary work on *Argo* floats, for instance deriving the subsurface two dimensional structure of ocean eddies.

- to use temperature as a non-reactive tracer and compare the eddies' effect on the former with their effect on *CHL*. For instance different spatial pattern in environments of similar large-scale gradients, or different decorrelation time scales could deliver hints on the extent of eddies impacting *CHL* purely as a passive tracer, or precisely as reactive tracer.

- analysis of ocean-atmosphere coupled model results, run presently over the south Atlantic; I will test the skill of the model system to reproduce my findings, and if it does so to investigate the impact of air-sea interactions associated with eddies on the ocean (for instance on temperature and salinity, i.e. ocean surface stratification).

- complete the set-up and evaluation of an ocean-biogeochemistry model for the SO, and subsequently test the skill of the model to reproduce my findings on the effect of eddies on *CHL*; potential future goals would be to disentangle the potential mechanisms for the *CHL* imprint of eddies with approaches as suggested above (e.g. switching on/off phytoplankton growth limitations), and an examination of the local carbon budget of the average eddy to obtain indications of their contribution to the SO carbon budget.

With that I would like to conclude that last but not least I wish for our work to inspire further research on SO eddies and their role in the Earth system.

List of Tables

List of Figures

A. Detection and Tracking of Mesoscale Oceanic Eddies

A.1. Detection-Matlab Routine

```
%-------------------------------------------------------------------------------------------------
%-------------------------------------------------------------------------------------------------
function [W lonf latf stdW u v w] = okubo_weiss(lon,lat,sla,date,timestp,name,threshOW);
%
lonmin=min(lon);
lonmax=max(lon);
latmin=min(lat);
latmax=max(lat);
plots=0;
% INPUT: lon: vector with longitudes
%        lat: vector with latitudes
%        sla: sea level anomalies
% of selected domain
%
%-------------------------------------------------------------------------------------------------
%% USERS DEFINED VARIABLES
%
g=9.81; % m/2ï£· acceleration due to gravity
Er=6371000; % m Earth's radius
omega=2*pi/(24*60*60); % 7.29*10^-5; % 1/s rotational speed of the Earth
%
% Matrix of latitudes & longitudes
[lonf latf]=meshgrid(lon,lat);
%
%-------------------------------------------------------------------------------------------------
% CALCULATIONS
%
% Okubo Weiss Parameter (see Okubo/Weiss)
%
% First the geostrophic velocities U=-g/f*dSLA/dy & V=g/f*dSLA/dx
slacirc=repmat(sla,[1,3]);
[dsla_xcirc,dsla_ycirc]=gradient(slacirc);% dsla_y=-dsla_y;
if length(lon)~=size(sla,2);stop;end
dsla_x=dsla_xcirc(:,length(lon)+1:length(lon)+length(lon));
dsla_y=dsla_ycirc(:,length(lon)+1:length(lon)+length(lon));
%
% Calculation of distances in m, radius Earth in Matlab 6371km
% distance in m
[dlonx,dlony]=gradient(lonf); %dlony=-dlony;
[dlatx,dlaty]=gradient(latf); %dlaty=-dlaty; % as gradient northward positive
%
% was dx, was dy?
for i=1:length(lat)
    dx(i,:)=abs(deg2km(dlonx(i,:),10^-3*max(Er*cos(deg2rad(latf(i,:))))).*10^3);
end
for i=1:length(lat)
    dy(i,:)=abs(deg2km(dlaty(i,:))).*10^3;
end%
%
f_x=2*omega*sin(deg2rad(latf));
f_y=2*omega*sin(deg2rad(latf));
%
u=-g./f_y.*dsla_y./dy.*10^-2;
v=+g./f_x.*dsla_x./dx.*10^-2;
%
ucirc=repmat(u,[1,3]);
vcirc=repmat(v,[1,3]);
[duxcirc,duycirc]=gradient(ucirc); %duy=-duy;
[dvxcirc,dvycirc]=gradient(vcirc); %dvy=-dvy;
if length(lon)~=size(u,2);stop;end;if length(lon)~=size(v,2);stop;end
dux=duxcirc(:,length(lon)+1:length(lon)+length(lon));
duy=duycirc(:,length(lon)+1:length(lon)+length(lon));
dvx=dvxcirc(:,length(lon)+1:length(lon)+length(lon));
dvy=dvycirc(:,length(lon)+1:length(lon)+length(lon));
%
% matlab sign (gradient from up) cancels because of double derivative?!
%
% Vorticity w=dv/dx-du/dy
w=dvx./dx-duy./dy;
%
```

```
% Normal component of the strain sn=du/dx-dv/dy
sn=dux./dx-dvy./dy;
%
% Shear component of the strain ss=dv/dx+du/dy
ss=dvx./dx+duy./dy;
%
% Okubo-Weiss parameter W=sn^2+ss^2-w^2
W=sn.^2+ss.^2-w.^2;
%
% Threshold value of OK-parameter (Isern-Fontanet 200x), -0.2 spatial-std-OW
stdW=nanstd(W(:));
%
% TESTPLOTS xxxxxxxxxxxxxxxxxxxxxxxxxxxxxxxx
if plots==1
%plot region of interest
figure
scrsz = get(0,'ScreenSize');
set(gcf, 'Visible','off','PaperPosition', [0 0 6 3.5],'PaperPositionMode','auto','PaperType','A2',...
   'Position',[1 scrsz(4)/1.46 scrsz(3)/1.5 scrsz(4)/1.46]);
set(gcf, 'PaperUnits', 'centimeters');
set(gcf, 'PaperPosition', [1 1 13 7]);
%
slaplot=sla;
slaplot(slaplot>900.)=NaN;
surface(lon,lat,slaplot,double(slaplot),'LineStyle','none','FaceAlpha',0.6);
xlim([lonmin lonmax])
ylim([latmin latmax])
%set(gca,'ZScale','log','ZMinorTick','on','CLim',[0 1])
colormap(gca,jet); colorbar;caxis([0 0.2]);
%
grid on;
caxis([-25 25])
colorbar
hold on
patch(surf2patch(lon,lat,Wo_ce),'LineStyle','none','FaceColor','w','FaceAlpha',0.6)
hold on
patch(surf2patch(lon,lat,Wo_ae),'LineStyle','none','FaceColor','k','FaceAlpha',0.6)
title(['MSLA ',date,' [cm] with eddies overlayed'])
%
print('-dtiff','-r100',[num2str(timestp),'_okubo-weiss_',date,name])
close gcf
end
% END PLOTS xxxxxxxxxxxxxxxxxxxxxxxxxxxxxxxx
%
%-------------------------------------------------------------------------------------------------------
%-------------------------------------------------------------------------------------------------------
```

A.2. Eddy Extraction and Collocation with Additional Observations

```
%-----------------------------------------------------------------------------------------------------
function [eddy_ee chl_mark chl_eedmark]=lable_eddies_io(eeflag,esize_min,lon_sel,lat_sel,sla_sel,...
    chl_sel,achl_sel,sst_sel,asst_sel,cf_sel,u_sel,v_sel,w_sel,wi_sel,rain_sel,chl_mark,count,Wo,...
    lonf,latf,datevect,name,ratio,testplot,chl_eedmark)
%
%% Extension _____________________________________________________________
% extend first all fields in x-direction, so that they are double (otherwise problem at
% edges with 'half-eddies'
sizex=length(lon_sel);
sizey=length(lat_sel);
limmin=sizex/36+2;
limmax=sizex+sizex/36+1;
%
lon_sel= repmat(lon_sel,[3,1]);    lon_sel=lon_sel(sizex-sizex/36:2*sizex+sizex/36);
sla_sel= repmat(sla_sel,[1,3]);    sla_sel=sla_sel(:,(sizex-sizex/36:2*sizex+sizex/36));
chl_sel= repmat(chl_sel,[1,3]);    chl_sel=chl_sel(:,(sizex-sizex/36:2*sizex+sizex/36));
achl_sel= repmat(achl_sel,[1,3]);  achl_sel=achl_sel(:,(sizex-sizex/36:2*sizex+sizex/36));
sst_sel= repmat(sst_sel,[1,3]);    sst_sel=sst_sel(:,(sizex-sizex/36:2*sizex+sizex/36));
asst_sel= repmat(asst_sel,[1,3]);  asst_sel=asst_sel(:,(sizex-sizex/36:2*sizex+sizex/36));
cf_sel= repmat(cf_sel,[1,3]);      cf_sel=cf_sel(:,(sizex-sizex/36:2*sizex+sizex/36));
u_sel= repmat(u_sel,[1,3]);        u_sel=u_sel(:,(sizex-sizex/36:2*sizex+sizex/36));
v_sel= repmat(v_sel,[1,3]);        v_sel=v_sel(:,(sizex-sizex/36:2*sizex+sizex/36));
w_sel= repmat(w_sel,[1,3]);        w_sel=w_sel(:,(sizex-sizex/36:2*sizex+sizex/36));
wi_sel= repmat(wi_sel,[1,3]);        wi_sel=wi_sel(:,(sizex-sizex/36:2*sizex+sizex/36));
rain_sel= repmat(rain_sel,[1,3]);        rain_sel=rain_sel(:,(sizex-sizex/36:2*sizex+sizex/36));
chl_mark= repmat(chl_mark,[1,3]);  chl_mark=chl_mark(:,(sizex-sizex/36:2*sizex+sizex/36));
chl_eedmark= repmat(chl_eedmark,[1,3]);chl_eedmark=chl_eedmark(:,(sizex-sizex/36:2*sizex+sizex/36));
Wo= repmat(Wo,[1,3]);              Wo=Wo(:,(sizex-sizex/36:2*sizex+sizex/36));
%
lonf= repmat(lonf,[1,3]);          lonf=lonf(:,(sizex-sizex/36:2*sizex+sizex/36));
latf= repmat(latf,[1,3]);          latf=latf(:,(sizex-sizex/36:2*sizex+sizex/36));
lonf(:,1:limmin-1)=lonf(:,1:limmin-1)-360;
lonf(:,limmax+1:end)=lonf(:,limmax+1:end)+360;
%
%-----------------------------------------------------------------------------------------------------
%-----------------------------------------------------------------------------------------------------
%
plots=1;
Er=6371000; % m Earth's radius
lonmin=min(lon_sel);
lonmax=max(lon_sel);
latmin=min(lat_sel);
latmax=max(lat_sel);
%
if testplot==1 % xxxxxxxxxxxxxxxxxxxxxxxxxxxxxxxxxxxxxxxxxxxxxxxxxxxxxxxx
%
figure;surface(lon_sel,lat_sel,double(sla_sel),'FaceAlpha',0.5)
caxis([-15 15])
colorbar
xlim([min(lon_sel)-1 max(lon_sel)+1])
hold on
        for test1=1:length(lon_sel)
         for test2=1:length(lat_sel)
           if Wo(test2,test1)==1
               plot(lon_sel(test1),lat_sel(test2),'bo')
           end
         end
        end
end % xxxxxxxxxxxxxxxxxxxxxxxxxxxxxxxxxxxxxxxxxxxxxxxxxxxxxxxxxxxxxxxxxxxxxx
%
display (['Check if eddy coincides with regional extremum (a little "blurred", meaning +1 box']);
tic
%
% Regional extrem values (NaN not possible)
sla_sel(isnan(sla_sel))=999.;
if strcmp(eeflag,'ae')
    ee=imregionalmax(sla_sel);
elseif strcmp(eeflag,'ce')
    ee=imregionalmin(sla_sel);
else
    stop
end
%
% Not only one box but possibility for shift, little more "soft"
x=size(sla_sel);
ee_test=ee;
for i=1:x(1)
    for j=1:x(2)
      if ee_test(i,j)==1
         if i~=x(1); ee(i+1,j)=1; end
         if i~= 1;   ee(i-1,j)=1; end
         if j~=x(2); ee(i,j+1)=1; end
         if j~= 1;   ee(i,j-1)=1; end
         if i~=x(1) && j~=x(2); ee(i+1,j+1)=1; end
         if i~= 1   && j~= 1;   ee(i-1,j-1)=1; end
         if i~=x(1) && j~= 1;   ee(i+1,j-1)=1; end
         if i~= 1   && j~=x(2); ee(i-1,j+1)=1; end
      end
    end
end
u=toc; display(['Time elapsed in min: ',num2str(u/60)])
%
display('Get # of eddies (bwboundaries)');tic
% mask out all eddies of 'the other sign' in vorticity
w_sel(isnan(w_sel))=999;
if strcmp(eeflag,'ae')
    temp=w_sel;temp(temp < 10^(-20)) = 0; temp(temp > 10^(-20)) = 1;
elseif strcmp(eeflag,'ce')
    temp=w_sel;temp(temp > -10^(-20)) = 0; temp(temp < -10^(-20)) = 1;
else
    stop
end
sla_sel(sla_sel>900)=NaN;
w_sel(w_sel>900)=NaN;
%
% Only sla where OW showed eddy + only where vorticity shows right sign
sla_wo=Wo.*sla_sel.*temp; clear temp;
%
sla_wo(isnan(sla_wo))=0;
[bou lab no]=bwboundaries(sla_wo,4);
% % clean up 'border-doubles'
```

```
% for i=1:length(chl_lat_sel)
%     if length(find(lab(i,:))~=0
%     end
% end
% %
u=toc; display(['Time elapsed in min: ',num2str(u/60)])
%
% Collect features eddies
%
display('Get regional properties (regionprops)');tic
% Derive features eddies
x=regionprops(lab,sla_wo,'MaxIntensity','MinIntensity',...
    'Area','Pixelvalues');
u=toc; display(['Time elapsed in min: ',num2str(u/60)])
%
%-------------------------------------------------------------------------------------------------
dlonf=gradient(lonf);
[dum dlatf]=gradient(latf); dlatf=-dlatf;
%
%-------------------------------------------------------------------------------------------------
%-------------------------------------------------------------------------------------------------
%% Loop over all eddies
%
display (['Collect eddy characteristics']);tic
eddy_ee=[];unmatched_ee=[];
for n=1:no
     % clear all variables from last eddy
      clear ampl edampl lonc latc ed_lon ed_lat ed_sla edampl meanampl esize loncm latcm ed_dlon...
          ed_dlat rchl_sel rachl_sel indeces ed_sst ed_asst ed_cf ed_u ed_v ed_w bouee
      %
      eddy_mask=(lab==n);
      ed_lon=lonf(eddy_mask);
      ed_lat=latf(eddy_mask);
      ed_dlon=dlonf(eddy_mask);
      ed_dlat=dlatf(eddy_mask);
      ed_sla=sla_sel(eddy_mask);
      ed_sst=sst_sel(eddy_mask);
      ed_asst=asst_sel(eddy_mask);
      ed_cf=cf_sel(eddy_mask);
      ed_u=u_sel(eddy_mask);
      ed_v=v_sel(eddy_mask);
      ed_w=w_sel(eddy_mask);
      ed_wi=wi_sel(eddy_mask);
      ed_rn=rain_sel(eddy_mask);
      esize=x(n).Area;
      %
      % in case switch from 0 to 360, add 360
      temp=ed_lon;
      if abs(max(temp)-min(temp)) > 200;temp(temp<50)=temp(temp<50)+360;end
      loncm=mean(temp);
      if loncm > 360;loncm=loncm-360; end
      if loncm < 0;loncm=loncm+360; end
      latcm=mean(ed_lat);
      %
%-------------------------------------------------------------------------------------------------
%
% criteria if eddy in that location
if strcmp(eeflag,'ae')
    isaneddyhere=(max(max(sla_sel.*eddy_mask.*ee))==x(n).MaxIntensity);
elseif strcmp(eeflag,'ce')
    isaneddyhere=(min(min(sla_sel.*eddy_mask.*ee))==x(n).MinIntensity);
else
    stop
end
%-------------------------------------------------------------------------------------------------
if isaneddyhere
%
% Only detected eddies greater than a certain box number
if (esize >= esize_min)
%
% if eddy onlly '1 grid box wide', skip
distx=max(ed_lon)-min(ed_lon); distx1box=max(ed_dlon);
disty=max(ed_lat)-min(ed_lat); disty1box=max(ed_dlat);
if (distx/distx1box <1) || (disty/disty1box <1);'test';continue;end
      %
      if strcmp(eeflag,'ae')
           ampl=(x(n).MaxIntensity);
           lonc=ed_lon(x(n).MaxIntensity==ed_sla);
           latc=ed_lat(x(n).MaxIntensity==ed_sla);
           [dum idx]=find(x(n).MaxIntensity==sla_sel & eddy_mask==1);
     elseif strcmp(eeflag,'ce')
           ampl=(x(n).MinIntensity);
           lonc=ed_lon(x(n).MinIntensity==ed_sla);
           latc=ed_lat(x(n).MinIntensity==ed_sla);
           [dum idx]=find(x(n).MinIntensity==sla_sel & eddy_mask==1);
      else
          stop
      end
      edampl=abs(x(n).MaxIntensity-x(n).MinIntensity);
      %
      bouee=bou;
      %
      earea=sum(areaquad(double(ed_lat(:)-ed_dlat(:)/2),double(ed_lon(:)-ed_dlon(:)/2),...
          double(ed_lat(:)+ed_dlat(:)/2),double(ed_lon(:)+ed_dlon(:)/2),Er));
      edia=sqrt(earea*4/pi())/1000;
      %
      ed_uedg=[];ed_vedg=[];ed_slaedg=[];
      for b=1:length(bouee{n}(1:end-1,1))
        ed_uedg(b)=u_sel(bouee{n}(b,1),bouee{n}(b,2));
        ed_vedg(b)=v_sel(bouee{n}(b,1),bouee{n}(b,2));
      end
      % eddy rotational speed
      ed_spedg=nanmean(sqrt(ed_uedg.^2 + ed_vedg.^2));
      ed_spin=nanmean(sqrt(ed_u.^2 + ed_v.^2));
      %
      rchl_sel=chl_sel(eddy_mask);
      rachl_sel=achl_sel(eddy_mask);
      rchl_sel(isnan(rachl_sel))=NaN;
      if (isempty(rchl_sel) || isempty(rachl_sel))
          save all;stop
      end
      %
      %-------------------------------------------------------------------------------------------
      % Inner and outer chlorophyll and eddy amplitude compared to
      % surrounding
      %
      % Create polygon with help from bou from bwboudaries
      ed_latb=[];ed_lonb=[];
      for b=1:length(bouee{n}(:,1))
         ed_latb=[ed_latb;latf(bouee{n}(b,1),bouee{n}(b,2))];
```

```
   ed_lonb=[ed_lonb;lonf(bouee{n}(b,1),bouee{n}(b,2))];
end
[ed_lonb ed_latb]=poly2cw(ed_lonb,ed_latb);
%ed_lonb=wrapTo360(ed_lonb);
%
% Mean gridspacing
gbar=(mean(abs(ed_dlon))+mean(abs(ed_dlat)))/2/2;
%
% Create buffer zone for inner part of eddy
if isempty(ed_lonb);
    ed_lonb
    bouee{n}
    stop
end
 % diameter, extend to eddy diameter
  disty=km2deg(edia/2,Er*10^-3);
  distx=km2deg(edia/2,Er*10^-3*cos(deg2rad(latcm)));
  mrad=(distx+disty)/2;
%
buffermsize=mrad;%4*double(gbar/0.9)
[ed_lato,ed_lono] = bufferm((ed_latb),(ed_lonb),buffermsize,'out',10);
%
% in case outer area weird (empty/too short)
if isempty(ed_lato) || isempty(ed_lono) || ...
  length(ed_lato)<length(ed_latb) || length(ed_lono)<length(ed_lonb)
  % polygon line... too many 'repetitions'? Works if last one is
  % skipped
 if ed_lonb(1)==ed_lonb(end) && ed_latb(1)==ed_latb(end)
   [ed_lato,ed_lono] = bufferm(ed_latb(1:end-1),ed_lonb(1:end-1),buffermsize,'out',10);
 end
 %
 if isempty(ed_lato) || isempty(ed_lono) || ...
  length(ed_lato)<length(ed_lat) || length(ed_lono)<length(ed_lon)
  count
  stop
 end
end
ed_lono=wrapTo360(ed_lono);
%
% if eddy at meridian, shift lons -
if abs(min(abs(ed_lono))-(max(abs(ed_lono)))) > 200
     save test ed_lono ed_lato
      tmped_lono=ed_lono;tmped_lono(tmped_lono<50)=tmped_lono(tmped_lono<50)+360;
      maskchl1=logical(inpolygon(lonf,latf,tmped_lono,ed_lato));
      tmped_lono=ed_lono;tmped_lono(tmped_lono>200)=tmped_lono(tmped_lono>200)-360;
      maskchl2=logical(inpolygon(lonf,latf,tmped_lono,ed_lato));
      maskchl=maskchl1 | maskchl2;
 else
      maskchl=logical(inpolygon(lonf,latf,ed_lono,ed_lato));
 end
%
% inner same as eddy detection, as OW underestimates eddy size
maskchli=eddy_mask;
maskchl=logical(maskchl & ~maskchli);
maskchli=logical(maskchli);
%
rchl_seli=chl_sel(maskchli);
rchl_selo=chl_sel(maskchl);
rachl_selo=achl_sel(maskchl);
if isempty(rchl_selo) || isempty(rachl_selo) ||  isempty(rchl_seli);stop
    count
end
rchl_seli(isnan(achl_sel(maskchli)))=NaN;
rchl_selo(isnan(achl_sel(maskchl)))=NaN;
%
maskchliindx=lonf(find(maskchli==1));
maskchliindy=latf(find(maskchli==1));
maskchloindx=lonf(find(maskchl==1));
maskchloindy=latf(find(maskchl==1));
%
ed_edgsla=sla_sel(maskchl);
% eddy amplitude
ed_slaedgampm=abs(ampl-(nanmean(ed_edgsla)));
%
% Dipole (include the ring around the core for this)
maskchlio=(maskchli | maskchl);
ed_lono=lonf(maskchlio);
ed_lato=latf(maskchlio);
%
% calculate dipole moment including outer
rchl_selio=[rchl_seli;rchl_selo];
 if sum(~isnan(rchl_selio))/length(rchl_selio) >= 0.8 ...
         && sum(~isnan(rachl_sel))/length(rachl_sel) >= 0.8
       coursex=NaN(length(ed_lono),1);coursey=NaN(length(ed_lono),1);
       distx=NaN(length(ed_lono),1);disty=NaN(length(ed_lono),1);
    for l=1:length(ed_lono)
        [coursex(l) distx(l)]=legs([latcm latcm],...
                                   [loncm ed_lono(l)]);
        [coursey(l) disty(l)]=legs([latcm ed_lato(l)],...
                                   [loncm loncm]);
     end
     distedx=distdim(distx,'nm','km');
     distedy=distdim(disty,'nm','km');
     %
     distedx(coursex >= 210)=-distedx(coursex >= 210);%distedx=distedx';
     distedy(coursey >=170 )=-distedy(coursey >= 170);%distedy=distedy';
     T
     %save test maskchlio achl_sel distedx distedy
     % Dipolemoment
     ed_dipox=(nansum(distedx.*achl_sel(maskchlio)));
     ed_dipoy=(nansum(distedy.*achl_sel(maskchlio)));
     clear dist course
     T
     % Monopolmoment
     ed_mono=nansum(achl_sel(maskchlio));
 else
     ed_dipox=NaN;
     ed_dipoy=NaN;
     ed_mono=NaN;
end
%
chl_eedmark(maskchl)=3;
chl_eedmark(maskchli)=1;
chl_eedmark(maskchli&maskchl)=4;
clear  maskchl maskchli maskchlia maskchlib maskchla maskchlb
% end inner/outer chl
%-------------------------------------------------------------------------------------------
%
 if min(min(chl_mark(eddy_mask)))<-900
     %display(['Chlorophyll of',num2str(length(chl_mark(eddy_mask)<-900))])
```

```
    %display('pixel collected multiple times.')
    chl_mark(chl_mark(eddy_mask)<-900)=chl_mark(chl_mark(eddy_mask)<-900)-1;
    chl_mark(chl_mark(eddy_mask)<-900)=chl_mark(chl_mark(eddy_mask)<-900)-1;
end
% Mark chlfield
chl_mark(eddy_mask)=-999;
%
%TESTPLOT xxxxxxxxxxxxxxxxxxxxxxxxxxxxxxxxxxxxxxxxxxxxxxxxxxxxxxxxxxxx
if testplot==1
for test=1:length(lon_sel(ilons))
 for test2=1:length(lat_sel(ilats))
  plot(lon_sel(ilons(test)),lat_sel(ilats(test2)),'g.')
 end;
end
title('Detected eddies (Wo, red and blue o) and matched chlorophyll with it (green .)')
end % xxxxxxxxxxxxxxxxxxxxxxxxxxxxxxxxxxxxxxxxxxxxxxxxxxxxxxxxxxxxxxx
%
%-------------------------------------------------------------------------------------------
%
% prepare data to be saved
% as detection possible to do parallel, do as much as possible here
% (not in tracking)
%Check occurence of missing values
if isempty(find(isnan(rachl_sel),1))
    chlmis=0;
else % At least one missing value
    chlmis=sum(isnan(rachl_sel))./length(rachl_sel);
end
if isempty(max(rchl_sel(~isnan(rachl_sel))));
    chlmax=NaN;
else
    chlmax=max(rchl_sel(~isnan(rachl_sel)));
end;
if isempty(min(rchl_sel(~isnan(rachl_sel))));
    chlmin=NaN;
else
   chlmin=min(rchl_sel(~isnan(rachl_sel)));
end;
if isempty(chlmax); chlmax=NaN; end;
if isempty(chlmin); chlmin=NaN; end;
%
chlmean =nanmean(rchl_sel);
achlmean=nanmean(rachl_sel);
%chlmeani=nanmean(rchl_seli);
chlmeano=nanmean(rchl_selo);
%achlmeani=nanmean(rachl_seli);
achlmeano=nanmean(rachl_selo);
%
sst     =nanmean(ed_sst);
asst    =nanmean(ed_asst);
cf      =nanmean(ed_cf);
eke=(ed_u.^2 + ed_v.^2)./2;
ekem    =nanmean(eke);
sla_edg =nanmean(ed_edgsla);
ed_vort =nanmean(ed_w);
stop
ed_wim =nanmean(ed_wi);
ed_rnm =nanmean(ed_rn);
%-------------------------------------------------------------------------------------------
%
    if isempty(eddy_ee)
    eddy_ee=struct('ampl',ampl,'edampl',edampl,'size',esize,'sla',ed_sla,'lon',ed_lon,'lat',ed_lat,...
      'lonc',lonc,'latc',latc,'loncm',loncm,'latcm',latcm,'chl',rchl_sel,'achl',rachl_sel,...
      'date',floor(str2num(datevect)),'dia',edia,'sla_edg',ed_edgsla,'maskchliind',...
      [maskchliindx maskchliindy],'maskchloind',[maskchloindx maskchloindy],...
      'chl_o',rchl_selo,'achl_o',rachl_sel,'sst',ed_sst,'asst',ed_asst,'cf',ed_cf,...
      'ed_u',ed_u,'ed_v',ed_v,'ed_w',ed_w,'ed_wi',ed_wim,'ed_rain',ed_rnm,'ed_spedg',...
      ed_spedg,'ed_spin',ed_spin,'ampl_slaedg',ed_slaedgampm,'bouee',bouee{n},...
      'chlmean',chlmean,'achlmean',achlmean,'achlmeano',achlmeano,'chlmeano',chlmeano,...
      'chlmin',chlmin,'chlmax',chlmax,'chlmis',chlmis,'sstm',sst,'asstm',asst,'cfm',cf,...
      'ekem',ekem,'sla_edgm',sla_edg,'ed_vort',ed_vort,'ed_dipox',ed_dipox,'ed_dipoy',ed_dipoy,...
      'ed_mono',ed_mono,'ed_idx',idx);
    else
    eddy_ee(end+1)=struct('ampl',ampl,'edampl',edampl,'size',esize,'sla',ed_sla,'lon',ed_lon,'lat',ed_lat,...
      'lonc',lonc,'latc',latc,'loncm',loncm,'latcm',latcm,'chl',rchl_sel,'achl',rachl_sel,...
      'date',floor(str2num(datevect)),'dia',edia,'sla_edg',ed_edgsla,'maskchliind',...
      [maskchliindx maskchliindy],'maskchloind',[maskchloindx maskchloindy],...
      'chl_o',rchl_selo,'achl_o',rachl_sel,'sst',ed_sst,'asst',ed_asst,'cf',ed_cf,...
      'ed_u',ed_u,'ed_v',ed_v,'ed_w',ed_w,'ed_wi',ed_wim,'ed_rain',ed_rnm,'ed_spedg',...
      ed_spedg,'ed_spin',ed_spin,'ampl_slaedg',ed_slaedgampm,'bouee',bouee{n},...
      'chlmean',chlmean,'achlmean',achlmean,'achlmeano',achlmeano,'chlmeano',chlmeano,...
      'chlmin',chlmin,'chlmax',chlmax,'chlmis',chlmis,'sstm',sst,'asstm',asst,'cfm',cf,...
      'ekem',ekem,'sla_edgm',sla_edg,'ed_vort',ed_vort,'ed_dipox',ed_dipox,'ed_dipoy',ed_dipoy,...
      'ed_mono',ed_mono,'ed_idx',idx);
    end
end % minsize
clear isaneddyhere
end % isaneddyhere
end % n: all eddies in this map
%
%-------------------------------------------------------------------------------------------
%% Sort out double eddies (from multiplication of x-dimension)
%
% first arrays
chl_mark= chl_mark(:,limmin:limmax);
chl_eedmark= chl_eedmark(:,limmin:limmax);
lonf= lonf(:,limmin:limmax);
latf= latf(:,limmin:limmax);
%
temp=[];
for nu=1:length(eddy_ee)
    if eddy_ee(nu).ed_idx >= limmin && eddy_ee(nu).ed_idx <= limmax
        if ~isstruct(temp)
            temp=eddy_ee(nu);
        else
            temp(end+1)=eddy_ee(nu);
        end
    end
end
%
checkdoub=zeros(sizey,sizex);
for nu=1:length(temp)
    idx=find(temp(nu).lonc==lonf & temp(nu).latc==latf);
    if isempty(idx);stop;end
    if checkdoub(idx)==1;stop;end
    checkdoub(idx)=1;
 %   if temp(nu).loncm < 181 & temp(nu).loncm > 179;stop;end
end
%
eddy_ee=temp;
```

```
%
%-------------------------------------------------------------------------
%-------------------------------------------------------------------------
%-------------------------------------------------------------------------
%% PLOTS
%
if plots==9
scrsz = get(0,'ScreenSize');
figure%*********************************
set(gcf, 'Visible','off','PaperPosition', [0 0 6 3],'PaperPositionMode','auto','PaperType','A2',...
    'Position',[1 scrsz(4)/1.46 scrsz(3)/1.5 scrsz(4)/1.46]);
slaplot=sla_sel;
slaplot(slaplot>900.)=NaN;
contourf(lon_sel,lat_sel,slaplot,'LevelStep',3)
%surface(lon_sel,lat_sel,slaplot,double(slaplot),'LineStyle','none','FaceAlpha',0.5)
hold on;
grid on;
pbaspect(ratio)
caxis([-25 25])
colorbar
xlim([lonmin lonmax])
ylim([latmin latmax])
for e=1:length(eddy_ae)
    plot(eddy_ae(e).lon,eddy_ae(e).lat,'w.')
    hold on;
    text(eddy_ae(e).lonc,eddy_ae(e).latc,['\bf\fontsize{9}\color{white}',num2str(e)])
end
for e=1:length(eddy_ce)
    plot(eddy_ce(e).lon,eddy_ce(e).lat,'k.')
    hold on;
    text(eddy_ce(e).lonc,eddy_ce(e).latc,['\bf\fontsize{9}\color{black}',num2str(e)])
end
for e=1:length(unmatched_ee)
    plot(unmatched_ee(e).lon,unmatched_ee(e).lat,'wo')
    hold on;
end
for e=1:length(unmatched_ee)
    plot(unmatched_ee(e).lon,unmatched_ee(e).lat,'ko')
    hold on;
end
title(['MSLA ',date,'[cm]']);

print('-dtiff','-r100',[num2str(count),'_lable-eddies_',date,name])
gcf;
%
end
%-------------------------------------------------------------------------
%-------------------------------------------------------------------------
```

A.3. Tracking-Matlab Routine


```
%-------------------------------------------------------------------------------------------------------
%-------------------------------------------------------------------------------------------------------
% Function which gets as input maps for each time step with eddies and
% returns the time series of eddies
%
%-------------------------------------------------------------------------------------------------------
function [eeddies]=track_eddies_io(eddies_ss,tsp_s,tsp_e,tsp,eeddies,...
    u_mean,v_mean,u_std,v_std,lon_sel,lat_sel,eddies_ampstd,eddies_diastd,eddies_sststd,eddies_vorstd,...
    lonsearch,latsearch,testplot,ro,skip,threshmaxtrav,eint,erotr,timestepping,threshsim,pathyd,name,...
    rotstr);
%
savethings=0;
if savethings==1;system('rm output.txt');fid = fopen('output.txt', 'a');end
%
histsim=[];
histell=[];
%
d=timestepping;
Er=6371000; % m Earth's radius
%
rolats=ro(:,1);
rolons=ro(:,2);
%
[lonsearchf latsearchf]=meshgrid(lonsearch,latsearch);
%
%-------------------------------------------------------------------------------------------------------
%-------------------------------------------------------------------------------------------------------
if isempty(eeddies)
display('Collect eddies of first time step (throw out afterwards as "none-complete").')
% FIRST TIME STEP: collect ALL eddies
eeddies=cell(length(eddies_ss{tsp_s}),1);
for e=1:length(eddies_ss{tsp_s})
    %
    % Features we want to collect: mean velocities and chl_orophyll
    %
    % Which month are we in? (from input file)
    datestr=num2str(eddies_ss{tsp_s}(e).date);
    monthstr=datestr(5:6); month=str2double(monthstr);
    u=u_mean{month};ustd=u_std{month};
    v=v_mean{month};vstd=v_std{month};
    uc=[];vc=[];ustdc=[];vstdc=[];
    for us=1:length(eddies_ss{tsp_s}(e).lon)
    indexlon=find(lon_sel==eddies_ss{tsp_s}(e).lon(us));
    indexlat=find(lat_sel==eddies_ss{tsp_s}(e).lat(us));
    uc=[uc u(indexlat,indexlon)];ustdc=[ustdc ustd(indexlat,indexlon)];
    vc=[vc v(indexlat,indexlon)];vstdc=[vstdc vstd(indexlat,indexlon)];
    end
    um=mean(uc); ustdm=mean(ustdc);
    vm=mean(vc); vstdm=mean(vstdc);
    %
    eddy_tsc=double([eddies_ss{tsp_s}(e).loncm eddies_ss{tsp_s}(e).latcm ...
            eddies_ss{tsp_s}(e).dia eddies_ss{tsp_s}(e).ampl ...
            (eddies_ss{tsp_s}(e).ed_wi) (eddies_ss{tsp_s}(e).ed_rain) ...
            max(eddies_ss{tsp_s}(e).ed_mono) min(eddies_ss{tsp_s}(e).lat) ...
            eddies_ss{tsp_s}(e).edampl tsp_s eddies_ss{tsp_s}(e).chlmean eddies_ss{tsp_s}(e).chlmax...
            eddies_ss{tsp_s}(e).chlmin eddies_ss{tsp_s}(e).chlmis ...
            eddies_ss{tsp_s}(e).date*10^-8 um vm eddies_ss{tsp_s}(e).achlmean ...
            eddies_ss{tsp_s}(e).achlmeano eddies_ss{tsp_s}(e).chlmeano eddies_ss{tsp_s}(e).sla_edgm...
            eddies_ss{tsp_s}(e).ampl_slaedg ustdm vstdm NaN NaN ...
            eddies_ss{tsp_s}(e).sstm eddies_ss{tsp_s}(e).asstm eddies_ss{tsp_s}(e).cfm...
            eddies_ss{tsp_s}(e).ekem eddies_ss{tsp_s}(e).ed_spedg eddies_ss{tsp_s}(e).ed_vort...
            eddies_ss{tsp_s}(e).ed_dipox eddies_ss{tsp_s}(e).ed_dipoy 0]);
    %
    % Collect time series of each eddy in a cell array
    eeddies{e}=eddy_tsc;
    tsp=tsp_s+1;
end
else
%    stop
    tsp=tsp+1;
end % First timestep, no eddies collected yet
%-------------------------------------------------------------------------------------------------------
%-------------------------------------------------------------------------------------------------------
%
% Allocate each eddy in the next time steps to one of the eddies before, if
% not possible, new eddy.
%-------------------------------------------------------------------------------------------------------
%-------------------------------------------------------------------------------------------------------
%
% For each time step AFTER THE FIRST ONE
checkend=0;
while checkend==0;
tic
%
% Marker if eddy will be taken
counted=zeros(2,length(eddies_ss{tsp}));
eddies_ellc=NaN(2,length(eddies_ss{tsp}));
% Reset
um=[];vm=[];ustdm=[];vstdm=[];
%
display(['tsp************************************************************'])
display(['Allocate eddies for timestep ',num2str(tsp),' and date ',num2str(eddies_ss{tsp}(1).date)])
%
%-------------------------------------------------------------------------------------------------------
%-------------------------------------------------------------------------------------------------------
% For each eddy of the time step before
for ee_col=1:length(eeddies)
    %
    % ---------------------------------------------------------------------
    if (ee_col==1.) % only once collect all eddies in the current time step
    %display(['Collect all uv/chl for eddies of map #',num2str(g)])
    for ee_attsp=1:length(eddies_ss{tsp})
    %testplot=0;

    % Same calculations as before for the selected eddies
    % Which month are we in? (from input file)
    datestr=num2str(eddies_ss{tsp}(ee_attsp).date);
    monthstr=datestr(5:6); month=str2double(monthstr);
```

```
    u=u_mean{month};ustd=u_std{month};
    v=v_mean{month};vstd=v_std{month};
    uc=[];vc=[];ustdc=[];vstdc=[];
    %
    for us=1:length(eddies_ss{tsp}(ee_attsp).lon)
    indexlon=find(lon_sel==eddies_ss{tsp}(ee_attsp).lon(us));
    indexlat=find(lat_sel==eddies_ss{tsp}(ee_attsp).lat(us));
    uc=[uc u(indexlat,indexlon)];ustdc=[ustdc ustd(indexlat,indexlon)];
    vc=[vc v(indexlat,indexlon)];vstdc=[vstdc vstd(indexlat,indexlon)];
    end
    %
    um(ee_attsp)=mean(uc); ustdm(ee_attsp)=mean(ustdc);
    vm(ee_attsp)=mean(vc); vstdm(ee_attsp)=mean(vstdc);
    %
    end % collect all features for eddies of this time step
    end % only firs t time
    %-----------------------------------------------------------------------
    %
    % Check if eddy (of final collection) existed in time step before
    % current one (or maybe only earlier)
if (eeddies{ee_col}(end,10)==tsp_s+tsp-1-1)
    %display(['Find eddy for eddy #',num2str(ee_col),' in last (',num2str(g-1),'th) timestep'])
    %
    % Then define characterstics which match-eddy has to have
    %
    % 1 eddies_ae_ss{tsp_s}(e).loncm
    % 2 eddies_ae_ss{tsp_s}(e).latcm
    % 3 eddies_ae_ss{tsp_s}(e).dia
    % 4 eddies_ae_ss{tsp_s}(e).ampl = maxint
    % 5 max(eddies_ae_ss{tsp_s}(e).ed_wi)
    % 6 min(eddies_ae_ss{tsp_s}(e).ed_rain)
    % 7 max(eddies_ae_ss{tsp_s}(e).ed_mono)
    % 8 min(eddies_ae_ss{tsp_s}(e).lat)
    % 9 eddies_ae_ss{tsp_s}(e).edampl
    %10 g
    %11 chlmean
    %12 chlmax
    %13 chlmin
    %14 chlmis
    %15 date
    %16 um
    %17 vm
    %18 achlmean
    %19 achlmeano
    %20 chlmeano
    %21 sla_oamplmean
    %22 sla_edgampl
    %23 ustdm
    %24 vstdm
    %25 direction
    %26 distance
    %27 sst
    %28 asst
    %29 cf
    %30 eke
    %31 rotational speed at edge
    %32 mean vorticity in eddy
    %33 dipole  moment x (include outer ring)
    %34 dipole  moment y
    %35 tsp-tsp1
    %
lon_eec=eeddies{ee_col}(end,1);
lat_eec=eeddies{ee_col}(end,2);
size_eec=eeddies{ee_col}(end,3);
ampl_eec=eeddies{ee_col}(end,22);
mampl_eec=abs(eeddies{ee_col}(end,4));
sst_eec=eeddies{ee_col}(end,27);
vor_eec=eeddies{ee_col}(end,32);
tstart_eec=eeddies{ee_col}(1,10);
%
% find idx of respective std in map:
diffidx=abs(lonsearchf-lon_eec) + abs(latsearchf-lat_eec);
idx=find(min(min(diffidx))==diffidx);
stdsize=eddies_diastd(idx);
if length(stdsize)>1;
    stdsize=stdsize(~isnan(stdsize));
    if isempty(stdsize);stdsize=NaN;end
    if length(stdsize)>1;stdsize=stdsize(1);end
end
if stdsize==0;stdsize=NaN; end
%
stdamp=eddies_ampstd(idx);
if length(stdamp)>1;
    stdamp=stdamp(~isnan(stdamp));
    if isempty(stdamp);stdamp=NaN;end
    if length(stdamp)>1;stdamp=stdamp(1);end
end
if stdamp==0;stdamp=NaN; end
%
stdsst=eddies_sststd(idx);
if length(stdsst)>1;
    stdsst=stdsst(~isnan(stdsst));
    if isempty(stdsst);stdsst=NaN;end
    if length(stdsst)>1;stdsst=stdsst(1);end
end
if stdsst==0;stdsst=NaN; end
%
stdvor=eddies_vorstd(idx);
if length(stdvor)>1;
    stdvor=stdvor(~isnan(stdvor));
    if isempty(stdvor);stdvor=NaN;end
    if length(stdvor)>1;stdvor=stdvor(1);end
end
if stdvor==0;stdvor=NaN; end
%
% Extrapolated travel distance ----------------------------------------
%
% If distance between old and projected new location smaller than eddy
% diameter, extend to eddy diameter (doch weggelassen, da spaeter
% draufgemacht)
disty=km2deg(size_eec,Er*10^-3);
distx=km2deg(size_eec,Er*10^-3*cos(deg2rad(lat_eec)));
distdia=(distx+disty)/2;
%
% Advection
londistv=eeddies{ee_col}(end,16)*60*60*24*d*10^-3;
latdistv=eeddies{ee_col}(end,17)*60*60*24*d*10^-3;

% Rossby wave speed from Chlton
% http://www-po.coas.oregonstate.edu/research/po/research/rossby_radius/index.html
```

```
%     * baroclinic gravity-wave phase speed c in m/s
xro=abs(rolats-lat_eec) + abs(rolons-lon_eec);
iroind=find(min(xro)==xro); if length(iroind)>1;iroind=iroind(1);end
rospd=ro(iroind,3);
% in m/sec
rodist=rospd*60*60*24*d*10^-3;
% as now SODA at steering level (see Smith 200x), which equals the phase speed of SLA var seen
% at surface
%rodist=0;
% subtract westward popagation of rossby waves as eddies propagate similar (Chelton2011)
% + rodist;
londistm=(londistv)+(rodist);
latdistm=(latdistv);
%
%totdist=(londistm^2+latdistm^2)^(1/2);
%
% Transfer to degrees
londistd=km2deg(londistm,10^-3*(Er*cos(deg2rad(lat_eec))));
latdistd=km2deg(latdistm);
%
% Extrapolated travelled distance  eddy centre to next time step
lonext=londistd;%sign(londistd) * min(abs(londistd),abs(2*distx/2));
latext=latdistd;%sign(latdistd) * min(abs(latdistd),abs(2*disty/2));
%
% Ellipse center (not further away from original position than 1
% diameter (visual evaluation), noe doch nicht...
ellonc=lon_eec + lonext;
ellatc=lat_eec + latext;
eddies_ellc(:,ee_col)=[ellonc,ellatc];
%
% Distance between the two locations and direction of movement
%[offset,dist] = legs([lat_eec latext],[lon_eec lonext]);
offset=0; % as now tilting of ellipse now
%
% Variability in current climatology (climatology not snap shot)
londiststd=km2deg(eeddies{ee_col}(end,23)*60*60*24*d*10^-3,Er*10^-3*cos(deg2rad(lat_eec)));
latdiststd=km2deg(eeddies{ee_col}(end,24)*60*60*24*d*10^-3);
%
% In deg, and add one diameter as well as
deltalon= nansum([3*londiststd]);%,londistd]);%,distx]);%, lonext/2]);
deltasho= nansum([3*latdiststd]);%,latdistd]);%,disty]);%, latext/2]);
%
if savethings==1;s=(['3*Londiststd:',num2str(3*deltalon),' 3*Latdiststd:',num2str(3*deltasho),'\n']);
    fprintf(fid, s);
end
%
% Include previous position in the search ellipse
%      if deltalon <lonext;s=(['Replace:  (',num2str(deltalon),') with maxaxis: ',...
%      num2str(lonext),'\n']);
%      fprintf(fid, s);end
%      if deltasho < latext;s=(['Replace:  (',num2str(deltasho),') with minaxis: ',...
%      num2str(latext),'\n']);
%      fprintf(fid, s);end
%     deltalon=max(abs(deltalon),abs(lonext)+0.001);
%     deltasho=max(abs(deltasho),abs(latext)+0.001);
%
semimajor_ax=deltalon;%max(semiaxes);
semiminor_ax=deltasho;%min(semiaxes);
%
% Sear ellipse at least size of eddy
if savethings==1;
if semimajor_ax < distx/2*2;s=(['Replace: Max of Diameter/2 (',num2str(distx/2*2),') and maxaxis: ',...
        num2str(semimajor_ax),'\n']);
    fprintf(fid, s);
end
if semiminor_ax < disty/2*2;s=(['Replace: Max of Diameter/2 (',num2str(disty/2*2),') and minaxis: ',...
        num2str(semiminor_ax),'\n']);
    fprintf(fid, s);
end
end
semimajor_ax = max(distx/2*2,semimajor_ax);
semiminor_ax = max(disty/2*2,semiminor_ax);
%
% Sear ellipse the most 3 times the radius of an eddy (eddy displaced/shifted once/former and
% current eddy still touching at edge)
%     if savethings==1;
%     if semimajor_ax > distdia/2*3;
%     s=(['Replace: Min of Diameter/2*3  (',num2str(distdia/2*3),') and maxaxis: ',...
%     num2str(semimajor_ax),'\n']);
%     fprintf(fid, s);end
%     if semiminor_ax > distdia/2*3;
%     s=(['Replace: Min of Diameter/2*3  (',num2str(distdia/2*3),') and minaxis: ',...
%     num2str(semiminor_ax),'\n']);
%     fprintf(fid, s);end
%     end
%    semimajor_ax = min(distdia/2*3,semimajor_ax);
%    semiminor_ax = min(distdia/2*3,semiminor_ax);
%
if isnan(semimajor_ax) | semimajor_ax==0 ;stop;end
if isnan(semiminor_ax) | semimajor_ax==0 ;stop;end
%
% Uncertainty ellipse around extrapolated position
% Do it manually, as I axes2ecc-function unclear
x=0:2*pi/100:2*pi;
ellon=semimajor_ax*cos(x)+ellonc;
ellat=semiminor_ax*sin(x)+ellatc;
%
%histell=[histell;semimajor_ax,semiminor_ax];
%
%   [ellat,ellon] = ellipse1(ellatc,ellonc,ellipse,0);
%ellon(ellon<0)=ellon(ellon<0)+360;
clear semimajor_ax semiminor_ax
%
%-------------------------------------------------------------------------------------------------
% If so check which eddy in the current time step matches
eddy_c=[];
% tsp: current time step: check all the eddies of the current time
% step, if they match the one of the last time step I am looking at
% right now
for ee_atg=1:length(eddies_ss{tsp})
%
% EDDY CENTRE WITHIN ALLOWED RANGE?  (it seems like inpolygon manages 360 to 0 trans)
% center location of maximum intensity (as lon/lat mean difficult
loncheck=eddies_ss{tsp}(ee_atg).loncm;
latcheck=eddies_ss{tsp}(ee_atg).latcm;
% HARDCODED
%
if min(ellon)<10 & max(ellon)>300
    ellon
    ellat
```

```
    stop
    ellon(ellon<10)=ellon(ellon<10)+360;
end
% in case ellipse posesses values greater 360...
if max(ellon)>359 & loncheck<10
        loncheck=loncheck+360;
        %ee_atg
end
...or values smaller 0.
if min(ellon)<1 & loncheck>350
        loncheck=loncheck-360;
        %ee_atg
end
%
%-------------------------------------------------------------------------------------------------
% Potential match-eddy must be in search ellipse ...
%
if inpolygon(loncheck,latcheck,ellon,ellat)
%... as well as the most 1 eddy-diameter away.
%if inpolygon(loncheck,latcheck,ellonedc,ellatedc)
%
[course,dist]=legs([eddies_ss{tsp}(ee_atg).latcm lat_eec],...
                   [eddies_ss{tsp}(ee_atg).loncm lon_eec]);
disted=distdim(dist,'nm','km') ;
if disted==0;course=NaN; end
%if disted > (threshmaxtrav*size_eec);stop;end % sec check
%
% Check if not 'dying eddy' (amplitude has decreased over the last x
% time steps
if length(eeddies{ee_col}(:,1)) >= 3
featasts=abs([eeddies{ee_col}(end-2:end,32);eddies_ss{tsp}(ee_atg).ed_vort]);
feattend=diff(abs(featasts));
%
% Conidtions for eddy to match
% if trend was negative in the last x time steps
% if trend between last time step and tobematched eddy positive
% if vorticity decreased by at least 50% compared to the first detection
% if increase to tobematched eddy at least 5% (try to exclude noise)
if min(feattend(1:length(feattend)-1) < 0) > 0  &&...
        feattend(end) > 0 && ...
        abs(featasts(end-1)/eeddies{ee_col}(1,32)) < 0.5 && ...
        abs(featasts(end)/featasts(end-1)) > 1.20;
        display(['Eddy #',num2str(ee_col),' Date',num2str(floor(eeddies{ee_col}(end,15)*10^8))])
    continue;
end
end
%
%    % TEST
%     if abs(max(eddies_ss{tsp}(ee_atg).lon) - min(eddies_ss{tsp}(ee_atg).lon)) > 5. ||...
%       abs(min(eddies_ss{tsp}(ee_atg).lon) - max(eddies_ss{tsp}(ee_atg).lon)) > 5.
%       eddies_ss{tsp}(ee_atg).lonc
%       eddies_ss{tsp}(ee_atg).lon
%       tsp
%       ee_atg
%       stop
%     end
%     if (abs(eddies_ss{tsp}(ee_atg).loncm - min(eddies_ss{tsp}(ee_atg).lon)) > 50) ...
%      & ( abs(eddies_ss{tsp}(ee_atg).loncm - min(eddies_ss{tsp}(ee_atg).lon)) < 350)||...
%       (abs(eddies_ss{tsp}(ee_atg).loncm - max(eddies_ss{tsp}(ee_atg).lon)) > 50) ...
%      & (abs(eddies_ss{tsp}(ee_atg).loncm - max(eddies_ss{tsp}(ee_atg).lon)) < 350)
%       eddies_ss{tsp}(ee_atg).lonc
%       eddies_ss{tsp}(ee_atg).lon
%       tsp
%       ee_atg
%       stop
%     end %TEST END
%
eddy_c=[eddy_c; eddies_ss{tsp}(ee_atg).loncm eddies_ss{tsp}(ee_atg).latcm...
    eddies_ss{tsp}(ee_atg).dia eddies_ss{tsp}(ee_atg).ampl...
    (eddies_ss{tsp}(ee_atg).ed_wi) (eddies_ss{tsp}(ee_atg).ed_rain)...
    max(eddies_ss{tsp}(ee_atg).ed_mono) min(eddies_ss{tsp}(ee_atg).lat) ...
    eddies_ss{tsp}(ee_atg).edampl tsp_s+tsp-1 eddies_ss{tsp}(ee_atg).chlmean...
    eddies_ss{tsp}(ee_atg).chlmax eddies_ss{tsp}(ee_atg).chlmin eddies_ss{tsp}(ee_atg).chlmis ...
    eddies_ss{tsp}(ee_atg).date*10^-8 um(ee_atg) vm(ee_atg)  eddies_ss{tsp}(ee_atg).achlmean...
    eddies_ss{tsp}(ee_atg).achlmeano eddies_ss{tsp}(ee_atg).chlmeano eddies_ss{tsp}(ee_atg).sla_edgm...
    eddies_ss{tsp}(ee_atg).ampl_slaedg ustdm(ee_atg) vstdm(ee_atg) course disted...
    eddies_ss{tsp}(ee_atg).sstm eddies_ss{tsp}(ee_atg).asstm eddies_ss{tsp}(ee_atg).cfm...
    eddies_ss{tsp}(ee_atg).ekem eddies_ss{tsp}(ee_atg).ed_spedg eddies_ss{tsp}(ee_atg).ed_vort...
    eddies_ss{tsp}(ee_atg).ed_dipox  eddies_ss{tsp}(ee_atg).ed_dipoy tsp-tstart_eec ee_atg];
%
end % in ellipse?
end % ee (check all eddies)
%if tsp==5 &  ee_col==50;stop;end
%
%
size_c=size(eddy_c);
if (~isempty(eddy_c)) % If there as it least one eddy in ellipse
%
% calculate 'similarity'
deltadist=[];deltasize=[];deltaampl=[];deltasst=[];deltavor=[];
%
for c=1:size_c(1,1) % For all the found eddies calculate...
    %
    % ...the distance to the centre at the previous time stpe
    [course,dist]=legs([eddy_c(c,2) ellatc],...
                       [eddy_c(c,1) ellonc]);
    if dist==0;course=NaN; end
    %
    dist=distdim(dist,'nm','km');
    % normalized to distance of eddies closed to extrapolated location,
    % subtracted later only
    if isempty(dist);stop;end
    deltadist=[deltadist;dist];
    %
    % ...the absolute difference in size
    sizee=abs(eddy_c(c,3)-size_eec);
    if isempty(sizee);stop;end
    deltasize=[deltasize;sizee];
    %
    % ...the absolute difference in amplitude
    ample=abs(abs(eddy_c(c,4))-mampl_eec);
    if isempty(ample);stop;end
    deltaampl=[deltaampl;ample];
    %
    % ...the absolute difference in vorticity
    vorte=abs(eddy_c(c,32)-vor_eec);
    if isempty(vorte);stop;end
    deltavor=[deltavor;vorte];
    %
    % ...the absolute difference in sst
```

```
    sste=abs(eddy_c(c,27)-sst_eec);
     if isempty(sste);stop;end
   deltasst=[deltasst;sste];
end
if max(isnan(deltasst))==1;deltasst=nan(size_c(1),1);end
dist_min=min(deltadist);
ampl_min=min(deltaampl);
%
% calculate 'similarity'
rel_delta=1/sqrt(4)*sqrt(nansum( ...
            [((abs(deltasst)/(1*stdsst)).^2),...
             ((abs(deltaampl)/(1*stdamp)).^2),...
             ((abs(deltavor)/(1*stdvor)).^2),...
             (((abs(deltadist)-abs(dist_min))/(1*dist_min)).^2)],2));
%
if testplot==1 % test-test-test-test-test-test-test-test-test-test-test-test
xmax=300;%40;
xmin=30;%10;
ymax=-32;
ymin=-62;
%
if eeddies{ee_col}(end,1) >xmin & eeddies{ee_col}(end,1) <xmax &...
   eeddies{ee_col}(end,2) >ymin & eeddies{ee_col}(end,2) <ymax &...
figure
set(gcf,'Visible','off')
%
hold on
plot(eeddies{ee_col}(end,1),eeddies{ee_col}(end,2),'r.','MarkerFaceColor','None') % center eddy1
text(eeddies{ee_col}(end,1),eeddies{ee_col}(end,2),'Initial position 1')
%
plot(ellon,ellat,'r-')  % sear ellipse of current eddy
plot(elloncc,ellatc,'ro') % center of ellipse (extrapolated location)
text(elloncc,ellatc,'Extrapolated position 1')
%
line([eeddies{ee_col}(end,1) elloncc],[eeddies{ee_col}(end,2) ellatc])
%
plot(eddy_c(:,1),eddy_c(:,2),'bo','MarkerFaceColor','b')
%text(eddy_c(:,1),eddy_c(:,2),'MatcheddyCenter')
%
x=0:2*pi/100:2*pi;
ellond=distx/2*cos(x)+elloncc;
ellatd=disty/2*sin(x)+ellatc;
plot(ellond,ellatd,'k--') % Diameter eddy in previous time step
%
% competiting eddy
plot(eddy_c(index,1),eddy_c(index,2),'ko','MarkerFaceColor','r') % center eddy1
% text(eeddies{ee_col2}(end-1,1),eeddies{ee_col2}(end-1,2),'Initial position 2')
%
%plot(elloncc2,ellatc2,'ko','MarkerFaceColor','None')
%text(elloncc2,ellatc2,'Extrapolated position 2')
%line([eeddies{ee_col2}(end-1,1) elloncc2],[eeddies{ee_col2}(end-1,2) ellatc2])
%
%plot(ellonedc,ellatedc,'k-')  % max ellipse of current eddy
axis equal
print('-dtiff','-r100',['Ellplots/ellipse_ee_col',num2str(ee_col),'_tsp',num2str(tsp)])
close all
%
end
end % test-test-test-test-test-test-test-test-test-test-test-test-test-test
%
if (size_c(1,1)>1) % If more than one matching eddy found
    %
    index=find(rel_delta==min(rel_delta));
    %
    % take "minimum eddy"
    eddy_c   =eddy_c(index,:);
    rel_delta=rel_delta(index);
    %
end % if more than one eddy
%
if rel_delta > threshsim;continue;end
%
% !!!!!!!!!!!!!!!! ADJUST COLUMN OF EDDY# (HARDCODED) !!!!!!!!!!!!!!!!!!!!!!!!!!!!!!!!!!!!!!!!!!!!!!!!!!!
e_c=eddy_c(36) ;
%
% if one eddy used more than ones check where it fits better
% Mark that eddy "taken" already
if counted(1,e_c)==1
    % eeddies{ee_col}(end,end)==g
    %
    ee_col2=counted(2,e_c);
    size_eec2=eeddies{ee_col2}(end-1,3);
    ampl_eec2=eeddies{ee_col2}(end-1,22);
    mampl_eec2=eeddies{ee_col2}(end-1,4);
    sst_eec2=eeddies{ee_col2}(end-1,27);
    vor_eec2=eeddies{ee_col2}(end-1,32);
    ellonc2=eddies_ellc(1,ee_col2);
    ellatc2=eddies_ellc(2,ee_col2);
    %
    deltadist=[];deltasize=[];deltaampl=[];deltasst=[];deltavor=[];
    % Which eddy of previous time step fits better?
    %
    % ...the distance to the centre at the previous time step
    [course,dist]=legs([eddy_c(2) ellatc],...
                       [eddy_c(1) elloncc]);
    dist=distdim(dist,'nm','km');
    deltadist=[dist];
    %
    [course,dist]=legs([eddy_c(2) ellatc2],...
                       [eddy_c(1) ellonc2]);
    dist=distdim(dist,'nm','km');
    deltadist=[deltadist;dist];
    %
    % ...the absolute difference in size
    sizee=abs(eddy_c(3)-size_eec);
    deltasize=[sizee];
    sizee=abs(eddy_c(3)-size_eec2);
    deltasize=[deltasize;sizee];
    %
    % ...the absolute difference in amplitude
    ample=abs(abs(eddy_c(4))-mampl_eec);
    deltaampl=[ample];
    ample=abs(abs(eddy_c(4))-mampl_eec2);
    deltaampl=[deltaampl;ample];
     % ...the absolute difference in amplitude
    %mple=abs(eddy_c(c,4)-mampl_eec);
    %if isempty(ample);stop;end
    %deltaampl=[deltaampl;ample];
    %
     % ...the absolute difference in vorticity
```

```
        vorte=abs(eddy_c(32)-vor_eec);
        deltavor=[vorte];
        vorte=abs(eddy_c(32)-vor_eec2);
        deltavor=[deltavor;vorte];
        %
        % ...the absolute difference in sst
        sste=abs(eddy_c(27)-sst_eec);
        deltasst=[sste];
        sste=abs(eddy_c(27)-sst_eec2);
        deltasst=[deltasst;sste];
        %
        dist_min=min(deltadist);
        ampl_min=min(deltaampl);
        %
        % calculate 'similarity'
        rel_delta=1/sqrt(4)*sqrt(nansum( ...
                [((abs(deltasst)/(1*stdsst)).^2),...
                 ((abs(deltaampl)/(1*stdamp)).^2),...
                 ((abs(deltavor)/(1*stdvor)).^2),...
                 (((abs(deltadist)-abs(dist_min))/(1*dist_min)).^2)],2));
      %
      index=find(rel_delta==min(rel_delta));
      %
      if index==1
           counted(2,e_c)=ee_col;
           eeddies{ee_col}=[eeddies{ee_col}; eddy_c(1,1:end-1)];
           eeddies{ee_col2}(end,:)=[];
       % else: just leave it like this, no matching eddy for ee_col
      end
       %
    else % If eddy was not allocated to an eddy of the previous time step yet
       %
       % Mark eddy and add info which eddy from previous time step got it
       counted(1,e_c)=1;
       counted(2,e_c)=ee_col;
       %
       % If a matching eddy found in tsp, add to eddy in g-1
       eeddies{ee_col}=[eeddies{ee_col}; eddy_c(1,1:end-1)];
       % display(['Eddy allocated: map ',num2str(g),' Eddy #',num2str(eddy_c(18)),', date ',...
       % num2str(dates(g,:))])
    %
    end % if eddy already allocated, check which one is more similar
    %
end % at leat one matching eddy found
end % if eddy existed in previous time step
 %   end %area
end % ee_col (all eddies in the previous time step)
%-------------------------------------------------------------------------------------------------
%-------------------------------------------------------------------------------------------------
```

```
%% SPECIAL SITUATIONS
%
% If not all eddies used, add as new eddy
       %save test.mat
if min(counted(1,:))<1
   newed=find(counted(1,:)<1);
   %
   for cne=1:length(newed) % all rest-eddies
        %
    eddy_c=[eddies_ss{tsp}(newed(cne)).loncm eddies_ss{tsp}(newed(cne)).latcm...
        eddies_ss{tsp}(newed(cne)).dia eddies_ss{tsp}(newed(cne)).ampl...
        (eddies_ss{tsp}(newed(cne)).ed_wi) (eddies_ss{tsp}(newed(cne)).ed_rain)...
        max(eddies_ss{tsp}(newed(cne)).ed_mono) min(eddies_ss{tsp}(newed(cne)).lat) ...
        eddies_ss{tsp}(newed(cne)).edampl tsp_s+tsp-1 eddies_ss{tsp}(newed(cne)).chlmean...
        eddies_ss{tsp}(newed(cne)).chlmax eddies_ss{tsp}(newed(cne)).chlmin...
        eddies_ss{tsp}(newed(cne)).chlmis eddies_ss{tsp}(newed(cne)).date*10^-8 ...
        um(newed(cne)) vm(newed(cne))  eddies_ss{tsp}(newed(cne)).achlmean...
        eddies_ss{tsp}(newed(cne)).achlmeano eddies_ss{tsp}(newed(cne)).chlmeano...
        eddies_ss{tsp}(newed(cne)).sla_edgm eddies_ss{tsp}(newed(cne)).ampl_slaedg...
        ustdm(newed(cne)) vstdm(newed(cne)) NaN NaN eddies_ss{tsp}(newed(cne)).sstm...
        eddies_ss{tsp}(newed(cne)).asstm eddies_ss{tsp}(newed(cne)).cfm...
        eddies_ss{tsp}(newed(cne)).ekem eddies_ss{tsp}(newed(cne)).ed_spedg ...
        eddies_ss{tsp}(newed(cne)).ed_vort eddies_ss{tsp}(newed(cne)).ed_dipox ...
        eddies_ss{tsp}(newed(cne)).ed_dipoy 0 newed(cne)];
        %
        eeddies{end+1}=eddy_c(1:end-1);
   end
end
%
if (mod(tsp,100)==0)
  save([pathyd,name,'_',rotstr,'-track.mat'],'eeddies','tsp')
end
%
tsp=tsp+1;
um=[];vm=[];ustdm=[];vstdm=[];
%
%if tsp >length(eddies_ss); checkend=1; end
if tsp >tsp_e; checkend=1; end
timec=toc; display(['Time elapsed in min: ',num2str(timec/60)]);disp(' ')
end % tsp (all time steps)
%
if savethings==1;
fclose(fid);
end
%
%save colldistributions_simell.mat histsim histell
%-------------------------------------------------------------------------------------------------
%-------------------------------------------------------------------------------------------------
```

B. Supplementary Material to Chapter 2: Eddy Characteristics

B.1. Supplementary Figure: Histogram of Selected Eddy Characteristics

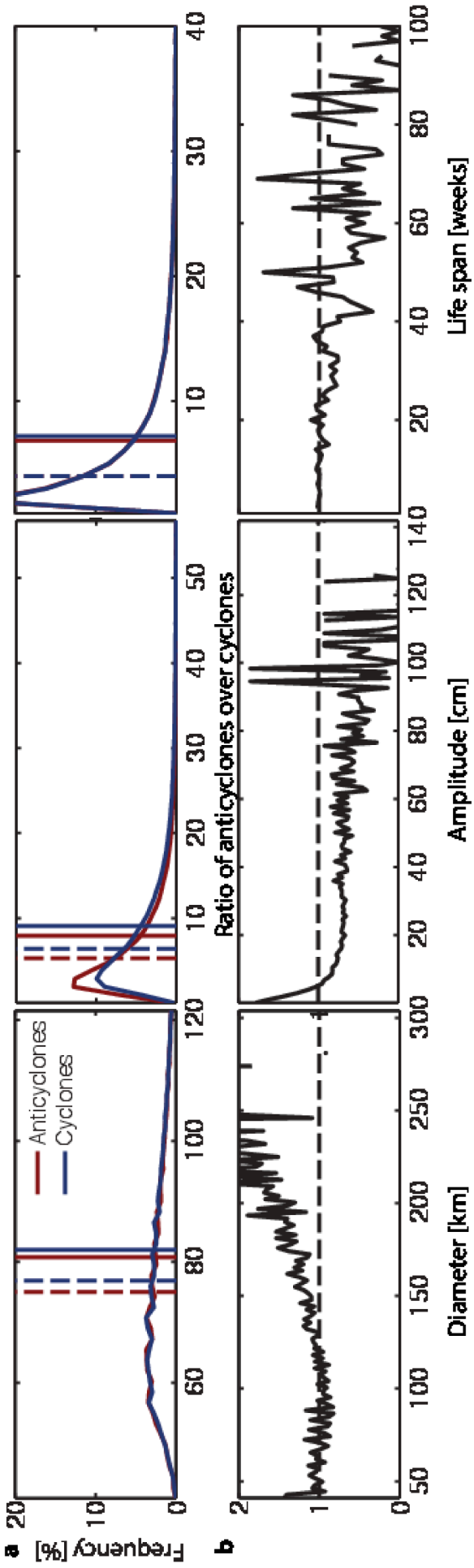

Figure B.1.: Histograms of eddy characteristics; ***a*** *distribution of absolute values and* ***b*** *ratio of distributions of anticyclones over cyclones; not the different x-axes for* ***a*** *and* ***b****, the former is a "zoom-in", the latter shows the complete range of values; solid line denotes the mean, dashed the median of the distributions; only eddies are included which exist two time steps or more; the median is the same for anticyclones and cyclones for life span; there tend to be more large anticyclones and in contrast more cyclones with larger amplitudes and longer life spans in the SO.*

B.2. Supplementary Figure and Note: Spatial Distribution of Eddy Characteristics

The basic eddy characteristics inferable from satellite *SLA* are the amplitude A and the length scale L_e (Supplementary Figures Figure B.2 and Figure B.3a). In the high energy regions, such as the *ACC*, they are greater than 20 cm and about 100 km, respectively. The high-energy regions are the same time areas of large *SSH* gradients (Supplementary Figure B.2b). CSS11 notes that the mean eddy amplitude scales well with the standard deviation of the *SSH* at the mesoscale.
It has been recognized that eddies are larger than anticipated from the scale of the first (surface-intensified) baroclinic mode, the first baroclinic Rossby radius of deformation (e.g. CSS11). This is the case especially for higher latitudes (Supplementary Figure Figure B.3b). One reason for this result is certainly the loss of resolution of the satellite *SLA* data with increasing latitude. Another one that indications exist for an "arresting scale"/energy being trapped in the larger barotropic mode (e.g. Ferrari and Wunsch, 2009).
If one examines histograms of distributions of L_e normalized with the Rossby radius for latitudinal bands, the *ACC* emerges as a band of especially large L_e relative to the local Rossby radius (not shown). In addition, the *ACC* stands out as an area featuring a wider range of deviations from the Rossby radius (wider distribution).
We find a strong correlation between A and L_e in the studied area (not shown), in contrast to the only weak correlation globally found by CSS11. Thus, we find a partial "self-similar structure" of eddies, i.e. it appears the structure of eddies scales. One would expect a constant ratio of these two properties in this case. However, A over L_e, labelled the "intensity" and an indication for the self-similarity, varies in space (not shown). Eddies are clearly more intense/steeper in the high energy regions than in the southern subtropical gyres.
One can examine the differences of characteristics of *AE* and *CE* by taking the ratio (not shown). The most prominent features are that *CE* are of larger A and L_e at the northern flank of the *ACC* but smaller for both properties south of the *ACC* and in the southern subtropical gyres. CE are overall more intense as their larger A outweighs their larger L_e (in agreement with CSS11, who found *CE* to be intense in the *SO*, in contrast to the northern hemisphere). The finding of more intense *CE* is rather intuitive as the centrifugal force pushes fluid outward in rotating eddies, which intensifies *CE* and "broadens" *AE* (cyclogeostrophic balance, Cushman-Roisin Benoit et al., 1989).
As for the eddy numbers (Section 2.3.2), we do not find a large seasonal variability for eddy characteristics, such as the intensity (not shown).

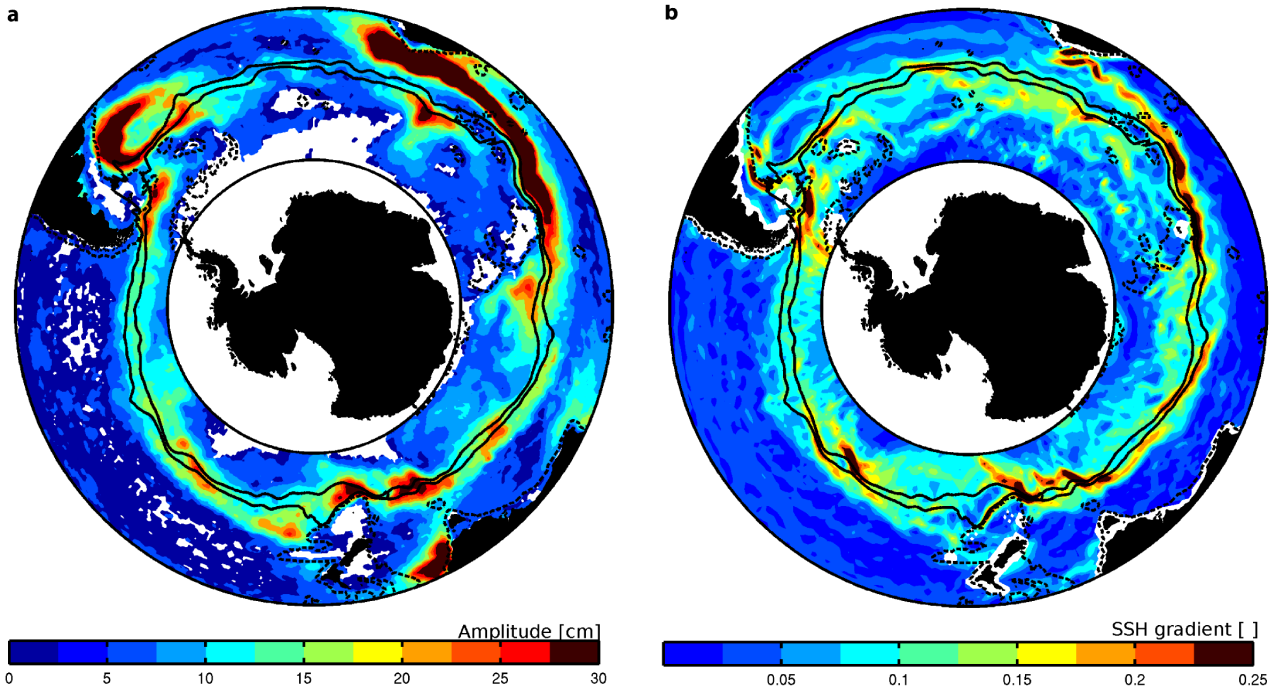

Figure B.2.: Eddy amplitudes; ***a*** *Mean amplitudes of eddies (maximum* SLA *anomaly relative to mean* SLA *at the core of the eddy's edge) and* ***b*** *gradient of the mean* SSH*; as before, solid black lines show the mean northern (SAF)/southern (PF) boundaries (major fronts) of the* ACC*; dashed black lines mark the -2000 m depth contour.*

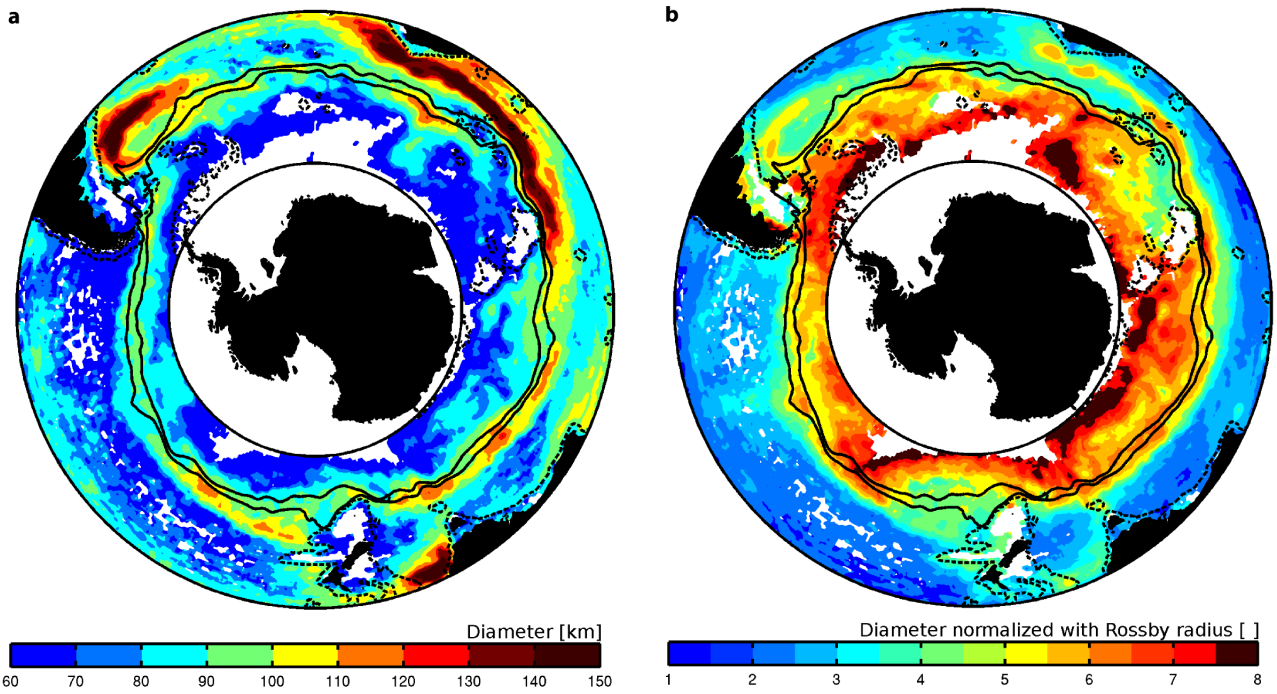

Figure B.3.: Eddy diameters; ***a*** *Mean diameter of eddies and* ***b*** *mean diameter normalized with the first baroclinic Rossby radius; as before, solid black lines show the mean northern (SAF)/southern (PF) boundaries (major fronts) of the* ACC*; dashed black lines mark the -2000 m depth contour.*

B.3. Supplementary Figure and Note: The Mean Eddy Life-Cycle

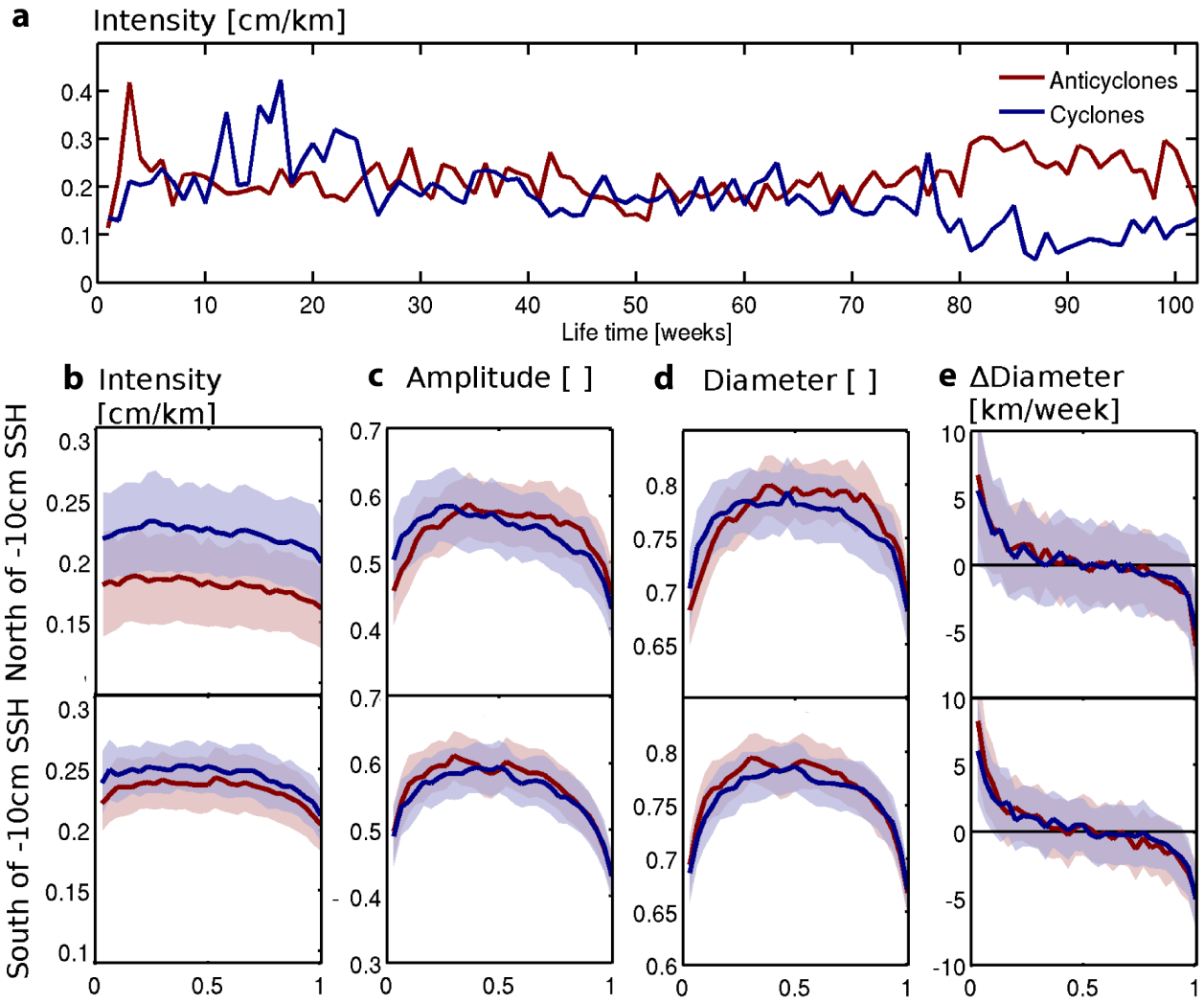

Figure B.4.: Eddy life cycle; a *Evolution of intensity of a single* AE *as well as a single* CE*;* ***b-e*** *average evolution of the respective quantity over the eddies lifetimes which were normalized with the respective lifespan of the individual eddies:* ***b*** *intensity,* ***c*** *amplitude (normalized for each individual eddies with the maximum amplitude during the life cycle),* ***d*** *diameter (normalized as in* ***c****) but with the maximum lifetime diameter) and* ***e*** *change of the eddy's diameter relative to the week before; the shading marks x standard deviations; red (blue) for* AE *(*CE*).*

How is the evolution of eddies over their lifetime? We expect properties of the eddies such as their intensity to be a function of the eddy's life stage/age. Similarly to atmospheric (low) pressure systems, we anticipate an initial growth or intensification versus a decay when the eddy ages (Rudeva and Gulev, 2007; Hewson and Titley, 2010).
This is not obvious from a time series of a characteristic of an individual eddy, such as the intensity (Supplementary Figure B.4). The eddies' intensities rather pulsate during the eddy's life time on timescales of weeks but also may exhibit longer scale variation O(months). To reveal a general tendency of the evolution of the eddy-properties, we scale the age of each individual eddy with its lifespan (Supplementary Figure B.4a-d). With this, it becomes clear that indeed, a growth period of eddy intensity, amplitude and diameter (absolute values not shown here) occurs over the first 10-30% of the eddy's life time (Supplementary Figure B.4a-c). Thereafter follows a "plateau" or weak decrease-phase. Finally, the last 10-30% of the life time features a decay period (in agreement with Liu et al., 2012). Finally, the growth period starts from a slightly higher level than the dissipation period ends.
The lifecycle of the eddy intensity is less pronounced than the lifecycle of the amplitude as well as diameter. Thus, while the eddy grows in size and increases its amplitude, its related *SLA* gradient changes less. Again, this implies some kind of "self-similar structure" in contrast to the finding of CSS11 (see also section B.2).
Even though the absolute magnitude of the eddy characteristics are dependent on polarity (see Supplementary Figure B.4a, not shown for diameter nor amplitude), it seems, the change over the lifetime, i.e. the slope is not (Supplementary Figure B.4e): here, representative for other eddy-properties, such as amplitude, intensity, vorticity and eddy kinetic energy, we show the diameter change from week to week, which is 5-10 km on average in the first and last 10-30% of the eddies' life time.
Supplementary Figure B.4b makes once more obvious that there is a tendency for *CE* to be on average more intense than *AE*. This can be due to the *CE* either being smaller or featuring a larger amplitude. North of the ACC (-10 cm *SSH* contour), *CE* are actually larger. However, the greater size is overcompensated by a much larger amplitude as well (not shown). Whereas in the ACC *CE* are of similar amplitude as *AE*, however they are smaller on average, which makes them again more intense. One reason for this could be a bias in the *SLA* due to surface intensification of *CE* in contrast to *AE*. A surface intensification was found for instance for the Humboldt current system (Chaigneau et al., 2011). However, this does not seem to be true for the *ACC* eddies (see Section 2.3.4.2).
We found this typical life cycle to be independent of the age group we considered (not shown).

B.4. Supplementary Note: Brief Comparison with a Global Eddy Tracking Study

Considering the tracked eddies of CSS11 (available at `http://cioss.coas.oregonstate.edu/eddies/`) only in our domain (which constitute almost 50% of all of the eddies tracked by CSS11) we find smaller lifespans of eddies in general and an average lifespan of eddies detected over at least 16 time steps to be 25 weeks in contrast to 32 weeks found by CSS11. This can be either due to the detection or the tracking algorithm. For instance Souza et al. (2011) found more identified and tracked eddies when a geometric criterion was used for eddy identification such as closed streamlines of *SLA* as CSS11 applied. Tracking algorithms have so far been validated by visual evaluation, hence are subjective to some extent and one expects deviations to some degree. Also, CSS11's method may result in a bias towards longer lifespans. Overall, the comparison with CSS11 highlights some of the uncertainties related to eddy detection and tracking. Nevertheless, we believe general trends robust findings on most of the eddies' properties are not hampered.

C. Supplementary Material to Chapter 3

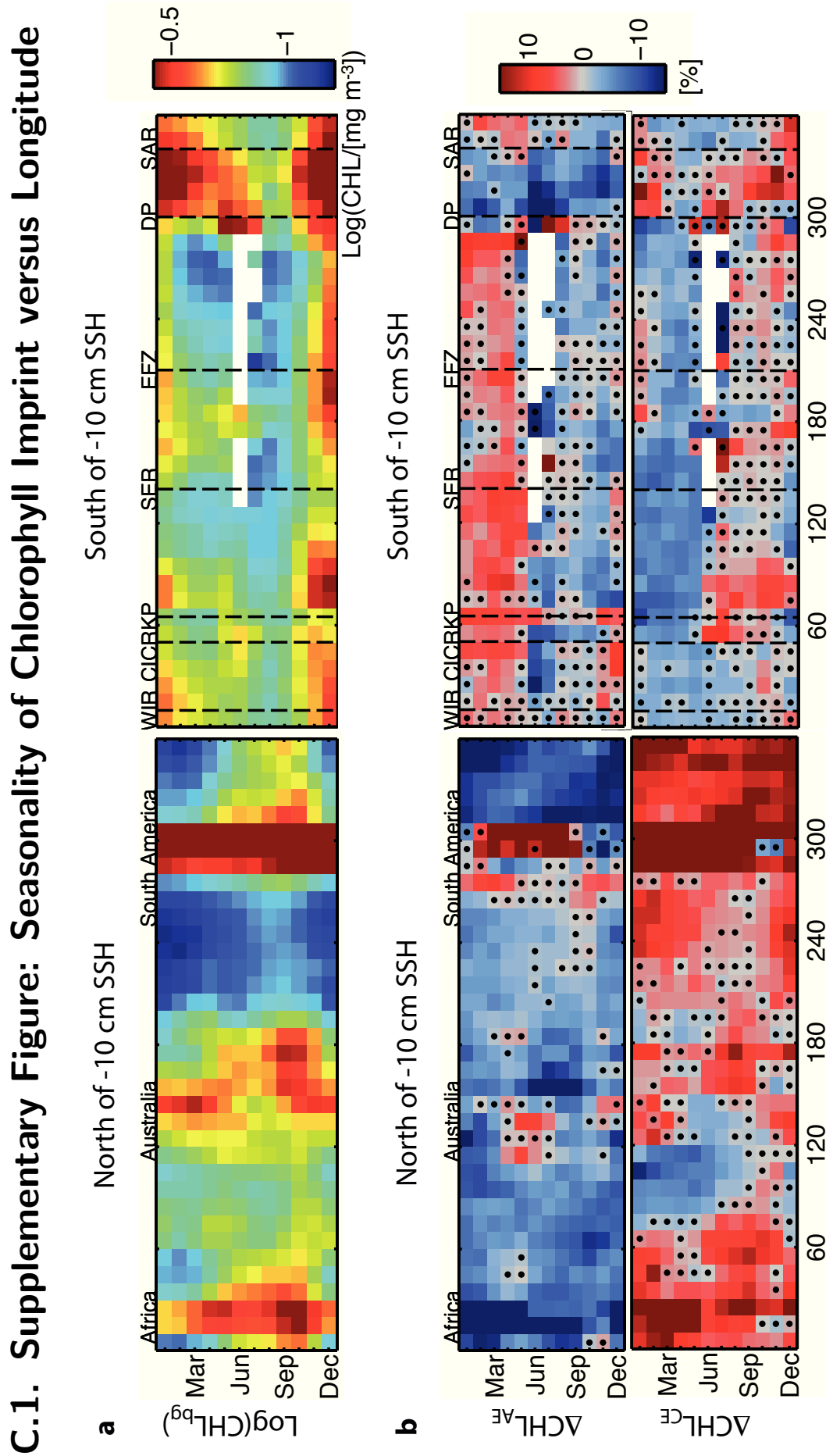

Figure C.1: *Caption on next page.*

Figure C.1.: Seasonality of chlorophyll (*CHL*) associated with eddies; *as Figure 3.4;* **a** *Common logarithm of the climatological chlorophyll (CHL) for reference, and* **b** *anomaly of* CHL *associated with eddies (*ΔCHL *related to anticyclones (AE, top) and cyclones (CE, bottom); left panels are for the area north of the -10 cm sea surface height (SSH) contour (figures look similar if the -20 cm SSH contour is chosen), the approximate locations of the continents in the domain are noted; right panels are for the area south of the -10 cm SSH contour, where distinct topographical obstacles along the Antarctic Circumpolar Current (ACC) are specified; the anomalies are the mean of all eddies existing at least 3 weeks binned in monthly 10° longitude bins; black dots mark bins where* ΔCHL *is not significant (t-test, p=0.05); the following abbreviations are used for topographical features: WIR for West Indian Ridge, CICRKP for Crozet Island/Conrad Rise/Kerguelen Plateau, SER for South East Ridge, EFZ for Eltanin Fracture Zone, DP for Drake Passage and SAR for South Atlantic Ridge.*

C.2. Supplementary Figure: Eddy Composite Separated by Large-Scale Chlorophyll Gradient

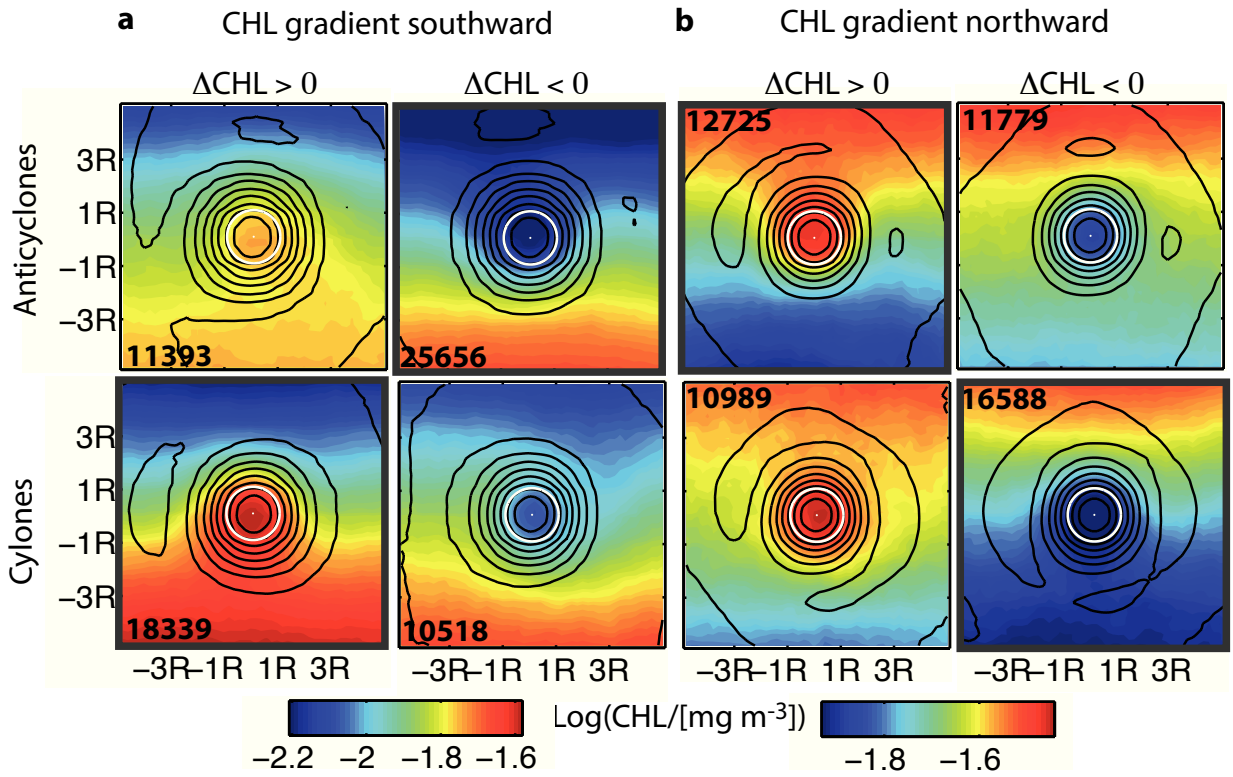

Figure C.2.: Eddy composite of chlorophyll (CHL) *of selected eddies; separated by anticyclones (top row) and cyclones (bottom row), and by positive and negative* CHL *imprint, respectively;* ***a*** *eddies located in situations of a southward directed large-scale* CHL *gradient (between 170° and 190°), and* ***b*** *eddies located in situations of a northward directed large-scale* CHL *gradient (between 350° and 10°); sea level anomaly contours are shown in black (0.05 spacing, normalized before averaging); the eddy core as detected with the Okubo-Weiss parameter and the eddy center are shown as white circle and dot, respectively; the individual eddies are scaled according to the eddy's radius (R), but here not rotated before averaging; thick frames mark "expected"* CHL *anomaly according to the theory of eddies entraining the "western part" (leading side) of the dipole into their core (Chelton et al., 2011a); indeed, these cases are more frequent (number of cases are noted in bold numbers within each figure), however, also the opposing cases frequently occur; visually, it appears that the "expected" cases after Chelton et al. (2011a) are characterized by a steeper* CHL *gradient, meaning entrainment in the core of the eddy is potentially more likely to have a significant effect.*

C.3. Supplementary Figure: Binned Chlorophyll Anomalies Versus Eddy Age

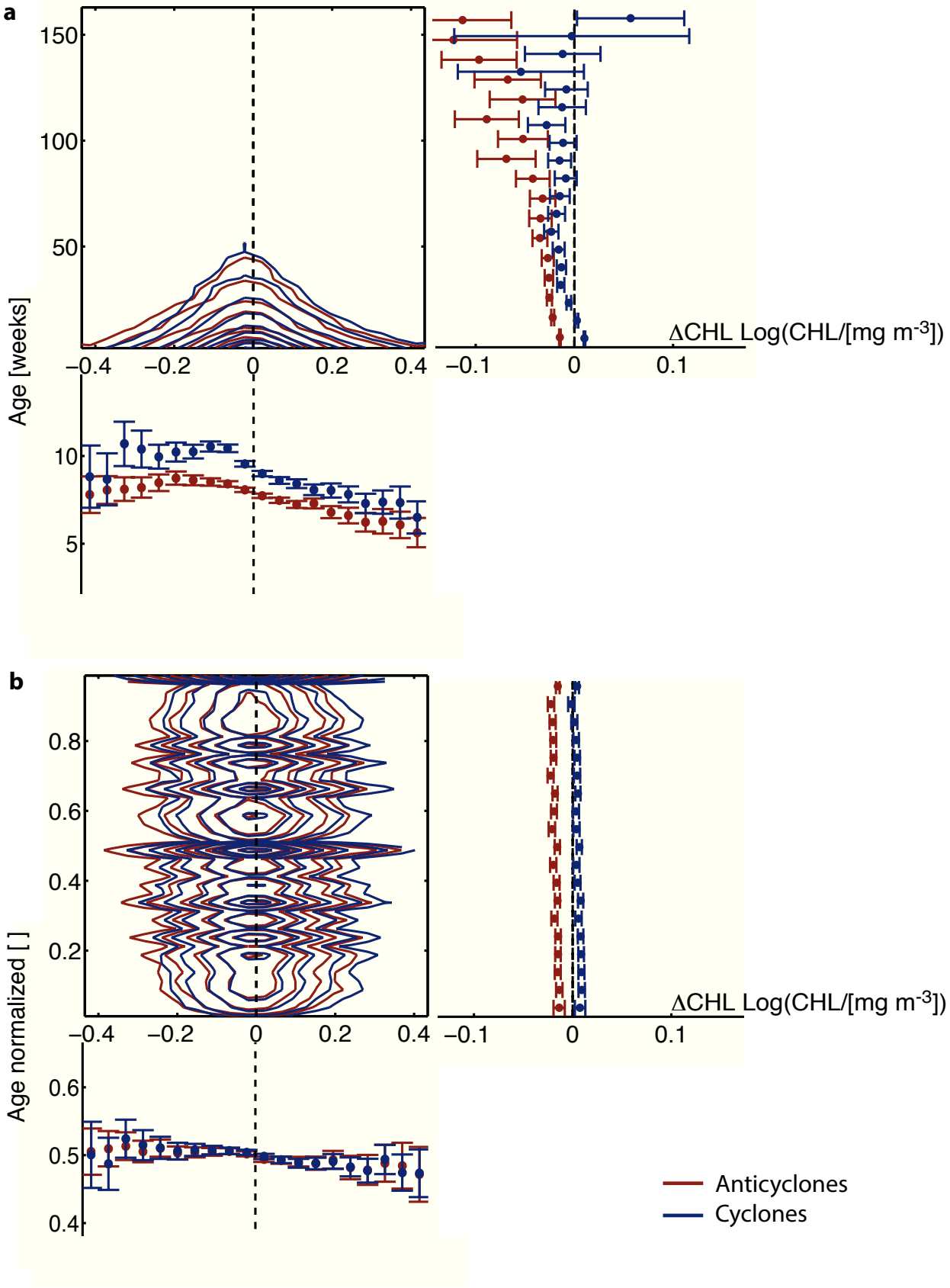

***Figure C.3**: Caption on next page.*

***Figure C.3.: "Chlorophyll (CHL)−chlorophyll relations"**; as Figure 3.7; two-dimensional histogram of **a** CHL anomalies associated with eddies (relative to surrounding, ΔCHL) and age of eddies, and **b** ΔCHL and normalized age of eddies, i.e. the present age for each individual eddy is normalized with the lifespan of the respective eddy, i.e. its age when it is detected the last time; "middle figure" (in **a** and **b**) binning according to the quantity of the x-axis and concurrently according to the quantity of the y-axis (about 40 bins for both); the normalized occurrences ranging from 0 to 1 are depicted with only selected (unevenly spaced) contours shown for reasons of clarity (contour 0.01, 0.02, 0.05, 0.1, 0.2, 0.3, 0.5, 0.7 and 0.99); the panels on the right and bottom of **a** and **b** figure show the projection onto the x- (19 bins) and y-axis (20 bins), respectively; three errors of the mean are marked with error bars; not the different scales for the projections (zoom-in).*

C.4. Supplementary Figure: Binned Scatterplot of "Chlorophyll Conditions"

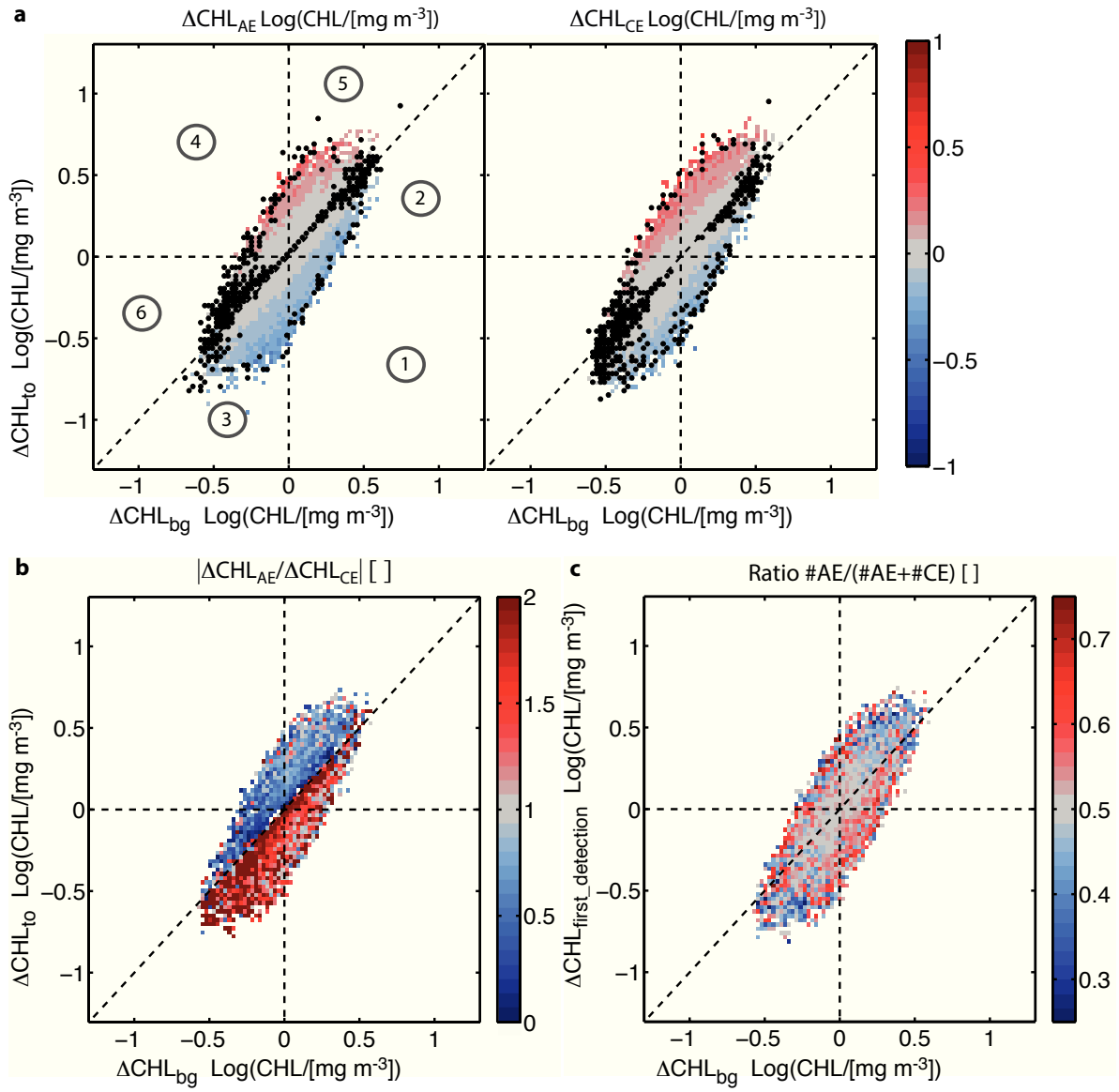

Figure C.4.: "Chlorophyll (CHL)−chlorophyll relations"; *as Figure 3.7, however three-dimensional histogram:* ***a*** $\Delta\mathrm{CHL}_{bg}$ *and the difference of the current* CHL *of an eddy relative to its* CHL *when it originated* ($\Delta\mathrm{CHL}_{to}$)*, with the color denoting the* CHL *anomalies of eddies relative to the background* (ΔCHL)*;* ***b*** *same as* ***a*** *but with colors denoting the absolute ratio of the left and right panel of* ***a****;* ***c*** *same as* ***b*** *but here the ratio of the numbers of data points of anticyclones (AE) over all data points (number AE plus number cyclones, CE) is shown for each bin; only eddies with an age of 3 to 12 weeks are considered; the slope larger 1 in* ***a*** *shows that eddies feature a larger* CHL *difference compared to the time of their origin than the difference is of the background* CHL *between the two locations/times, indicating an effect of eddies on* CHL *as reactive tracer;* ***a*** *looks similar for AE and CE; the absolute ration of the two,* ***b****, shows again the larger negative* |ΔCHL| *and smaller positive* |ΔCHL| *for AE, compared to CE, resulting in a smaller mean* ΔCHL *of AE;* ***c*** *visualizes that AE and CE tend to show similar numbers in the different sections 1-6 which are indicated in* ***a****, with AE showing somewhat less occurrences in 5 and 3, but some more in the other sections; the sections as indicated in* ***a*** *are interpreted in Supplementary Figure C.5.*

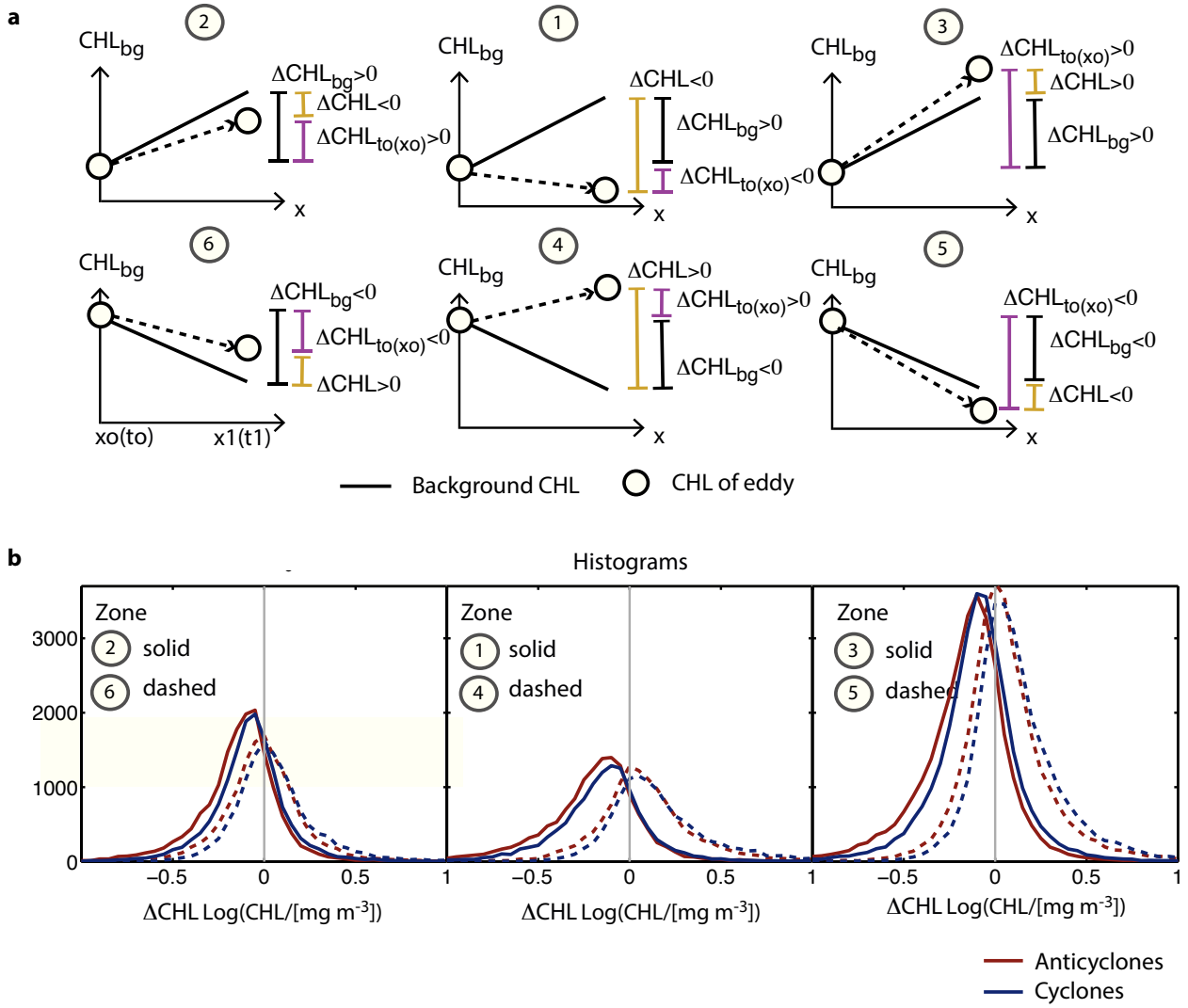

Figure C.5.: Changes of chlorophyll (CHL) associated with eddies relative to the background CHL. *Here, the zones as indicated in Supplementary Figure C.4* ***a*** *are illustrated in* ***a*** *and the frequency of* CHL *of eddies in the sections 1-6 is quantified in* ***b****; we separate in a positive background* CHL *gradient (in* ***a****, top row,* $\Delta\text{CHL}_{bg} > 0$*) and a negative background* CHL *gradient (bottom row,* $\Delta\text{CHL}_{bg} < 0$*); further we distinguish by the change of the* CHL *of an eddy while it is propagating over time from the location of its origin (*x_o *at* t_o*) to a later position (*x_1 *at* t_1*): firstly, we check the* CHL *of the eddy relative the* CHL *at the location of origin (*$CHL_{to(xo)}$*), and secondly we check the* CHL *of an eddy relative to the background at the current position* x_1 *(*ΔCHL*); at position* x_1 *(at* t_1*), the eddie's* CHL *is expected to be the same as the background* CHL *in the case of "perfect entrainment", i.e. constant exchange with its surroundings (evolution of CHL along the black line); in contrast, the* CHL *of the eddy is anticipated to be the same as at the time of its origin (*x_o *at* t_o*) in the case of perfect trapping; situation 2 and 6 (left panels) illustrate a case in between, i.e. some trapping and some entrainment; 1 and 4 (middle panels) illustrate cases where the* CHL *of the eddy appears to develop independently of the background* CHL*; and 3 and 5 (right panel) illustrate cases where the* CHL *of the eddy shows the same trend as the background* CHL *but amplified; the middle and right panels are the cases where we anticipate an influence of the eddy on* CHL *as a reactive tracer, both by enhancing and damping* CHL *intensity;* ***b*** *quantifies the number of eddies occurring in each of the sections/cases: 1 and 3 as well as 1 and 4 account each for abut 10% of all cases, 3 and 5 for almost 30% each; hence, we find a large fraction of eddies showing a development of* CHL *which indicates an impact on phytoplankton growth; the assumption here is a monotonic background* CHL *gradient.*

D. Supplementary Material to Chapter 4

D.1. Supplementary Methods

Data

The altimeter product, i.e. sea level anomalies exploited for eddy identification are produced by Ssalto/Duacs and distributed by Aviso, with support from Cnes (version v3.0.0, available at `http://www.aviso.oceanobs.com/duacs/`). The AMSR-E and QuikSCAT data are produced by Remote Sensing Systems (available at `http://www.remss.com`) and sponsored by the NASA Ocean Vector Winds Science Team as well as the NASA Earth Science MEaSUREs DISCOVER Project and the AMSR-E Science Team. The cloud fraction data are processed and distributed by the ACRI-ST GlobColour service (available at `http://www.globcolour.info`), supported by EU FP7 MyOcean & ESA GlobColour Projects, using ESA ENVISAT MERIS data, NASA MODIS and SeaWiFS data.

D.1.1. Eddy Tracking

The eddies were tracked over time to be able to select eddies which were detected in at least two consecutive time steps (see Methods Section): to track an eddy, we determined the location of the matching eddy in the consecutive time step by first estimating its possible position taking into account the advection by the mean currents and the eddies' intrinsic phase speed, which is assumed to be close to the one of linear baroclinic Rossby waves (Chelton et al., 1998). We then drew a search ellipse around our projection of the eddy location considering the variability of currents and eddy behaviour. If we found more than one potentially matching eddy for e_1 within the search ellipse, for instance e_2 and e_3, we applied a similarity-criteria similar to studies before (e.g. Penven et al. 2005), i.e. selected the âĂIJmost similar eddyâĂİ as matching eddy: $\min(D_{e_1,e_{2,3}})$ with $D_{e_1,e_{2,3}} = \frac{1}{\sqrt{4}}\sqrt{\left(\frac{\Delta\omega}{\sigma_\omega}\right)^2 + \left(\frac{\Delta a}{\sigma_a}\right)^2 + \left(\frac{\Delta SST}{\sigma_{SST}}\right)^2 + \left(\frac{\Delta d}{d_{min}}\right)^2}$, and $\Delta\omega = |\omega_{e_1} - \omega_{e_{2,3}}|$, $\Delta SST = |SST_{e_1} - SST_{e_{2,3}}|$, $\Delta a = |a_{e_1} - a_{e_{2,3}}|$ and $\Delta d = |d_{min} - d_{e_{2,3}}|$, where a is the individual eddy amplitude, d_{min} the minimum of the spatial distances of all eddies located within the search ellipse from the projected location of e_1, SST the sea surface temperature and σ_ω, σ_a and σ_{SST}, i.e., the temporal standard deviations of ω, a and SST, are taken from maps of temporal standard deviations which we derived based

on all identified (not yet tracked) eddies. We applied two final constraints concerning the match-up: firstly, we allowed a match only if $D_{e_1,e_{2,3}} < 1$ to exclude a match which would involve highly unlikely changes in eddy properties from e_1 to $e_{2,3}$. Secondly, we aimed to filter out "dying eddies" by not allowing an (5%) increase in vorticity if the eddy's vorticity had decreased the previous three time steps and also showed a 50% decease of vorticity compared to the time of first detection. In case that either no eddy centre was located within the search ellipse or all eddies within the search ellipse were rejected as matching eddies, e_1 was assumed to have died. We did not try to search for lost eddies in the following time steps.

D.1.2. Note About the Mean Composite Eddy (Fig. 4.2 and Supplementary Fig. D.5)

The variables were averaged in a rotated coordinate system according to the large-scale wind direction as one anticipates a different state of the atmosphere up- and downstream of the SST perturbation, and in addition a downwind shift of the perturbed atmosphere relative to the SST anomaly. The large-scale wind direction was defined as the average wind direction in a square of 14 eddy radii centred relative to the eddy-core. The SST anomaly and sea level anomaly contours are closely linked in the mean composite figure. A pronounced shift of the SST anomaly associated with oceanic eddies (relative to sea level anomalies contours) was detected in quiescent areas, whereas it is very small and not directly visible in dynamic areas, such as the Antarctic Circumpolar Current (ACC) (Hausmann and Czaja, 2012). If we distinguish eddies related to the ACC from the ones to the north, we find a clear dipole structure/shift of the SST anomaly and the sea level anomalies in the more quiescent region north of the ACC, too (not shown). However, in our domain, as the mean composite of eddies is dominated by eddies of dynamic areas which generally show a larger SST anomaly than eddies in quiescent regions, the dipole pattern due the shift has a much weaker amplitude (Hausmann and Czaja, 2012). Also, the feature of the SST and sea level anomaly shift is not directly relevant for the point of air-sea interaction we would like to make in this paper.

D.2. Supplementary Note: Scaling Argument Concerning the Impact of Oceanic Eddies on the Lower Atmosphere

The scaling argument entails two steps. First, we need to show that the overlying atmosphere responds quickly to anomalous surface fluxes associated with SST anomalies, and second, we need to demonstrate that the anomalous heat fluxes are of a magnitude large enough to modify the marine atmospheric boundary layer significantly. We first discuss the adjustment time-scale, and then provide a brief scaling estimate of the energy added to the atmospheric boundary layer due the effect of oceanic eddies.

D.2.1. Time-scale of adjustment

While air-sea fluxes will respond instantaneously to a disequilibrium, it will take time for the overlying atmosphere to adjust, and this time-scale has to be shorter than the time the air spends over the eddy and its associated SST anomalies. We estimate the latter to be about 4.5 to 5.5 hours, assuming an air-speed of 10 $^{m}/_{s}$ and an extent of 160 to 240 km of the eddy-induced SST anomalies (2 to 3 times larger than the pure eddy core). This is longer than the time-scale associated with the subsequent modification of the marine atmospheric boundary layer turbulence, i.e., about 1 hour, as estimated by Park et al. (2006) based on satellite observations and model simulations. Therefore, we can assume that the boundary layer above the SST anomalies will have sufficient time to adjust to them.

The tight spatial coupling between the SST and atmospheric anomalies with only a small downwind displacement further supports this conclusion. The somewhat larger displacements of cloud properties and rainfall compared to wind speed (at least for anticyclones), indicates that near surface wind responds quickest, whereas the responses of clouds and rainfall, which are related to processes at the top of the atmospheric boundary layer, are slightly delayed.

Our arguments are also consistent with what is known about the diurnal cycle of the atmospheric boundary layer over land (although clearly the magnitude of the forcing is much larger there). During the day, when the surface is being heated and the vertical momentum exchange increases, the near-surface wind speeds are higher – analogous to the increased wind over a positive SST anomaly. During the night, surface cooling stabilizes the atmospheric boundary layer and decreases the vertical momentum transport, i.e. turbulence. As a result, near-surface wind speeds tend to be very low and a nocturnal jet may develop aloft.

D.2.2. Energy flux scaling argument

For a typical warm-core eddy SST anomaly for Southern Ocean conditions of $\Delta\mathrm{SST} = 0.3\ ^{\circ}\mathrm{C}$ (mean over core and peripheral area), a standard bulk formula for surface fluxes provides an estimate of the additional heat flux into the atmospheric boundary layer of $\Delta Q = 20\ \mathrm{W\ m^{-2}}$ (Messager et al. 2012, 200 W m^{-2} for $\sim 3\ ^{\circ}\mathrm{C}$). For an exposure

time to this SST anomaly of $t = 4$ h and an atmospheric boundary layer height of $H = 500$ m this leads to a mean temperature change in the atmospheric boundary layer of $\Delta T = \Delta Q t/(H \rho_{\mathrm{air}} c_p) = 0.6$ °C (density of air ρ_{air} =1 kg m^{-3}, specific heat capacity of air c$_p$=10^3 J kg^{-1} K^{-1}). Finally, assuming a well mixed atmospheric boundary layer and a standard tropospheric lapse rate above of $\gamma = 6.5$ °C km^{-1}, we estimate an atmospheric boundary layer height change of $\Delta H \approx 100$ m or 20%, which is in the range of observations and modeling studies (e.g. Sweet et al. 1981; Kwon et al. 1998; Spall 2007). Hence, the SST anomalies associated with ocean mesoscale eddies provide enough energy to cause measurable changes in the lower atmosphere despite their moderate size and the swiftly moving atmosphere.

D.3. Supplementary Figure: Seasonality of correlations of SST anomalies of oceanic eddies with anomalies of atmospheric properties

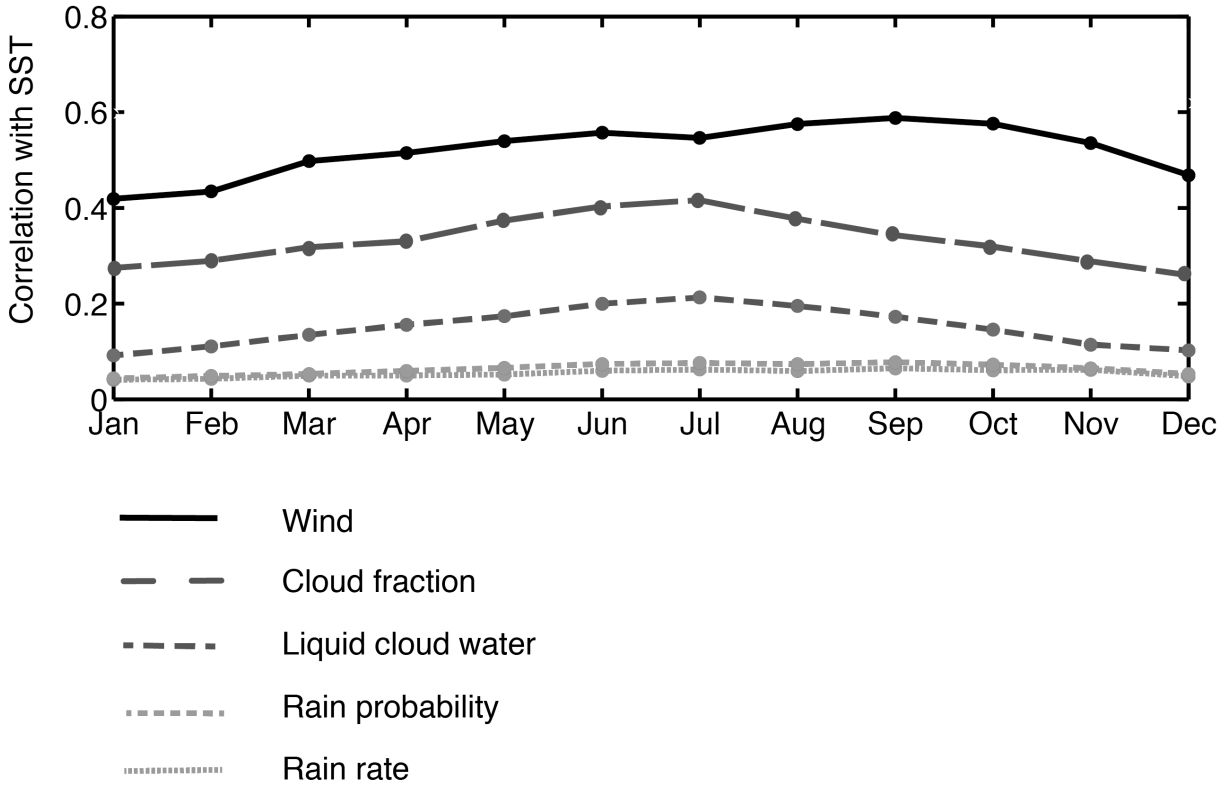

Figure D.1.: Seasonality of correlations of SST anomalies of oceanic eddies with anomalies of atmospheric properties *(wind speed, cloud fraction, liquid cloud water, rain probability and rain rate); all eddies south of 30°S (>600,000) are considered in this Figure, i.e. several 10,000 data points contribute to the correlation for each month; correlations are significant for all months ($p<0.01$).*

D.4. Supplementary Figure: Polar orthographic maps of the eddy statistics (continued from Fig. 4.1)

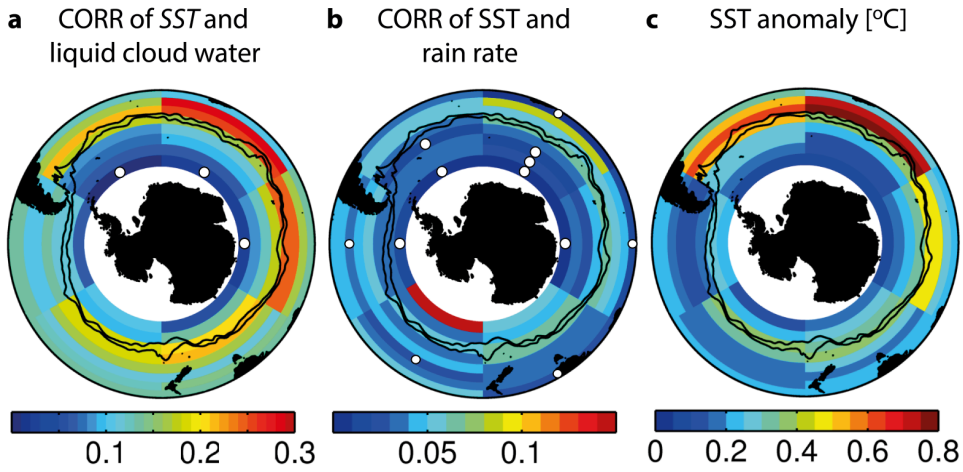

Figure D.2.: Polar orthographic maps of the eddy statistics (continued from Fig. 4.1). *Correlations (CORR) in each 60°×4° bin of anomalies of SST of oceanic eddies with anomalies of* **a** *liquid cloud water and* **b** *rain rate;* **c** *shows the mean absolute SST anomaly in each bin. White dots mark bins in* **a** *and* **b** *where correlations are not significant (p>0.01) and white areas feature insufficient data; black contours denote the two major fronts of the Antarctic Circumpolar Current (the Subantarctic and the Polar Fronts).*

D.5. Supplementary Figure: Autocorrelation of total cloud cover over various locations in the Southern Ocean

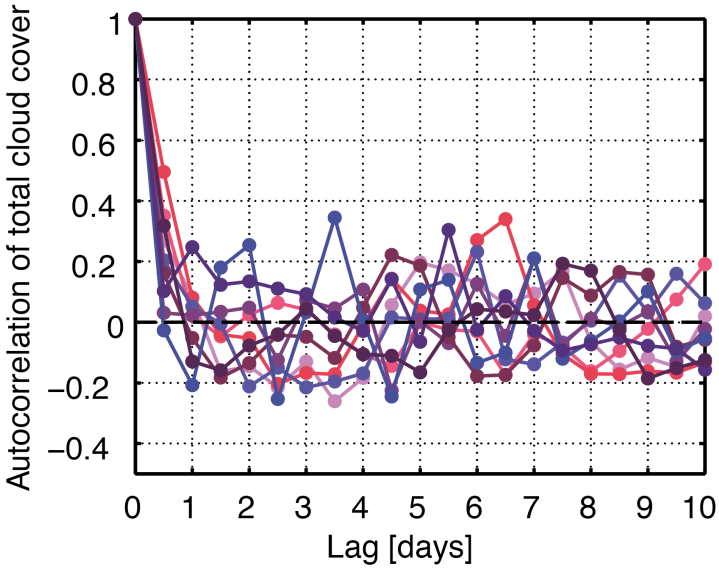

Figure D.3.: Autocorrelation of total cloud cover over various locations in the Southern Ocean *(south of 30°S and north of 60°S at different latitudes over the Pacific, Atlantic and Indian Ocean) based on 12-hourly atmospheric reanalysis data (ERA-interim, http://www.ecmwf.int/research/era/do/get/era-interim) for a summer month, i.e., January 2008.*

At all locations the autocorrelation of total cloud cover drops below 0.2 within 1 to 2 days (see Supplementary Fig. D.3). The autocorrelations of other atmospheric quantities drop off similarly quickly (not shown). This confirms our expectation since atmospheric weather systems pass by quickly in the Southern Ocean, where there are no blocking situations over/next to land masses/topography that could induce longer persistence. Hence, we consider the weekly atmospheric data as statistically independent.

D.6. Supplementary Figure: Linear relationship of SST anomalies of oceanic eddies and anomalies of atmospheric quantities.

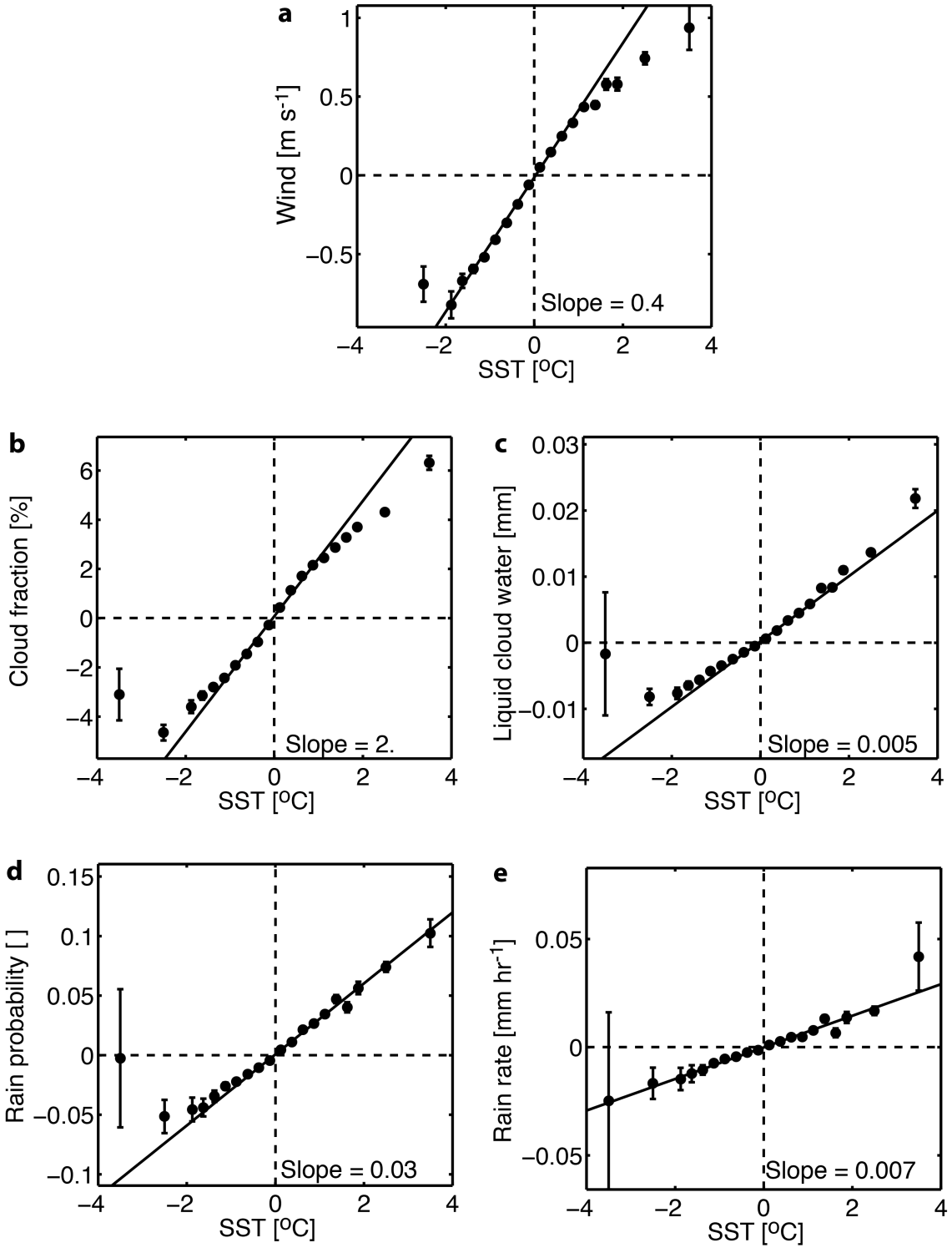

***Figure D.4**: Caption on next page.*

Figure D.4.: Linear relationship of SST anomalies of oceanic eddies and anomalies of atmospheric quantities. *The atmospheric quantities, i.e.* ***a*** *wind speed,* ***b*** *cloud fraction,* ***c*** *liquid cloud water,* ***d*** *rain probability and* ***e*** *rain rate are binned according to the eddies' SST anomalies and averaged thereafter; the bin sizes are of 0.25°C and of 1°C spacing for anomalies smaller and larger than |2°C|, respectively; the vertical bars show the error of the mean; the slope of the least square fit to the unbinned data shown as black line is noted in each panel; all eddies in the region south of 30°S (>600,000) are considered in this Figure.*

The relationship of SST anomalies and atmospheric quantities is mostly linear with a change of wind of 0.4 m s^{-1}, of cloud fraction of 2%, of liquid cloud water of 0.005 mm, rain probability of 3% and rain rate of 0.007 mm h^{-1} per 1°C of SST anomaly; a robust fit (not shown) features the same slopes except for the rain rate where it is smaller (0.005 mm h^{-1}); the slope expressed relative to the background state is about 5% for wind, 3% for cloud fraction, 6% for liquid cloud water and 8% for both, rain rate and probability. The steepness of the slopes is relatively independent of the magnitude of the SST anomalies included in the regression and of the area, i.e. independent for instance of the Agulhas area with its large SST anomalies and high correlations. The steepness of the slopes increases with increasing large-scale wind speeds (not shown, in agreement with Spall (2007))
The slopes from our results agree well with previous findings of 0.2-0.4 m s^{-1} $°C^{-1}$ for wind speed over the Agulhas Return Current and the Malvinas-Brazil Confluence Zone (Liu et al., 2007; O'Neill et al., 2005, 2012); further, absolute SST perturbations in the range of 1.5 to 3 °C in the Agulhas Return Current are associated with absolute liquid cloud water anomalies in the range of 0.01 to 0.02 mm (O'Neill et al. 2005, Fig. 18 therein), matching approximately our results.

D.7. Supplementary Figure: Mean eddy and and pattern of its atmospheric imprint (continued from Fig. 4.2)

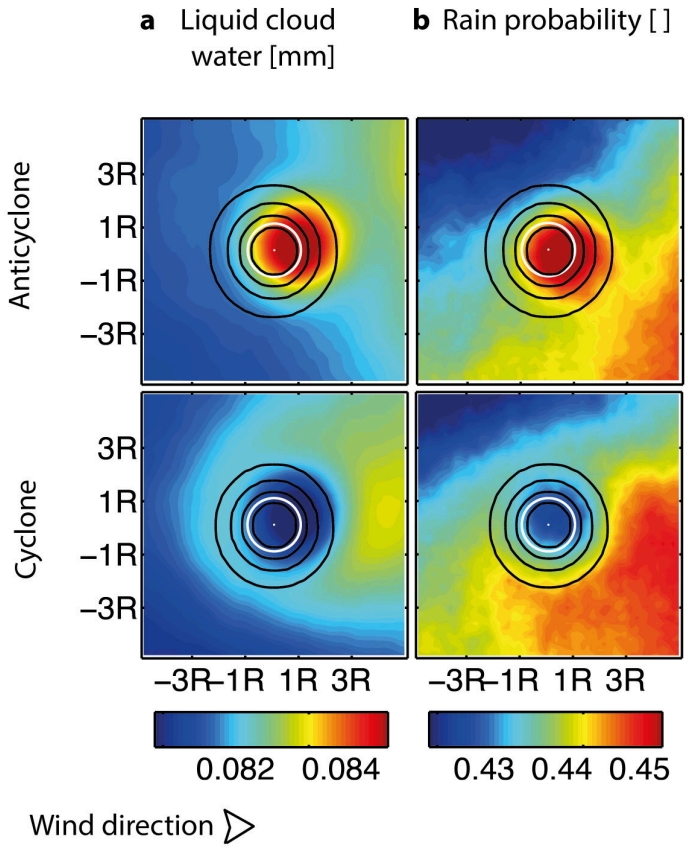

Figure D.5.: Mean eddy and and pattern of its atmospheric imprint (continued from Fig. 4.2). ***a*** *Liquid cloud water* ($\pm 0.3 \times 10^{-3}$ *mm) and* ***b*** *rain probability* ($\pm 3 \times 10^{-3}$)*; mean composite maps of the >600,000 individual eddy realizations south of 30° S, divided into anticyclones and cyclones; white circles mark the eddy-core as detected with the Okubo-Weiss parameter; black lines denote sea level anomaly contours associated with the eddy; before averaging, the eddies were scaled according to their individual eddy amplitude and radius (R), interpolated and rotated so that the large-scale wind is from left to right.*

The large-scale gradient of SST is positive towards the equator (the wind direction is predominantly westerly); in contrast, the large-scale gradient is largely positive towards high latitudes for the atmospheric quantities, which reflects the increasing wind speed, cloud fraction and rain towards the "core-latitudes" of the westerlies.
A small downwind displacement is visible in the imprint of eddies on the atmosphere especially for the cloud properties and rain (see also Fig. 4.2 in the main text and Supplementary Note D.2 about the response time-scale of the marine atmospheric boundary layer).

D.8. Supplementary Figure: Polar orthographic maps of the eddy statistics

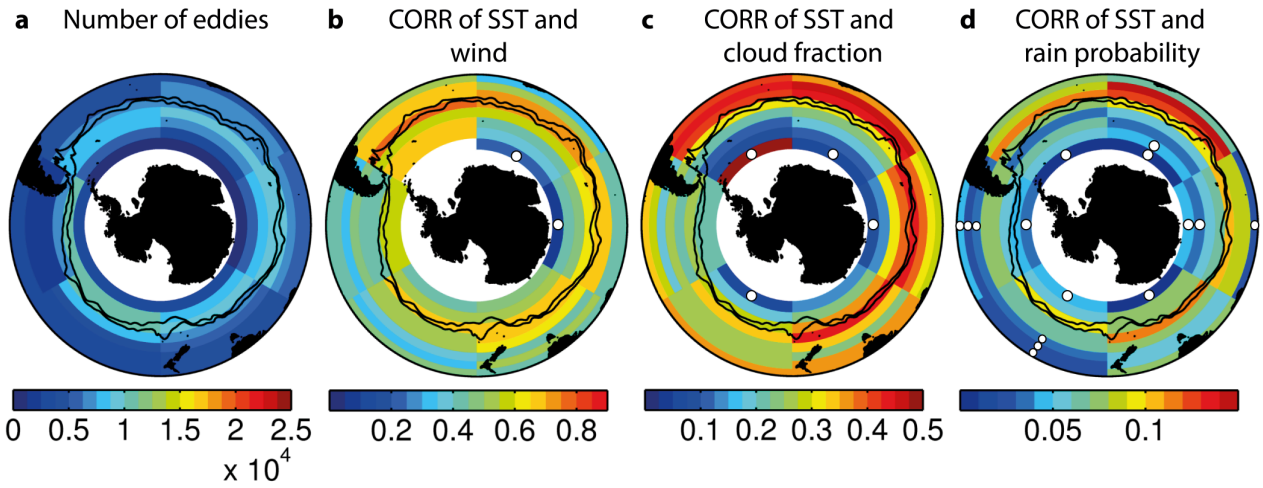

Figure D.6.: Polar orthographic maps of the eddy statistics: *as Fig. 4.1 but with a reduced sample size (see Methods Section); only biweekly atmospheric data are considered and eddies with a minimum life time of 1 month.*

D.9. Supplementary Figure: Polar orthographic maps of the eddy statistics

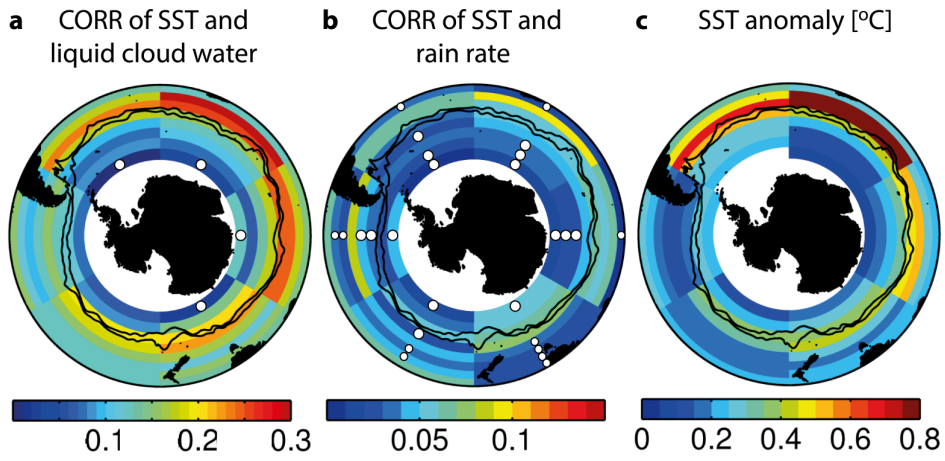

Figure D.7.: Polar orthographic maps of the eddy statistics: *as Supplementary Fig. D.2 but with a reduced sample size (see Methods Section); only biweekly atmospheric data are considered and eddies with a minimum life time of 1 month.*

D.10. Supplementary Figure: Mean eddy and and pattern of its atmospheric imprint

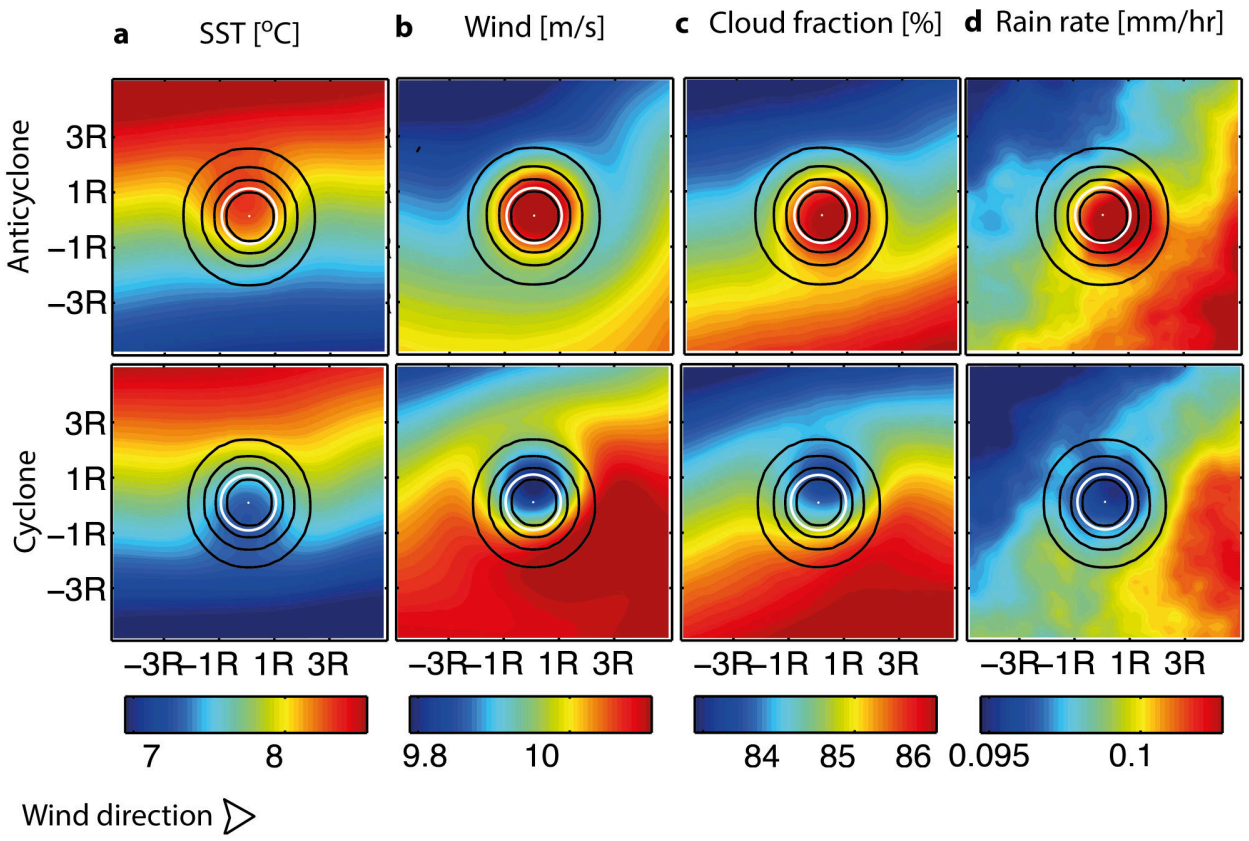

Figure D.8.: Mean eddy and and pattern of its atmospheric imprint: *as Fig. 4.2 but with a reduced sample size (see Methods Section); only biweekly atmospheric data are considered and eddies with a minimum life time of 1 month.*

D.11. Supplementary Figure: Mean eddy and and pattern of its atmospheric imprint

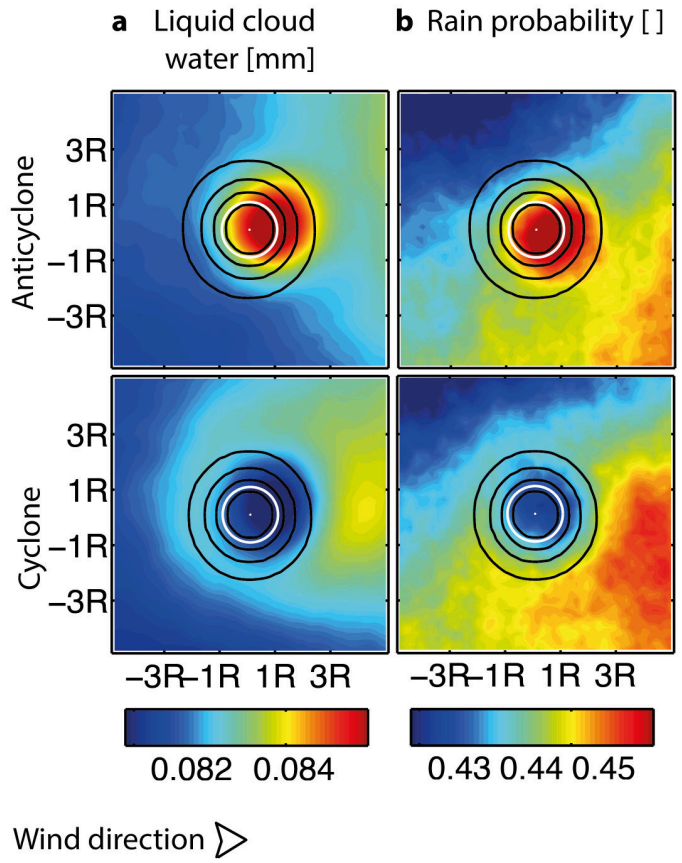

Figure D.9.: Mean eddy and and pattern of its atmospheric imprint: *as Supplementary Fig. D.5 but with a reduced sample size (see Methods Section); only biweekly atmospheric data are considered and eddies with a minimum life time of 1 month.*

Bibliography

Adams, D. K., McGillicuddy, D. J., Zamudio, L., Thurnherr, A. M., Liang, X., Rouxel, O., German, C. R., and Mullineaux, L. S. (2011). Surface-generated mesoscale eddies transport deep-sea products from hydrothermal vents. *Science (New York, N.Y.)*, 332(6029):580–3.

Ansorge, I. J., Pakhomov, E. A., Kaehler, S., Lutjeharms, J. R. E., and Durgadoo, J. V. (2009). Physical and biological coupling in eddies in the lee of the South-West Indian Ridge. *Polar Biology*, 33(6):747–759.

Arhan, M., Speich, S., Messager, C., Dencausse, G., Fine, R., and Boye, M. (2011). Anticyclonic and cyclonic eddies of subtropical origin in the subantarctic zone south of Africa. *Journal of Geophysical Research*, 116(C11):1–22.

Bailleul, F., Cotté, C., and Guinet, C. (2010). Mesoscale eddies as foraging area of a deep-diving predator, the southern elephant seal. *Marine Ecology Progress Series*, 408:251–264.

Behrenfeld, M. J., Boss, E., Siegel, D. A., and Shea, D. M. (2005). Carbon-based ocean productivity and phytoplankton physiology from space. *Global Biogeochemical Cycles*, 19(1):GB1006, doi:10.1029/2004GB002299.

Bernard, A., Ansorge, I., Froneman, P., Lutjeharms, J., Bernard, K., and Swart, N. (2007). Entrainment of Antarctic euphausiids across the Antarctic Polar Front by a cold eddy. *Deep Sea Research Part I: Oceanographic Research Papers*, 54(10):1841–1851.

Bigorre, S. (2005). *Topographic Effects on Wind Driven Oceanic Circulation*. PhD thesis, The Florida State University.

Boehlert, G. W. (1988). Current-topography interactions at mid-ocean seamounts and the impact on pelagic ecosystems. *GeoJournal*, 16(1):45–52.

Böning, C. W., Dispert, A., Visbeck, M., Rintoul, S. R., and Schwarzkopf, F. U. (2008). The response of the Antarctic Circumpolar Currrent to recent climate change. *Nature Geoscience*, 1:864–869.

Boyd, P. W., Arrigo, K. R., Strzepek, R., and van Dijken, G. L. (2012). Mapping phytoplankton iron utilization: Insights into Southern Ocean supply mechanisms. *Journal of Geophysical Research*, 117(C6):C06009.

Bracco, A., Provenzale, A., and Scheuring, I. (2000). Mesoscale vortices and the paradox of the plankton. *Proceedings. Biological sciences / The Royal Society*, 267(1454):1795–1800.

Bryan, F. O., Tomas, R., Dennis, J. M., Chelton, D. B., Loeb, N. G., and McClean, J. L. (2010). Frontal scale air-sea interaction in high-resolution coupled climate models. *Journal of Climate*, 23:6277–6291.

Calbet, A., Saiz, E., Almeda, R., Movilla, J. I., and Alcaraz, M. (2011). Low microzooplankton grazing rates in the Arctic Ocean during a Phaeocystis pouchetii bloom (summer 2007): fact or artifact of the dilution technique? *J. Plankton Res.*, 33(5):687–701.

Campbell, J. W. (1995). The lognormal distribution as a model for bio-optical variability in the sea. *Journal of Geophysical Research*, 100(C7):13237–13254.

Carton, J. A. and Giese, B. S. (2008). A reanalysis of ocean climate using simple ocean data assimilation (SODA). *Monthly Weather Review*, 136(8):2999–3017.

Casey, K. S., Brandon, T. B., Cornillon, P., Evans, R., Barale, V., Gower, J., and Alberotanza, L. (2010). The past, present and future of the AVHRR Pathfinder SST program. In Barale, V., Gower, J., and Alberotanza, L., editors, *Oceanography from Space*, pages 273–287. Springer Netherlands, Dordrecht.

Chaigneau, A., Eldin, G., and Dewitte, B. (2009). Eddy activity in the four major upwelling systems from satellite altimetry (1992-2007). *Progress In Oceanography*, 83(1-4):117–123.

Chaigneau, A., Gizolme, A., and Grados, C. (2008). Mesoscale eddies off Peru in altimeter records: Identification algorithms and eddy spatio-temporal patterns. *Progress In Oceanography*, 79(2-4):106–119.

Chaigneau, A., Le Texier, M., Eldin, G., Grados, C., and Pizarro, O. (2011). Vertical structure of mesoscale eddies in the eastern South Pacific Ocean: A composite analysis from altimetry and Argo profiling floats. *Journal of Geophysical Research*, 116:C11025.

Charlson, R. J., Lovelock, J. E., Andreae, M. O., and Warren, S. G. (1987). Oceanic phytoplankton, atmospheric sulphur, cloud albedo and climate. *Nature*, 326(16):655–661.

Charney, J. G. (1971). Geostrophic Turbulence. *Journal of the Atmospheric Sciences*, 28(6):1087–1095.

Chelton, D. B., DeSzoeke, R. A., Schlax, M. G., El Naggar, K., and Siwertz, N. (1998). Geographical variability of the first baroclinic Rossby radius of deformation. *Journal of Physical Oceanography*, 28(3):433–460.

Chelton, D. B., Gaube, P., Schlax, M. G., Early, J. J., and Samelson, R. M. (2011a). The influence of nonlinear mesoscale eddies on near-surface oceanic chlorophyll. *Science*, 334:328–332.

Chelton, D. B., Schlax, M. G., Freilich, M. H., and Milliff, R. F. (2004). Satellite measurements reveal persistent small-scale features in ocean winds. *Science*, 303:978–983.

Chelton, D. B., Schlax, M. G., and Samelson, R. M. (2011b). Global observations of nonlinear mesoscale eddies. *Progress in Oceanography*, 91(2):167–216.

Chelton, D. B., Schlax, M. G., Samelson, R. M., and de Szoeke, R. A. (2007). Global observations of large oceanic eddies. *Geophysical Research Letters*, 34(15):L15606.

Chelton, D. B., Schlax, M. G., Witter, D. L., and Richman, J. G. (1990). Geosat altimeter observations of the surface circulation of the Southern Ocean. *Journal of Geophysical Research*, 95(C10):17877–17903.

Chelton, D. B. and Xie, S.-P. (2010). Coupled ocean-atmosphere interaction at oceanic mesoscales. *Oceanography*, 23(4):52–69.

Cipollini, P., Cromwell, D., Challenor, P. G., and Raffaglio, S. (2001). Rossby waves detected in global ocean colour data. *Geophysical Research Letters*, 28(2):323–326.

Comiso, J. C., McClain, C. R., Sullivan, C. W., Ryan, J. P., and Leona, C. L. (1993). Coastal zone color scanner pigment concentrations in the Southern Ocean and relationships to geophysical surface features. *Journal of Geophysical Research*, 98(C2):2419–2451.

Cushman-Roisin Benoit, Chassignet, E. P., and Tang, B. (1989). Westward motion of mesoscale eddies. *Journal of Physical Oceanography*, 20:758–768.

Czaja, A. and Marshall, J. (2006). The partitioning of poleward heat transport between the atmosphere and ocean. *Journal of the Atmospheric Sciences*, 63:1498–1511.

Dandonneau, Y., Vega, A., Loisel, H., du Penhoat, Y., and Menkes, C. (2003). Oceanic Rossby waves acting as a "hay rake" for ecosystem floating by-products. *Science*, 302(5650):1548–1551.

D'Asaro, E., Lee, C., Rainville, L., Harcourt, R., and Thomas, L. (2011). Enhanced turbulence and energy dissipation at ocean fronts. *Science*, 332(6027):318–322.

De Steur, L. and Van Leeuwen, P. (2009). The influence of bottom topography on the decay of modeled Agulhas rings. *Deep Sea Research Part I: Oceanographic Research Papers*, 56(4):471–494.

De Szoeke, R. A. and Levine, M. D. (1981). The advective flux of heat by mean geostrophic motions in the Southern Ocean. *Deep Sea Research Part A. Oceanographic Research Papers*, 28(10):1057–1085.

Dehairs, F., Kopczynska, E., Nielsen, P., Lancelot, C., Bakker, D. C. E., Koeve, W., and Goeyens, L. (1997). δ13C Southern Ocean suspended organic matter during spring and early summer: regional and temporal variability. *Deep-Sea Research II*, 44(1-2):129–142.

Dencausse, G., Arhan, M., and Speich, S. (2010). Routes of Agulhas rings in the southeastern Cape Basin. *Deep Sea Research Part I: Oceanographic Research Papers*, 57(11):1406–1421.

Doney, S. C. (2003). Mesoscale variability of Sea-viewing Wide Field-of-view Sensor (SeaWiFS) satellite ocean color: Global patterns and spatial scales. *Journal of Geophysical Research*, 108(C2):3024.

Dong, C., Nencioli, F., Liu, Y., and McWilliams, J. C. (2011). An automated approach to detect oceanic eddies from satellite remotely sensed sea surface temperature data. *IEEE Geoscience and Remote Sensing Letters*, 8(6):1055–1059.

D'Ovidio, F., Isern-Fontanet, J., Lopez, C., Hernández-García, E., and García-Ladona, E. (2009). Comparison between Eulerian diagnostics and finite-size Lyapunov exponents computed from altimetry in the Algerian basin. *Deep Sea Research Part I: Oceanographic Research Papers*, 56(1):15–31.

Dufour, C. O., Le Sommer, J., Zika, J. D., Gehlen, M., Orr, J. C., Mathiot, P., and Barnier, B. (2012). Standing and transient eddies in the response of the Southern Ocean meridional overturning to the Southern Annular Mode. *Journal of Climate*, 25(20):6958–6974.

Early, J. J., Samelson, R. M., and Chelton, D. B. (2011). The evolution and propagation of quasigeostrophic ocean eddies. *Journal of Physical Oceanography*, 41(8):1535–1555.

Everett, J. D., Baird, M. E., Oke, P. R., and Suthers, I. M. (2012). An avenue of eddies: Quantifying the biophysical properties of mesoscale eddies in the Tasman Sea. *Geophysical Research Letters*, 39(16):L16608.

Falkowski, P. (2012). Ocean Science: The power of plankton. *Nature*, 483(7387):S17–20.

Falkowski, P. G., Ziemann, D., Kolber, Z., and Bienfang, P. K. (1991). Role of eddy pumping in enhancing primary production in the ocean. *Nature*, 352(6330):55–58.

Fasullo, J. T. and Trenberth, K. E. (2008). The annual cycle of the energy budget. Part II: meridional structures and poleward transports. *Journal of Climate*, 21(10):2313–2325.

Fernandes, A. M., Nascimento, S., and Boutov, D. (2011). Automatic identification of oceanic eddies in infrared satellite images. *Computers & Geosciences*, 37(11):1783–1792.

Ferrari, R. (2011). Ocean science. A frontal challenge for climate models. *Science*, 332:316–317.

Ferrari, R. and Wunsch, C. (2009). Ocean circulation kinetic energy: reservoirs, sources, and sinks. *Annual Review of Fluid Mechanics*, 41(1):253–282.

Field, C. B. (1998). Primary production of the biosphere: integrating terrestrial and oceanic components. *Science*, 281(5374):237–240.

Flierl, G. G. R. (1981). Particle motions in large-amplitude wave fields. *Geophysical & Astrophysical Fluid Dynamics*, 18(1-2):39–74.

Fu, L.-L. (2009). Pattern and velocity of propagation of the global ocean eddy variability. *Journal of Geophysical Research*, 114:C11017.

Fyfe, J. C. and Saenko, O. A. (2006). Simulated changes in the extratropical Southern Hemisphere winds and currents. *Geophysical Research Letters*, 33:1–4.

Garabato, A. C. N., Polzin, K. L., King, B. a., Heywood, K. J., and Visbeck, M. (2004). Widespread intense turbulent mixing in the Southern Ocean. *Science*, 303(5655):210–3.

Gent, P. R. and McWilliams, J. C. (1990). Isopycnal mixing in ocean circulation models. *Journal of Physical Oceanography*, 20:150–155.

Gill, A., Green, J., and Simmons, A. (1974). Energy partition in the large-scale ocean circulation and the production of mid-ocean eddies. *Deep Sea Research and Oceanographic Abstracts*, 21(7):499–528.

Gillett, N. P., Stone, D. a., Stott, P. a., Nozawa, T., Karpechko, A. Y., Hegerl, G. C., Wehner, M. F., and Jones, P. D. (2008). Attribution of polar warming to human influence. *Nature Geoscience*, 1(11):750–754.

Godø, O. R., Samuelsen, A., Macaulay, G. J., Patel, R., Hjø llo, S. S. t., Horne, J., Kaartvedt, S., and Johannessen, J. a. (2012). Mesoscale eddies are oases for higher trophic marine life. *PloS one*, 7(1):e30161, doi:10.1371/journal.pone.0030161.

Gomez-Enri, J., Quartly, G. D., Navarro, G., and Villares, P. (2007). Characterizing and following eddies in the Drake Passage. In *IGARSS 2007: Sensing and Understanding our Planet, Barcelona, Spain, 23-27 July 2007.*, page 4pp, Barcelona, Spain.

Gordon, A. and Taylor, H. W. (1975). Heat and salt balance within the cold waters of the world ocean. In *Numerical models of ocean circulation*, pages 54–56.

Gower, J. F. R., Denman, K. L., and Holyer, R. J. (1980). Phytoplankton patchiness indicates the fluctuation spectrum of mesoscale oceanic structure. *Nature*, 288(5787):157–159.

Griffa, A., Lumpkin, R., and Veneziani, M. (2008). Cyclonic and anticyclonic motion in the upper ocean. *Geophysical Research Letters*, 35(1):L01608.

Gruber, N., Gloor, M., and Mikaloff Fletcher, S. E. (2009). Oceanic sources, sinks, and transport of atmospheric CO2. *Global Biogeochemical Cycles*, 23:GB1005, doi:10.1029/2008GB003349.

Hallberg, R. and Gnanadesikan, A. (2006). The role of eddies in determining the structure and response of the wind-driven southern hemisphere overturning: results from the modeling eddies in the Southern Ocean (MESO) Project. *Journal of Physical Oceanography*, 36:2232–2252.

Hausmann, U. and Czaja, A. (2012). The observed signature of mesoscale eddies in sea surface temperature and the associated heat transport. *Deep Sea Research Part I: Oceanographic Research Papers*, 70:60–72.

Henson, S. (2008). A census of oceanic anticyclonic eddies in the Gulf of Alaska. *Deep Sea Research Part I: Oceanographic Research Papers*, 55(2):163–176.

Hewson, T. D. and Titley, H. A. (2010). Objective identification, typing and tracking of the complete life-cycles of cyclonic features at high spatial resolution. *Meteorological Applications*, 17(3):355–381.

Hilburn, K. A., Wentz, F. J., Smith, D. K., and Ashcroft, P. D. (2006). Correcting active scatterometer data for the effects of rain using passive radiometer data. *Journal of Applied Meteorology and Climatology*, 45(3):382–398.

Hobbs, P. V. (1987). The Gulf Stream rainband. *Geophysical Research Letters*, 14:1142–1145.

Hogg, A. M. and Blundell, J. R. (2006). Interdecadal variability of the Southern Ocean. *Journal of Physical Oceanography*, 36:1626–1645.

Hogg, A. M., Meredity, M. P., Blundell, J. R., and Wilson, C. (2008). Eddy heat flux in the Southern Ocean: response to variable wind forcing. *Journal of Climate*, 21:608–620.

Hogg, N. G. (1973). On the stratified Taylor column. *Journal of Fluid Mechanics*, 58(3):517–537.

Iizuka, S. (2010). Simulations of wintertime precipitation in the vicinity of Japan: sensitivity to fine-scale distributions of sea surface temperature. *Journal of Geophysical Research*, 115:D10107, doi:10.1029/2009JD012576.

Isern-Fontanet, J., García-Ladona, E., and Font, J. (2003). Identification of marine eddies from altimetric maps. *Journal of Atmospheric and Oceanic Technology*, 20(5):772–778.

Isern-Fontanet, J., García-Ladona, E., and Font, J. (2006). Vortices of the Mediterranean Sea: An altimetric perspective. *Journal of Physical Oceanography*, 36(1):87–103.

Ito, T., Woloszyn, M., and Mazloff, M. (2010). Anthropogenic carbon dioxide transport in the Southern Ocean driven by Ekman flow. *Nature*, 463(7277):80–3.

Itoh, S. and Yasuda, I. (2010). Characteristics of mesoscale eddies in the Kuroshio-Oyashio extension region detected from the distribution of the sea surface height anomaly. *Journal of Physical Oceanography*, 40(5):1018–1034.

Jin, X., Dong, C., Kurian, J., McWilliams, J. C., Chelton, D. B., and Li, Z. (2009). SSTâĂŞwind interaction in coastal upwelling: oceanic simulation with empirical coupling. *Journal of Physical Oceanography*, 39(11):2957–2970.

Johnson, E. R. (1977). Stratified taylor columns on a beta-plane. *Geophysical & Astrophysical Fluid Dynamics*, 9(1):159–177.

Joyce, T. M., Patterson, S. L., and Millard, R. C. (1981). Anatomy of a cyclonic ring in the drake passage. *Deep Sea Research Part A. Oceanographic Research Papers*, 28(11):1265–1287.

Kahru, M., Gille, S. T., Murtugudde, R., Strutton, P. G., Manzano-Sarabia, M., Wang, H., and Mitchell, B. G. (2010). Global correlations between winds and ocean chlorophyll. *Journal of Geophysical Research*, 115:C12040, doi:10.1029/2010JC006500.

Kahru, M., Mitchell, B. G., Gille, S. T., Hewes, C. D., and Holm-Hansen, O. (2007). Eddies enhance biological production in the Weddell-Scotia confluence of the Southern Ocean. *Geophysical Research Letters*, 34:L14603.

Keffer, T. and Holloway, G. (1988). Estimating Southern Ocean eddy flux of heat and salt from satellite altimetry. *Nature*, 332(6165):624–626.

Kelly, K. A., Beardsley, R. C., Limeburner, R., Brink, K. H., Paduan, J. D., and Chereskin, T. K. (1998). Variability of the near-surface eddy kinetic energy in the California Current based on altimetric, drifter, and moored current data. *Journal of Geophysical Research*, 103(C6):13067–13083.

Koshlyakov, M. N. and Monin, A. S. (1978). Synoptic eddies in the ocean. *Annual Review of Earth and Planetary Sciences*, 6:495–523.

Kurczyn, J. A., Beier, E., Lavín, M. F., and Chaigneau, A. (2012). Mesoscale eddies in the northeastern Pacific tropical-subtropical transition zone: Statistical characterization from satellite altimetry. *Journal of Geophysical Research*, 117:C10021, doi:10.1029/2012JC007970.

Kwon, B., Bénech, B., and Lambert, D. (1998). Structure of the marine atmospheric boundary layer over an oceanic thermal front: SEMAPHORE experiment. *Journal of Geophysical Research*, 103(C11):25159–25180, doi::10.1029/98JC02207.

Lachkar, Z., Orr, J. C., Dutay, J.-C., and Delecluse, P. (2007). Effects of mesoscale eddies on global ocean distributions of CFC-11, CO2, and δ14C. *Ocean Science*, 3:461–482.

Lehahn, Y., D'Ovidio, F., Lévy, M., Amitai, Y., and Heifetz, E. (2011). Long range transport of a quasi isolated chlorophyll patch by an Agulhas ring. *Geophysical Research Letters*, 38(16):L16610.

Lévy, M. (2008). The modulation of biological production by oceanic mesoscale turbulence. *Transport and Mixing in Geophysical Flows, Creators of Modern Physics*, 744:219–261.

Liang, X. and Thurnherr, A. M. (2012). Eddy-modulated internal waves and mixing on a midocean ridge. *Journal of Physical Oceanography*, 42(7):1242–1248.

Liu, W., Xie, X., and Tang, W. (2010). Scatterometer's unique capability in measuring ocean surface stress. In Barale, V., Alberotanza, L., and Gower, J., editors, *Oceanography from Space: Revisited*, chapter 6, pages 93–111. Springer Dordrecht Heidelberg London New York.

Liu, W. T., Xie, X., and Niiler, P. P. (2007). Ocean-atmosphere interaction over Agulhas extension meanders. *Journal of Climate*, 20(23):5784–5797.

Liu, Y., Dong, C., Guan, Y., Chen, D., McWilliams, J., and Nencioli, F. (2012). Eddy analysis in the subtropical zonal band of the North Pacific Ocean. *Deep Sea Research Part I: Oceanographic Research Papers*, 68:54–67.

Llido, J. (2005). Event-scale blooms drive enhanced primary productivity at the Subtropical Convergence. *Geophysical Research Letters*, 32(15):L15611.

Mahadevan, A., D'Asaro, E., Lee, C., and Perry, M. J. (2012). Eddy-driven stratification initiates North Atlantic spring phytoplankton blooms. *Science*, 337(6090):54–58.

Maritorena, S., D'Andon, O. H. F., Mangin, A., and Siegel, D. a. (2010). Merged satellite ocean color data products using a bio-optical model: Characteristics, benefits and issues. *Remote Sensing of Environment*, 114(8):1791–1804.

Maritorena, S. and Siegel, D. A. (2005). Consistent merging of satellite ocean color data sets using a bio-optical model. *Remote Sensing of Environment*, 94(4):429–440.

Marshall, J. and Shutts, G. (1981). A note on rotational and divergent eddy fluxes. *Journal of Physical Oceanography*, 11(12):1677–1680.

Maximenko, N., Niiler, P., Rio, M.-H., Melnichenko, O., Centurioni, L., Chambers, D., Zlotnicki, V., and Galperin, B. (2009). Mean dynamic topography of the ocean derived from satellite and drifting buoy data using three different techniques. *Journal of Atmospheric and Oceanic Technology*, 26:1910–1919.

McGillicuddy, D. J., Robinson, A. R., Siegel, D. A., Jannasch, H. W., Johnson, R., Dickey, T. D., McNeil, J., Michaels, A. F., and Knap, A. H. (1998). Influence of Mesoscale Eddies on New Production in the Sargasso Sea. *Nature*, 394(6690):263–266.

McGillicuddy et al., D. J. (2007). Eddy/wind interactions stimulate extraordinary mid-ocean plankton blooms. *Science*, 316(5827):1021–6.

Melander, M. V., Mcwilliams, J. C., and Zabusky, N. J. (1987). Axisymmetrization and vorticity-gradient intensification of an isolated two-dimensional vortex through filamentation. *Journal of Fluid Mechanics*, 178:137–159.

Meredith, M. P. (2003). An anticyclonic circulation above the Northwest Georgia Rise, Southern Ocean. *Geophysical Research Letters*, 30(20):2061.

Meredith, M. P., Naveira Garabato, A. C., Hogg, A. M., and Farneti, R. (2012). Sensitivity of the overturning circulation in the Southern Ocean to decadal changes in wind forcing. *Journal of Climate*, 25(1):99–110.

Messager, C., Speich, S., and Key, E. (2012). Marine atmospheric boundary layer over some Southern Ocean fronts during the IPY BGH 2008 cruise. *Ocean Science*, 8(6):1001–1023.

Mignone, B. K., Gnanadesikan, A., Sarmiento, J. L., and Slater, R. D. (2006). Central role of Southern Hemisphere winds and eddies in modulating the oceanic uptake of anthropogenic carbon. *Geophysical Research Letters*, 23:L01604, doi:10.1029/2005GL024464.

Mikaloff Fletcher, S. E., Gruber, N., Jacobson, a. R., Doney, S. C., Dutkiewicz, S., Gerber, M., Follows, M., Joos, F., Lindsay, K., Menemenlis, D., Mouchet, A., Müller, S. a., and Sarmiento, J. L. (2006). Inverse estimates of anthropogenic CO2 uptake, transport, and storage by the ocean. *Global Biogeochemical Cycles*, 20:GB2002, doi:10.1029/2005GB002530.

Minobe, S., Kuwano-Yoshida, A., Komori, N., Xie, S.-P., and Small, R. J. (2008). Influence of the Gulf Stream on the troposphere. *Nature*, 452(7184):206–9.

Morrison, A. and Hogg, A. (2013). On the relationship between Southern Ocean overturning and ACC transport. *Journal of Physical Oceanography*, 140-14:43.

Morrow, R. (2004). Divergent pathways of cyclonic and anti-cyclonic ocean eddies. *Geophysical Research Letters*, 31:L24311.

Morrow, R. and Le Traon, P.-Y. (2012). Recent advances in observing mesoscale ocean dynamics with satellite altimetry. *Advances in Space Research*, 50(8):1062–1076.

Moutin, T., Van Wambeke, F., and Prieur, L. (2012). Influence of anticyclonic eddies on the biogeochemistry from the oligotrophic to the ultraoligotrophic Mediterranean (BOUM cruise). *Biogeosciences Discussions*, 8:8091–8160.

Naveira Garabato, A. C., Ferrari, R., and Polzin, K. L. (2011). Eddy stirring in the Southern Ocean. *Journal of Geophysical Research*, 116:C09019.

Naveira Garabato, A. C., Polzin, K. L., King, B. A., Heywood, K. J., and Visbeck, M. (2004). Widespread intense turbulent mixing in the Southern Ocean. *Science*, 303:210–213.

Nel, D., Lutjeharms, J., Pakhomov, E., Ansorge, I., Ryan, P., and Klages, N. (2001). Exploitation of mesoscale oceanographic features by grey-headed albatross Thalassarche chrysostoma in the southern Indian Ocean. *Marine Ecology Progress Series*, 217:15–26.

Neu, U., Akperov, M. G., Bellenbaum, N., Benestad, R., Blender, R., Caballero, R., Cocozza, A., Dacre, H. F., Feng, Y., Fraedrich, K., Grieger, J., Gulev, S., Hanley, J., Hewson, T., Inatsu, M., Keay, K., Kew, S. F., Kindem, I., Leckebusch, G. C., Liberato, M. L. R., Lionello, P., Mokhov, I. I., Pinto, J. G., Raible, C. C., Reale, M., Rudeva, I., Schuster, M., Simmonds, I., Sinclair, M., Sprenger, M., Tilinina, N. D., Trigo, I. F., Ulbrich, S., Ulbrich, U., Wang, X. L., and Wernli, H. (2012). IMILAST - a community effort to intercompare extratropical cyclone detection and tracking algorithms: assessing method-related uncertainties. *Bulletin of the American Meteorological Society, Early Online Release*, pages doi: http://dx.doi.org/10.1175/BAMS–D–11–00154.1.

Nikurashin, M., Vallis, G. K., and Adcroft, A. (2012). Routes to energy dissipation for geostrophic flows in the Southern Ocean. *Nature Geoscience*, 6(1):48–51.

Oh, I. S. and Zhurbas, V. (2000). Study of spatial spectra of horizontal turbulence in the ocean using drifter data. *Journal of Physical Oceanography*, 30(7):1790–1801.

Okubo, A. (1970). Horizontal dispersion of floatable particles in the vicinity of velocity singularities such as convergences. *Deep-Sea Research*, 17:445–454.

Olbers, D., Borowski, D., Völker, C., and Wölff, J.-O. (2004). The dynamical balance, transport and circulation of the Antarctic Circumpolar Current. *Antarctic Science*, 16(4):439–470.

Omta, A. W., Kooijman, B., and Dijkstra, H. (2007). Influence of (sub)mesoscale eddies on the soft-tissue carbon pump. *Journal of Geophysical Research*, 112(C11):1–14.

O'Neill, L. W. (2012). Wind speed and stability effects on coupling between surface wind stress and SST observed from buoys and satellite. *Journal of Climate*, 25(5):1544–1569.

O'Neill, L. W., Chelton, D. B., and Esbensen, S. K. (2012). Covariability of surface wind and stress responses to sea surface temperature fronts. *Journal of Climate*, 25(17):5916–5942.

O'Neill, L. W., Chelton, D. B., Esbensen, S. K., and Wentz, F. J. (2005). High-resolution satellite measurements of the atmospheric boundary layer response to SST variations along the Agulhas Return Current. *Journal of Climate*, 18(14):2706–2723.

Oschlies, A. (2002). Can eddies make ocean deserts bloom? *Global Biogeochemical Cycles*, 16(4).

Park, K.-A., Cornillon, P., and Codiga, D. L. (2006). Modification of surface winds near ocean fronts: Effects of Gulf Stream rings on scatterometer (QuikSCAT, NSCAT) wind observations. *Journal of Geophysical Research*, 111(C3):C03021, doi:10.1029/2005JC003016.

Pascual, A., Faugere, Y., Larnicol, G., and Le Traon, P.-Y. (2006). Improved description of the ocean mesoscale variability by combining four satellite altimeters. *Geophysical Research Letters*, 33:L02611.

Pasquero, C., Provenzale, A., and Babiano, A. (2001). Parameterization of dispersion in two-dimensional turbulence. *J. Fluid Mech.*, 439:279–303.

Penven, P., Echevin, V., Pasapera, J., Colas, F., and Tam, J. (2005). Average circulation, seasonal cycle, and mesoscale dynamics of the Peru Current System: A modeling approach. *Journal of Geophysical Research*, 110:C10021, doi:10.1029/2005JC002945.

Perissinotto, R., Lutjeharms, J. R. E., and Ballegooyen, R. C. (2000). Biological-physical interactions and pelagic productivity at the Prince Edward Islands, Southern Ocean. *Journal of Marine Science*, 24:327–341.

Petersen, M. R., Williams, S. J., Maltrud, M. E., Hecht, M. W., and Hamann, B. (2013). A three-dimensional eddy census of a high-resolution global ocean simulation. *Journal of Geophysical Research: Oceans*, 118:1759–1774, doi:10.1002/jgrc.20155.

Peterson, T., Crawford, D., and Harrison, P. (2011). Mixing and biological production at eddy margins in the eastern Gulf of Alaska. *Deep Sea Research Part I: Oceanographic Research Papers*, 58(4):389–377.

Qiu, B. and Chen, S. (2005). Eddy-induced heat transport in the subtropical North Pacific from Argo, TMI, and altimetry measurements. *Journal of Physical Oceanography*, 35(4):458–473.

Rae, C. M. D., Garzoli, S. L., and Gordon, A. L. (1996). The eddy field of the southeast Atlantic Ocean: A statistical census from the Benguela Sources and Transports Project. *Journal of Geophysical Research*, 101(C5):11,949–11,964.

Redfield, A. C. (1958). The biological control of chemical factors in the environment. *American Scientist*, 46(3):205–221.

Rhines, P. B. and Young, W. R. (1983). How rapidly is a passive scalar mixed within closed streamlines? *Journal of Fluid Mechanics*, 133:133–145.

Rintoul, S. R., Hughes, C. W., and Olbers, D. (2001). The Antarctic Circumpolar Current System. In Siedler, G., Church, J., and Gould, J., editors, *Ocean Circulation and Climate*, pages 271–302. Academic Press.

Robinson, I. S. (2010). *Discovering the Ocean from Space*. Springer Berlin Heidelberg, Berlin, Heidelberg.

Rudeva, I. and Gulev, S. K. (2007). Climatology of cyclone size characteristics and their changes during the cyclone life cycle. *Monthly Weather Review*, 135:2568–2587.

Sallée, J., Speer, K., and Rintoul, S. (2011). Mean-flow and topographic control on surface eddy-mixing in the Southern Ocean. *Journal of Marine Research*, 69(4):753–777.

Sallée, J.-B., Matear, R. J., Rintoul, S. R., and Lenton, A. (2012). Localized subduction of anthropogenic carbon dioxide in the Southern Hemisphere oceans. *Nature Geoscience*, 5(8):579–584.

Sallée, J. B., Speer, K., and Morrow, R. (2008). Response of the antarctic circumpolar current to atmospheric variability. *Journal of Climate*, 21(12):3020–3039.

Sallée, J.-B., Speer, K., Rintoul, S., and Wijffels, S. (2010a). Southern Ocean thermocline ventilation. *Journal of Physical Oceanography*, 40(3):509–529.

Sallée, J. B., Speer, K. G., and Rintoul, S. R. (2010b). Zonally asymmetric response of the Southern Ocean mixed-layer depth to the Southern Annular Mode. *Nature Geoscience*, 3(4):273–279.

Sallée, J.-B. B. and Rintoul, S. R. (2011). Parameterization of eddy-induced subduction in the Southern Ocean surface-layer. *Ocean Modelling*, 39:146–153.

Sarmiento, J. L., Gruber, N., Brzezinski, M. A., and Dunne, J. P. (2004). High-latitude controls of thermocline nutrients and low latitude biological productivity. *Nature*, 427:56–60.

Shats, M., Xia, H., Punzmann, H., and Falkovich, G. (2007). Suppression of turbulence by self-generated and imposed mean flows. *Physical Review Letters*, 99(16):2–5.

Shuckburgh, E., Maze, G., Ferreira, D., Marshall, J., Jones, H., and Hill, C. (2011). Mixed layer lateral eddy fluxes mediated by air-sea interaction. *Journal of Physical Oceanography*, 41(1):130–144.

Siegel, D. A., Court, D. B., Menzies, D. W., Peterson, P., Maritorena, S., and Nelson, N. B. (2008). Satellite and in situ observations of the bio-optical signatures of two mesoscale eddies in the Sargasso Sea. *Deep Sea Research Part II: Topical Studies in Oceanography*, 55(10-13):1218–1230.

Siegel, D. A., Peterson, P., McGillicuddy, D. J., Maritorena, S., and Nelson, N. B. (2011). Bio-optical footprints created by mesoscale eddies in the Sargasso Sea. *Geophysical Research Letters*, 38(13):L13608.

Small, R., DeSzoeke, S., Xie, S., O'Neill, L., Seo, H., Song, Q., Cornillon, P., Spall, M., and Minobe, S. (2008). Air-sea interaction over ocean fronts and eddies. *Dynamics of Atmospheres and Oceans*, 45(3-4):274–319.

Smith, K. S. (2007). The geography of linear baroclinic instability in Earth's oceans. *Journal of Marine Research*, 65(5):655–683.

Sokolov, S. and Rintoul, S. R. (2007). On the relationship between fronts of the Antarctic Circumpolar Current and surface chlorophyll concentrations in the Southern Ocean. *Journal of Geophysical Research*, 112:C07030.

Sokolov, S. and Rintoul, S. R. (2009a). Circumpolar structure and distribution of the Antarctic Circumpolar Current fronts: 1. Mean circumpolar paths. *Journal of Geophysical Research*, 114:C11018, doi:10.1029/2008JC005108.

Sokolov, S. and Rintoul, S. R. (2009b). Circumpolar structure and distribution of the Antarctic Circumpolar Current fronts: 2. Variability and relationship to sea surface height. *Journal of Geophysical Research*, 114:C11019, doi:10.1029/2008JC005248.

Souza, J. M. A. C., de Boyer Montégut, C., and Le Traon, P. Y. (2011). Comparison between three implementations of automatic identification algorithms for the quantification and characterization of mesoscale eddies in the South Atlantic Ocean. *Ocean Science*, 7(3):317–334.

Spall, M. A. (2007). Midlatitude wind stress-sea surface temperature coupling in the vicinity of oceanic fronts. *Journal of Climate*, 20(15):3785–3801.

Stammer, D. (1997). Global characteristics of ocean variability estimated from regional TOPEX/POSEIDON altimeter measurements. *Journal of Physical Oceanography*, 27(8):1743–1769.

Swart, N. C., Ansorge, I. J., and Lutjeharms, J. R. E. (2008). Detailed characterization of a cold Antarctic eddy. *Journal of Geophysical Research*, 113:CO1009.

Sweet, W., Fett, R., Kerling, J., and La Violette, P. (1981). Air-sea interaction effects in the lower troposphere across the north wall of the Gulf Stream. *Monthly Weather Review*, 109(5):1042–1052.

Takahashi, T., Sweeney, C., Hales, B., Chipman, D., Newberger, T., Goddard, J., Iannuzzi, R., and Sutherland., S. (2012). The changing carbon cycle in the Southern Ocean. *Oceanography*, 25(3):26–37.

Terry, P. W. (2000). Suppression of turbulence and transport by sheared flow. *Reviews of Modern Physics*, 72(1):109–165.

Thompson, A. F. (2008). The atmospheric ocean: eddies and jets in the Antarctic Circumpolar Current. *Philosophical Transactions Royal Society*, 366:4529–4541.

Thompson, A. F., Haynes, P. H., Wilson, C., and Richards, K. J. (2010). Rapid Southern Ocean front transitions in an eddy-resolving ocean GCM. *Geophysical Research Letters*, 37(23):1–5.

Thompson, A. F. and Sallée, J.-B. (2012). Jets and topography: jet transitions and the impact on transport in the Antarctic Circumpolar Current. *Journal of Physical Oceanography*, 42(6):956–972.

Thompson, D. W. J., Solomon, S., Kushner, P. J., England, M. H., Grise, K. M., and Karoly, D. J. (2011). Signatures of the Antarctic ozone hole in Southern Hemisphere surface climate change. *Nature Geoscience*, 4(11):741–749.

Thompson, K. R. and Demirov, E. (2006). Skewness of sea level variability of the world's oceans. *Journal of Geophysical Research*, 111(C5):1–11.

Thoppil, P. G., Richman, J. G., and Hogan, P. J. (2011). Energetics of a global ocean circulation model compared to observations. *Geophysical Research Letters*, 38:L15607.

Treguier, A., England, M., Rintoul, S., Madec, G., Le Sommer, J., and Molines, J.-M. (2007). Southern Ocean overturning across streamlines in an eddying simulation of the Antarctic Circumpolar Current. *Ocean Science Discussions*, 4:653–698.

Trenberth, K. E. and Caron, J. M. (2001). Estimates of meridional atmosphere and ocean heat transports. *Journal of Climate*, 14:3433–3443.

Tulloch, R., Marshall, J., Hill, C., and Smith, K. S. (2011). Scales, growth rates, and spectral fluxes of baroclinic instability in the ocean. *Journal of Physical Oceanography*, 41(6):1057–1076.

Van Aken, H., Van Veldhoven, A., Veth, C., De Ruijter, W., Van Leeuwen, P., Drijfhout, S., Whittle, C., and Rouault, M. (2003). Observations of a young Agulhas ring, Astrid, during MARE in March 2000. *Deep Sea Research Part II: Topical Studies in Oceanography*, 50(1):167–195.

Van Leeuwen, P. J. (2007). The propagation mechanism of a vortex on the β plane. *Journal of Physical Oceanography*, 37(9):2316–2330.

Velasco Fuentes, O. (2009). Kelvin's discovery of Taylor columns. *European Journal of Mechanics - B/Fluids*, 28(3):469–472.

Von Schuckmann, K., Gaillard, F., and Le Traon, P.-Y. (2009). Global hydrographic variability patterns during 2003-2008. *Journal of Geophysical Research*, 114:C09007, doi:10.1029/2008JC005237.

Walkden, G. J., Heywood, K. J., and Stevens, D. P. (2008). Eddy heat fluxes from direct current measurements of the Antarctic Polar Front in Shag Rocks Passage. *Geophysical Research Letters*, 35(6):1–6.

Wanninkhof, R., Park, G., Chelton, D. B., and Risien, C. M. (2011). Impact of small-scale variability on air-sea CO2 fluxes. In Komori, S., McGillis, W., and Kurose, R., editors, *Gas Transfer at Water Surfaces, 2010*, pages 431–444. Kyoto University Press, Kyoto.

Weiss, J. (1991). The dynamics of enstrophy transfer in two-dimensional hydrodynamics. *Physica D: Nonlinear Phenomena*, 48(2-3):273–294.

Wentz, F. J. (1997). A well-calibrated ocean algorithm for special sensor microwave/imager. *Journal of Geophysical Research*, 102(C4):8703–8718, doi:10.1029/96JC01751.

Whalen, C. B., Talley, L. D., and MacKinnon, J. a. (2012). Spatial and temporal variability of global ocean mixing inferred from Argo profiles. *Geophysical Research Letters*, 39:L18612.

White, W. B. and Annis, J. L. (2003). Coupling of extratropical mesoscale eddies in the ocean to westerly winds in the atmospheric boundary layer. *Journal of Physical Oceanography*, 33(5):1095–1107.

Wunsch, C. (2005). The total meridional heat flux and its oceanic and atmospheric partition. *Journal of climate*, 18:4374–4380.

Xie, S.-P. (2004). Satellite observations of cool ocean-atmosphere interaction. *Bulletin of the American Meteorological Society*, 85(2):195–208.

Xiu, P., Palacz, A. P., Chai, F., Roy, E. G., and Wells, M. L. (2011). Iron flux induced by Haida eddies in the Gulf of Alaska. *Geophysical Research Letters*, 38(13):L13607.

Xu, C., Shang, X.-D., and Huang, R. X. (2011a). Estimate of eddy energy generation/dissipation rate in the world ocean from altimetry data. *Ocean Dynamics*, 61(4):525–541.

Xu, H., Xu, M., Xie, S.-P., and Wang, Y. (2011b). Deep atmospheric response to the spring Kuroshio over the East China Sea. *Journal of Climate*, 24(18):4959–4972.

Xu, Y. and Fu, L.-L. (2011). Global variability of the wavenumber spectrum of oceanic mesoscale turbulence. *Journal of Physical Oceanography*, 41(4):802–809.

Zhai, X., Johnson, H. L., and Marshall, D. P. (2010). Significant sink of ocean-eddy energy near western boundaries. *Nature Geoscience*, 3(9):608–612.

Zickfeld, K., Fyfe, J. C., Saenko, O. A., Eby, M., and Weaver, A. J. (2007). Response of the global carbon cycle to human-induced changes in Southern Hemisphere winds. *Geophysical Research Letters*, 34:L12712, doi:10.1029/2006GL028797.

Thanks to ...

... Niki and Reto, who initiated this project and whose doors were always open for discussion of results, or to give back the big picture if I got lost in detail. Thanks to Niki for giving guidance through my PhD life.

... Matt for countless discussions, technical hints and help, without you this project would not have been possible.

... Matt and David for struggling through my drafts.

... Bianca for making administrative processes run so smoothly I did not even realize they existed.

... Heini for providing help with the eddy-tracking algorithm.

... Andreas for being a great host while I visited GEOMAR, and for making the trip to Zurich for my defense.

... all the UP group members who were there when I started my PhD and made me feel welcome in the office with the view on the concrete bridge, and thanks especially to Ilaria for making me quickly feel at home in Zurich.

... to my office mates to give me company and together with Mark keep our table brimming with food for the brain.

... all former and current UP group members for providing a great work-atmosphere, in addition to great times we had on private ventures. Thanks to our hallway- and coffeeroom-colleagues for friendly exchanges in between.

... the ClimPhys group for the nice coffee chats in addition to the work-talks and discussions which gave me the opportunity to keep in touch with the atmospheric sciences.

... my parents for providing me with everything I needed to pursue my studies, and my husband Moritz for giving me any support I could ever need.

... the Center for Climate Systems Modeling (C2SM) at ETH Zürich which provided the financial support for most of this project.